THE ACTIVATION OF CARBON OXIDES BY LOW VALENT GROUP IV AND THORIUM COMPLEXES

BY

ZOË EMILY BUTTON

SUBMITTED FOR THE DEGREE OF DOCTOR OF PHILOSOPHY

UNIVERSITY OF SUSSEX

DECEMBER, 2011

The work described in this thesis was carried out at the University of Sussex from October 2008 to December 2011, under the supervision of Professor F. G. N. Cloke. All the work is my own, unless stated to the contrary and has not been previously submitted for any degree at this or any other university.

Zoë Emily Button

December, 2011

ACKNOWLEDGEMENTS

This thesis is dedicated to my late Grandad, Pte. Thomas Henry Doidge, nuclear test veteran with Operation Hurricane on HMS Campania.

With thanks to:

The members of Lab 14 past and present

Prof. F. G. N. Cloke
Dr J. F. C. Turner
Dr I. R. Crossley
Dr A. S. Frey
Dr J. H. Farnaby
Dr M. P. Coles
Dr S. M. Roe
Dr P. B. Hitchcock
Dr I. J. Day
Dr A. Abdul-Sada
A. Kilpatrick
Prof. L. Maron
Roger, Ken, Alex, Barry, Mick, Fran, JMS stores
EPSRC
University of Sussex

With thanks to my wonderful family and friends who have supported me throughout my studies.

And finally, to Sam.

SUMMARY

Following discoveries in our laboratory that mixed-ring uranium(III) complexes reductively couple CO to produce new C-C bonds and transform this small molecule into potentially useful small organic things, further research has taken place into the synthesis, characterisation and reactivity of the zirconium, hafnium and thorium analogues. The first part of this thesis describes the preparation of the novel zirconium(IV) and hafnium(IV) mixed-sandwich chloride complexes using sterically demanding cyclopentadienyl and cyclooctatetraenyl ligands, and their subsequent reduction into the desired low valent M(III) compounds.

The second part considers the reaction between carbon oxides and three different zirconium(III) complexes in which differently substituted cyclopentadienyl ligands are employed. Reaction with CO generated two novel complexes that displayed C-C bond formation, with the products influenced by the sterics of the systems. Reaction with CO_2 produced products resulting from reduction and/or reductive disproportionation of CO_2, which were independent of the steric bulk of the cyclopentadienyl ligand.

The third and final part of the thesis considers the synthesis of two novel mixed-ring thorium(IV) halide species, before a description of their *in situ* reduction in the presence of CO_2 to yield products different to those previously described in this work. The reactivity illustrated here demonstrates a new approach to the reductive coupling of CO *via* characterised zirconium(III) complexes and provides insight into the reactivity of a transient thorium(III) sandwich complex.

LIST OF NEW COMPOUNDS

$[Zr(\eta^8\text{-}C_8H_6\{Si^iPr_3\text{-}1,4\}_2)Cl_2(THF)]$ (**2.5**)

$[Hf(\eta^8\text{-}C_8H_6\{Si^iPr_3\text{-}1,4\}_2)Cl_2(THF)]$ (**2.6**)

$[Hf(\eta^8\text{-}C_8H_6\{Si^iPr_3\text{-}1,4\}_2)(Cp^{Me4H})Cl]$ (**2.8**)

$[Hf(\eta^8\text{-}C_8H_6\{Si^iPr_3\text{-}1,4\}_2)(Cp^{Me5})Cl]$ (**2.10**)

$[Zr(\eta^8\text{-}C_8H_6\{Si^iPr_3\text{-}1,4\}_2)(Cp^{Me(TMS)})Cl]$ (**2.11**)

$[Hf(\eta^8\text{-}C_8H_6\{Si^iPr_3\text{-}1,4\}_2)(Cp^{Me4(TMS)})Cl]$ (**2.12**)

$[Zr(\eta^8\text{-}C_8H_6\{Si^iPr_3\text{-}1,4\}_2)(Ind^{Me7})Cl]$ (**2.13**)

$[Hf(\eta^8\text{-}C_8H_6\{Si^iPr_3\text{-}1,4\}_2)(Ind^{Me7})Cl]$ (**2.14**)

$[Zr(\eta^8\text{-}C_8H_6\{Si^iPr_3\text{-}1,4\}_2)(Cp^{Me4H})]$ (**3.1**)

$[Zr(\eta^8\text{-}C_8H_6\{Si^iPr_3\text{-}1,4\}_2)(Cp^{Me5})]$ (**3.2**)

$[Zr(\eta^8\text{-}C_8H_6\{Si^iPr_3\text{-}1,4\}_2)(Cp^{Me4(TMS)})]$ (**3.3**)

$[Hf(\eta^8\text{-}C_8H_6\{Si^iPr_3\text{-}1,4\}_2)(Cp^{Me4H})]$ (**3.4**)

$[Hf(\eta^8\text{-}C_8H_6\{Si^iPr_3\text{-}1,4\}_2)(Cp^{Me5})]$ (**3.5**)

$[Hf(\eta\text{-}Cp^{Me4H})]_2(\mu\text{-}\eta^7.\eta^7\text{-}(C_8H_6\{Si^iPr_3\text{-}1,4\}_2C_8H_6\{Si^iPr_3\text{-}1,4\}_2)]$ (**3.6**)

$[Hf(\eta\text{-}Cp^{Me5})]_2(\mu\text{-}\eta^7.\eta^7\text{-}(C_8H_6\{Si^iPr_3\text{-}1,4\}_2C_8H_6\{Si^iPr_3\text{-}1,4\}_2)]$ (**3.7**)

$[Hf(\eta\text{-}Cp^{Me4(TMS)})]_2(\mu\text{-}\eta^7.\eta^7\text{-}(C_8H_6\{Si^iPr_3\text{-}1,4\}_2C_8H_6\{Si^iPr_3\text{-}1,4\}_2)]$ (**3.8**)

$[Zr(\eta^4\text{-}C_8H_6\{Si^iPr_3\text{-}1,4\}_2)(Cp^{Me5})^{13}CO]_2$ (**4.1**)

$[Zr(\eta^4\text{-}C_8H_6\{Si^iPr_3\text{-}1,4\}_2)(Cp^{Me4H})^{13}CO]_2$ (**4.2**)

$[OZr_2(CO_3)_2Zr_2O]^{Me4H}$ (**4.3**)

$[OZr_2(CO_3)_2Zr_2O]^{Me5}$ (**4.4**)

$[OZr_2(CO_3)_2Zr_2O]^{Me4(TMS)}$ (**4.5**)

$[Th(\eta^8\text{-}C_8H_6\{Si^iPr_3\text{-}1,4\}_2)(Cp^{Me5})Cl]$ (**5.4**)

$[Th(\eta^8\text{-}C_8H_6\{Si^iPr_3\text{-}1,4\}_2)(Cp^{Me5})I]$ (**5.7**)

$[Th(\eta^8\text{-}C_8H_6\{Si^iPr_3\text{-}1,4\}_2)(Cp^{Me5})]_2C_2O_4$ (**5.8**)

$[Th(\eta^8\text{-}C_8H_6\{Si^iPr_3\text{-}1,4\}_2)(Cp^{Me5})]_2CO_3$ (**5.9**)

LIST OF ABBREVIATIONS USED IN THE TEXT

ATP	Adenosine triphosphate
CHT	Cycloheptatrienyl
COD	Cyclooctadiene
COT	Cyclooctatetraene, cyclooctatetraenyl
Cp	Cyclopentadienyl
Cp^{Me4H}	Tetramethylcyclopentadienyl
Cp^{Me5}	Pentamethylcyclopentadienyl
$Cp^{Me4(TMS)}$	Trimethylsilyl tetramethylcyclpentadienyl
CV	Cyclic Voltammetry/ Cyclic Voltammogram
Cy	Cyclohexane
d	Doublet
δ	Chemical shift
DFT	Density Functional Theory
DME	1,2-Dimethoxyethane
dmpe	1,2-Bis(methylphosphino)ethane
dppe	1,2-Bis(diphenylphosphino)ethane
EI	Electron Impact
$\{^1H\}$	Proton Decoupled
Ind	Indenyl
Ind^{Me7}	Permethylindenyl
^{i}Pr	*iso*-Propyl
IR	Infrared
Ln	Lanthanide
M	Metal
m	Multiplet
Me	Methyl
NMR	Nuclear Magnetic Resonance
^{n}Bu	*n*-Butyl
OTf	Triflate
Pent	Pentalene

Ph	Phenyl
ppm	parts per million
s	Singlet
t	Triplet
^{t}Bu	*t*-butyl
THF	Tetrahydrofuran
TMEDA	*N,N,N',N'*-tetramethylethylenediamine
TMS	Trimethylsilyl
X	Halide or non-coordinating anion

TABLE OF CONTENTS

Bazinga!

Sheldon Cooper *(Big Bang Theory)*

1 CHAPTER ONE: INTRODUCTION

1.1 General Introduction

Small molecule activation, in particular that of N_2, CO and CO_2, has been an active area of research for over 40 years. Notably, this field of research has identified the significant reactivity of organometallic complexes of the Group IV metals (titanium, zirconium and hafnium) towards these small molecules. In this chapter, the activity of organometallic transition metal and f-element complexes towards N_2, CO and CO_2 will be discussed, with emphasis on the reactivity of Group IV metals in this context.

1.2 Introduction to the Group IV metals titanium, zirconium and hafnium

Despite the discovery of the elements titanium and zirconium in the latter part of the 18th century, it was not until the 1920s that hafnium, the heaviest Group IV metal, was definitively identified, following predictions about the missing elements of the periodic table. This belated discovery is due to the similar physical properties of zirconium and hafnium, meaning that they occur in the same ores and are difficult to separate. Consequently, its chemistry was slow to develop and it is only in recent years that hafnium has been shown to possess different chemical reactivity to that of its lighter counterparts. This can, in part, be attributed to the differences in redox potential down the group as summarised in **Table 1.1**, with titanium only a mild reducing agent compared to zirconium and hafnium when the identical substituted metallocene dichlorides are considered.[1]

Table 1.1: Selected reduction potentials *versus* the standard calomel electrode in 0.2 M $[N^nBu_4][BF_4]$ in THF at a platinum electrode at 20 °C.

Complex	$E_{1/2}^{red}$/V	ΔG/kJ.mol^{-1}
$[TiCl_2\{\eta\text{-}C_5H_3(SiMe_3)_2\}_2]$	-0.70	67.5
$[ZrCl_2\{\eta\text{-}C_5H_3(SiMe_3)_2\}_2]$	-1.55	149.6
$[HfCl_2\{\eta\text{-}C_5H_3(SiMe_3)_2\}_2]$	-1.87	180.4

When the electropotentials of titanium and zirconium congeners from **Table 1.1** are compared a large difference in $E_{1/2}$ values is observed, equating to 82.1 kJ.mol^{-1}. This would indicate that different reactivity should be detected between these two Group IV neighbours. The hafnium analogue requires an energy input of 180.4 kJ.mol^{-1} to reach the +3 oxidation state with the same ligands, indicating further difference still from its lighter congeners: this metal is thought to possess the most negative of reduction potential of all the transition elements. The presence of full f-orbitals in the core and the associated lanthanide contractions of hafnium lead to behaviour distinctive from titanium and zirconium, elements that do not possess f-orbitals in their cores. Although zirconium and hafnium(IV) compounds have previously been noted to behave similarly, it is now clear that they display subtly different modes of activity and stability towards different ligands, reagents and conditions, whilst titanium assumes a pronouncedly dissimilar reactivity.

Titanium, zirconium and hafnium are most well known for their use in polymerisation chemistry. Over 50 years ago, Ziegler *et al.* observed that $TiCl_4$-$AlClEt_2$ was active towards the polymerisation of ethene,[2] with Natta discovering shortly afterwards that this catalyst could be used to prepare stereoregular polymers.[3] This catalysis occurred in a heterogeneous system, leading to a broad molecular weight distribution. Andresen *et al.* noted that addition of trimethyl aluminium with trace water to a homogeneous metallocene catalyst greatly increased the reactivity of the complex, with molecular weight governed by temperature of the system. Since then, cationic alkyl complexes of Group IV metallocenes of the type $[MCp_2R]^+$ (M = Ti, Zr, Hf; R = alkyl) have been recognised as the catalytically active species. Differently substituted and tethered Cp

rings such as ethylene-tethered *bis*(indenyl) and *bis*(tetrahydroindenyl),[4] ethylene bridged permethylated metallocenes[5] and tetramethylethylene bridged metallocenes[6] have allowed control of polymer tacticity. Most stereoselectivity has been seen through the application of the *ansa*-bridged zirconocenes, particularly those containing substituted indenyl ligands, as these impart significant rigidity to the molecule.[7] Through these now relatively well-defined 14 electron systems, highly stereoselective polymers are accessible in excellent yields.

1.3 Activation of N_2

Nitrogen is an essential element for all life and vital in plant fertilisation. At the beginning of the 20th century, natural sources of non-elemental nitrogen such as saltpetre were nearing depletion. Although dinitrogen itself is abundant in the Earth's atmosphere, accessing an activated or functionalised form of this element for application is a non-trivial process: N_2 is apolar and possesses one of the strongest bonds known of 945 kJ.mol^{-1}.

With this challenge and immediate need in mind, fixation of nitrogen became an area of immense scientific interest. It was with the development of the Haber-Bosch process in the early 20th century that it became possible to transform the naturally inert dinitrogen molecule into ammonia, a fundamental feedstock for fertiliser production. This industrial process requires the pressurisation of one equivalent of N_2 and three equivalents of H_2 to approximately 200 atm at 400 °C over an iron or ruthenium catalyst, resulting in two equivalents of ammonia. This is in stark contrast to the nitrogenase enzymes present in certain plants that are capable of dinitrogen activation under extremely mild conditions. However, to proceed under these conditions, these enzymes require a large energy input of up to sixteen equivalents of MgATP.

Although the Haber-Bosch process is unlikely to be superseded in the near future by other commercially practical means, the activation of N_2 under mild conditions, as seen with nitrogenases, is still of great interest. The elucidation of this mechanism has been subject to speculation, but has been greatly hindered by the complexity of the enzymes involved. The activation of N_2 by organometallic systems has been widely reported as

chemists attempt to synthesise a complex that may provide insight into the finer details of nitrogenase activity.

Despite being apolar and both a poor σ-donor and π-acceptor, many examples of N_2 bound to an organometallic transition metal centre are known, in a number of coordination modes (**Figure 1.1**).

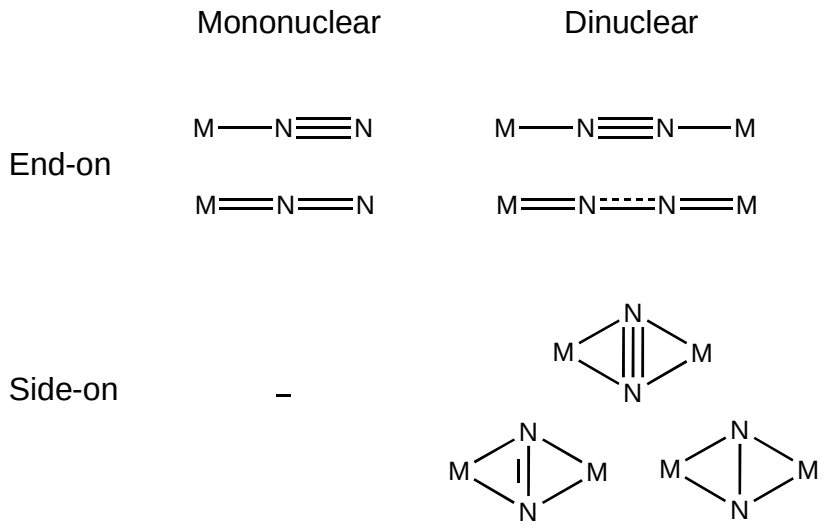

Figure 1.1: Bonding modes of dinitrogen.[8]

The extent of N_2 activation is largely dependent on the choice of metal oxidation state and the ligand environment. Bonding of dinitrogen to two metal centres, relative to one, results in a "more activated" N_2 moiety, with greater back-bonding from the metal to the Nπ* orbitals. This back-bonding lengthens the N-N distance, with this bond length frequently cited as the measure of the extent of activation when compared to that of free N_2 at 1.0977 Å. This lengthening also leads to a decrease in the stretching frequency observed in IR and/or Raman spectroscopy as the bond order of the N_2 moiety decreases.

1.3.1 Activation of N_2 by organometallic transition metal complexes

Although not synthesised directly from the addition of dinitrogen to an organometallic complex, the reaction of ruthenium(III) or (IV) salts with hydrazine resulted in what is considered to be the first example of a molecular nitrogen ligand, terminally bound to the metal as $[Ru(NH_3)_5N_2]X_2$ (**1.1**, X = Cl; **1.2**, X = Br; **1.3**, X = I; **1.4**, X = BF_4; **1.5**, X = PF_6).[9, 10] The molecular arrangement of **1.1** was confirmed by IR spectroscopy and later by a single crystal X-ray diffraction study.[11]

Following this first example of the ligating dinitrogen moiety, further instances were swiftly discovered by other research groups. This included the discovery of the first coordinated N_2 complex synthesised directly from gaseous dinitrogen, $[(Ph_3P)_3Co(N_2)H]$ (**1.6**).[12] Subsequent work by Chatt *et al.* with tungsten and molybdenum documented further N_2 activation when $[M(N_2)_2(dppe)_2]$ (**1.7**, M = Mo; **1.8**, M = W) was reacted with hydrogen halides, resulting in a bound N_2H_2 moiety, *i.e.* as $[MX_2(N_2H_2)(dppe)_2]$ (**1.9**).[13] Although acquisition of structural data was not possible, ^{1}H NMR and IR spectroscopy confirmed the presence of the diazene core. Terminal functionalisation of the dinitrogen ligand by *n*-butanol was possible, upon irradiation in the presence of methyl bromide, and confirmed by X-ray diffraction studies (**Scheme 1.1**).[14] This group expanded these investigations and documented a variety of C-N bond formations mediated *via* irradiation of **1.8** in the presence of alkyl bromides, acyl chlorides and aryl chlorides yielding organohydrazido and diazenido compounds.[15]

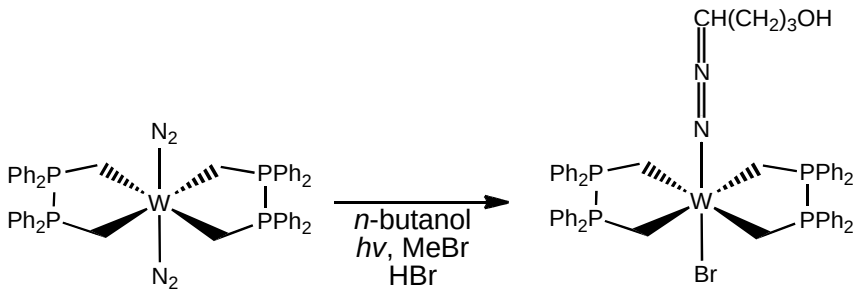

1.8

Scheme 1.1: Reaction of **1.8** with *n*-butanol results in functionalisation of one dinitrogen ligand and bromination of the central metal atom.

In the early 1980s attention shifted to compounds of Group V, following the discovery of a vanadium-containing nitrogenase. It was research by Schrock and coworkers that led to the isolation of the first structurally characterised dinitrogen complex containing a Group V metal, the ditantalum complex **1.10** (**Scheme 1.2**).[16] This complex is significant due to the considerably lengthened N-N distance of 1.298(12) Å and shorter metal-nitrogen lengths than previously observed, measuring 1.837(8) and 1.842(8) Å. Compound **1.10** can be described as consisting of an N_2^{4-} hydrazido core with imido-like N-Ta bonds, where electrons have been donated into the antibonding orbitals of the dinitrogen moiety, thus decreasing its bond order.

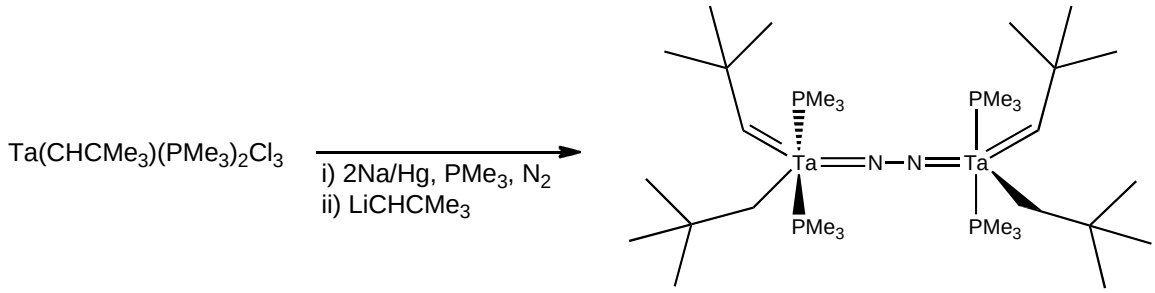

1.10

Scheme 1.2: Reduction of N≡N by tantalum complex resulting in the bridging imido moiety.

Schrauzer and Palmer found that the highly reducing vanadium(II) complex [V(benzene-1,2-diolate)] **1.11** in methanol allowed complete reduction of N_2 to ammonia in <10 % yields, with the yield being highly dependent on pH and solvent.[17] Further work by Luneva *et al.* into the related complex [V(4,5-di-*tert*-butylbenzene-1,2-diolate)] **1.12,** under similarly basic and methanolic conditions, showed that the metal extracts hydrogen from the solvent, resulting in formation of ammonia in yields that vary with concentration of the base, peaking at 40-45 % where [$NaOCH_3$] is 0.8 M.[18] However, in this example 75 atmospheres of N_2 are required.

Further studies by Berno and Gambarotta led to isolation of the divanadium salt **1.13** from trihydridodivanadium and nitridodivanadium fragments, shown in **Figure 1.2**.[19] The short V-N distances of 1.771(4) and 1.776(4) Å are consistent with multiple bond character, while the N-N distance of 2.420(3) Å rules out a side-on bound dinitrogen moiety. This compound was formed from [{[$(Me_3Si)_2N$]V[$CH_2(SiMe_2)N(SiMe_3)$}(PMe_3)] under 60 atm hydrogen, with "fortuitous nitrogen exposure" during work-up. It is believed that the hydride moieties in **1.13** arise from hydrogenolysis of the silyl ligands, with the electrons required for nitrogen reduction also presumed by the author to be provided by this source. However, though it is believed that the nitrogen atoms did not come from the amide ligands, this has not been unequivocally established.

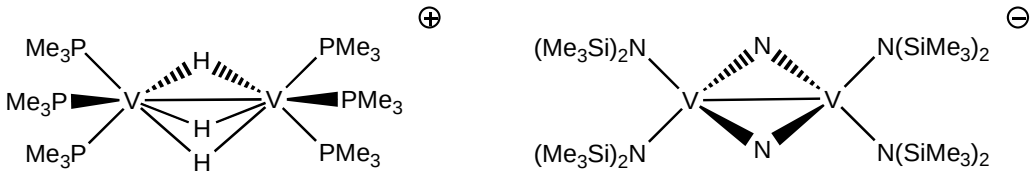

Figure 1.2: Vanadium cation/anion complex **1.13** demonstrating complete cleavage of N_2.

Work by Cloke and coworkers showed a less ambiguous N_2 reduction by the vanadium diamidoamine complex [V[$(Me_3Si)N\{CH_2CH_2N(SiMe_3)\}_2$]Cl]$_2$ (**1.14**). Addition of one equivalent of nitrogen gas and one equivalent of KC_8 to **1.14** resulted in the dinuclear dinitrogen bridged vanadium product (**1.15**) as shown in **Scheme 1.3**. The origin of the bridging nitrogen was proven by ^{15}N NMR spectroscopic studies not to result from

ligand reactivity in this case.[20, 21] In contrast to previously documented examples, a large overpressure of dinitrogen was not required. In this example the N-N distance is 2.50(2) Å, indicating complete N_2 cleavage.

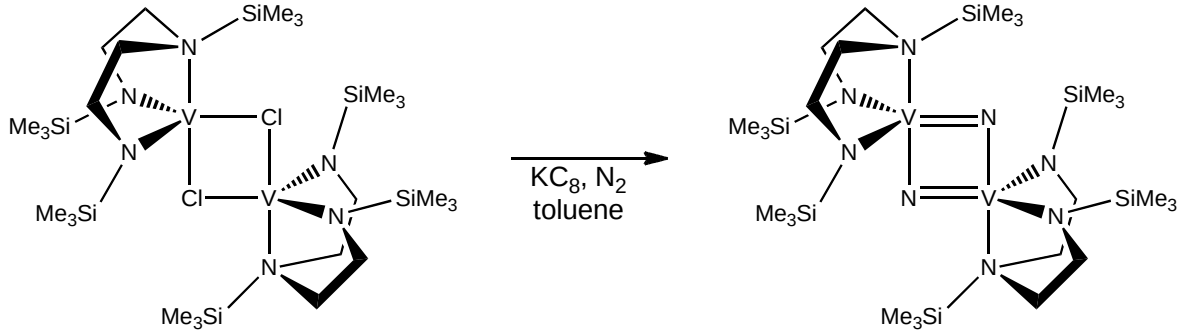

1.14 **1.15**

Scheme 1.3: Complete cleavage of dinitrogen by Cloke's vanadium complex in the presence of KC_8 under ambient pressures of N_2

Only two other indisputable examples of complete N_2 cleavage to nitrido compounds are currently known. The first of these is the three-coordinate molybdenum amido complex[22-24] $[Mo(NRAr)_3]$ (R = $C(CD_3)_2CH_3$, Ar = 3,5-$C_6H_3(CH_3)_2$, **1.16**), which is active under extremely mild conditions (-35 °C, ≤ 1 atm N_2). A number of kinetic interrogations revealed the unstable end-on N_2-bridged dimeric intermediate **1.17**, which breaks apart to afford the monomeric molybdenum nitrido complex **1.18** (**Scheme 1.4**). Molecule **1.18** has a short Mo-N distance of 1.658(5) Å, and, unlike other examples discussed in this section, exists as a mononuclear compound. Due to the preservation of the ligand set during this reaction, one could hope for the development of a catalytic system that facilitates the removal of the nitrido moiety from **1.18** and thus reduces the metal centre from Mo(VI) back to the Mo(III) starting material **1.16**.

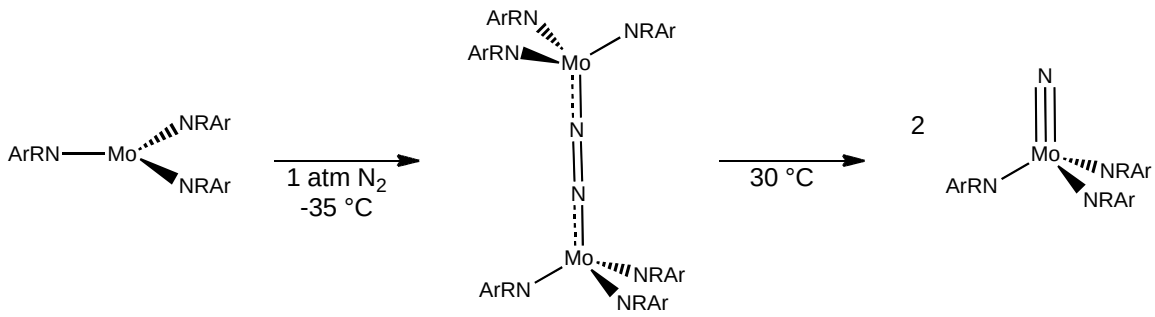

1.16 **1.17** **1.18**

Scheme 1.4: Complete dinitrogen cleavage by molybdenum(III) complex **1.16**, via unstable intermediate **1.17**, resulting in the terminal nitrido molecule **1.18**.

In a further example, only a blanket of dinitrogen was required to ensure reaction with niobium calix[4]arene **1.19,** based on the methylphenol subunit (**Scheme 1.5**).[25] Subsequent reductions with sodium led to the nitrido complex **1.20** with a side-on bridging Nb_2N_2 core, structurally similar to that seen in Cloke's vanadium molecule, but with a slightly greater N-N separation of 2.598(8) Å. In **1.20**, the N_2 moiety bridges both niobium centres η^2, with each nitrogen atom engaging in long range interactions (2.433(8) Å) with one sodium atom.

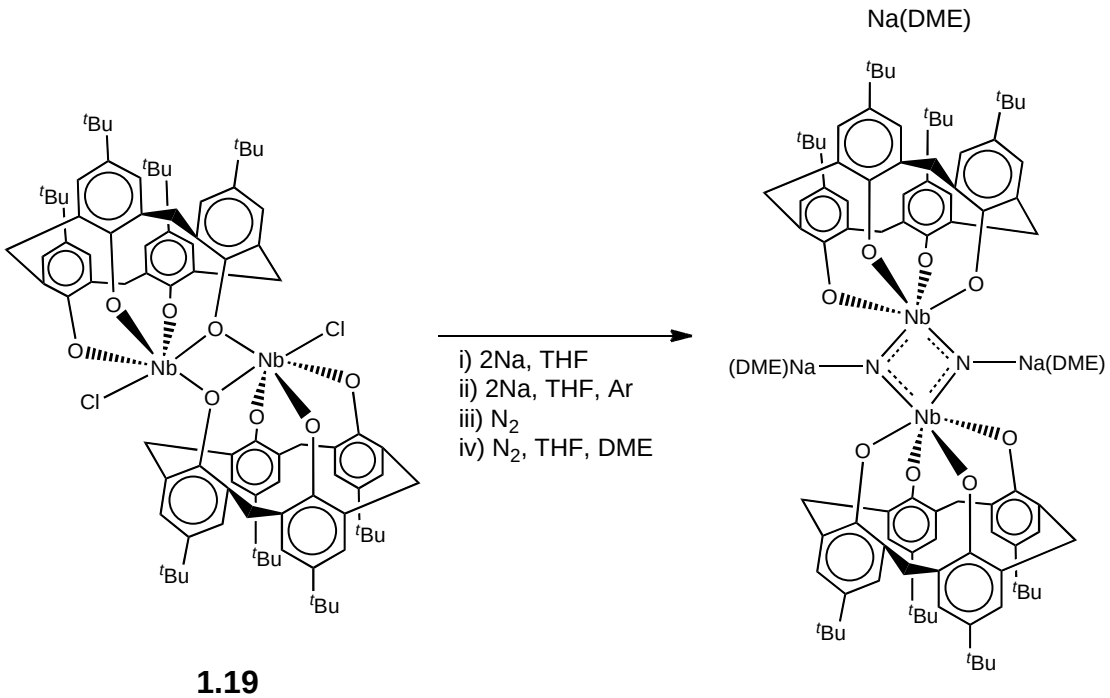

1.19 **1.20**

Scheme 1.5: Complete reduction of dinitrogen by niobium calixarene complex with sodium.

1.3.2 Activation of N_2 by organometallic Group IV complexes

Titanocenes have proven particularly problematic to isolate and characterise and, for the unsubstituted Cp variant, remains elusive in the solid state, only existing as a poorly characterised species in the solution state. During investigations it was observed that $TiCp^R_2$ would absorb dinitrogen, carbon monoxide and dihydrogen;[26] with hydrazine or ammonia observed on hydride addition in the case of nitrogen absorption.[27-29]

Five years after these initial observations, X-ray analysis confirmed the identity of the titanocene compound resulting from N_2 absorption as the end-on bound dinuclear complex **1.21** (**Figure 1.3)**.[30] In this structure, the N-N bond distance is 1.165(14) Å, longer than seen in the free molecule. Similar examples of titanocene-based dinitrogen activation are plentiful, with the steric influence of the Cp ligand being thoroughly explored (Cp^{Me4R}: R = H, Me, Et, TMS, ^{t}Bu, $SiMe_2Ph$, 3,5-Me_2-C_6H_3; Cp^{TMS2}), albeit exerting little effect.[31-35]

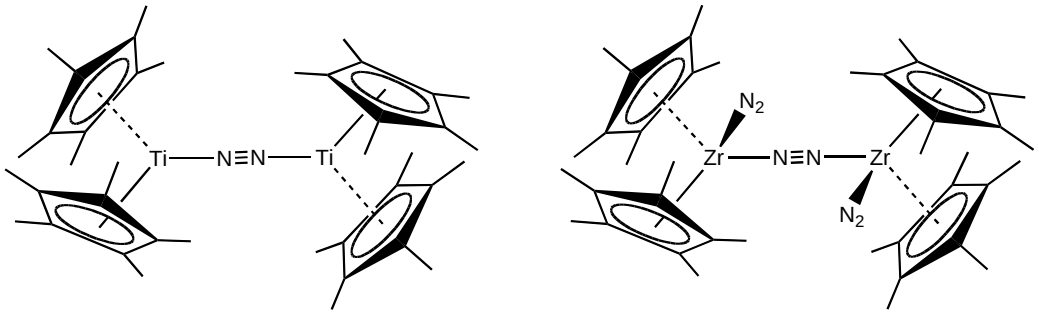

1.21 **1.22**

Figure 1.3: Dinitrogen bonding in titanocene and zirconocene. The larger zirconium atoms allow end-on coordination of two additional N_2 molecules.

Further investigations by Bercaw led to the structural identification of the related zirconium complex $[Zr(Cp^{Me5})_2(N_2)]_2N_2$ (**1.22**) containing both an end-on bridging dinitrogen fragment and two terminal molecular nitrogen molecules bound end-on to each metal centre (**Figure 1.3**).[36, 37] These two terminal nitrogen groups display a torsion angle of 87.3(2)° through the ZrNNZr core, and N-N bond lengths only marginally longer than the free N_2 molecule (1.116(8) and 1.115(7) Å versus 1.0976 Å). The bridging dinitrogen moiety has a slightly elongated bond length when compared with **1.21** of 1.182(5) Å, indicating activation, although this cannot be considered a true example of N_2^{2-}. This complex released hydrazine upon addition of HCl, with half a mole produced per zirconium atom. The hafnocene congener, identified spectroscopically ten years after the initial observation of **1.21**, is yet to be crystallographically characterised, though it is believed to be structurally similar to **1.22**, on the basis of IR spectroscopic studies that indicate three prominent υ(NN) bands, while ^{1}H NMR spectroscopy indicates two pairs of inequivalent Cp^{Me5} ligands, as seen for the zirconium congener.[38]

Despite further investigations into related titanocenes by Teuben and coworkers, only compounds similar to **1.21** were detected, with functionalisation of the dinitrogen moiety not observed.[39-41] Employing the unsubstituted cyclopentadienyl ligand, Pez *et al.* were able to synthesise the dinuclear compound $[\mu\text{-}(\eta^1\text{:}\eta^5\text{-}C_5H_4)](\eta\text{-}C_5H_5)_3Ti_2$ (**1.23**), and found that this reacts with N_2 to produce a variety of products depending on

the solvent system utilised. When solvents of low polarity such as toluene, hexane and diethyl ether were employed under mild conditions, a simple N_2-bridged dinuclear complex was observed.[42] Alternatively, when DME and an overpressure (10 atm) of dinitrogen were employed, a compound containing the unprecedented μ_3-N_2 moiety (**1.24**), in which the nitrogen is bound both side- and end-on, resulted (**Figure 1.4**). Due to the unusual binding mode, the N_2 fragment has a significantly longer N-N bond distance of 1.301 Å, as expected for a doubly-bonded N-N moiety. On aqueous treatment of a diglyme solution of **1.24**, ammonia is detected, although this has not been quantified.

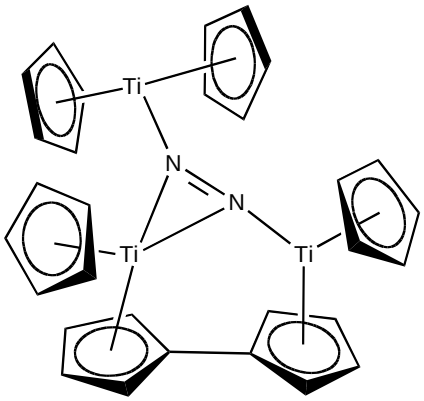

1.24

Figure 1.4: Dinitrogen bound in an unusual end- and side-on mode to three titanocene units.

The most successful example of N_2 activation by Group IV complexes have typically afforded side-on bound examples. In the first of these examples,[43] the more common Cp ligands are abandoned and NMe_2 groups employed instead. This resulted in the first example of two molecules of N_2 bound between two titanium atoms in an anionic complex (**1.25**) (**Figure 1.5**), with the N-N distance of 1.379(21) Å consistent with that of a single bond.

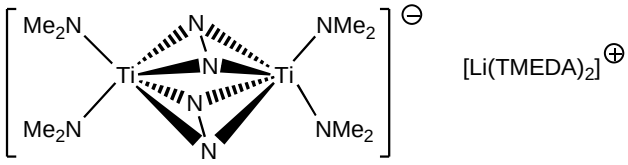

1.25

Figure 1.5: The first example of side-on bound dinitrogen in a Group IV organometallic complex.

The first example of side-on bound N_2 by zirconium resulted in a Zr_2N_2 moiety (**1.26**) in which the dinitrogen has been indisputably reduced to N_2^{4-} (**Scheme 1.6**).[44] The N-N bond distance of 1.548(1) Å is considerably longer than anything seen before in Group IV chemistry, equating to a single N-N bond, longer than that of hydrazine (typical N-N_{N2H4} = 1.45 Å). As expected with the level of activation shown in **1.26**, the metal-nitrogen distances (2.024(4) and 2.027(4) Å) are significantly shorter than typical Zr-N single bonds (*ca*. 2.25 Å).[45-47] Addition of HCl results in liberation of one equivalent of hydrazine per dinuclear molecule. However, this accompanies complete decomposition of the organometallic compound, precluding this reaction from being utilised catalytically. Later work showed that functionalisation of the above compound was possible, with the creation of an N-C bond, through addition of aryl ethynes (aryl = Ph, *p*-Me-C_6H_4, *p*-^{t}Bu-C_6H_4).[48] Synthesis of a hafnium analogue has proven difficult, with the dinitrogen complex so far proving to be unisolable in the solid state.[49]

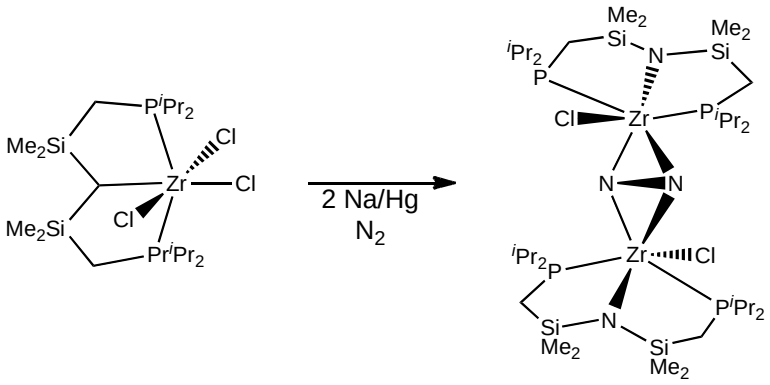

1.26

Scheme 1.6: Dinuclear zirconium compound showing reduction of N_2 to a bridging N_2^{4-} moiety.

A large number of examples of side-on bound Zr_2N_2 complexes have been identified by Chirik *et al.*, with subtle changes in the ligand environment of the zirconocene moiety, however these show a lesser degree of activation than observed with **1.26**, with N-N bond distances of 1.241(3) to 1.377(3) Å recorded.[50] Some of these complexes have shown success with regards to dinitrogen reduction, with hydrazine or ammonia detectable upon acidic work-up, whilst one such complex has been amenable to further functionalisation with CO_2, as discussed in more detail in **Section 1.4**. A hafnocene molecule containing the side-on bound N_2 moiety was characterised by X-ray diffraction, with the N-N distance observed to be significantly longer (1.423(11) Å) than that seen in the zirconocene congener. This result highlights the more pronounced back bonding that is possible from a hafnium core compared to zirconium.[51]

Functionalisation of hafnium-bound dinitrogen has recently been the subject of intensive investigation by Chirik and coworkers, with many publications appearing in the past decade. The small molecules CO,[52-54] CO_2[55] and PhNCO[56] have each been used in this nitrogen functionalisation, yielding a range of interesting results. Addition of MeOTf to the functionalised dinitrogen product resulted in a mixture of products including the methylated N-N core,[57] however the main product of this reaction was the end-on bridged hafnocene system with a triflate group attached to each metal. Carbon monoxide and dioxide functionalisation of the dinitrogen moiety will be examined more thoroughly in **Sections 1.4** and **1.5**.

1.4 Activation of CO

The possibility of using CO as a C_1 feedstock is of great industrial interest as economic pressure mounts on the petrochemical industry to pursue alternative fuel options. Although isoelectronic with N_2 and containing the strongest bond in nature (1076 kJ.mol^{-1}), the inherent polarity and polarisability (1.95×10^{-24} cm^3) of carbon monoxide can allow access to a wider range of chemistry. As for N_2, the degree of activation can be ascertained by the increase in interatomic distance ($d_{C\equiv O}$ = 1.128 Å) and decrease in $\upsilon_{C=O}$ stretching frequency. Although carbonyl complexes are known for most transition metals, there are few examples in which the CO moiety undergoes further M-CO reactivity

1.4.1 Activation of CO by organometallic transition metal complexes

Following the fuel crisis of the 1970s, extensive research was conducted into CO insertion into metal-metal bonds in diphosphine- and diarsine-bridged 'A-frame' complexes (such as that illustrated in **Scheme 1.7**), where the metal atoms were commonly late transition metals such as palladium,[58, 59] and platinum[60] It was found that these relatively weak M-M interactions were amenable to small molecule insertion or activation, with either formation of MC(O)M or MCO.

Brown *et al.*[60] identified reversible binding of one CO unit to the dimeric complex bis-μ-[bis(diphenylphosphino)methane]-bis(chloroplatinum)(Pt-Pt), with subsequent CO insertion into the Pt-Pt bond. Similar results were seen by a number of research groups and investigations eventually led to isolation of crystalline material suitable for X-ray diffraction studies[58,59] One group examined the palladium complex (**1.27**) shown in **Scheme 1.7**, produced by addition of CO to a solution of a Pd-Pd bound dimer under mild conditions. The resulting product decomposed slowly at room temperature, releasing CO and presumably reforming the metal-metal bond.

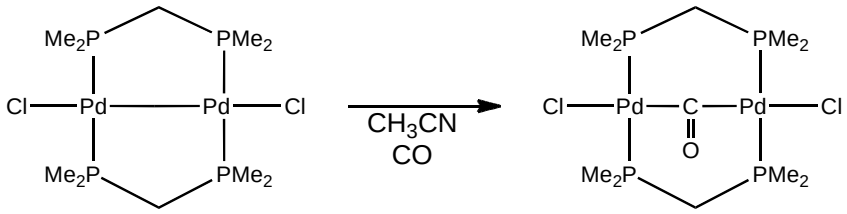

1.27

Scheme 1.7: Carbon monoxide insertion in an A-frame palladium phosphine complex.

Further investigations were made into rhodium(II) porphyrins, including $[Rh(OEP)]_2$, Rh(TMP) and Rh(TTiPP) (OEP = octaethylporphirinato, **1.28**; TMP = tetrakis-(2,4,6-trimethylphenyl)porphyrinato, **1.29**; TTiPP = tetrakis-(2,4,6-triisopropylphenyl)-porphyrinato, **1.30**; see **Figure 1.6** for a description of these rings) maintaining the interest in the late transition metal complexes.[61, 62] In each case, reversible carbonylation was observed by ^{1}H, $^{13}C\{^{1}H\}$ NMR and IR spectroscopic techniques. Mono-insertion into the metal-metal bond in **1.28** resulted from addition of 1 atm of CO, with 12 atm required for di-insertion (**Scheme 1.8**). The bulkier porphyrin moieties employed in **1.29** and **1.30** precluded dimerisation in the starting materials, resulting in a stable rhodium(II) radical that reacts with less than 1 atm of CO under mild conditions, allowing observation of the terminal mononuclear metal carbonyls. Although a second carbonylation was not possible with the sterically encumbered compound **1.30**, it was possible with **1.29** with an increase of CO pressure.

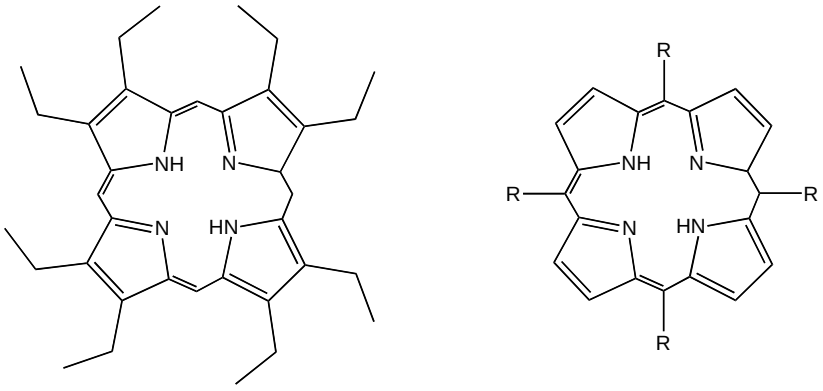

Figure 1.6: Left: octaethyl porphyrin. Right: R = 2,4,6-trimethylphenyl or 2,4,6-tri*iso*propylphenyl.

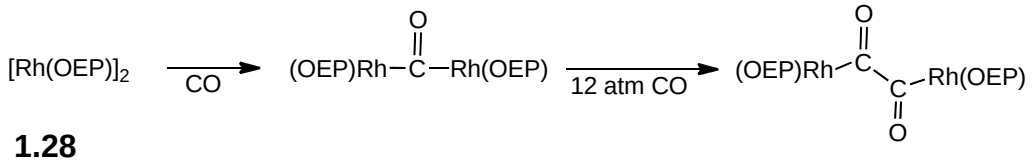

1.28

Scheme 1.8: Mono and dicarbonylation resulting in the first 1,2-ethanedionyl bridged metal complex from CO addition.

As with dinitrogen, some success has been seen towards CO activation *via* organometallic tantalum systems. This started with the isolation of a seven-coordinate tantalum diphosphine system $[TaH(CO)_2(dmpe)_2]$,[63] characterised *via* single crystal X-ray diffraction.[64] Although this example was synthesised by addition of carbon monoxide at 102 atm and 80 °C, a similar tantalum complex was synthesised under more mild conditions, with *in situ* sodium naphthalenide reduction of $[Ta(dmpe)_2Cl_4]$ under a stream of CO under ambient temperatures.[65]

Wood and Schrock looked further into the reactivity of tantalum complexes with respect to carbonylation by CO. They discovered that $[(Cp^{Me5})TaMe_4]$ reacts at room temperature with a stoichiometric amount of carbon monoxide, leading to CO insertion into the metal-carbon bond.[66] With two equivalents of CO a second insertion is possible, resulting in C-C coupling. The tantalum cyclopentadienyl phosphine polyhydrides $[(Cp^{Me5})TaL_2H_{4-n}C1_n]$ (n = 0, L = PMe_3, $PMe_2(C_6H_5)$, $P(OMe)_3$, and $Me_2PCH_2CH_2PMe_2$; n = 1, L = PMe_3) also showed significant reactivity towards double carbonylation under mild conditions in subsequent work by Mayer and Bercaw.[67]

Extensive isocyanide and carbonyl coupling studies led to the discovery that sodium amalgam reduction of a seven-coordinate tantalum dicarbonyl with subsequent trimethylsilyl chloride addition could result in a functionalised, coupled, CO moiety (**1.31**). A comparable result was obtained with the niobium analogue **1.32,** with different stoichiometries of silyl chlorides affording differently substituted products.[68] In the same report, the resulting silyl moieties in **1.31** and **1.32** (**Scheme 1.9**) could be removed under low pressures of H_2 (0.5 atm) to liberate the C_2 unit as a *cis*-disiloxyethylene.

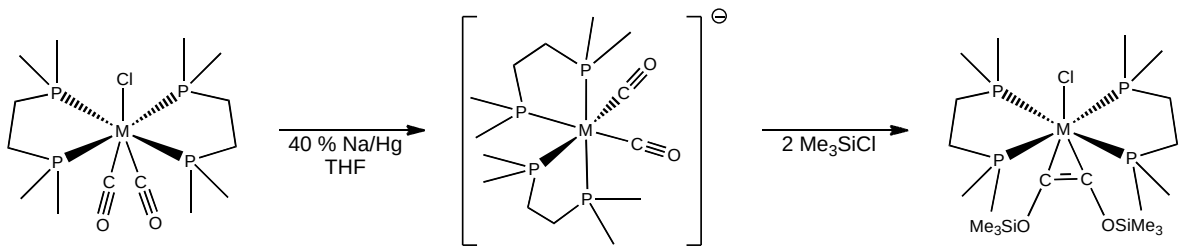

M = Ta (**1.31**)

M = Nb (**1.32**)

Scheme 1.9: C-C coupling and subsequent functionalisation by trimethylsilyl chloride. M = Ta, Nb.

1.4.2 Activation of CO by organometallic Group IV complexes

Metallocenes and derivatives with η^1-CO moieties have been characterised by X-ray diffraction studies for titanium, zirconium and hafnium[69-74] and some cationic derivatives have been observed spectroscopically.[75] Mono- and di-carbonyl compounds of the open metallocenes *bis*-2,3-dimethylpentadienyl zirconium and hafnium have also been fully described.[76]

The first zirconium acyl complexes produced *via* CO insertion into a metal-carbon bond proved that such insertions could occur cleanly in high yields, while judicious work-up facilitated extraction of a number of functionalised alkanes.[77] These zirconium complexes react more swiftly than the titanocene alkyls observed previously,[78] with reactivity seen at room temperature and under 1.4 atm of CO. This work was subsequently extended to consider the reactivity of hafnium alkyls, with similar results, both zirconium and hafnium examples illustrating reversible insertion of the carbon monoxide unit to be possible.[79, 80] Single crystal X-ray diffraction studies of the insertion product $[(Cp)_2Zr(COMe)Me]$ (**1.33**) (**Scheme 1.10**) implied the η^2-coordination of the CO moiety to the metal centre, rationalising the notably low IR stretching frequencies recorded for the acyl moieties.[79] The permethylated zirconocene

derivative reacts with a second equivalent of CO at 70 °C in a similar fashion, before rearranging to yield but-2-ene-2,3-diolate.[81]

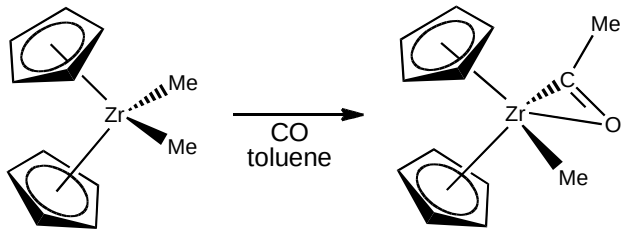

1.33

Scheme 1.10: CO insertion resulting in an acylated ligand.

Migratory insertion of CO into a zirconium-hydride bond, resulting in a formyl group, has also been described.[82-84] The zirconium formyl complex exists in the dimeric state, as suggested by ^{1}H NMR spectroscopy, with methanol isolated upon acid hydrolysis.[83] It has also been shown that CO will insert into bridging hydrides to form a μ_2-formyl under ambient conditions when COT and arlyoxide ligands are employed.[85]

Further in-depth studies[81, 86] into CO activation by zirconocene dihydride led to near quantitative isolation of enolate **1.34**, which results from C-C coupling of the labile CO moieties, as described in **Scheme 1.11**. Although not characterised by X-ray diffraction, spectroscopic analysis and analytical data support this formulation; with the IR $\upsilon_{C\text{-}O}$ stretch being particularly low. Similar reactivity was reported in subsequent articles considering the hafnium congener, although little further was elucidated about the mechanisms involved.[38]

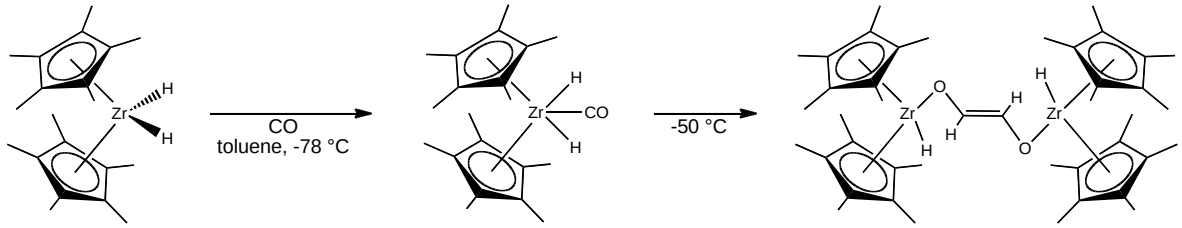

1.34

Scheme 1.11: Formation of enolate-bridged zirconocene dimer through C-C coupling.

Complete cleavage of CO at ambient pressures is also possible, as seen in its reaction with [$(Cp^{Me5})_2$M(2,3-dimethylbutadiene)Cl] (**1.35**, M = Zr; **1.36**, M = Hf) at ambient temperature to produce [$(Cp^{Me5})_2$M(Cl)O] (**1.37**) and 1,2-dimethyl-cyclopentadienyl, where the carbon supplied by the small molecule is incorporated into the newly formed Cp ring.[87] A similar mode of reactivity is seen in the case of $[(Me_3Si)_2N]_2ZrMe_2$ (**1.38**), when exposed to 1-2 atm of CO under ambient temperatures.[88] Here, a μ-oxo complex $\{[(Me_3Si)_2N]_2ZrMe\}_2O$ (**1.39**) results, as identified by X-ray diffraction studies, and is formed alongside the spectroscopically identified enolate complex $[(Me_3Si)_2N]_2(Me)Zr(OC(Me)=CMe_2]$ (**1.40**).

More comprehensively characterised C-C coupling products were described by Calderazzo *et al*. Here, two CO moietes bound to zirconocene or hafnocene were converted to an μ_2-CCO ligand and μ_3-oxo in a trinuclear metal complex in moderate to high yields, with analysis by single crystal X-ray diffraction and spectroscopic techniques.[89] When the dicarbonyl metallocene was heated to reflux with one equivalent of $[M(O_2CNR_2)_4]$, $[M_2Cp_2(\mu_2\text{-}CCO)(\mu_3\text{-}O)(O_2CNR_2)_6]$ (**1.41**, R = Et, M = Zr; **1.42**, R = ^{i}Pr, M = Zr; **1.43**, R = ^{i}Pr, M = Hf) resulted (**Figure 1.7**). The formation of the ketenylidene ligand was confirmed by ^{13}C labelling experiments and results from the reductive coupling of the metal-coordinated carbonyl groups, with electrons provided by the M-Cp cleavage. No reactivity was observed for the permethylated metallocenes, due perhaps to the greater strength of the M-Cp^{Me5} bonds.

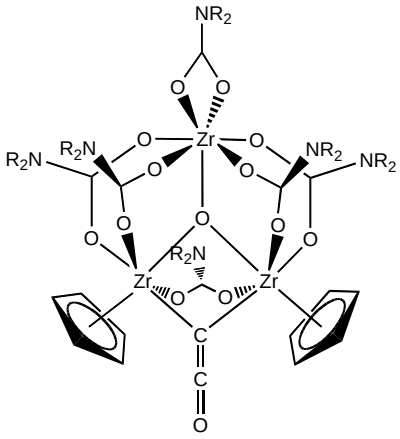

R = Et, **1.41**

R = ^{i}Pr, **1.42**

Figure 1.7: Carbon-carbon coupling to form μ_2-CCO and μ_3-O core.

Functionalisation of coordinated CO and subsequent regeneration of the active organometallic complex is highly sought after in the field of small molecule activation, representing a desirable step toward catalysis. Something akin to this has very recently been described by Chirik and coworkers.[52, 54] In this work, the reactivity of the side-on bridged N_2 tetramethylcyclpentadienyl hafnocene (**1.44**) is described alongside the dimethylsilyl-tethered congener (**1.45**). These compounds are produced *via in situ* reduction of hafnocene diiodide by sodium amalgam under an atmosphere of dinitrogen. Subsequent addition of 1-4 atm of CO to these compounds results in a metal-bound oxamimide compound **1.46** in good yield, with the molecular structure confirmed by single crystal X-ray diffractions studies. The bridging oxamimide moiety can be functionalised on both nitrogen atoms by alkyl halides and silanes (RX) affording **1.47** (**Scheme 1.12**), before cleavage with hydrochloric acid to afford the dichloro hafnocene and organic fragment. Yields have yet to be discussed by the authors, however if high, this could prove significant in the development of a catalytic system.

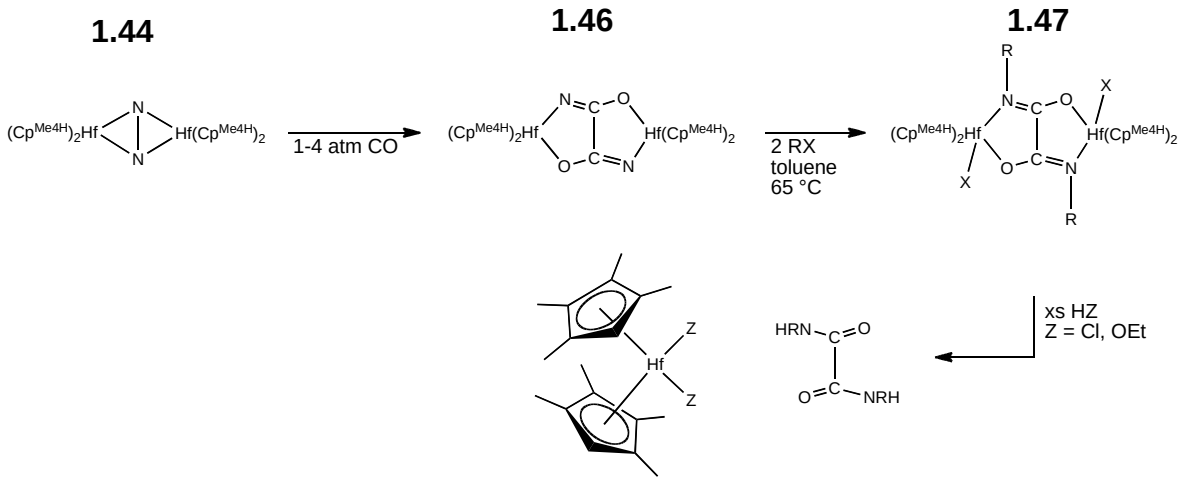

Scheme 1.12: Activation of N_2 and CO by **1.44** to synthesise a functionalised oxamimide (R = Et, X = Br and R = Me, X = I).

1.5 Activation of CO_2

Carbon dioxide contains longer and weaker bonds (1.16 Å and 805 kJ.mol^{-1}) than carbon monoxide and is thus easier to activate than the other small molecules so far discussed here. This small molecule displays similar reactivity to dinitrogen and carbon monoxide in that it can act as an innocent ligand or insert into existing metal-R bonds. However, coordinated carbon dioxide also disproportionates and thus leads to more unusual products, containing a mixture of carbonate and carbonyl moieties.

1.5.1 Activation of CO_2 by organometallic transition metal complexes

Previously considered to be an inert gas, the first true example of carbon dioxide coordinated to an organometallic complex of a transition metal was reported by Pu *et al.* in 1968, shortly after that group's discovery of the dinitrogen complex $H(N_2)Co[P(C_6H_5)_3]_3$ (**1.48**).[12, 90] Carbon dioxide was bubbled through a solution of **1.48**, yielding a metal-bound formate moiety $HCOOCo[P(C_6H_5)_3]_3$ as confirmed by IR spectroscopy and combustion analysis. Further reaction with methyl bromide led to

isolation of methyl formate. Subsequent publications by other groups identified similar formate synthesis *via* CO_2 insertion into a metal-hydride bond with concomitant loss of an η^1-bound dinitrogen ligand in the cases of $[Ru(N_2)H_2(PPh_3)_3]$[91] and $[Fe(N_2)H_2(PEtPh_2)_3]$.[92]

A large number of products generated from the activation of carbon dioxide possess a bound CO_2 moiety behaving as a ligand in its own right rather than undergoing a chemical transformation. An early report detailed the infrared spectroscopic identification of CO_2 ligating to iridium and rhodium, yielding $[(CO_2)M(OH)(CO)(PPh_3)_2]$ (**1.49**, M = Ir, **1.50**, M = Rh).[93] In each case, coordination was reversible, with **1.49** more unstable to vacuum than **1.50**, with both complexes affording a carbonate complex on addition of ethanol.

A subsequent report by Chatt *et al.* identified another example of carbon dioxide acting as a ligand.[94] Only poor quality structural data could be obtained for this product, presumably due to the inherent instability of this particular complex, which ultimately leads to a spontaneous change to the CO-ligated, carbonato bridged dimer **1.51** (**Scheme 1.13**) *via* presumed disproportionation. Shortly after this report, a mononuclear iridium complex incorporating a C_2O_4 unit (**1.52**) was described (**Scheme 1.14**).[95] Exhibiting the unusual bonding mode where the two carbon atoms are bridged by a single oxygen atom, it has been postulated that **1.52** represents an intermediary complex before disproportionation of the bound CO_2 units. Here, the bridging oxygen atom has distinctly elongated bonds to both carbon atoms of 1.39(2) and 1.36(1) Å, showing that this disproportionation is effectively already taking place. Thermal decomposition at 150 °C results in a carbonyl compound, as detected by IR spectroscopy.

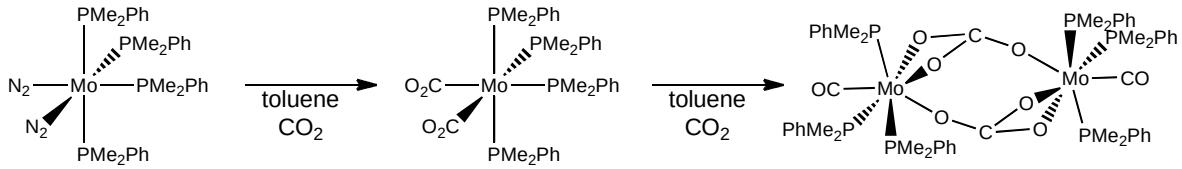

1.51

Scheme 1.13: Ligation of CO_2 before disproportionation, with a bridging CO_3 moiety and CO bound directly to metal centres.

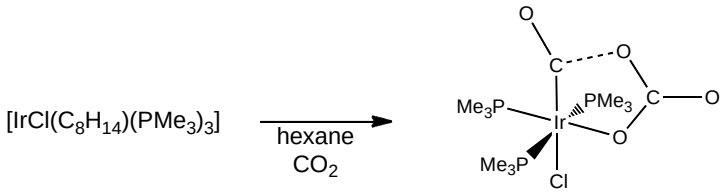

1.52

Scheme 1.14: Unusual coordination mode of CO_2 to iridium compound. This could represent a step in the disproportion of bound CO_2 to carbonate and carbonyl.

Following this example, other instances of ligated CO_2 were published in quick succession[95-97] including $[Ni(CO_2)(PCy_3)_2]$ (**1.53**), isolated following facile dinitrogen displacement from $[\{Ni(PCy_3)_2\}_2N_2]$.[98] Characterised by single crystal X-ray diffraction, the CO_2 moiety was observed to be η^2-bound to the metal centre. The C-O bond was longer than that seen in free carbon dioxide, measuring 1.22 Å, with the OCO moiety significantly bent to 133°. On heating, this product largely decomposed to the starting material and a small quantity of a nickel carbonyl carbonate.

Lappert and coworkers synthesised and fully characterised a niobocene complex that displayed reactivity towards carbon dioxide, the first example of an early d-block compound binding CO_2 (**1.54**, **Figure 1.8)**.[99] Again, an η^2 bonding mode is observed in the molecular structure, with a similar bending of the CO_2 moiety to 132.4°. Lengthened C-O bond distances (compared to the free molecule: $d_{C=O}$ = 1.16 Å) of 1.283(8) and 1.216(8) Å were observed, with the former corresponding to the atoms bound to the central metal. Consistent with previous reports of carbon dioxide binding

to a metal centre, small amounts of carbonato and carbonyl species were also observed as the bound CO_2 moiety undergoes disproportionation. Interestingly, despite the presence of an alkyl group bound to the niobium atom, no insertion product was observed.

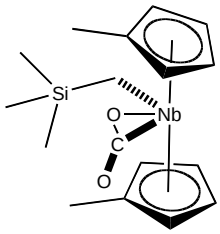

1.54

Figure 1.8: Binding of CO_2 to an alkyl niobocene.

Molybdenum has proven popular in carbon dioxide ligation following Chatt's earlier report, with structurally characterised examples of η^2-C,O in the cases of $[Mo(CO_2)_2(PMe_3)_3(CN^iPr)]$ (**1.55**) and $[Mo(CO_2)_2(PMe_3)_3(CNCH_2Ph)]$ (**1.56**), synthesised from the molybdenum dinitrogen complex.[100, 101] In each case, two CO_2 moieties are bound *trans*, with OCO angles between 128(2) to 134(1)°, with the smaller angles noted for the bulkier phenyl derivative. Lengthened bond distances between the carbon and oxygen atoms bound to the metal are also noted (1.20(2) to 1.28(3) Å). These molecules show moderate thermal stability up to 60 °C, indicating that the Mo-C and Mo-O bonds are strong. Gambarotta *et al.* found that the carbene-like molybdenocene $[Mo(Cp)_2(PhCCPh)]$ could bind CO_2, *via* displacement of weakly bound diphenylacetylene in toluene at room temperature[102] resulting in another example of η^2-bound CO_2. Once again, the C-O bond distance between the coordinating atoms is elongated with respect to the terminal C-O linkage, measuring 1.288(14) and 1.201(14) Å respectively.

Carbon dioxide insertion reactions do not only occur with metal hydride bonds, they are also possible into metal-nitrogen and metal-oxygen bonds under equally mild conditions. Single crystal X-ray diffraction studies have shown the product from three CO_2 molecules mono-inserting into three M-N bonds of the tungsten compound

$[W(NMe_2)_6]$ (**1.57**).[103] Multiple insertions into one M-N bond were not observed and the carbon dioxide insertions were seen to occur in a stepwise fashion, on the same face of **1.57** as confirmed by ^{1}H NMR spectroscopy. Insertion into a M-O bond was shown later by the same group when the reactivity of the dimolybdenum compound $[Mo_2(OR)_6]$ (**1.58**, R = $SiMe_3$; **1.59**, R = ^{t}Bu; **1.60**, R = $CHMe_2$, **1.61**, R = $CH_2{}^t$Bu) was probed,[104] with resultant generation of dicarboxylated complexes that are stable under ambient temperatures, with heating to 90 °C required to decarboxylate and decompose the material. The insertion reaction occurred at a greater rate for **1.61**, with single crystal X-ray diffraction studies possible for R = ^{t}Bu (**1.62**), shown in **Scheme 1.15**. Here, two bridging carboxylate moieties are generated following insertion of two CO_2 molecules into two Mo-O bonds, before formation of further Mo-O bonds thus linking the two metal centres. The O-C-O angle in this example is significantly more acute than seen in end-on bound CO_2 ligands described previously, measuring 122.4(8) and 124.5(9)°. The C-O bond distances are also much longer (1.27(1) to 1.29(1) Å) as the bond order has significantly decreased from the original C-O double bond in the free gas towards that of a single bond.

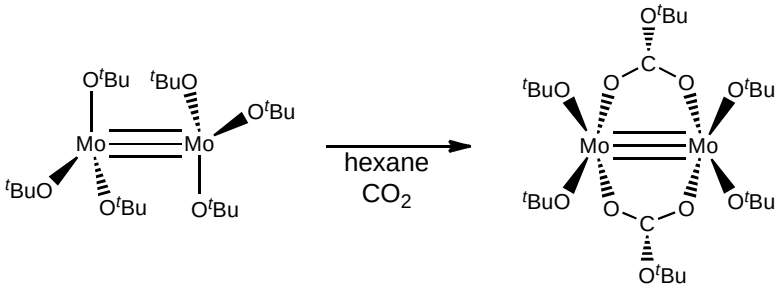

1.59 **1.62**

Scheme 1.15: CO_2 insertion into M-O bond, resulting in a bridging dicarboxylate dinuclear complex.

In more recent publications, research has begun focussing on heterometallic systems, with the idea that two metals with widely differing electron donor and acceptor properties would facilitate binding and activation of CO_2. The first account of a fully characterised heterometallic compound displaying reactivity towards CO_2 described the trimetallic dirhodium monoosmium μ_3-η^3 CO_2 complex

[{(COD)Rh}$_2$OsH$_2$(CO$_2$)(PMe$_2$Ph)$_3$] **1.63** (**Figure 1.9**), with data from single crystal X-ray diffractions analysis.[105] This is produced *via* addition of 1.5 atm of CO_2 to a THF solution of the bimetallic compound [(COD)RhOsH$_3$(PMe$_2$Ph)$_3$] (**1.64**), resulting in an amount of a hydrolysed osmium compound and osmium carbonyl species in addition to **1.63**, suggesting that disproportionation has occurred during the course of the reaction. Compound **1.63** is isolated as the major product and shows the CO_2 moiety bound to each of the three metal atoms, with C-O bond distances of 1.300(21) and 1.309(22) Å and an acute O-C-O angle of 116.3(16)°: significantly different from the free gaseous molecule. An unusual tetrametallic complex results from addition of $ZnBr_2$, with the zinc atom bonding to both oxygen atoms of the CO_2 moiety, though no further lengthening of the C-O bonds, or change in O-C-O angle are observed. Further reactions of the trimetallic complex **1.63** to form C-H bonds or cleave C-O bonds proved impossible, most likely due to the steric shielding of the metallic core by the phosphine and alkyl ligands employed.

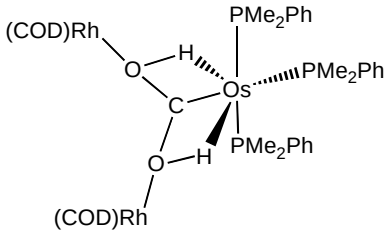

1.63

Figure 1.9: Trimetallic carbon dioxide complex.

Bergman and coworkers discovered that the heterobimetallic compound [Cp$_2$Zr(μ-N^{t}Bu)IrCp^{Me5}] (**1.65**) undergoes facile addition of CO_2, with the carbon and one oxygen adding across the metal-metal bond yielding [Cp$_2$Zr(μ-N^{t}Bu)(μ-OC(O))IrCp^{Me5}] (**1.66**) in 67 % yield, which was fully characterised by IR and NMR spectroscopies and single crystal X-ray diffraction.[106] If, however, carbon dioxide is added to the related dihydride complex [(H)Cp$_2$Zr(μ-N^{t}Bu)(μ-H)IrCp^{Me5}] (**1.67**), terminal Zr-H insertion leads to formation of the bimetallic formato complex **1.68** (**Scheme 1.16**), in a 75 % overall yield, with stoichiometric conversion into formic acid also reported, although no details are given of the method employed. Addition of phenyllithium to **1.68** led to

generation of lithium formate and regeneration of **1.65** in low to moderate yields, leading the authors to propose that this process could be made catalytic.

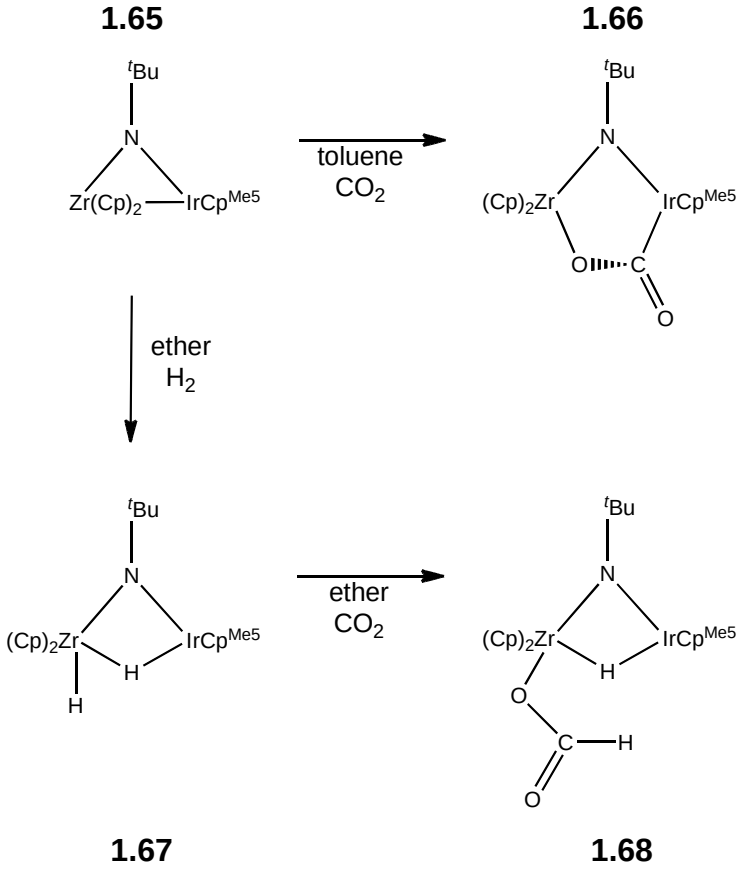

Scheme 1.16: Reactivity of the early-late heterobimetallic zirconium-iridium complex towards CO_2.

So far, few publications have discussed the functionalisation of carbon dioxide bound to organometallic transition metal complexes. Creating C-C bonds is vital if fuel feedstocks are to be synthesised *via* metal catalysis of the small molecule. However, the tendency of bound carbon dioxide to disproportionate to afford the carbonato moiety[107] makes this research even more difficult, despite the relative ease with which carbon dioxide can be attached as a ligand under mild conditions.

1.5.2 Activation of CO_2 by organometallic Group IV complexes

Insertions of carbon dioxide into Group IV M-C and M-H bonds are less well defined, with reports of CO_2 activation by hafnium being particularly rare. Early reports of insertion have demonstrated success in the employment of titanocene alkyls, such as the example described by Kolomnikov *et al*. Here, CO_2 inserts into one M-C bond of diphenyltitanocene with concomitant loss of benzene and formation of the cyclic compound **1.69** (**Scheme 1.17**).[108] This reaction occurred between 80 – 90 °C under ambient pressures to produce **1.69** as a crystalline material in 35 % yield. The C-O and C=O bond distances are as expected for the singly and doubly bonded atoms,[109] measuring 1.35(3) and 1.24(3) Å, with the O-C-O angle 119(3)° nearing that typical for an sp^2 carbon.

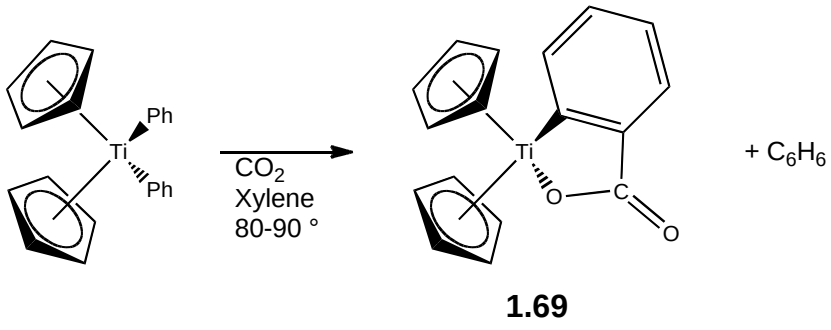

1.69

Scheme 1.17: CO_2 insertion into an Ti-C bond.

Other reported examples rely largely on IR and NMR spectroscopic data for product identification, as in the cases of chlorozirconocene methoxide (**1.70**) and μ-oxo dizirconocene chloride (**1.71**) (**Figure 1.10**), which are synthesised in the same reaction *via* addition of excess CO_2 to a THF solution of hydridochlorozirconocene.[83, 110] Though dialkyl zirconocenes (dimethyl, diphenyl and dibenzyl) failed to show any reactivity towards carbon dioxide under similarly mild conditions, this could be effected for dimethyl zirconocene at 80 °C and 50 atm of CO_2.[111] The product from this reaction was ill-defined, but believed to contain a symmetrically bound acetato group.

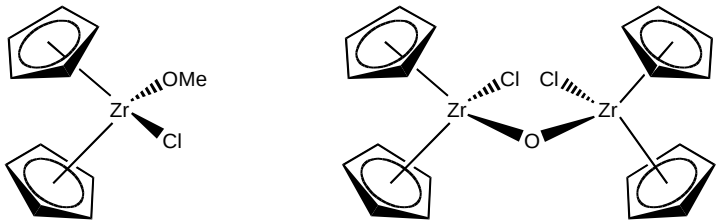

1.70 **1.71**

Figure 1.10: Representation products resulting from CO_2 addition.

Cohen and Bercaw documented carbon dioxide insertion into decamethyl titanocene ethene, resulting in the carbometallocycle **1.72**, (**Scheme 1.18)**[112] with IR and NMR spectroscopies suggesting an ester-type linkage. Titanocene but-2-ene displayed different reactivity (**Scheme 1.19**), with CO_2 inserting linearly to yield **1.73**, which possesses a carboxylate moiety which can be hydrolysed to produce 2-methylbutanoic acid.[113]

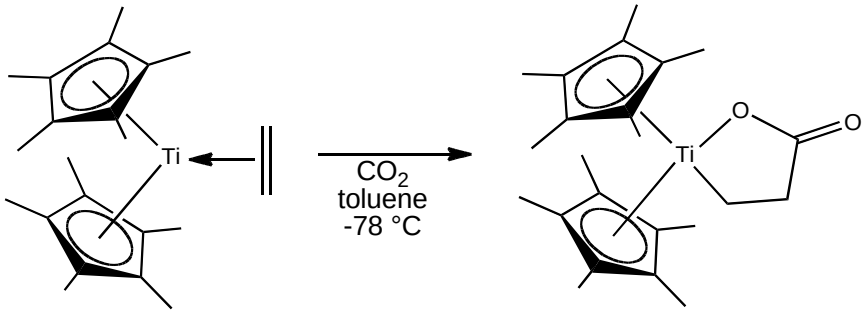

1.72

Scheme 1.18: Cyclometallation of ethene induced by CO_2 addition.

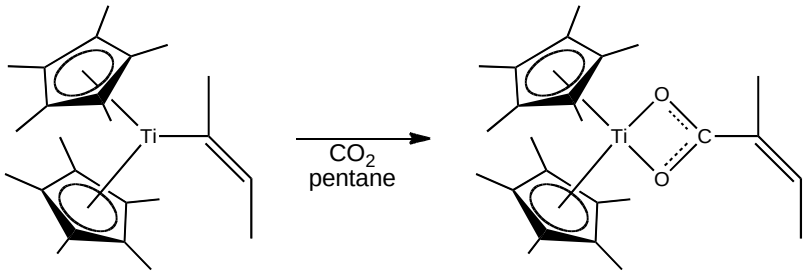

1.73

Scheme 1.19: Insertion of CO_2 into Ti-C bond.

As already mentioned, investigations have taken place into carbon dioxide functionalisation of Group IV-coordinated dinitrogen compounds, largely completed by Chirik and coworkers in the past five years. Considerable detail is available regarding the functionalisation of the nitrogen atoms in the tetramethylcyclopenatadienyl hafnocene complex **1.43** (**Scheme 1.20)**. Here, two equivalents of CO_2 are added to a toluene solution of **1.43** to yield the double insertion product **1.74**, in moderate yield.[55] The identity of **1.74** was confirmed by single crystal X-ray diffraction analysis and IR, ^{1}H NMR and $^{13}C\{^{1}H\}$ NMR spectroscopy. The carbonyl moieties possess bond lengths of 1.208(8) and 1.228(8) Å, consistent with localised carbon-oxygen double bonds, while the neighbouring C-O and N-N bond distances are suggestive of single bonds, measuring 1.323(7), 1.303(8) and 1.471(7) Å respectively. Stepwise addition of TMSI to **1.74** results in extrusion of the organic core $(Me_3Si)_2N_2(CO_2SiMe_3)_2$ and hafnocene diiodide in good yields. Though not yet realised, the regeneration of $[(Cp^{Me4H})_2HfI_2]$ may afford scope for catalytic cycling *via* further reduction under N_2.

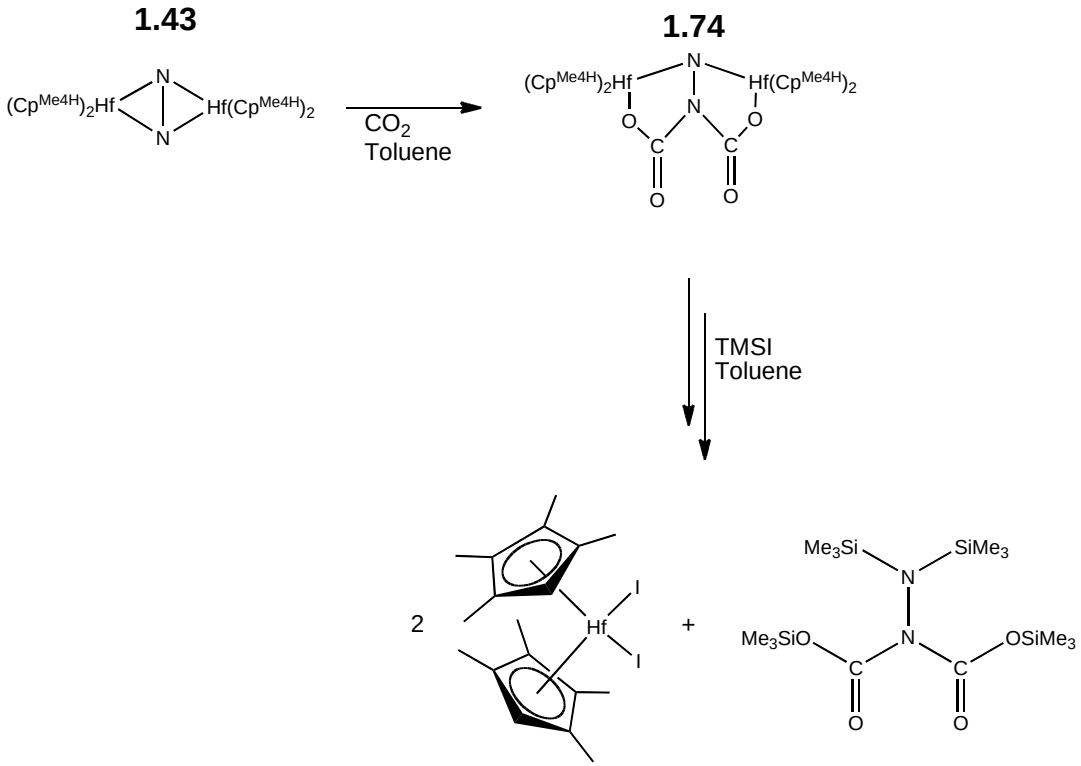

Scheme 1.20: Functionalisation of hafnocene dinitrogen compound by carbon dioxide.

Addition of CO_2 to the zirconocene dinitrogen complex $[Me_2Si(\eta^5\text{-}C_5Me_4)(\eta^5\text{-}C_5H_3\text{-}3\text{-}^tBu)Zr]_2(\mu^2,\eta^2,\eta^2\text{-}N_2)$ (**1.75**) resulted in one carbon dioxide molecule adding to each nitrogen atom, generating **1.76** in high yields, as illustrated in **Scheme 1.21**, in contrast to **1.74**, in which both CO_2 molecules bonding to the same nitrogen atom (*vide supra*).[114] The resulting substituted hydrazine core in **1.76** can be cleaved with TMSI, or alternatively *via* addition of methyl triflate to yield **1.77** before subsequent TMSI addition. In each case, regeneration of the zirconocene diiodide starting material was observed alongside isolation of a highly functionalized hydrazine core, again offering promise of future catalytic behaviour.

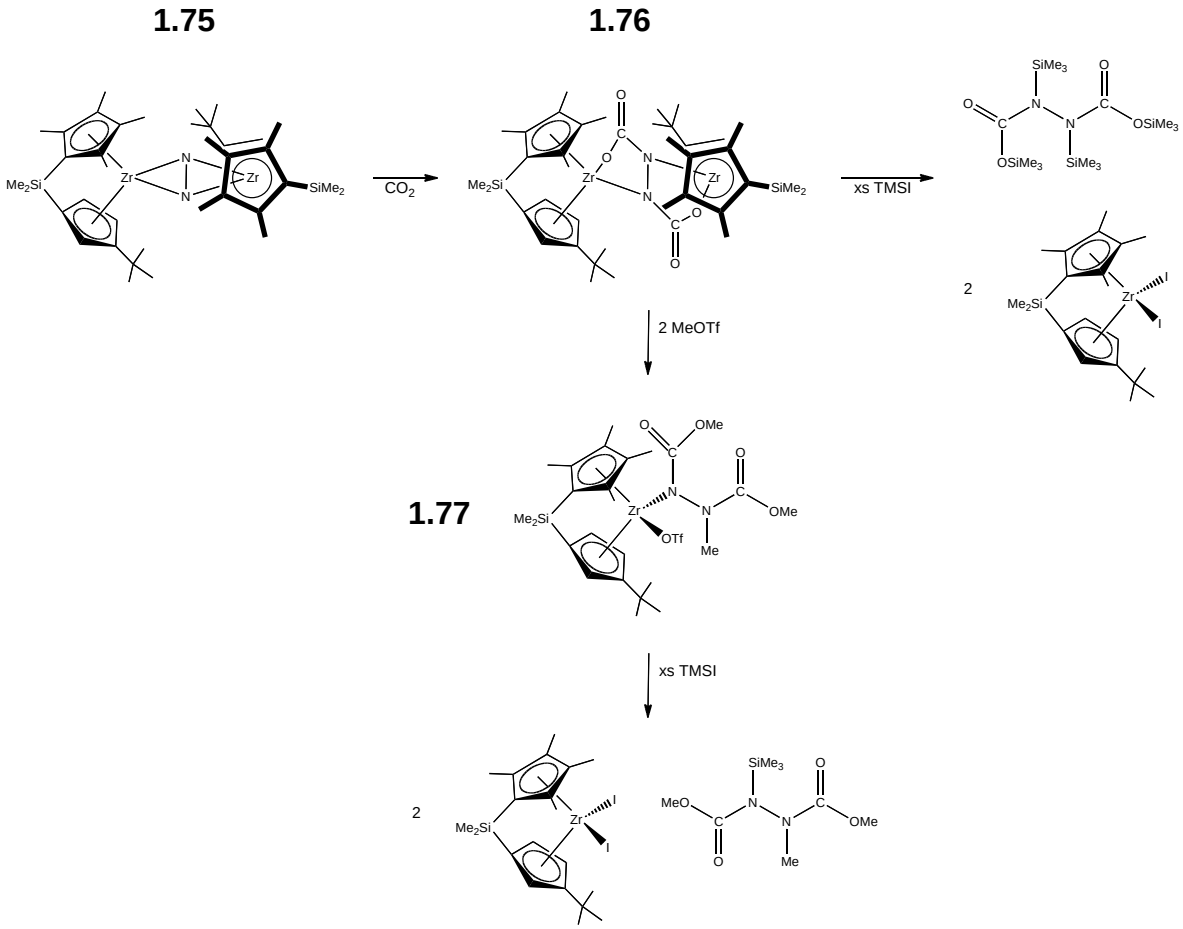

Scheme 1.21: Functionalisation of N_2 moiety in a zirconocene derivative with CO_2.

1.6 Reactivity of divalent lanthanides towards small molecules

Following advances in recent years, this area has been extensively reviewed.[115, 116] This section will thus provide a brief overview of the reactivity of divalent lanthanide organometallic complexes towards carbon monoxide, carbon dioxide and dinitrogen.

Due to their instability, divalent organo-lanthanide compounds were considered inaccessible for many years. However, studies by Evans *et al.* illustrated that dicyclopentadienyl lanthanide complexes could indeed be isolated, and that they would react with small molecules. The initial communication to this effect in 1988[117] detailed the synthesis of the first dinitrogen complex of an f-element, the samarocene derivative **1.78** (**Figure 1.11**), obtained by slow crystallisation of decamethyl samarocene (**1.79**) under a blanket of dinitrogen. The observed binding of dinitrogen proved to be

reversible upon dissolution in toluene and consistent with this, the N-N bond distance is short (1.088(12) Å) and similar to that in free N_2, suggesting negligible activation.

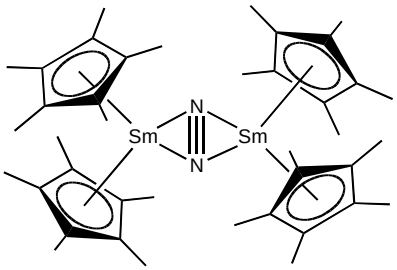

1.78

Figure 1.11: Nitrogen activation *via* divalent permethylated samarocene.

Similar chemistry has been seen with substituted thulium analogues, resulting in $[(Cp^R)_2Tm(N_2)Tm(Cp^R)_2]$ (R = Me_5, **1.80**; R = TMS_2H_3, **1.81**; R = $TMSH_4$, **1.82**).[118, 119] Although the structural data for **1.80** proved poor and precluded detailed analysis of bond lengths, **1.81** and **1.82** showed a distinct lengthening of the N-N distance (1.259(4) and 1.236(8) Å) compared to the samarium analogue **1.78**.

In the following years, there were a large number of publications by this group, debating further examples of N_2 activation by complexes of lanthanum, cerium, praseodymium, neodymium, gandolinium, terbium, dysprosium, holmium, erbium, thulium and lutetium.[120-125] Among these examples, the range of ligands employed was expanded to include Cp^{Me4H}, $N(TMS)_2$ and OAr (Ar = $C_6H_3{}^tBu_2$-2,6). The resultant N-N bond distances ranging from 1.233(5) Å for $[(Cp^{Me5})_2(THF)La]_2(N_2)$ (**1.83**) to 1.305(6) Å for $[(N(TMS)_2)_2(THF)Dy]_2(N_2)$ (**1.84**) and corresponding to an $[N_2]^{2-}$ imido core.

Despite the impressive reactivity of these divalent lanthanides toward N_2, few examples exist of carbon monoxide or carbon dioxide activation *via* similar systems. Evans and coworkers provided the first example of reactivity towards CO, with generation of the samarocene ketene carboxylate compound $[(Cp^{Me5})_4Sm_2(O_2CCCO)(THF)]$ (**1.85, Figure 1.12**) when **1.79** was exposed to six atmospheres of CO.[126] This result was

subsequently repeated with permethyl lanthanocene to produce a structurally similar ketene carboxylate.[127]

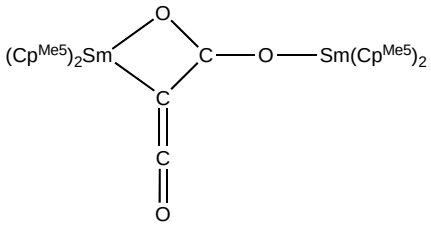

1.85

Figure 1.12: Disamarocene ketene carboxylate.

Samarocene **1.78** has proven versatile toward CO_2 activation, facilitating C-C coupling of two carbon dioxide units to afford the bridging oxalate compound $[(Cp^{Me5})_2Sm]_2(\mu\text{-}\eta^2\text{:}\eta^2\text{-}O_2CCO_2)$ (**1.86**), in high yields upon treatment with one atmosphere of CO_2 at ambient temperature.[128] Unfortunately poor quality diffraction data precluded discussion of the bond lengths and angles present in the organic core. Later work by Gardiner and coworkers[129] with a samarium(II) porphyrinogen complex led to disproportionation of carbon dioxide and formation of the bridging carbonate disamarium compound **1.87** (**Figure 1.13**) in moderate yield, thus identifying the first example of reductive disproportionation of CO_2 by a lanthanide complex.

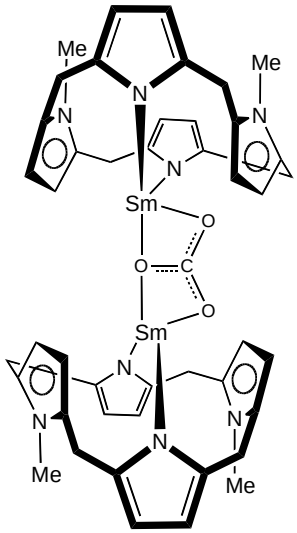

1.86

Figure 1.13: The first example of reductive disproportionation by an f-block element complex.

1.7 Reactivity of organometallic thorium complexes towards small molecules

There are few examples of small molecule activation mediated by organometallic thorium complexes. Early studies into carbon monoxide activation involved insertion of CO into a thorium-alkyl or thorium-amide bond, to afford η^2-formyls, often followed by further coupling (**Scheme 1.22**).[130-133] These complexes are generated under mild conditions and were isolable as crystalline materials, with the thorocene alkyl starting materials showing reactivity similar to that observed with the zirconocene analogues described earlier. Similar studies continued investigations into the CO chemistry of permethylated thoracene alkyls, with double insertion resulting in the first example of a metalloxy ketene complex **1.88** (**Figure 1.14**) when the starting material is subjected to over two atmospheres of carbon dioxide.

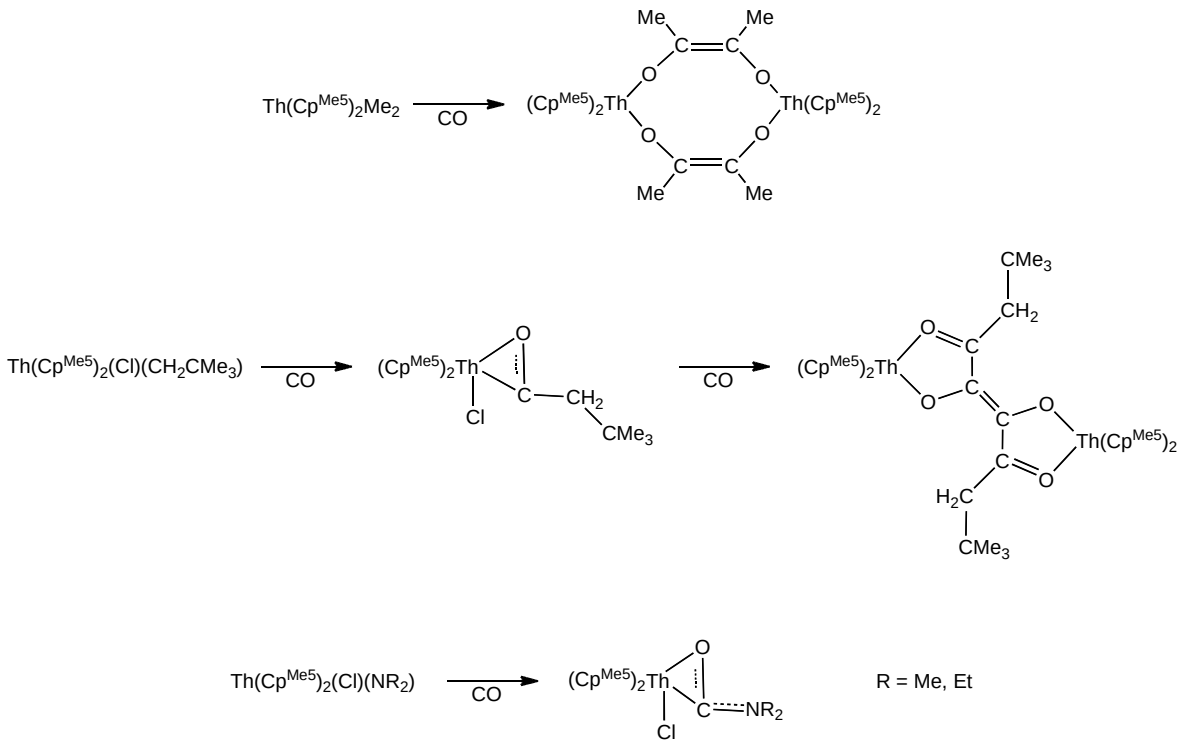

Scheme 1.22: Insertion of CO into Th-C and Th-N bonds.

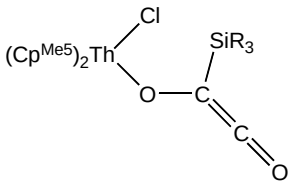

1.88

Figure 1.14: Double CO insertion into Th-Si bond leading to a metalloxy ketene (R = $SiMe_3$, $^tBuPh_2$).

A further example of CO insertion and activation considered the reactivity of the dialkylphosphide complex $Th[P(CH_2CH_2PMe_2)_2]_4$ (**1.89**) with CO to afford **1.90** (**Figure 1.15**).[134] However, no details are provided by the author as to the conditions required for this reactivity.

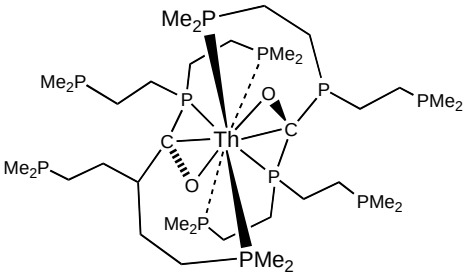

1.90

Figure 1.15: Thorium phosphide complex resulting from double CO insertion.

Thorium alkyls show reactivity toward carbon dioxide, which inserts into the Th-R bonds (R = Me, ^{i}Pr) of [$(Cp^{Me5})_3$ThR] (**1.91**)[135] and [$(Cp^{Me5})_2$Th(R)Me] (**1.92**)[136] to afford mono- or di-carboxylates, although these have yet to be structurally characterised. Similar results were obtained regarding activation of CO_2 by [$(Ind^{Me7})_2ThR_2$] (R = Me, **1.93**; R = NMe_2, **1.94**), with the resulting carboxylate confirmed by IR spectroscopic data. [137]

There is little published research concerning dinitrogen activation by thorium complexes, the only current example documenting complete N_2 cleavage and hydrogen abstraction by a zero-valent thorium synthon (**Scheme 1.23**). Reaction of the thorium starting material (**1.95**) with one equivalent of potassium naphthalenide, in DME, under N_2 yielded the coordinated amide **1.96**, isolated in moderate yields as X-ray quality crystals. The source of hydrogen has yet to be established.

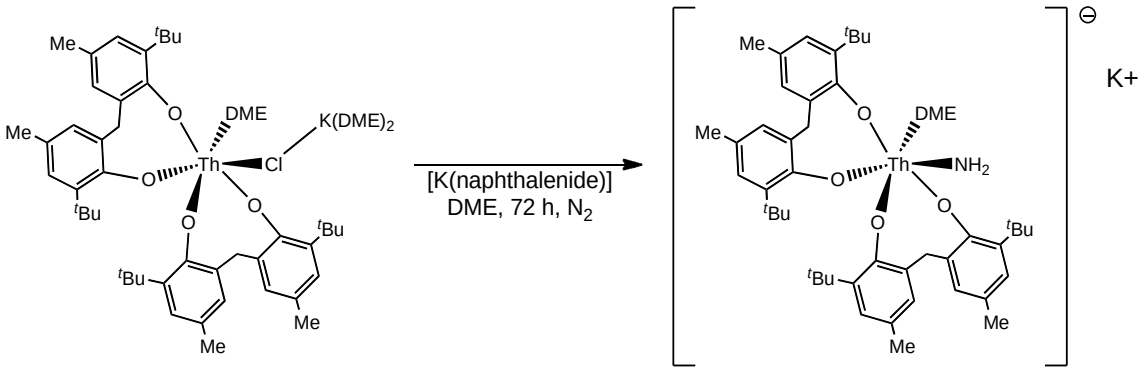

1.95 **1.96**

Scheme 1.23: Dinitrogen cleavage by a organometallic thorium compound under reducing conditions.

1.8 Reactivity of organometallic uranium complexes towards small molecules

Investigations into the reactivity of uranium complexes towards small molecules has been aided by a wider range of accessible oxidation states. The first uranium complex to activate dinitrogen was synthesised by Roussel and Scott in 1998 in the form of the U(III) complex [U{N($CH_2CH_2NSi^tBuMe_2$)$_3$}] (**1.97**).[138] Compound **1.97** was found to reversibly bind dinitrogen, in a side-on bridging mode between two uranium atoms, with an N-N distance of 1.109(7) Å, showing little activation of the triple bond from the free N_2 molecule. This reaction occurred at ambient temperature, under one atmosphere of dinitrogen, and afforded **1.97** in good yields.[139] Other examples of reversibly-coordinated dinitrogen have been published by Evans[140] with end-on bound N_2 in [U(Cp^{Me5})$_3$(N_2)] (**1.98**), and Cloke with side-on bridging N_2 in [U_2(μ^2-N_2)(Cp^{Me5})$_2$(Pent{1,4-Si^iPr_3}$_2$)$_2$] (**1.99**).[141, 142] Within **1.98**, the N-N bond length is not significantly lengthened from that observed in free N_2 (1.120(14) Å), whilst for **1.99** it is more akin to a N-N double bond (1.232(10) Å). However, in both cases, the dinitrogen moiety is easily removed under reduced pressure to yield the U(III) starting material. Nitrogen can also be reduced by a bimetallic uranium/molybdenum compound[143] in a similar manner as observed with the molybdenum amindo compound described earlier in this chapter.

Similar results have been communicated by Arnold and coworkers,[144] with addition of dinitrogen (1 atm) to uranium(III) aryloxide compounds. This addition affords the side-on bridged dimeric complexes $[U(OAr)_3]_2(N_2)$ (Ar = O-2,6-^{t}Bu$_2$C$_6$H$_3$, **1.100**; Ar = O-2,4,6-^{t}Bu$_3$C$_6$H$_2$, **1.101**), with N-N bond lengths consistent with a double bond (1.189(19) Å for **1.100**, 1.236(5) Å for **1.101**). In neither case is N_2 lost under reduced pressure, although it can be displaced on addition of carbon monoxide to yield the bridging ynediolate complexes in good yields (**Scheme 1.24**). The similar ynediolate complex, $[U\{N(SiMe_3)_2\}_3]_2(\mu\text{-}\eta^1\text{:}\eta^1\text{-}C_2O_2)$, can be formed in high yields following exposure of $[U\{N(SiMe_3)_2\}_3]$ to CO (1 atm) at ambient temperatures.[145]

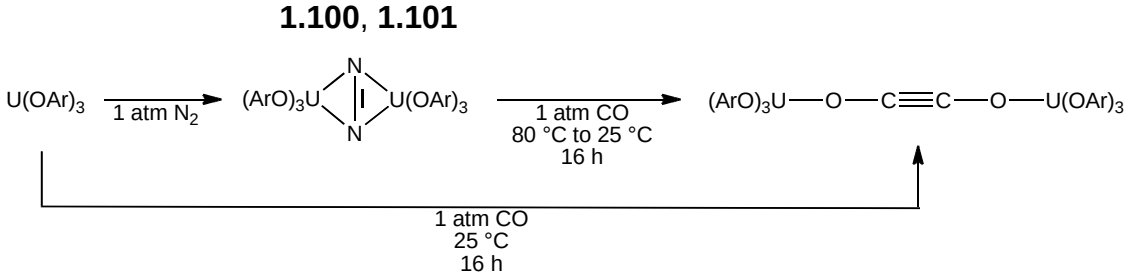

Scheme 1.24: Ynediolate formation *via* uranium aryl oxide dinitrogen complex

Activation of carbon monoxide by organometallic uranium complexes largely involved the coordination of the carbonyl ligand to the metal centre, or its insertion into a U-R bond,[146-149] with the first example of CO acting as a bridging ligand between two uranium atoms reported by Meyer.[150] More unusual reactivity was observed by Cloke and coworkers, with the observation that CO can be reductively coupled by the mixed-ring uranium(III) compound $[U(COT\{1,4\text{-}Si^iPr_3\}_2(Cp^{Me4R})]$.[151, 152] The products of this reaction can be tuned by varying the sterics and electronics of the cyclopentadienyl ring (R = Me, **1.102**; R = H, **1.103**) to selectively generate the deltate (**1.104**) and squarate (**1.105**) members of the oxocarbon dianion series (**Figure 1.16**), when an excess of gas is added under extremely mild conditions (-78 °C, < 1 atm CO, **Scheme 1.25**). In the squarate moiety, the C-C bond lengths are as expected for an aromatic moiety, measuring 1.449(10) to 1.460(11) Å; the less symmetrical deltate unit contains slightly shorter C-C bond lengths of 1.377(6) to 1.436(7) Å. In both instances, the C-O distances are as expected for a carbonyl group with double or partially double-bonded character.

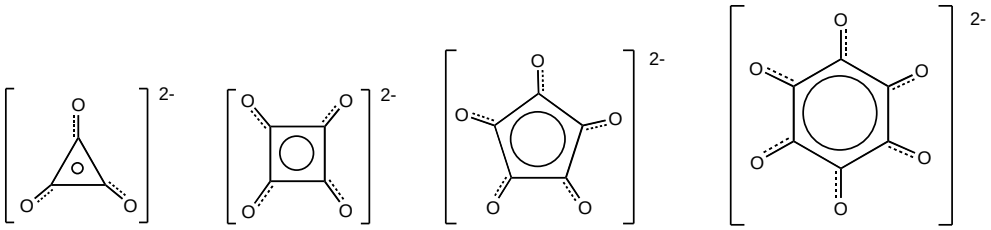

Figure 1.16: The oxocarbon dianion series.

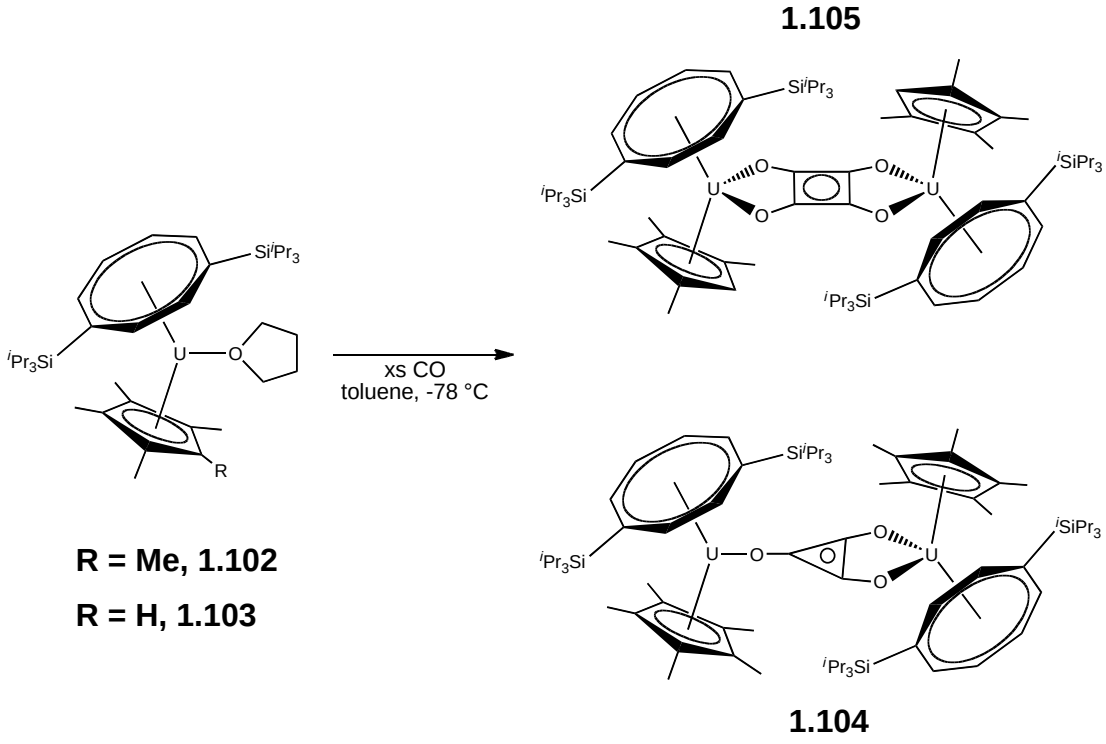

Scheme 1.25: Coupling of carbon monoxide via U(III) organometallic complexes.

Interestingly, if CO is added to **1.102** in a 1:1 ratio, the ynediolate complex **1.105** (**Figure 1.17)** results.[153] This compound contains a short C-C bond of 1.177(12) Å, consistent with a triply-bonded moiety, which appears stable towards further carbon monoxide addition, with no formation of bridging deltate being observed. Further studies noted that this product was also stable towards dihydrogen. However, if a mixture of one equivalent of CO and two equivalents of H_2 is added simultaneously to **1.102**, the sole product is [U(COT{1,4-Si^{i}Pr$_3$}$_2$(Cp^{Me5})(OMe)].[154] It was found that

treatment of the uranium methoxide complex with hydrochloric or triflic acid would not result in methanol, although addition of trimethylsilyltriflate liberated uranium(IV) triflate and Me_3SiOMe. The metal triflate can be reduced back to **1.102** (> 60%) upon addition of potassium amalgam, over a period of four hours.

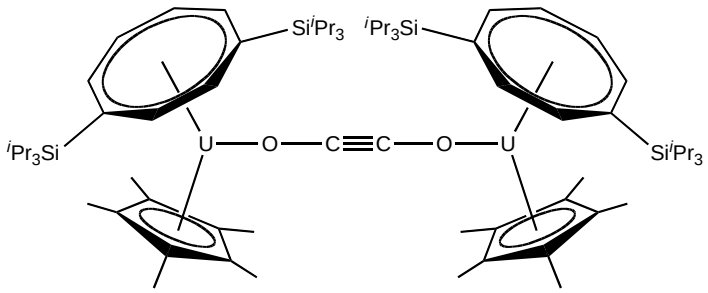

1.106

Figure 1.17: Bridging ynediolate complex resulting from 1:1 addition of carbon monoxide to **1.102**.

Both **1.102** and **1.103** react with excess carbon dioxide under similarly mild conditions, affording moderate yields of the μ-carbonate and μ-oxo complexes, resulting from disproportionation in a similar manner to those discussed in **Sections 1.5.1** and **1.5.2**.[155] A small amount of **1.104** or **1.105** was also observed, due to generation of carbon monoxide during the course of the reaction, making this was the first example of a member of the oxocarbon dianion family being synthesised from carbon dioxide.

Although reactions between **1.102** and **1.103** and carbon dioxide fail to produce significant products containing new C-C bonds, it is the ability of these uranium compounds to couple carbon atoms from the CO unit that is particularly significant. These deltate and squarate moieties could be cleaved from the product, and further functionalised for use in fuel or synthetic chemistry.

However, due to the economic and environmental costs of employing uranium, it was decided that this successful ligand system be applied to a chemically similar metal that was cheaper and more environmentally friendly. Taking into account electron counting

considerations with this particular ligand set and the need for a metal centre that can exist in two adjacent oxidation states, the lower of which is supported only by the ligands. On further investigation, when reduction potentials are considered, zirconium and hafnium IV/III half cell measurements are much closer to that of the uranium IV/III half cell than that of titanium.[156] Taking these factors into consideration, it was believed that the most successful transition metal analogues that could duplicate the reactivity seen with the mixed-ring uranium compounds would be those of zirconium and hafnium. Investigations into this area will be described in this thesis.

1.9 References for Chapter One

1. D. J. Cardin, M. F. Lappert and C. L. Raston, *Chemistry of Organo-Zirconium and -Hafnium Compounds*, 1st edn., Ellis Horwood Limited, Chichester, 1986.
2. E. H. K. Ziegler, E. Holzkamp, H. Breil and H. Martin, *Angew. Chem.*, 1955, **67**, 541-547.
3. G. Natta, *Angew. Chem.*, 1956, **68**, 393-403.
4. F. R. W. P. Wild, M. Wasiucionek, G. Huttner and H. H. Brintzinger, *J. Organomet. Chem.*, 1985, **288**, 63-67.
5. F. Wochner, L. Zsolnai, G. Huttner and H. H. Brintzinger, *J. Organomet. Chem.*, 1985, **288**, 69-77.
6. H. Schwemlein, W. Tritschler, H. Kiesele and H. H. Brintzinger, *J. Organomet. Chem.*, 1985, **293**, 353-364.
7. M. Bochmann, *J. Chem. Soc., Dalton Trans.*, 1996, 255-270.
8. M. D. Fryzuk and S. A. Johnson, *Coord. Chem. Rev.*, 2000, **200-202**, 379-409.
9. A. D. Allen and C. V. Senoff, *J. Chem. Soc. Chem. Comm.*, 1965, 621-622.
10. A. D. Allen, F. Bottomley, R. O. Harris, V. P. Reinsalu and C. V. Senoff, *J. Am. Chem. Soc.*, 1966, **89**, 5595-5599.
11. F. Bottomley and S. C. Nyburg, *J. Chem. Soc., Chem. Commun.*, 1966, 897-898.
12. A. Yamamoto, S. Kitazume, L. S. Pu and S. Ikeda, *Chem. Commun.*, 1967, 79-80.
13. J. Chatt, G. A. Heath and R. L. Richards, *J. Chem. Soc., Chem. Commun.*, 1972, 1010-1011.
14. P. C. Bevan, J. Chatt, R. A. Head, P. B. Hitchcock and G. J. Leigh, *J. Chem. Soc., Chem. Commun.*, 1976, 509-510.
15. J. Chatt, A. A. Diamantis, G. A. Heath, N. E. Hooper and G. J. Leigh, *J. Chem. Soc., Dalton Trans.*, 1977, 688-697.
16. S. M. Rocklage, H. W. Turner, J. D. Fellmann and R. R. Schrock, *Organometallics*, 1982, **1**, 703-707.
17. G. N. Schrauzer and M. R. Palmer, *J. Am. Chem. Soc.*, 1981, **193**, 2659-2667.
18. N. P. Luneva, S. A. Mironova, A. E. Shilov, M. Y. Antipin and Y. T. Struchkov, *Angew. Chem. Int. Ed.*, 1993, **32**, 1178-1179.
19. P. Berno and S. Gambarotta, *Angew. Chem. Int. Ed.*, 1995, **34**, 822-824.

20. G. K. B. Clentsmith, V. M. E. Bates, P. B. Hitchcock and F. G. N. Cloke, *J. Am. Chem. Soc.*, 1999, **121**, 10444-10445.
21. V. M. E. Bates, G. K. B. Clentsmith, F. G. N. Cloke, J. C. Green and H. D. L. Jenkinb, *Chem. Commun.*, 2000, 927-928.
22. C. E. Laplaza and C. C. Cummins, *Science*, 1995, **268**, 861-863.
23. C. E. Laplaza, A. R. Johnson and C. C. Cummins, *J. Am. Chem. Soc.*, 1996, **118**, 709-710.
24. C. E. Laplaza, M. J. A. Johnson, J. C. Peters, A. L. Odom, E. Kim, C. C. Cummins, G. N. George and I. J. Pickering, *J. Am. Chem. Soc.*, 1996, **118**, 8623-8638.
25. A. Zanotti-Gerosa, E. Solari, L. Giannini, C. Floriani, A. Chiesi-Villa and C. Rizzoli, *J. Am. Chem. Soc.*, 1998, **120**, 437-438.
26. H. H. Brintzinger and J. E. Bercaw, *J. Am. Chem. Soc.*, 1971, **93**, 2045-2046.
27. Y. G. Borodko, I. N. Ivleva, L. M. Kachapina, S. I. Salienko, A. K. Shilova and A. E. Shilov, *J. Chem. Soc., Chem. Commun.*, 1972, 1178a-1178a.
28. Y. G. Borodko, I. N. Ivleva, L. M. Kachapina, E. F. Kvashina, A. K. Shilova and A. E. Shilov, *J. Chem. Soc., Chem. Commun.*, 1973, 169-170.
29. J. E. Beraw, *J. Am. Chem. Soc.*, 1974, **96**, 5087-5095.
30. R. D. Sanner, D. M. Duggan, T. C. McKenzie, R. E. Marsh and J. E. Bercaw, *J. Am. Chem. Soc.*, 1976, **98**, 8358-8365.
31. D. H. Berry, L. J. Procopio and P. J. Carroll, *Organometallics*, 1988, **7**, 570-572.
32. J. M. d. Wolf, R. Blaauw, A. Meetsma, J. H. Teuben, R. Gyepes, V. Varga, K. Mach, N. Veldman and A. L. Spek, *Organometallics*, 1996, **15**, 4977-4983.
33. T. E. Hanna, E. Lobkovsky and P. J. Chirik, *J. Am. Chem. Soc.*, 2004, **126**, 14688-14689.
34. T. E. Hanna, I. Keresztes, E. Lobkovsky, W. H. Bernskoetter and P. J. Chirik, *Organometallics*, 2004, **23**, 3448-3458.
35. T. E. Hanna, E. Lobkovsky and P. J. Chirik, *Organometallics*, 2009, **28**, 4079-4088.
36. J. M. Manriquez and J. E. Beraw, *J. Am. Chem. Soc.*, 1974, **96**, 6229-6230.
37. R. D. Sanner, J. M. Manriquez, R. E. Marsh and J. E. Bercaw, *J. Am. Chem. Soc.*, 1976, **98**, 8351-8357.
38. D. M. Roddick, M. D. Fryzuk, P. F. Seidler, G. L. Hillhouse and J. E. Bercaw, *Organometallics*, 1985, **4**, 97-104.

39. J. H. Teuben, *J. Organomet. Chem.*, 1973, **57**, 159-167.
40. F. W. van der Weij and J. H. Teuben, *J. Organomet. Chem.*, 1976, **105**, 203-207.
41. J. D. Zeinstra, J. H. Teuben and F. Jellinek, *J. Organomet. Chem.*, 1979, **170**, 39-50.
42. G. P. Pez, P. Apgar and R. K. Crissey, *J. Am. Chem. Soc.*, 1982, **104**, 482-490.
43. R. Duchateau, S. Gambarotta, N. Beydoun and C. Bensimon, *J. Am. Chem. Soc.*, 1991, **113**, 8986-8988.
44. M. D. Fryzuk, T. S. Haddad and S. J. Rettig, *J. Am. Chem. Soc.*, 1990, **112**, 8185-8186.
45. D. A. Fletcher, R. F. McMeeking and D. Parkin, *J. Chem. Inf. Comput. Sci.*, 1996, **46**, 746-749.
46. F. H. Allen, *Acta Crystallogr., Sect. B: Struct. Sci*, 2002, **58**, 380-388.
47. I. J. Bruno, J. C. Cole, P. R. Edgington, M. Kessler, C. F. Macrae, P. McCabe, J. Pearson and R. Taylor, *Acta Crystallogr., Sect. B: Struct. Sci*, 2002, **58**, 389-397.
48. L. Morello, J. B. Love, B. O. Patrick and M. D. Fryzuk, *J. Am. Chem. Soc.*, 2004, **126**, 9480-9481.
49. M. D. Fryzuk, J. R. Corkin and B. O. Patrick, *Can. J. Chem.*, 2003, **81**, 1376-1387.
50. P. J. Chirik, L. M. Henling and J. E. Bercaw, *Organometallics*, 2001, **20**, 534-544.
51. C. Marschner, *Angew. Chem. Int. Ed.*, 2007, **46**, 6770-6771.
52. D. J. Knobloch, E. Lobkovsky and P. J. Chirik, *J. Am. Chem. Soc.*, 2010, **132**, 15340-15350.
53. D. J. Knobloch, E. Lobkovsky and P. J. Chirik, *J. Am. Chem. Soc.*, 2010, **132**, 10553-10564.
54. D. J. Knobloch, E. Lobkovsky and P. J. Chirik, *Nature Chemistry*, 2010, **2**, 30-35.
55. W. H. Bernskoetter, E. Lobkovsky and P. J. Chirik, *Angew. Chem. Int. Ed.*, 2007, **46**, 2858-2861.
56. W. H. Bernskoetter, A. V. Olmos, J. A. Pool, E. Lobkovsky and P. J. Chirik, *J. Am. Chem. Soc.*, 2006, **128**, 10696-10697.

57. D. J. Knobloch, D. Benito-Garagorri, W. H. Bernskoetter, I. Keresztes, E. Lobkovsky, H. Toomey and P. J. Chirik, *J. Am. Chem. Soc.*, 2009, **131**, 14903-14912.
58. L. S. Benner and A. L. Balch, *J. Am. Chem. Soc.*, 1978, **100**, 6099-6106.
59. M. L. Kullberg and C. P. Kubiak, *Inorg. Chem.*, 1986, **25**, 26-30.
60. M. P. Brown, R. J. Puddephatt, M. Rashidi, L. Manojlović-Muir, K. W. Muir, T. Solomun and K. R. Seddon, *Inorg. Chim. Acta*, 1977, **23**, L33-L34.
61. V. L. Coffin, W. Brennen and B. B. Wayland, *J. Am. Chem. Soc.*, 1988, **110**, 6063-6069.
62. B. B. Wayland, A. E. Sherry, G. Poszmik and A. G. Bunn, *J. Am. Chem. Soc.*, 1992, **114**, 1673-1681.
63. F. N. Tebbe, *J. Am. Chem. Soc.*, 1973, **95**, 5823-5824.
64. P. Meakin, L. J. Guggenberger, F. N. Tebbe and J. P. Jesson, *Inorg. Chem.*, 1974, **13**, 1025-1032.
65. S. Datta and S. S. Wreford, *Inorg. Chem.*, 1977, **16**, 1134-1137.
66. C. D. Wood and R. R. Schrock, *J. Am. Chem. Soc.*, 1979, **101**, 5421-5422.
67. J. M. Mayer and J. E. Bercaw, *J. Am. Chem. Soc.*, 1982, **104**, 2157-2165.
68. E. M. Carnahan, J. D. Protasiewicz and S. J. Lippard, *Acc. Chem. Res.*, 1993, **26**, 90-97.
69. D. J. Sikora, M. D. Rausch, R. D. Rogers and J. L. Atwood, *J. Am. Chem. Soc.*, 1981, **103**, 1265-1267.
70. B. H. Edwards, R. D. Rogers, D. J. Sikora, J. L. Atwood and M. D. Rausch, *J. Am. Chem. Soc.*, 1983, **105**, 416-426.
71. M. D. Rausch, K. J. Moriarty, J. L. Atwood, W. E. Hunter and E. Samuel, *J. Organomet. Chem.*, 1987, **327**, 39-54.
72. W. H. Bernskoetter, A. V. Olmos, E. Lobkovsky and P. J. Chirik, *Organometallics*, 2006, **25**, 1021-1027.
73. T. E. Hanna, I. Keresztes, E. Lobkovsky and P. J. Chirik, *Inorg. Chem.*, 2007, **46**, 1675-1683.
74. D. Pun, S. M. Leopold, C. A. Bradley, E. Lobkovsky and P. J. Chirik, *Organometallics*, 2009, **28**, 2471-2484.
75. G. Pampaloni and G. Tripepi, *J. Organomet. Chem.*, 2000, **593**, 19-26.
76. T. E. Waldman, L. Stahl, D. R. Wilson, A. M. Arif, J. P. Hutchinson and R. D. Ernst, *Organometallics*, 1993, **12**, 1543-1552.

77. C. A. Bertelo and J. Schwartz, *J. Am. Chem. Soc.*, 1975, **97**, 228-230.
78. G. Fachinetti and C. Floriani, *J. Organomet. Chem.*, 1974, **71**, C5-C7.
79. G. Fachinetti, C. Floriani, F. Marchetti and S. Merlino, *J. Chem. Soc., Chem. Commun.*, 1976, 522-523.
80. G. Fachinetti, G. Fochi and C. Floriani, *J. Chem. Soc. Dalton Trans.*, 1977, 1946-1950.
81. J. M. Manriquez, D. R. McAlister, R. D. Sanner and J. E. Bercaw, *J. Am. Chem. Soc.*, 1978, **100**, 2716-2724.
82. J. M. Manriquez, D. R. McAlister, R. D. Sanner and J. E. Bercaw, *J. Am. Chem. Soc.*, 1976, **98**, 6733-6735.
83. G. Fachinetti, C. Floriani and S. Pucci, *J. Chem. Soc., Chem. Commun.*, 1978, 269-270.
84. M. D. Fryzuk, M. Mylvaganam, M. J. Zaworotko and L. R. MacGillivray, *Organometallics*, 1996, **15**, 1134-1138.
85. P. Berno, C. Floriani, A. Chiesi-Villa and C. Guastini, *J. Chem. Soc., Chem. Commun.*, 1991, 109-110.
86. P. T. Wolczanski and J. E. Bercaw, *Acc. Chem. Res.*, 1980, **13**, 121-127.
87. J. Blenkers, H. J. D. L. Meijer and J. H. Teuben, *Organometallics*, 1983, **2**, 1483-1484.
88. R. P. Planalp and R. A. Andersen, *J. Am. Chem. Soc.*, 1983, **105**, 7774-7775.
89. F. Calderazzo, U. Englert, A. Guarini, F. Marchetti, G. Pampaloni, A. Segre and G. Tripepi, *Chem. Eur. J.*, 1996, **2**, 412-419.
90. L. S. Pu, A. Yamamoto and S. Ikeda, *J. Am. Chem. Soc.*, 1968, **90**, 3896.
91. I. S. Kolomnikov, A. I. Gusev, G. G. Aleksandrov, T. S. Lobeeva, Y. T. Struchkov and M. E. Vol'pin, *J. Organomet. Chem.*, 1973, **59**, 349-351.
92. V. D. Bianco, S. Doronzo and M. Rossi, *J. Organomet. Chem.*, 1972, **35**, 337-339.
93. B. R. Flynn and L. Vaska, *J. Chem. Soc., Chem. Commun.*, 1974, 703-704.
94. J. Chatt, M. Kubota, J. Leigh, F. March, R. Mason and D. J.Yarrow, *J. Chem. Soc. Chem. Comm.*, 1974, 1033-1034.
95. T. Herskovitz, *J. Am. Chem. Soc.*, 1977, **99**, 2391-2392.
96. M. Aresta and C. F. Nobile, *Inorg. Chim. Acta*, 1977, **24**, L49-L50.
97. J. C. Calabrese, T. Herskovitz and J. B. Kinney, *J. Am. Chem. Soc.*, 1983, **105**, 5914-5915.

98. M. Aresta, C. F. Nobile, V. G. Albano, E. Forni and M. Manassero, *J. Chem. Soc., Chem. Commun.*, 1975, 636-637.

99. G. S. Bristow, P. B. Hitchcock and M. F. Lappert, *J. Chem. Soc., Chem. Commun.*, 1981, 1145-1146.

100. R. Alvarez, E. Carmona, E. Gutierrez-Puebla, J. M. Marín, A. Monge and M. L. Poveda, *J. Chem. Soc., Chem. Commun.*, 1984, 1326-1327.

101. R. Alvarez, E. Carmona, J. M. Marin, M. L. Poveda, E. Gutierrez-Puebla and A. Monge, *J. Am. Chem. Soc.*, 1986, **108**, 2286-2294.

102. S. Gambarotta, C. Floriani, A. Chiesi-Villa and C. Guastini, *J. Am. Chem. Soc.*, 1985, 2985-2986.

103. M. H. Chisholm and M. Extine, *J. Am. Chem. Soc.*, 1974, **96**, 6214-6216.

104. M. H. Chisholm, F. A. Cotton, M. W. Extine and W. W. Reichert, *J. Am. Chem. Soc.*, 1978, **100**, 1727-1734.

105. E. G. Lundquist, J. C. Huffman, K. Folting, B. E. Mann and K. G. Caulton, *Inorg. Chem.*, 1990, **29**, 128-134.

106. T. A. Hanna, A. M. Baranger and R. G. Bergman, *J. Am. Chem. Soc.*, 1995, **117**, 11363-11364.

107. S. Krogsrud, S. Komiya, T. Ito, J. A. Ibers and A. Yamamoto, *Inorg. Chem.*, 1976, **15**, 2798–2805.

108. I. S. Kolomnikov, T. S. Loveeva, V. V. Gorbachevskaya, G. G. Aleksandrov, Y. T. Struckhov and M. E. Vol'pin, *J. Chem. Soc., Chem. Commun.*, 1971, 972-973.

109. D. R. Lide, ed., *CRC Handbook of Chemistry and Physics*, 89 edn., CRC Press, Boca Raton, 2008.

110. S. Gambarotta, S. Strologo, C. Floriani, A. Chiesi-Villa and C. Guastini, *J. Am. Chem. Soc.*, 1985, **107**, 6278-6282.

111. S. Gambarotta, S. Strologo, C. Floriani, A. Chiesi-Villa and C. Guastini, *Inorg. Chem.*, 1985, **24**, 654-660.

112. S. A. Cohen and J. E. Bercaw, *Organometallics*, 1985, **4**, 1006-1014.

113. E. Klei and J. H. Teuben, *J. Organomet. Chem.*, 1981, **222**, 79-88.

114. D. J. Knobloch, H. E. Toomey and P. J. Chirik, *Organometallics*, 2008, **130**, 4248-4249.

115. M. N. Bochkarev, *Coord. Chem. Rev.*, 2004, **248**, 835-851.

116. W. J. Evans, *Inorg. Chem.*, 2007, **46**, 3435-3449.

117. W. J. Evans, T. A. Ulibarri and J. W. Ziller, *J. Am. Chem. Soc.*, 1988, **110**, 6877-6879.

118. W. J. Evans, N. T. Allen and J. W. Ziller, *J. Am. Chem. Soc.*, 2001, **123**, 7927-7928.

119. W. J. Evans, N. T. Allen and J. W. Ziller, *Angew. Chem.*, 2002, **114**, 369.

120. W. J. Evans, G. Zucchi and J. W. Ziller, *J. Am. Chem. Soc.*, 2003, **125**, 10-11.

121. W. J. Evans, D. S. Lee and J. W. Ziller, *J. Am. Chem. Soc.*, 2004, **126**, 454-455.

122. W. J. Evans, D. S. Lee, D. B. Rego, J. M. Perotti, S. A. Kozimor, E. K. Moore and J. W. Ziller, *J. Am. Chem. Soc.*, 2004, **126**, 14574-14582.

123. W. J. Evans, D. S. Lee, C. Lie and J. W. Ziller, *Angew. Chem. Int. Ed.*, 2004, **43**, 5517-5519.

124. W. J. Evans, D. B. Rego and J. W. Ziller, *Inorg. Chem.*, 2006, **45**, 10790-10798.

125. W. J. Evans, M. Fang, G. Zucchi, F. Furche, J. W. Ziller, R. M. Hoekstra and J. I. Zink, *J. Am. Chem. Soc.*, 2009, **131**, 11195-11202.

126. W. J. Evans, J. W. Grate, L. A. Hughes, H. Zhang and J. L. Atwood, *J. Am. Chem. Soc.*, 1985, **107**, 3728-3730.

127. W. J. Evans, D. S. Lee, J. W. Ziller and N. Kaltsoyannis, *J. Am. Chem. Soc.*, 2006, **128**, 14176-14184.

128. W. J. Evans, C. A. Seibel and J. W. Ziller, *Inorg. Chem.*, 1998, **37**, 770-776.

129. N. W. Davies, A. S. P. Frey, M. G. Gardiner and J. Wang, *J. Chem. Soc., Chem. Commun.*, 2006, 4853-4855.

130. J. M. Manriquez, P. J. Fagan, T. J. Marks, C. S. Day and V. W. Day, *J. Am. Chem. Soc.*, 1978, **100**, 7112-7114.

131. P. J. Fagan, J. M. Manriquez, T. J. Marks, V. W. Day, S. H. Vollmer and C. S. Day, *J. Am. Chem. Soc.*, 1980, **102**, 5393-5396.

132. K. G. Moloy and T. J. Marks, *J. Am. Chem. Soc.*, 1984, **106**, 7051-7064.

133. K. G. Moloy, P. J. Fagan, J. M. Manriquez and T. J. Marks, *J. Am. Chem. Soc.*, 1986, **108**, 56-67.

134. P. G. Edwards, M. B. Hursthouse, K. M. A. Malik and J. S. Parry, *J. Chem. Soc., Chem. Commun.*, 1994, 1249-1250.

135. D. C. Sonnenberger, E. A. Mintz and T. J. Marks, *J. Am. Chem. Soc.*, 1984, **106**, 3484-3491.

136. K. G. Moloy and T. J. Marks, *Inorg. Chim. Acta*, 1985, **110**, 127-131.

137. T. M. Trnka, J. B. Bonanno, B. M. Bridgewater and G. Parkin, *Organometallics*, 2001, **20**, 3255-3264.

138. P. Roussel and P. Scott, *J. Am. Chem. Soc.*, 1998, **120**, 1070-1071.

139. P. Roussel, W. Errington, N. Kaltsoyannis and P. Scott, *J. Organomet. Chem.*, 2001, **635**, 69-74.

140. W. J. Evans, S. A. Kozimor and J. W. Ziller, *J. Am. Chem. Soc.*, 2003, **125**, 14264-14265.

141. F. G. N. Cloke and P. B. Hitchcock, *J. Am. Chem. Soc.*, 2002, **124**, 9352-9353.

142. F. G. N. Cloke, J. C. Green and N. Kaltsoyannis, *Organometallics*, 2004, **23**, 832-835.

143. A. L. Odom, P. L. Arnold and C. C. Cummins, *J. Am. Chem. Soc.*, 1998, **120**, 5836-5837.

144. S. M. Mansell, N. Kaltsoyannis and P. L. Arnold, *J. Am. Chem. Soc.*, 2011, **133**, 9036-9051.

145. P. L. Arnold, Z. R. Turner, R. M. Bellabarba and R. P. Tooze, *Chemical Science*, 2011, **2**, 77-79.

146. O. E. Cramer, R. B. Maynard, J. C. Paw and J. W. Gilje, *Organometallics*, 1982, **1**, 869-871.

147. J. G. Brennan, R. A. Andersen and J. L. Robbins, *J. Am. Chem. Soc.*, 1986, **108**, 335-336.

148. J. Parry, E. Carmon, S. Coles and M. Hursthouse, *J. Am. Chem. Soc.*, 1995, **117**, 2649-2650.

149. M. d. M. Conejo, J. S. Parry, E. Carmona, M. Schultz, J. G. Brennann, S. M. Beshouri, R. A. Andersen, R. D. Rogers, S. Coles and M. B. Hursthouse, *Chem. Eur. J.*, 1999, **5**, 3000-3009.

150. I. Castro-Rodriguez and K. Meyer, *J. Am. Chem. Soc.*, 2005, **127**, 11242-11243.

151. O. T. Summerscales, F. G. N. Cloke, P. B. Hitchcock, J. C. Green and N. Hazari, *Science*, 2006, **331**, 829-831.

152. O. T. Summerscales, F. G. N. Cloke, P. B. Hitchcock, J. C. Green and N. Hazari, *J. Am. Chem. Soc.*, 2006, **128**, 9602-9603.

153. A. S. Frey, F. G. N. Cloke, P. B. Hitchcock, I. J. Day, J. C. Green and G. Aitken, *J. Am. Chem. Soc.*, 2008, **130**, 13816-13817.

154. A. S. P. Frey, F. G. N. Cloke, M. P. Coles, L. Maron and T. Davin, *Angew. Chem. Int. Ed.*, 2011, **50**, 6881-6883.

155. O. T. Summerscales, A. S. P. Frey, F. G. N. Cloke and P. B. Hitchcock, *Chem. Commun.*, 2009, 198-200.

156. D. E. Morris, R. E. Da Re, K. C. Jantunen, I. Castro-Rodriguez and J. L. Kiplinger, *Organometallics*, 2004, **23**, 5142-5153.

2 CHAPTER TWO: SYNTHESIS OF MIXED SANDWICH Zr(IV) AND Hf(IV) CHLORIDES

2.1 Introduction

Mixed-ring zirconium complexes that incorporate both COT and Cp ligands are rare, with the hafnium analogues even rarer still, despite the chemical similarities between zirconium and hafnium compounds. The first instance of this type of mixed-ring Group IV compound was published in 1985 by Teuben and co-workers[1, 2] and was the first example of a thermally stable, paramagnetic, organo-zirconium(III) compound to be successfully isolated in the solid state. The hafnium(III) equivalent was, however, unable to be isolated as the reduced compound underwent hydrogen abstraction to afford the mixed-ring hydride. The results of this initial investigation were expanded by Spencer and co-workers,[3] characterising twelve examples of 18-electron compounds of the form [Zr(COT)(Cp^{Me4R})R'], and successfully collecting X-ray data on the mixed-ring compound [Zr(COT)(Cp^{Me5})H] in the +4 oxidation state. Attempts to reduce the compound when R = Me and R' = Cl led to a black crystalline pyrophoric product believed to be [Zr(COT)(Cp^{Me5})], although this was not fully characterised, presumably due to its unstable nature. In this chapter, the synthesis of the mixed ring chlorides of both the hafnium(IV) and zirconium(IV) compounds will be discussed.

2.2 Synthesis of $[Zr(\eta^8\text{-}C_8H_6\{Si^iPr_3\text{-}1,4\}_2)Cl_2]_2$ and $[Hf(\eta^8\text{-}C_8H_6\{Si^iPr_3\text{-}1,4\}_2)Cl_2]_2$

To a white suspension of one equivalent $ZrCl_4$ in THF was added a pale green solution of $K_2C_8H_6\{Si^iPr_3\text{-}1,4\}_2$ (2 eq) in THF at ambient temperature, immediately affording a deep wine-red colour. This mixture was heated to reflux at 65 °C overnight resulting in the appearance of a pale precipitate, but with no further colour change. Extraction into 40-60 petroleum ether and subsequent removal of solvent yielded $[Zr(C_8H_6\{Si^iPr_3\text{-}1,4\}_2)_2]$ (**2.1**) in quantitative yield as a sticky dark red solid, the identity of which was confirmed by ^1H NMR spectroscopy. The COT ring protons appeared as a sharp singlet at δ_H 6.5 and two broad singlets at δ_H 6.4 and 6.2: each integrating to two hydrogen atoms. A septet integrating to six protons was observed at 1.2 ppm indicating the *iso*propyl methine groups, while two doublets each integrating to 18 and therefore indicative of the presence of *iso*propyl methyl groups were seen at δ_H 0.9 and 0.8 ppm. MS identified the parent ion at m/z 923, further confirming the identity and of **2.1**, which was not purified further before subsequent reaction. Compound **2.1** was dissolved in toluene before addition of a further equivalent of $ZrCl_4$ as a white suspension in toluene with stirring. No colour changes were observed on addition and the mixture was heated to reflux at 120 °C for 48 hours. Removal of volatiles and washing with pentane yielded **2.2** as a pale orange solid in good yield. ^1H NMR spectroscopy showed a slight downfield shift in all resonances with respect to **2.1** and the ring proton singlets previously observed resolved into the characteristic second-order AA'BB'X_2 splitting pattern of the COT ring protons. The identity of **2.2** was confirmed by $^{29}Si\{^1H\}$ and $^{13}C\{^1H\}$ NMR spectroscopy, with spectral assignment by COSY, HSQC and HMBC experiments. Elemental analysis and mass spectrometry confirmed the identity and purity of the product with the parent ion at m/z 1156 corroborating the dimeric nature of **2.2** as shown in (**Scheme 2.1**), as previously reported by Floriani and co-workers using the $C_8H_6\{SiMe_3\text{-}1,4\}_2$ moiety.[4]

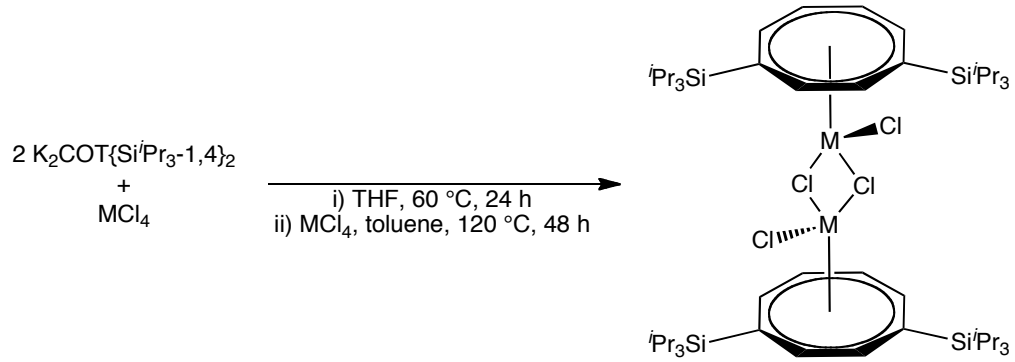

Scheme 2.1: General synthesis for mixed-ring M(IV) where M = Zr (**2.2**) and Hf (**2.4**).

The hafnium congener **2.4** was prepared analogously to **2.2**, with the intermediate compound [Hf(C_8H_6{Si^{i}Pr$_3$-1,4}$_2$)$_2$] (**2.3**) observed to be deep pink-red in colour and its identity confirmed by ^{1}H NMR spectroscopy and mass spectrometry as with the zirconium analogue. The ultimate compound **2.4** was isolated as a pale yellow powder in similar yield to **2.2**. The purity of **2.4** was confirmed by elemental analysis and ^{1}H, ^{13}C{^{1}H} and ^{29}Si{^{1}H} NMR spectroscopy, with resonances at comparable shifts to the zirconium congener, however, its identity could not be confirmed by mass spectrometry. Although a dimeric compound isostructural to that assumed for **2.2** is expected due to the chemically similar nature of zirconium and hafnium compounds, the observed parent ion is only at m/z 666, corresponding to the monomeric unit [Hf(η^8-C_8H_6{Si^{i}Pr$_3$-1,4}$_2$)Cl_2]. This result suggests that the dimeric unit **2.4** shown in **Scheme 2.1** fragments in the conditions used for mass spectrometry.

Attempts to crystallise **2.2** and **2.4** have so far proven unsuccessful due to their insolubility, however, they do crystallise from THF at -50 °C as a stable monomeric THF adduct, consistent with similar, previously reported compounds.[4-6] X-ray diffraction studies have been possible for both the zirconium and hafnium congeners **2.5** and **2.6** (**Figure 2.1** and **Figure 2.2**). These adducted complexes both crystallise in the triclinic space group P$\bar{1}$. Compound **2.5** crystallises with two monomers in the unit cell, with the four chlorine atoms directed towards the centre of the cell. The COT rings are planar and parallel to one another, and there are no interactions between the two monomers in the cell. In the case of **2.6**, however, six monomers are observed in the unit cell which are arranged such that the

chlorine atoms all point towards the outside of the cell, again with no intermolecular interactions between the monomeric units and with the COT moieties parallel with respect to each other.

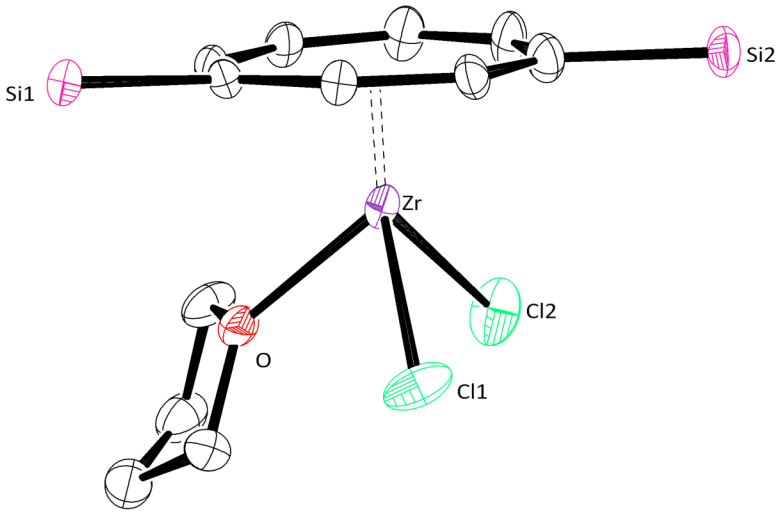

Figure 2.1: Molecular structure of [Zr(η^8-C_8H_6{Si^{i}Pr$_3$-1,4}$_2$)Cl_2(THF)] (**2.5**). Hydrogen atoms and ^{i}Pr groups are omitted for clarity. Thermal ellipsoids at 50 % probability level.

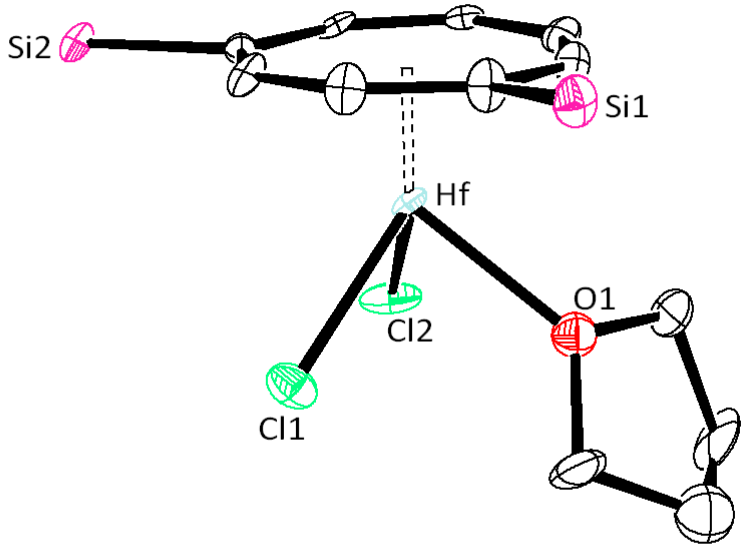

Figure 2.2: Molecular structure of [Hf(η^8-C_8H_6{Si^{i}Pr$_3$-1,4}$_2$)Cl_2(THF)] (**2.6**). Hydrogen atoms and ^{i}Pr groups are omitted for clarity. Thermal ellipsoids at 50 % probability level.

Table 2.1: Selected bond angles (deg) and distances (Å) for **2.5** and **2.6**. COT_{cent} indicates the centroid of the COT ring.

Compound	**2.5**	**2.6**
M-$COT_{cent.}$	1.6521(4)	1.6257(3)
Av. COT C-C	1.415(6)	1.423(9)
M-O	2.281(3)	2.254(5)
$COT_{cent.}$-M-O	127.96(7)	127.63(15)
M-Cl(1)	2.4809(11)	2.4585(17)
M-Cl(2)	2.482(4)	2.4647(16)
$COT_{cent.}$-M-Cl(1)	129.71(3)	129.74(5)
$COT_{cent.}$-M-Cl(2)	130.40(4)	130.84(5)

The Zr-COT_{cent} distance is the same as that reported by Krüger and Brauer[7] for the monomeric compound bearing the unsubstituted COT (1.650(5) Å), but longer than that documented for the dimeric COT(1,4-$SiMe_3$)$_2$ chloro-bridged compound by Berno *et al*[4], which measures 1.610(6) Å. The average C-C bond length calculated for **2.5** is slightly longer than expected for an aromatic ring system at 1.415(6) Å.

The Zr-Cl bond lengths determined for **2.5** are shorter than the Zr-Cl bond length in the previously reported monomer [Zr(COT)Cl_2(THF)], which measures 2.496(1) Å. Whilst the metal-halide distances observed for the bridging chlorides in the dimeric compounds[4] are considerably longer at 2.634(2) and 2.638(2) Å as would be expected for this mode, the distance between the metal and terminal chloride is comparable at 2.442(2) Å. The Zr-O distances are very similar in **2.5** and the monomeric example at 2.281(3) and 2.l74(2) Å respectively.

The COT_{cent}-Zr-Cl angle in **2.5** is much greater than seen in Krüger and Brauer's example at 129.71(3) and 130.40(4)° versus 116.4(4)°: this is most likely due to the steric effects of the bulky *iso*propyl groups. This effect is also manifest in the slightly smaller COT_{cent}-Zr-O angle in the unsubstituted example at 126.436(4) Å compared to 127.96(7) Å for the 1,4-tri*iso*propyl COT compound **2.5**.

When compound **2.6** is compared to the only similar example in the literature of [Hf(η^8-C_8H_6)Cl_2(THF)] reported by Berno *et al*,[4] it is clear that all the measurements are in agreement. This is despite the employment of the bulky COT moiety in the case of the complex synthesised here compared to the unsubstituted compound.

2.3 Synthesis and characterisation of [M(η^8-C_8H_6{Si^{i}Pr$_3$-1,4}$_2$)(Cp^{Me4R})Cl]

Previous work by the author for the M.Chem degree generated the mixed-ring chloride compounds [M(η^8-C_8H_6{Si^{i}Pr$_3$-1,4}$_2$)(Cp^{Me4R})Cl] (M = Zr, R = H, Me): the same general procedure was followed for [M(η^8-C_8H_6{Si^{i}Pr$_3$-1,4}$_2$)(Cp^{Me4R})Cl] (M = Zr, R = TMS; M = Hf, R = H, Me, TMS) (**Scheme 2.2**). Addition of a white suspension of two equivalents of KCp^{Me4R} in toluene to a stirring orange solution of one equivalent of **2** or **4** in toluene at ambient temperature yielded a green solution in the case of the zirconium compound and yellow solution for the hafnium congeners. This mixture was allowed to stir at reflux (120 °C) overnight, darkening slightly in colour with the appearance of a fine precipitate. Extraction with pentane and subsequent storage at -50 °C yielded bright yellow crystals of the product in moderate to good yield. For compounds **2.7**, **2.8**, **2.9**, **2.10** and **2.11**, these crystals were suitable for single crystal diffraction studies while **2.12** required recrystallisation from DME. Selected bond distances and angles for complexes **2.7** – **2.12** are summarised in **Table 2.2**.

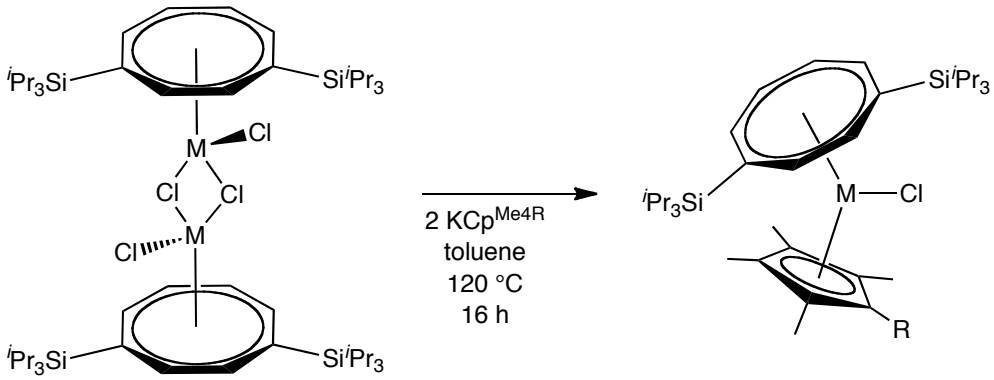

Scheme 2.2: General synthesis for mixed-ring M(IV) compounds **2.7** (M = Zr, R = H), **2.8** (M = Hf, R = H), **2.9** (M = Zr, R = Me), **2.10** (M = Hf, R = Me), **2.11** (M = Zr, R = TMS), **2.12** (M = Hf, R = TMS).

In each case, mass spectrometry revealed the anticipated parent ion and purity was confirmed by elemental analysis. The same resonances for the substituted COT ligand as described with previous compounds **2.2** and **2.4** were generated by ^{1}H NMR spectroscopy. For **2.7**, three singlets were seen for the Cp^{Me4H} moiety at 4.93, 1.86 and 1.70 ppm, integrating 1:6:6 respectively. In the case of the hafnium analogue **2.8**, these resonances were observed at δ_H 4.82, 1.94 and 1.77. For compounds bearing the pentamethylated Cp ligand (**2.9** and **2.10**), only a singlet integrating to 15 protons was observed at *ca.* δ_H 1.75. Finally, with the bulkier silylated Cp ligand, three singlets at 1.98, 1.70, 0.34 ppm (**2.11**) and 2.05, 1.76 and 0.30 ppm (**2.12**) were recorded with relative integration 6:6:9, with the most upfield shift corresponding to the trimethylsilyl protons. Full assignment of ^{1}H, ^{13}C{^{1}H} and ^{29}Si{^{1}H} shifts were by recourse to 2D techniques including COSY, HSQC and HMBC experiments. In the case of **2.11** and **2.12**, ^{29}Si{^{1}H} spectroscopy resolved the TMS resonance upfield from the TIPS resonance at *ca.* δ_{Si} -7.2 ppm.

Table 2.2: Selected bond angles (deg) and distances (Å) for [M(η^8-C_8H_6{Si^{i}Pr$_3$-1,4}$_2$)(Cp^{Me4R})Cl]: **2.7** (M = Zr, R = H), **2.8** (M = Hf, R = H), **2.9** (M = Zr, R = Me), **2.10** (M = Hf, R = Me), **2.11** (M = Zr, R = TMS), **2.12** (M = Hf, R = TMS). $COT_{cent.}$ and $Cp_{cent.}$ indicate the centroid of the COT and Cp rings.

Compound	M-Cl	M-$COT_{cent.}$	M-$Cp_{cent.}$	$COT_{cent.}$-M-$Cp_{cent.}$	COT C-C range	Av.Cp C-C
2.7	2.5691(8)	1.731(3)	2.240(3)	144.0(1)	1.399(4) – 1.423(4)	1.413(5)
2.8	2.5283(11)	1.7182(2)	2.2230(2)	144.440(10)	1.402(6) – 1.427(5)	1.418(7)
2.9	2.5584(5)	1.730(2)	2.254(2)	145.5(6)	1.403(3) – 1.421(3)	1.414(4)
2.10	2.4968(10)	1.72(4)	2.23(4)	145.9(19)	1.390(6) – 1.424(6)	1.408(7)
2.11	2.5574(6)	1.746(15)	2.260(15)	147.4(9)	1.399(3) – 1.423(3)	1.424(3)
2.12	2.525(1)	1.74(2)	2.24(2)	148.7(6)	1.393(7) – 1.434(7)	1.428(8)

In the case of compounds **2.7** – **2.12**, the M-Cl bond lengths are consistent with those reported and summarised in **Figure 2.3**. The average Zr-Cl and Hf-Cl distances calculated from these data measure 2.45(5) and 2.42(4) Å respectively, across a wide range of compounds where the chloride is a terminal moiety.

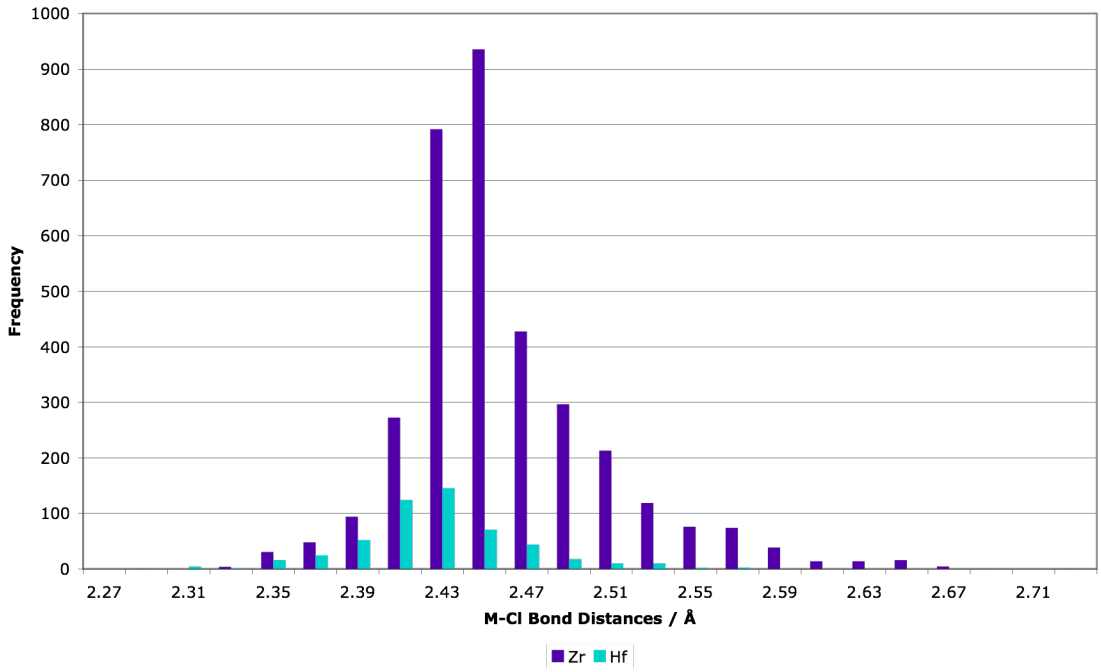

Figure 2.3: Published Zr-Cl and Hf-Cl distances where the halide is a terminal moiety.[8-10]

As similar compounds have not before been reported, data are not available for direct comparative analysis of metal-centroid distances regarding the bis(tri*iso*propylsilyl)-substituted COT moiety and either zirconium or hafnium centres. In this case, comparisons to unsubstituted or similarly substituted COT moieties η^8-bound to zirconium and hafnium have been conducted (**Figure 2.4**).

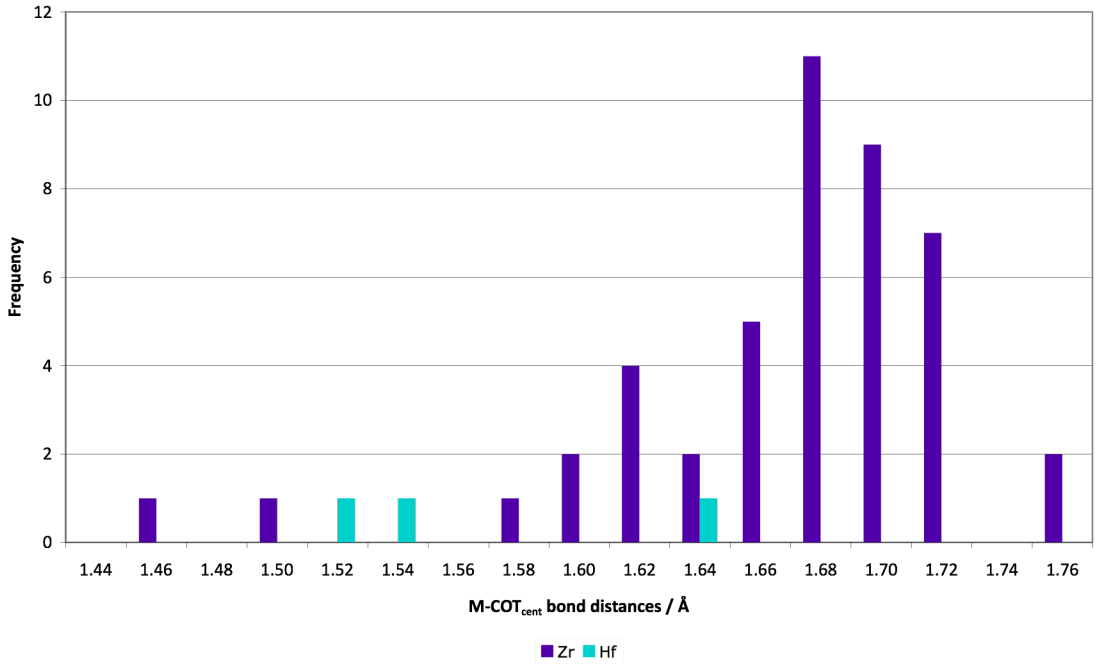

Figure 2.4: Zr-COT_{cent} and Hf-COT_{cent} distances where the COT moiety is bound η^8 to the central metal atom.[8-10]

The average Zr-COT_{cent} distance calculated from the available data summarised in **Figure 2.4** is 1.66(6) Å, consistent with the same parameter measured for compounds **2.7**, **2.9** and **2.11** (1.731(3), 1.730(2) and 1.746(15) Å) within standard deviations. The Zr-COT_{cent} distances observed for the zirconium complexes summarised in **Table 2.2**. These are directly comparable to those seen for more sterically crowded examples of zirconium in the +4 oxidation state bonded to either bis(trimethylsilyl)COT[11] or other bulky ligands including Cp^{Me5}, 2,6-di-*tert*-butylphenol and η^1-1,3,5-tri-*tert*butylbenzene.[3, 12, 13] Compounds **2.7**, **2.9** and **2.11** are all sterically congested, containing bulky *iso*propyl groups that will experience unfavourable steric interactions with the methyl and trimethylsilyl groups present on the Cp ligand. This results in Zr-COT_{cent} lengths that are longer than those seen in examples with less bulky ligands. Significantly different Zr-COT_{cent} distances are seen for Zr(III) compounds at 1.449 and 1.498 Å,[11, 14] distinctly shorter than compounds **2.7**, **2.9** and **2.11**, and those observed for the Zr(IV) compounds which constitute the remainder of the supplied data.

As can be seen from **Figure 2.4**, only three compounds containing the Hf-η^8COT moiety have been reported previously. There is one example containing the unsubstituted COT ligand[4] and two with bistrimethylsilyl COT.[15, 16]. The Hf-COT_{cent} bond distances reported for these compounds (1.629, 1.519 and 1.524 Å respectively) are shorter than those observed for compounds **2.8**, **2.10** and **2.12** (1.7182(2), 1.72(4) and 1.74(2) Å respectively). The latter compounds contain bulkier ligands, leading to an increase in this measurement, making these values more comparable with those seen for the zirconium analogues.

For all the compounds synthesised and discussed in this section, COT_{cent}-M-Cp_{cent} angles have been calculated. These measure between 144.0(1)° for **2.7** and 148.7(6)° for **2.12** and it is apparent that the two substituted rings are not parallel. Clear similarities between the zirconium and hafnium analogues are seen as the angles reflect the effect of the combined steric bulk of the H, Me or TMS group and bulky *iso*propyl groups. No literature values are available for direct comparison with these measurements, but these values are consistent within the group of compounds synthesised in this chapter.

Despite the non-planarity of the COT ligand for compounds **2.7** – **2.12** (**Figures 2.5**, **2.6**, **2.8**, **2.9**, **2.11** and **2.12**), spectroscopic data support the assumption of the diamagnetic +4 metal centre, with sharp resonances observed by ^{1}H NMR spectroscopy, which could only be achieved *via* the dianionic (X_2) COT moiety. For each compound, the COT C-C bond lengths vary (**Table 2.2**), although no correlation can be seen between shorter bond distances in the COT ring and relative orientation of the Cp ligand. The COT C-C bond lengths do not alternate between short and long, and are as expected for an aromatic system. The destabilisation of the d_{xy} and $d_{x^2-y^2}$ orbitals relative to the d_{z^2}, d_{xz} and d_{yz} orbitals due to the η^5-bonding of the Cp ligand results in loss of δ bonding between the metal atom and COT ring leading to a puckered conformation.[17] However, it is believed that maximum hapticity of each ligand is achieved in the case of **2.7** – **2.12**. With respect to the Cp moiety, the range of C-C distances is much more narrow, although the bond lengths are still longer than expected for a five-membered aromatic ring.

2.4 Characterisation of [M(η^8-C_8H_6{Si^{i}Pr$_3$-1,4}$_2$)(Cp^{Me4H})Cl] (2.7 & 2.8)

In the case of **2.7** and **2.8** (**Figure 2.5** and **Figure 2.6**), both compounds crystallise in the triclinic space group $P\bar{1}$. In both cases, the Cp^{Me4H} ring is oriented so that the protonated ring carbon is opposite to the chloride and closer to the COT ligand than the methylated Cp carbons.

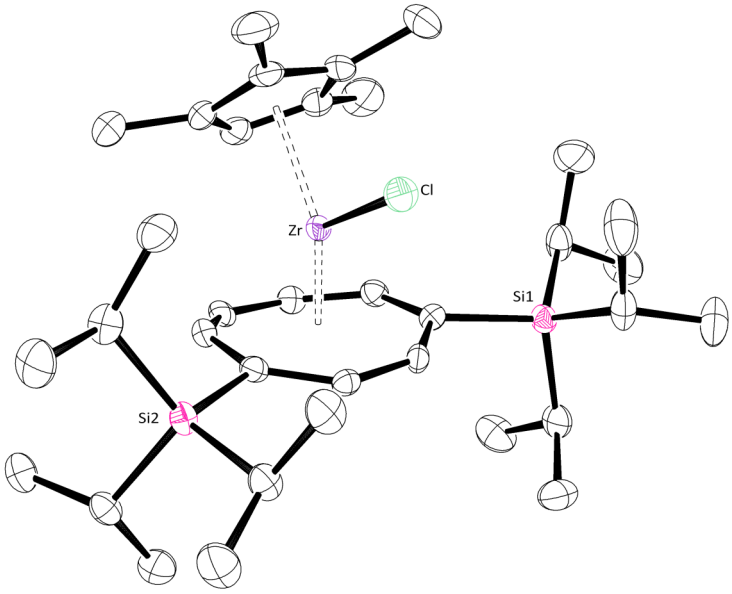

Figure 2.5: Molecular structure of [Zr(η^8-C_8H_6{Si^{i}Pr$_3$-1,4}$_2$)(Cp^{Me4H})Cl] (**2.7**). Hydrogen atoms are omitted for clarity. Thermal ellipsoids at 50 % probability level.

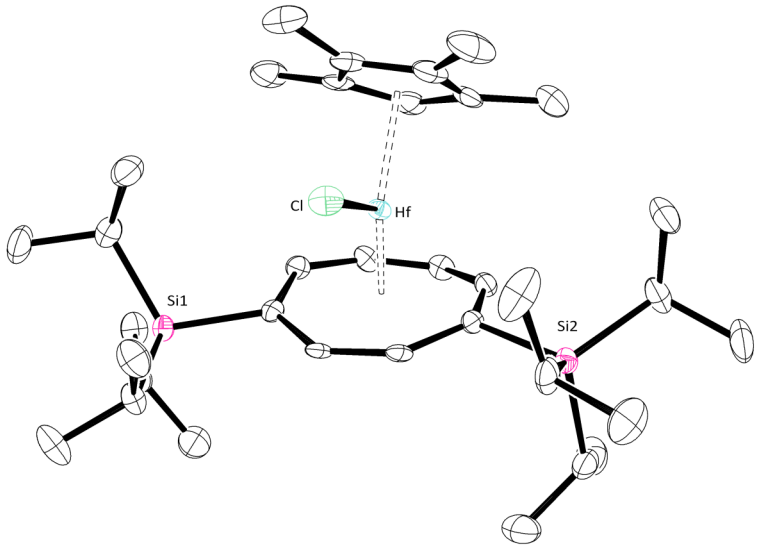

Figure 2.6: Molecular structure of [Hf(η^8-C_8H_6{Si^{i}Pr$_3$-1,4}$_2$)(Cp^{Me4H})Cl] (**2.8**). Hydrogen atoms are omitted for clarity. Thermal ellipsoids at 50 % probability level.

Again, there is little published crystallographic data relating to the M-Cp$^{Me4H}_{cent.}$ distances (where M = Zr, Hf). Regarding the Zr-Cp$^{Me4H}_{cent.}$ distances, most examples relate to zirconocene derivatives and average 2.25(3) Å, whilst figures for Hf-Cp$^{Me4H}_{cent.}$ largely correspond to mono-Cp compounds and average 2.24(3) Å. These values are in agreement with those observed in **2.7** and **2.8**. The outlying zirconium complex with a Zr-Cp$_{cent}$ length of 2.34 Å corresponds to (μ^2-Methyl)(μ^2-*t*-butylamido)-bis(η^5-tetramethylcyclopentadienyl)(THF)-lithium zirconium. It is not clear why the bond distance for this molecule is significantly greater than the average, although it is a very different type of compound and due to its unusual nature it will be omitted from this comparison.

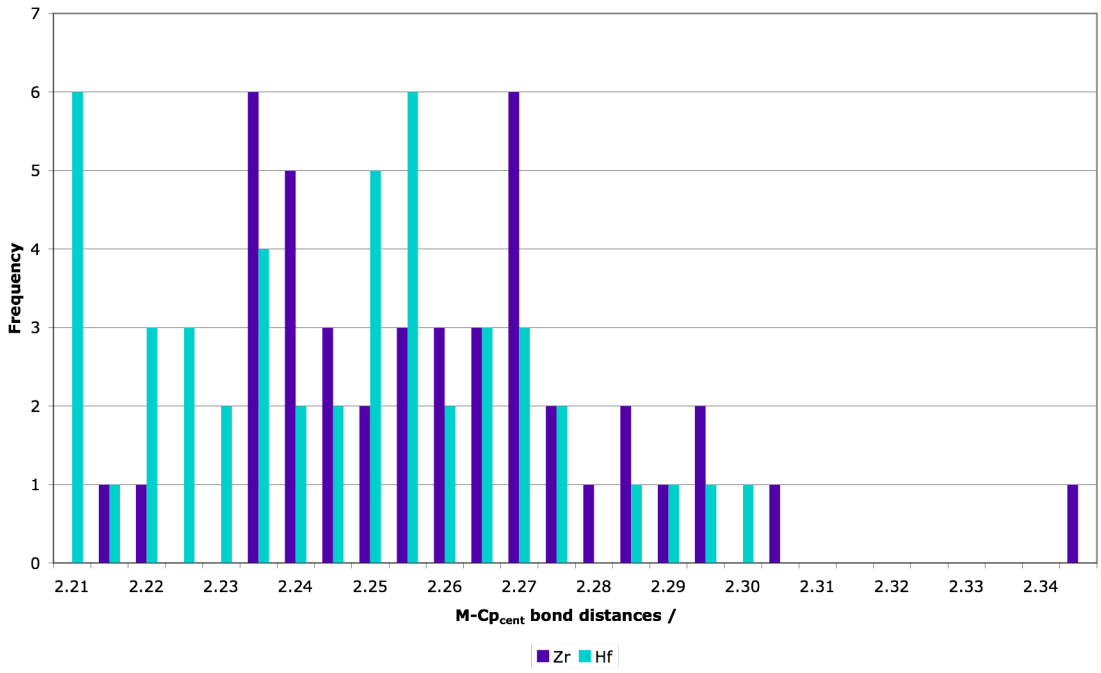

Figure 2.7: Zr-Cp$^{Me4H}{}_{cent.}$ and Hf-Cp$^{Me4H}{}_{cent.}$ distances where the Cp moiety is bound η^5 to the central metal atom.[8-10]

2.5 Characterisation of [M(η^8-C_8H_6{Si^{i}Pr$_3$-1,4}$_2$)(Cp^{Me5})Cl] (2.9 & 2.10)

Compounds **2.9** and **2.10** (**Figure 2.8** and **Figure 2.9**) crystallise in the triclinic space group $P\bar{1}$ and contain the pentamethylated cyclopentadienyl ligand. A large volume of data regarding published distances between the zirconium or hafnium and η^5-bound Cp^{Me5} are available, represented in **Figure 2.10**, and the average the Zr-Cp$^{Me5}{}_{cent.}$ and Hf-Cp$^{Me5}{}_{cent.}$ bond distances are calculated as 2.25(4) and 2.21(3) Å respectively: comparable to the measurements for **2.9** and **2.10** (2.254(2) and 2.23(4) Å).

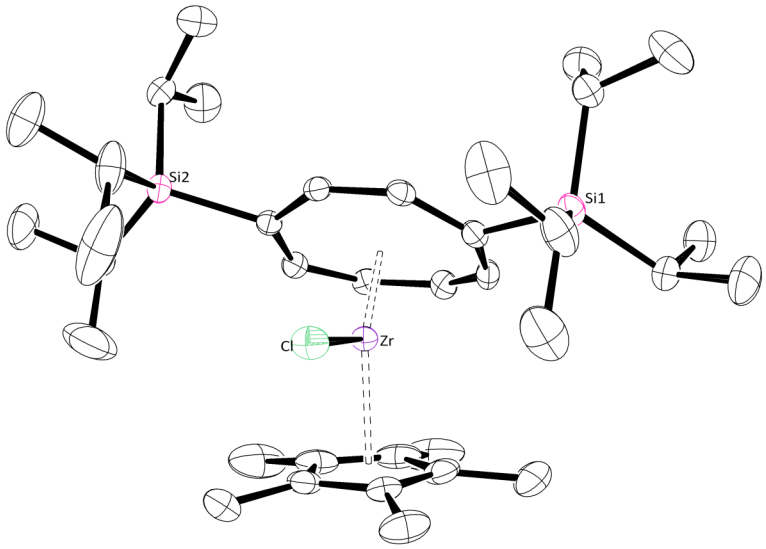

Figure 2.8: Molecular structure of [Zr(η^8-C_8H_6{Si^{i}Pr$_3$-1,4}$_2$)(Cp^{Me5})Cl] (**2.9**). Hydrogen atoms are omitted for clarity. Thermal ellipsoids at 50 % probability level.

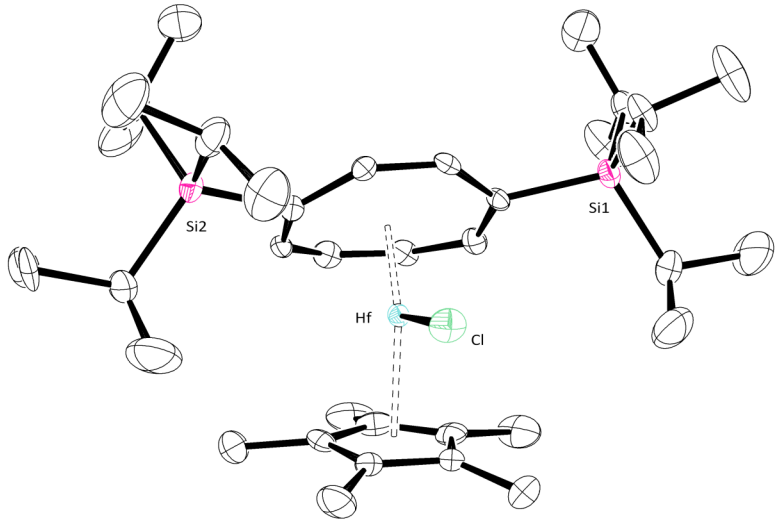

Figure 2.9: Molecular structure of [Hf(η^8-C_8H_6{Si^{i}Pr$_3$-1,4}$_2$)(Cp^{Me5})Cl] (**2.10**). Hydrogen atoms are omitted for clarity. Thermal ellipsoids at 50 % probability level.

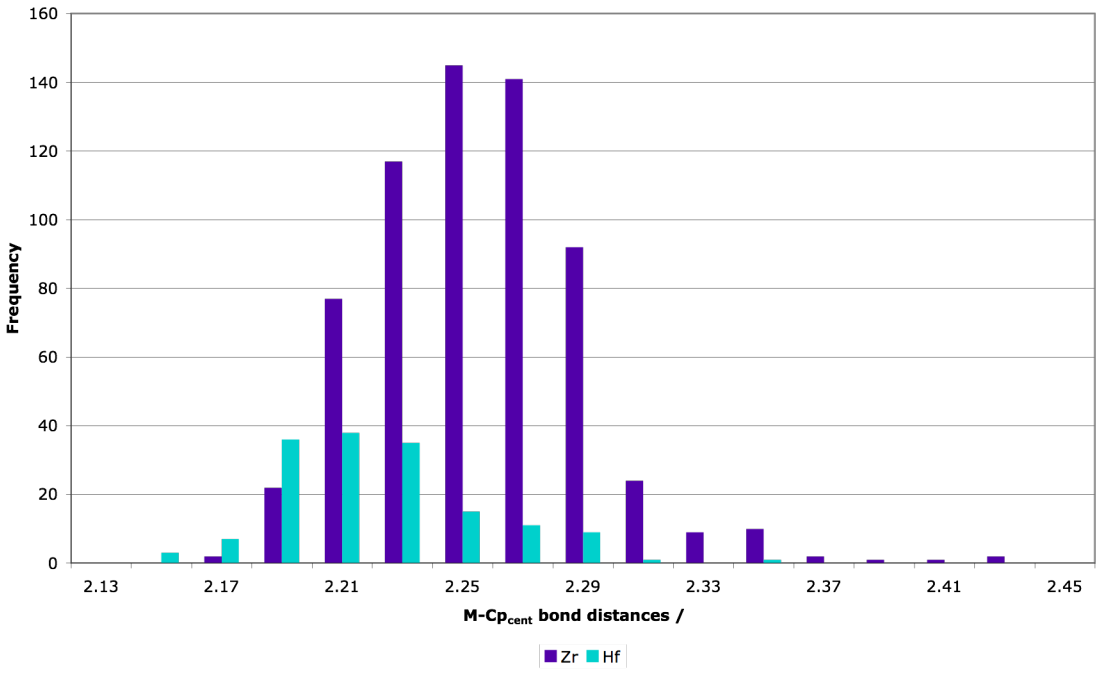

Figure 2.10: Zr-Cp$^{Me5}{}_{cent}$ and Hf-Cp$^{Me5}{}_{cent}$ distances where the Cp moiety is bound η^5 to the central metal atom.[8-10]

2.6 Characterisation of [M(η^8-C_8H_6{Si^{i}Pr$_3$-1,4}$_2$)(Cp$^{Me4(TMS)}$)Cl] (2.11 & 2.12)

Unlike previous compounds **2.7** – **2.10**, **2.11** and **2.12** both crystallise in the monoclinic space group C2/c (**Figure 2.11** and **Figure 2.12**). There are very few examples of compounds that contain a zirconium atom π-bonded to a Cp$^{Me4(TMS)}$ ligand, with instances described only by Mu *et al*[18] and Mach and coworkers[19]. Mu's work calculates the Zr-Cp$^{Me4(TMS)}{}_{cent.}$ distances as 2.2712(3) and 2.2698(12) Å, whilst Mach quotes lengths of 2.221(2), 2.226(9), 2.271(3) and 2.279(3) Å, all similar to the length seen in **2.11** at 2.260(15) Å. Data have not been published for Hf-Cp$^{Me4(TMS)}{}_{cent.}$ distances, but due to the similarity in size and chemical nature of zirconium and hafnium, the length measured in **2.12** can be easily compared to values calculated for zirconium examples, and are seen to be similar.

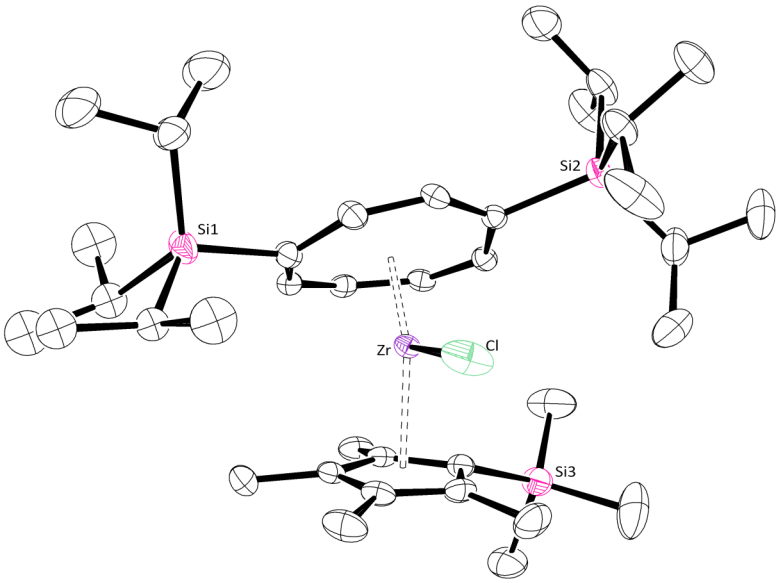

Figure 2.11: Molecular structure of [Zr(η^8-C_8H_6{Si^{i}Pr$_3$-1,4}$_2$)(Cp$^{Me(TMS)}$)Cl] (**2.11**). Hydrogen atoms are omitted for clarity. Thermal ellipsoids at 50 % probability level.

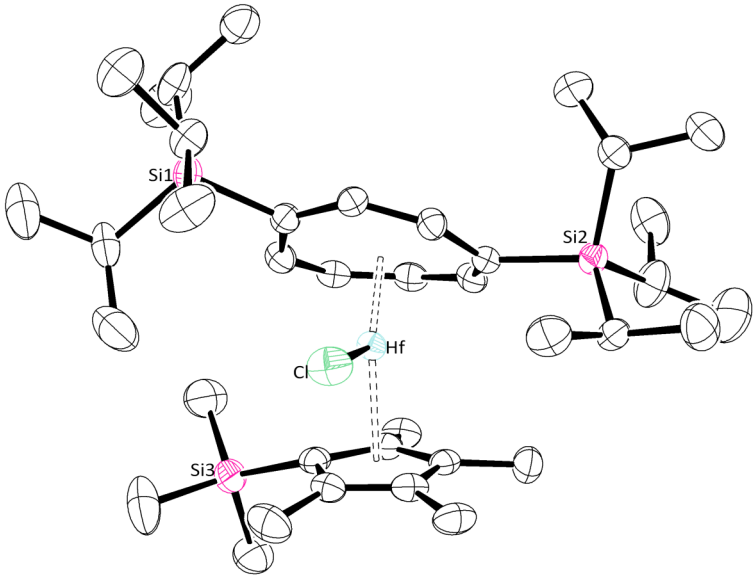

Figure 2.12: Molecular structure of [Hf(η^8-C_8H_6{Si^{i}Pr$_3$-1,4}$_2$)(Cp$^{Me4(TMS)}$)Cl] (**2.12**). Hydrogen atoms are omitted for clarity. Thermal ellipsoids at 50 % probability level.

For both **2.11** and **2.12**, the trimethylsilyl group is aligned with one of the tri*iso*propylsilyl groups in an eclipsed configuration, rather then occupying a less sterically conflicted staggered formation in the molecule. Also of note is the deviation of the TMS moiety from the plane of the Cp ring. This is due to the increase in p-character of the ring carbons on π-bonding to the metal centre, however, no unusual bonding modes are observed for the Cp ligand.

2.7 Cyclic voltammetry of [M(η^8-C_8H_6{Si^iPr_3-1,4}$_2$)(Cp^{Me4R})Cl]

Compounds **2.7** – **2.12** were further analysed by cyclic voltammetry, in order to obtain a more accurate redox potential for zirconium and hafnium centres bonded to the specific ligands discussed in this chapter, with the aim that these results could assist in the prediction or discussion of any reactivity towards small molecules. The results are summarised in **Table 2.3** and **Figure 2.13**.

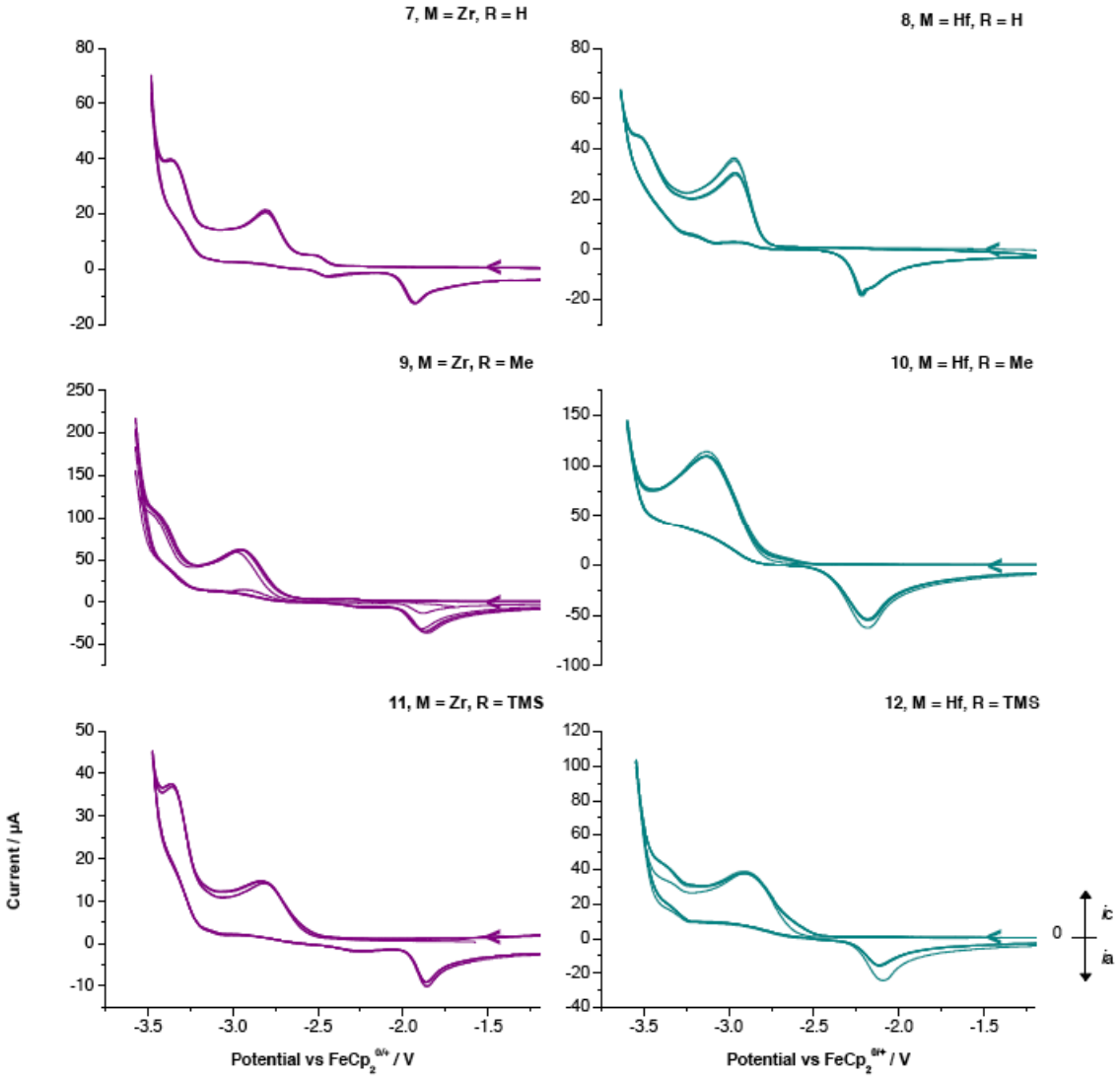

Figure 2.13: Six overlaid cyclic voltammograms of **2.7** (4.2 mM), **2.8** (4.5 mM), **2.9** (5.9 mM), **2.10** (6.5 mM), **2.11** (3.3 mM), **2.12** (3.2 mM) in THF containing 0.1 M $[N^nBu_4][PF_6]$. The scan rate was 100 $mV.s^{-1}$.

Table 2.3: Electrode potentials *versus* $FeCp_2^{0/+}$ in 0.1 M $[N^nBu_4][PF_6]$ in THF at a silver electrode at 27 °C.

Compound	M	R	E_p^{red} / V	E_p^{ox} / V
2.7	Zr	H	-2.81	-1.93
2.9	Zr	Me	-2.96	-1.88
2.11	Zr	$SiMe_3$	-2.83	-1.87
2.8	Hf	H	-2.98	-2.18
2.10	Hf	Me	-3.12	-2.18
2.12	Hf	$SiMe_3$	-2.91	-2.11

In each case, a clear reduction event was observed at approximately -3 V with respect to the ferrocene/ferrocenium couple, corresponding to a one electron reduction of the metal centre. The corresponding oxidation process is seen at approximately -2 V in each case. This *ca*. 1V separation between the reductive and oxidative peaks suggests that this could be either: (i) a chemically reversible, but electrochemically irreversible redox process that requires the application of a significant overpotential to overcome the electron transfer kinetics; (ii) that the initial reduction product of these complexes undergoes further homogeneous follow-up chemistry that generates a redox active species that can be oxidised at much more positive potentials. Further investigation does confirm that the oxidation wave observed upon reversing the scan direction is not present without the initial reduction of the Zr/Hf complexes **2.7** – **2.12** and that the peaks do not significantly decrease in intensity over time.

More negative potentials result in breakdown of the electrolyte or solvent with no overall effect on the quasi-reversible wave discussed above. More positive oxidation potentials beyond the ferrocene/ferrocenium waves were analysed, however, large unidentified peaks resulted with concurrent deposition on the surface of the working electrode.

When the E_p^{red} values for the zirconium compounds (**2.7**, **2.9** and **2.11**) are compared to the hafnium congeners (**2.8**, **2.10** and **2.12**) there is a difference, with slightly more positive values calculated for all zirconium complexes. This is as expected, based on the current information available regarding electrode potentials of similar zirconium and hafnium compounds.[20] Hafnium compounds are considered to have more negative redox potentials than their zirconium analogues, thus leading to different reactivity. The most reducing compounds for each metal seem to be those with the Cp^{Me5} moiety, with the Cp^{Me4H} derivatives giving similar results to the $Cp^{Me4(TMS)}$ complexes.

2.8 Synthesis and characterisation of [M(η^8-C_8H_6{Si^{i}Pr$_3$-1,4}$_2$)(Ind^{Me7})Cl] (M = Zr, 2.13) (M = Hf, 2.14)

In a similar manner to the previous zirconium mixed-ring chlorides described, a pale orange suspension of two equivalents of $KInd^{Me7}$ in toluene was added to an orange solution of **2.2** in toluene. The mixture turned green and was allowed to reflux at 120 °C for 24 hours resulting in a fine, pale precipitate. Extraction into pentane and subsequent crystallisation afforded **2.13** (**Figure 2.14**) as large, round orange crystals in moderate yield which were suitable for X-ray crystal diffraction studies. Mass spectrometry confirmed the identity of the **2.13** with the parent ion at m/z 755. The purity and identity of this product was further confirmed by ^1H NMR spectroscopy with the characteristic COT resonances observed as previously described. Also exhibited are three singlets with relative intensity 2:2:2:1 at 2.47, 2.32, 2.11 and 1.81 ppm, indicative of the heptamethylated indenyl moiety. $^{13}C\{^1H\}$ and $^{29}Si\{^1H\}$ NMR spectroscopy and 2D correlation experiments HSQC and HMBC were in agreement with the identity of **2.13**.

The hafnium analogue **2.14** was prepared similarly to **2.13**, appearing orange/red in colour during reflux ultimately affording small yellow crystals in poor yield that were unsuitable for single crystal diffraction studies. Resonances observed in ^1H, $^{13}C\{^1H\}$ and $^{29}Si\{^1H\}$

NMR spectroscopy were as noted previously with **2.13**. The anticipated parent ion peak was not detected by mass spectrometry, with m/z 826 the greatest value seen and corresponding to the loss of one methyl group.

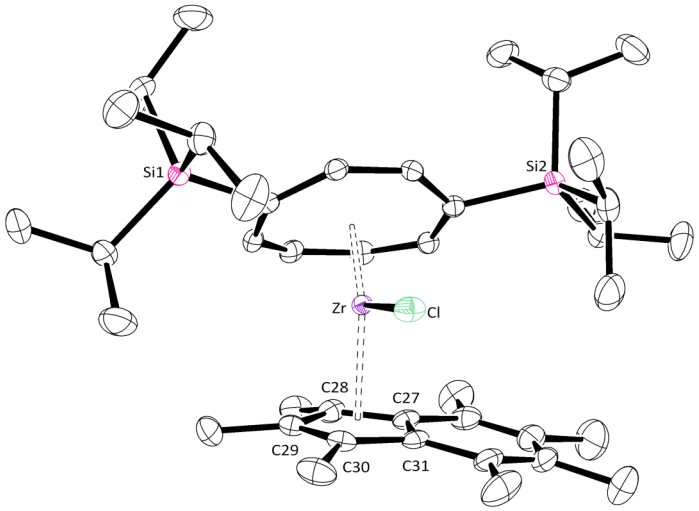

Figure 2.14: Molecular structure of [Zr(η^8-C_8H_6{Si^{i}Pr$_3$-1,4}$_2$)(Ind^{Me7})Cl] (**2.13**). Hydrogen atoms are omitted for clarity. Thermal ellipsoids at 50 % probability level.

Table 2.4: Selected bond angles (deg) and distances (Å) for **2.13**. $COT_{cent.}$ and $Ind_{cent.}$ indicate the centroid of the COT and Cp rings.

Zr-Cl	2.5565(4)
Zr-COT_{cent}	1.731(7)
Zr-Ind_{cent}	2.28(2)
COT_{cent}-Zr-Ind_{cent}	144.3(3)

The Zr-Cl and Zr-COT distances described in **Table 2.4** are consistent with those calculated for the zirconium compounds **2.7**, **2.9** and **2.11** (*vida supra*) and those figures available in the literature (**Figure 2.3** and **Figure 2.4**). The only published example containing the $ZrInd^{Me7}$ moiety $[Zr(\eta^5\text{-}C_9Me_7)_2Cl_2]$[21], shows Zr-$Ind_{cent.}$ distances of 2.511(4) and 2.612(4) Å, significantly longer than seen in **2.13**. These longer distances are due to the substantial methyl-methyl interactions in the bis(heptamethylindenyl) compound. The Zr-$Ind_{cent.}$ distance observed in **2.13** is more comparable to those seen in examples of compounds containing zirconium directly bound to an unsubstituted indenyl moiety, with distances typically observed between 2.196 and 2.303 Å.[22-39]

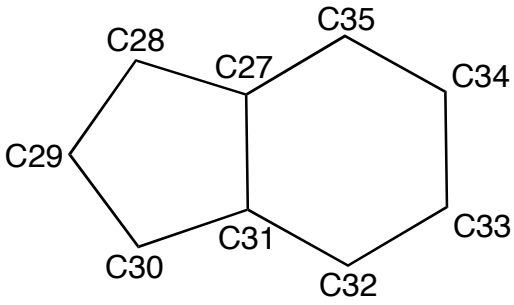

Figure 2.15: The hinge angle is defined as the angle between the planes [C28, C29, C30] and [C27, C28, C30, C31]. The fold angle is defined as the angle between the planes [C27, C28, C29, C30, C31] and [C27, C31, C32, C33, C34, C35].

Typically, distortions in metal-indenyl complexes can be defined in several ways (**Table 2.5**). The slip parameter is defined by Parkin and coworkers[40] as the difference in the average metal to ring-junction carbons C27, C31 and the other metal to carbon distances in the five-membered ring C28, C29, C30. In the case of **2.13**, this value is small at 0.05 Å, indicating no η^5 to η^3 ring slippage. However, the relatively large hinge and fold angles (**Figure 2.15**) suggest a significant distortion from planarity in the indenyl ligand. This could be due to steric repulsion between the methyl and *iso*propyl groups.

Table 2.5: Distortion parameters (deg, Å) for **2.13**.

Slip Parameter Δ_{M-C}	0.05
Hinge Angle	6.59
Fold Angle	35.93

2.9 Attempted synthesis of [Zr(η^8-C_8H_6{Si^{i}Pr$_3$-1,4}$_2$)(Cp$^{Me4(nBu)}$)Cl]

Attempts were made to synthesise a more sterically encumbered mixed-ring chloride complex of zirconium by employing Cp^{Me4nBu}. However, despite heating **2.2** to reflux over two days with 50 % excess of KCp^{Me4nBu} in toluene, only the starting material and a negligible amount of the desired product were observed by ^{1}H NMR spectroscopy. This synthesis was not pursued further.

2.10 Conclusions

Direct comparisons here show that the bond angles and lengths are similar between the zirconium and hafnium analogues described, whilst Zr(IV) and Hf(IV) compounds are structurally very similar, a fact supported by literature.[20] Yields from each synthesis described in this chapter are generally good and range from 39 to 66 %, with no significant difference in product yield between the Hf and Zr analogues, with upscaling of the reactions not affecting the amount of product successfully isolated.

2.11 Experimental details for Chapter Two

2.11.1 Synthesis of [Zr(η^8-C_8H_6{Si^{i}Pr$_3$-1,4}$_2$)Cl$_2$]$_2$ (2.2)

A green solution of [K_2(η^8-C_8H_6{Si^{i}Pr$_3$-1,4}$_2$)] (5.142 g, 10.409 mmol) in THF (100 cm^3) was added *via* cannula to a white suspension of $ZrCl_4$ (1.247 g, 5.398 mmol) in THF (30 cm^3) at ambient temperature with stirring. The mixture turned a deep wine-red colour on addition and was allowed to stir at reflux (65 °C) for 24 hours, with no further colour change observed. Volatiles were removed at reduced pressure before extraction with 3 x 20 cm^3 40-60 petroleum ether (filtered on a frit through dry Celite). Removal of the solvent at reduced pressure yielded [Zr(η^8-C_8H_6{Si^{i}Pr$_3$-1,4}$_2$)$_2$] as deep red sticky solids. This was dissolved in toluene (100 cm^3) before addition of a further equivalent of $ZrCl_4$ (1.225 g, 5.303 mmol) as a white suspension in toluene (30 cm^3) *via* cannula at ambient temperature with stirring. This was allowed to reflux (120 °C) with stirring for 48 hours yielding a dark orange-red solution. Removal of solvent at reduced pressure yielded brown residues. Washing with 4 x 25 cm^3 pentane yielded **2.2** as a pale orange powder.
Yield = 3.968 g (3.432 mmol), 66 % w.r.t. [K_2(η^8-C_8H_6{Si^{i}Pr$_3$-1,4}$_2$)].

MS (EI)$^+$: m/z = 535 (100 %), 1156 (2% M^+), 1121 (28% M^+ -Cl), 578 (24% M^+ - Zr(η^8-C_8H_6{Si^{i}Pr$_3$-1,4}$_2$)Cl$_2$), 535 (100% M^+ - Zr(η^8-C_8H_6{Si^{i}Pr$_3$-1,4}$_2$)Cl$_2$, -Cl).
Elemental analysis calcd (%) for $C_{52}H_{96}Cl_4Si_4Zr_2$: C 53.94, H 8.36; found: C 54.06, H 8.24.

2.11.2 Synthesis of [Zr(η^8-C_8H_6{Si^{i}Pr$_3$-1,4}$_2$)Cl$_2$(THF)] (2.5)

Compound **2.5** was synthesised as per **2.2**, obtaining X-ray quality crystals through recrystallisation from THF at -50 °C.

^{1}H NMR (THF-d_8, 399.5 MHz, 303 K): δ_H 7.04 (s, 4 H, COT-H), 7.02 (m, 4 H, COT-H), 6.92 (m, 4 H, COT-H), 1.73 (m, 12 H, ^{i}Pr-CH), 1.26 (d, $|^3J_{HH}|$ = 2.40 Hz, 36 H, CH_3), 1.24 (d, $|^3J_{HH}|$ = 2.46 Hz, 36 H, ^{i}Pr-CH_3).
^{13}C{^{1}H} NMR (THF-d_8, 100.5 MHz, 303 K): δ_C 107.96 (COT-*C*H), 105.33 (COT-*C*H), 104.00 (COT-*C*H), 101.49 (COT-*C*Si), 19.67 (^{i}Pr-*C*H$_3$), 19.59 (^{i}Pr-*C*H), 13.18 (^{i}Pr-*C*H$_3$).
^{29}Si{^{1}H} NMR (THF-d_8, 79.4 MHz, 303 K): δ_{Si} 11.60 (Si-^{i}Pr).
Elemental analysis calcd (%) for $C_{26}H_{48}Cl_2OSi_2Zr$: C 55.34, H 8.67; found: C 55.46, H 8.80.
Crystal data for **5**: Orange air-sensitive plate 0.14 × 0.04 × 0.03 mm^3, $C_{30}H_{56}Cl_2OSi_2Zr$, a = 7.4101(2), b = 13.1605(4), c = 18.6254(5) Å, α = 72.431(1)°, β = 79.710(2)°, γ = 76.160(2)°, U = 1670.21(8) Å^3, triclinic, $P\bar{1}$, Z = 2, total reflections 38048, independent reflections 7657, R_{int} = 0.077, θ_{max} = 27.48, R_1 [I >2σ(I)] = 0.062, wR^2 = 0.141 and 317 parameters.

2.11.3 Synthesis of $[Hf(\eta^8\text{-}C_8H_6\{Si^iPr_3\text{-}1,4\}_2)Cl_2]_2$ (2.4)

A green solution of $[K_2(\eta^8\text{-}C_8H_6\{Si^iPr_3\text{-}1,4\}_2)]$ (5.072 g, 10.267 mmol) in THF (100 ml) was added *via* cannula to a white suspension of $HfCl_4$ (1.636 g, 5.145 mmol) in THF (30 cm^3) at ambient temperature with stirring. The mixture turned pink/red in colour on addition and was allowed to stir at reflux (65 °C) for 24 hours, with no further colour change observed. Volatiles were removed at reduced pressure before extraction with 3 x 20 cm^3 40-60 petroleum ether (filtered on a frit through dry Celite). Removal of the solvent at reduced pressure yielded $[Hf(\eta^8\text{-}C_8H_6\{Si^iPr_3\text{-}1,4\}_2)_2]$ as a deep orange/red sticky matrix. This was dissolved in toluene (100 cm^3) before addition of a further equivalent of $HfCl_4$ (1.646 g, 5.176 mmol) as a white suspension in toluene (30 cm^3) *via* cannula at ambient temperature with stirring. This was allowed to reflux with stirring for 48 hours at 120 °C yielding a dark orange-red solution. Removal of solvent at reduced pressure yielded orange residues. Washing with 4 x 25 cm^3 pentane yielded **2.4** as a yellow powder.
Yield = 3.996 g (3.009 mmol), 58 % w.r.t. $HfCl_4$.

MS $(EI)^+$: m/z = 59 (100 %), 666 (25% M^+ -$(Hf(\eta^8\text{-}C_8H_6\{Si^iPr_3\text{-}1,4\}_2)Cl_2)$, 623 (95% M^+ -$(Hf(\eta^8\text{-}C_8H_6\{Si^iPr_3\text{-}1,4\}_2)Cl_2)$, -^{i}Pr).
Elemental analysis calcd (%) for $C_{52}H_{96}Cl_4Hf_2Si_4$: C 46.87, H 7.26; found: C 46.84, H 7.16.
Crystal data for **2.6**: Yellow air-sensitive plate 0.20 × 0.20 × 0.20 mm^3, $C_{26}H_{46}Cl_2OSi_2Hf$, a = 16.5996(3), b = 17.3425(4), c = 18.6224(4) Å, α = 85.7860(10)°, β = 71.5670(10)°, γ = 82.0410(10)°, U = 5034.43(18) $Å^3$, triclinic, $P\bar{1}$, Z = 7, total reflections 73390, independent reflections 21935, R_{int} = 0.0752, θ_{max} = 27.06, R_1 [I >2σ(I)] = 0.0568, wR^2 = 0.1237 and 958 parameters.
Elemental analysis calcd (%) for $C_{26}H_{48}Cl_2HfOSi_2$: C 48.80, H 7.64; found: C 48.89, H 7.74.

2.11.4 Synthesis of [Hf(η^8-C_8H_6{Si^{i}Pr$_3$-1,4}$_2$)Cl$_2$(THF)] (2.6)

This was synthesised as **2.4**, with recrystallisation from THF at -35 °C yielding material suitable for X-ray diffraction studies.

^{1}H NMR (THF-d_8, 399.5 MHz, 303K): δ 6.94 (s, 4H, COT-H), 6.90 (m, 4H, COT-H), 6.80 (m, 4H, COT-H), 1.68 (m, 12H, ^{i}Pr-CH), 1.22 (d, $|^3J_{HH}|$ =1.48 Hz, 36H, ^{i}Pr-CH$_3$), 1.20 (d, $|^3J_{HH}|$ = 1.76 Hz, 36H, ^{i}Pr-CH$_3$).
^{13}C{^{1}H} NMR (THF-d_8, 100.5 MHz, 303 K): δ_C 104.10 (COT-*C*H), 101.46 (COT-*C*H), 98.76 (COT-*C*H), 97.29 (COT-*C*Si), 18.45 (^{i}Pr-*C*H$_3$), 18.37 (^{i}Pr-*C*H$_3$), 12.04 (^{i}Pr-*C*H).
^{29}Si{^{1}H} NMR (THF-d_8, 79.4 MHz, 303 K): δ_{Si} 13.29 (Si-^{i}Pr).
Elemental analysis calcd (%) for $C_{26}H_{48}Cl_2HfOSi_2$: C 48.80, H 7.64; found: C 48.89, H 7.74.

2.11.5 Synthesis of [Zr(η^8-C_8H_6{Si^{i}Pr$_3$-1,4}$_2$)(Cp^{Me4H})Cl] (2.7)

A white suspension of KCp^{Me4H} (0.468 g, 2.925 mmol) in toluene (25 cm^3) was added dropwise with stirring, *via* cannula to an orange suspension of **2** (1.647 g, 1.425 mmol) in toluene (40 cm^3) to give a green solution. This was allowed to stir at reflux (120 °C), with the mixture appearing dark green-yellow after 90 minutes and darker green after heating overnight with the appearance of a dark precipitate. Solvent was removed at reduced pressure to yield green and pale brown solids before addition of pentane (60 cm^3) and freeze-thawing twice in liquid nitrogen. Filtration *via* filter cannula gave a clear olive-green solution that when concentrated and stored to -50 °C afforded yellow needle-like crystals of **2.7** suitable for X-ray diffraction studies.
Yield = 0.874 g (1.318 mmol), 46 % w.r.t. **2.2**.

^{1}H NMR (benzene-d_6, 399.5 MHz, 303 K): δ_H 6.87 (s, 2H, COT-H), 5.94 (m, 2H, COT-H), 5.66 (m, 2H, COT-H), 4.93 (s, 1H, Cp-H), 1.86 (s, 6H, Cp-CH$_3$), 1.70 (s, 6H, Cp-CH$_3$), 1.56 (septet, $|^3J_{HH}|$ = 7.44 Hz, 6H, ^{i}Pr-CH), 1.33 (d, $|^3J_{HH}|$ = 7.45 Hz, 18H, ^{i}Pr-CH$_3$), 1.22

(d, $|^3J_{HH}|$ = 7.44 Hz, 18H, ^{i}Pr-CH_3).

$^{13}C\{^1H\}$ NMR (benzene-d_6, 100.5 MHz, 303 K): δ_C 120.63 (Cp-*C*CH_3), 118.75 (Cp-*C*CH_3), 112.70 (COT-*C*H), 110.64 (Cp-*C*H), 100.94 (COT-*C*H), 98.21 (COT-*C*Si), 94.08 (COT-*C*H), 19.48 (^{i}Pr-*C*H_3), 14.58 (Cp-*C*H_3), 12.61 (^{i}Pr-*C*H), 11.85 (Cp-*C*H_3).

$^{29}Si\{^1H\}$ NMR (benzene-d_6, 79.4 MHz, 303 K): δ_{Si} 10.66 (s, Si^{i}Pr$_3$).

MS $(EI)^+$: m/z = 157 (100 %), 663 (3 % M^+), 628 (10 % M^+ -Cl), 545 (80 % M^+ - Cp^{Me4H}).

Elemental analysis calcd (%) for $C_{35}H_{61}ClSi_2Zr$: C 63.70, H 9.36; found: C 63.42, H 9.36.

Crystal data for **2.7**: Yellow air-sensitive prism 0.30 × 0.08 × 0.05 mm^3, $C_{35}H_{61}ClSi_2Zr$, a = 8.2098(2), b = 12.8103(5), c = 18.2306(7) Å, α = 70.354(2)°, β = 83.543(2)°, γ = 86.825(2)°, U = 1793.93(11) Å^3, triclinic, $P\bar{1}$, Z = 2, total reflections 27512, independent reflections 7011, R_{int} = 0.082, θ_{max} = 25.99, R_1 [I >2σ(I)] = 0.047, wR^2 = 0.080 and 368 parameters.

2.11.6 Synthesis of [Hf(η^8-C_8H_6{Si^{i}Pr$_3$-1,4}$_2$)(Cp^{Me4H})Cl] (2.8)

A pale yellow suspension of KCp^{Me4H} (0.370 g, 2.312 mmol) in toluene (20 cm^3) was added *via* cannula to a stirring, yellow solution of **2.4** (1.500 g, 1.129 mmol) in toluene (30 cm^3) at ambient temperature. This was allowed to stir under reflux overnight (120 °C), during which the mixture turned dark orange in colour with appearance of a fine precipitate. The mixture was extracted into pentane and free-thawed in liquid nitrogen before filtration *via* filter cannula. Storage in pentane at - 50 °C yielded fine needle-like pale yellow crystals of **2.8** suitable for single crystal diffraction study.

Yield = 1.058 g (1.407 mmol), 62 % w.r.t. **2.4**.

^1H NMR (benzene-d_6, 399.5 MHz, 303 K): δ_H 6.86 (s, 2H, COT-*H*), 5.88 (m, 2H, COT-*H*), 5.64 (m, 2H, COT-*H*), 4.82 (s, 1H, Cp-H), 1.94 (s, 6H, Cp-CH_3), 1.77 (s, 6H, Cp-CH_3) 1.57 (septet, $|^3J_{HH}|$ = 7.44 Hz, 6H, ^{i}Pr-CH), 1.34 (d, $|^3J_{HH}|$ = 7.48 Hz, 18H, ^{i}Pr-CH_3), 1.22 (d, $|^3J_{HH}|$ = 7.42 Hz, 18H, ^{i}Pr-CH_3).

$^{13}C\{^1H\}$ NMR (benzene-d_6, 100.5 MHz, 303 K): δ_C 119.50 (Cp-*C*CH_3), 117.06 (Cp-*C*CH_3), 111.99 (COT-*C*H), 108.66 (Cp-*C*H_3), 99.71 (COT-*C*H), 96.01 (COT-*C*Si), 91.03 (COT-*C*H), 20.00 (*i*Pr-*C*H_3), 19.93 (*i*Pr-*C*H_3), 15.02 (Cp-*C*H_3), 13.19 (^{i}Pr-*C*H), 12.20 (Cp-*C*H_3).
$^{29}Si\{^1H\}$ NMR (benzene-d_6, 79.4 MHz, 303 K): δ_{Si} 10.80 (s, Si^{i}Pr$_3$).
MS $(EI)^+$: m/z = 631 (100 %), 752 (M^+, 14 %), 709 (M^+ - ^{i}Pr, 4 %), 631 (M^+ - Cp^{Me4H}, 100 %).
Elemental analysis calcd (%) for $C_{35}H_{61}ClSi_2Hf_2$: C 55.69, H 8.10; found: C 55.90, H 8.18.
Crystal data for **2.8**: Yellow air-sensitive prism 0.18 × 0.11 × 0.05 mm^3, $C_{35}H_{61}ClSi_2Hf$, a = 8.2152(2), b = 12.7941(4), c = 18.2350(5) Å, α = 70.215(2)°, β = 83.412(2)°, γ = 86.929(2)°, U = 1791.34(9) Å^3, triclinic, $P\bar{1}$, Z = 2, total reflections 29302, independent reflections 8150, R_{int} = 0.078, θ_{max} = 27.48, R_1 [I >2σ(I)] = 0.040, wR^2 = 0.070 and 356 parameters.

2.11.7 Synthesis of [Zr(η^8-C_8H_6{Si^{i}Pr$_3$-1,4}$_2$)(Cp^{Me5})Cl] (2.9)

A white suspension of KCp^{Me5} (0.558 g, 3.206 mmol) in toluene (20 cm^3) was added dropwise with stirring, *via* cannula to an orange suspension of **2.2** (1.800 g, 1.557 mmol) in toluene (30 cm^3), turning green on addition. The reaction mixture was allowed to stir at reflux (120 °C) overnight, after which the solution had darkened and a pale precipitate was observed. Solvent was removed at reduced pressure yielding yellow-green residues which were extracted into pentane (50 cm^3) before freeze-thawing in liquid nitrogen. Filtration and subsequent cooling to - 50 °C of a concentrated solution resulted in yellow rectangular crystals of **2.9** suitable for X-ray diffraction study.
Yield = 0.974 g (1.439 mmol), 46 % w.r.t. **2.2**.

^1H NMR (benzene-d_6, 399.5 MHz, 303 K): δ_H 6.88 (s, 2H, COT-H), 5.85 (m, 2H, COT-H), 5.60 (m, 2H, COT-H), 1.73 (s, 15H, Cp-CH_3), 1.56 (septet, $|^3J_{HH}|$ = 7.43 Hz, 6H, ^{i}Pr-CH), 1.34 (d, $|^3J_{HH}|$ = 7.43 Hz, 18H, ^{i}Pr-CH_3), 1.22 (d, $|^3J_{HH}|$ = 7.43 Hz, 18H, ^{i}Pr-CH_3).
$^{13}C\{^1H\}$ NMR (benzene-d_6,100.5 MHz, 303 K): δ_C 119.67 (Cp-*C*CH_3), 113.32 (COT-*C*H), 101.03 (COT-*C*H), 98.62 (COT-*C*Si), 94.85 (COT-*C*H), 19.72 (^{i}Pr-*C*H_3), 13.06 (^{i}Pr-*C*H),

12.56 (Cp-*C*H_3).

^{29}Si{^{1}H} NMR (benzene-d_6, 79.4 MHz, 303 K): δ_{Si}10.73 (s, Si^{i}Pr$_3$).

MS (EI)$^+$: m/z = 677 (2 % M^+), 633 (2 % M^+ - ^{i}Pr), 541 (69 % M^+ - Cp^{Me5}).

Elemental analysis calcd (%) for $C_{36}H_{63}ClSi_2Zr$: C 63.24, H 9.25; found: C 63.16, H 9.04.

Crystal data for **2.9**: Yellow air-sensitive prism 0.25 × 0.20 × 0.05 mm^3, $C_{36}H_{63}ClSi_2Zr$, a = 8.5410(2), b = 13.0372(2), c = 18.6994(4) Å, α = 69.615(1)°, β = 88.160(1)°, γ = 71.287(1)°, U = 1841.16(6) Å^3, triclinic, $P\bar{1}$, Z = 2, total reflections 29392, independent reflections 7200, R_{int} = 0.044, θ_{max} = 26.02, R_1 [I >2σ(I)] = 0.032, wR^2 = 0.073 and 378 parameters.

2.11.8 Synthesis of [Hf(η^8-C_8H_6{Si^{i}Pr$_3$-1,4}$_2$)(Cp^{Me5})Cl] (2.10)

A white suspension of KCp^{Me5} (0.242 g, 1.391 mmol) in toluene (20 cm^3) was added *via* cannula to a yellow solution of **2.4** (0.857 g, 0.645 mmol) in toluene (30 cm^3) at ambient temperature, turning brighter yellow on addition. The reaction mixture was allowed to stir at reflux overnight (120 °C) after which a pale precipitate was observed. Removal of solvent at reduced pressure yielded a sticky orange solid which was extracted into pentane (30 cm^3) before freeze-thawing in liquid nitrogen. Filtration and storage of a concentrated solution at - 50 °C yielded yellow rectangular crystals of **2.10** suitable for single crystal diffraction study.

Yield = 0.407 g (0.533 mmol), 41 % w.r.t. **2.4**.

^{1}H NMR (benzene-d_6, 399.5 MHz, 303 K): δ_H 6.88 (s, 2H, COT-H), 5.78 (m, 2H, COT-H), 5.57 (m, 2H, COT-H), 1.80 (s, 15H, Cp-CH_3), 1.57 (septet, $|^3J_{HH}|$= 7.39 Hz, 6H, ^{i}Pr-CH), 1.35 (d, $|^3J_{HH}|$ = 7.37 Hz, 18H, ^{i}Pr-CH_3), 1.22 (d, $|^3J_{HH}|$= 7.10 Hz, 18H, ^{i}Pr-CH_3).

^{13}C{^{1}H} NMR (benzene-d_6, 100.5 MHz, 303 K): δ_C 117.82 (Cp-*C*CH_3), 112.65 (COT-*C*H), 99.27 (COT-*C*H), 96.29 (COT-*C*Si), 90.83 (COT-*C*H), 19.83 (^{i}Pr-*C*H_3), 12.87 (^{i}Pr-*C*H), 12.21 (Cp-*C*H_3).

^{29}Si{^{1}H} NMR (benzene-d_6, 79.4 MHz, 303 K): δ_{Si} 10.20 (s, Si^{i}Pr$_3$).

MS (EI)$^+$: m/z = 631 (100 %), 766 (14 % M^+), 723 (4 % M^+ - ^{i}Pr), 631 (100 % M^+ - Cp^{Me5}).

Elemental analysis calcd (%) for $C_{36}H_{63}ClHfSi_2$: C 56.45, H 8.29; found: C 56.68, H 8.12. Crystal data for **2.10**: Yellow air-sensitive prism 0.18 × 0.14 × 0.10 mm^3, $C_{36}H_{63}ClSi_2Hf$, a = 11.7530(2), b = 16.8027(3), c = 19.6881(3) Å, α = 99.778(1)°, β = 107.251(1)°, γ = 90.039(1)°, U = 3653.82(11) $Å^3$, triclinic, $P\bar{1}$, Z = 4, total reflections 56162, independent reflections 14702, R_{int} = 0.061, θ_{max} = 26.73, R_1 [I >2σ(I)] = 0.034, wR^2 = 0.069 and 741 parameters.

2.11.9 Synthesis of [Zr(η^8-C_8H_6{Si^{i}Pr$_3$-1,4}$_2$)(Cp$^{Me4(TMS)}$)Cl] (2.11)

A white suspension of $KCp^{Me4(TMS)}$ (0.675 g, 2.909 mmol) in toluene (20 cm^3) was added *via* cannula to a stirring dark orange solution of **2.2** (1.640 g, 1.419 mmol) in toluene (40 cm^3) at ambient temperature. This was allowed to heat under reflux (120 °C) overnight after which the solution appeared dark orange in colour with the appearance of a pale precipitate. Solvent was removed at reduced pressure before the addition of pentane and freeze-thawing in liquid nitrogen. The product was then filtered to yield a clear, dark orange solution that when concentrated and cooled to - 50 °C, yielded small, yellow, needle-like crystals of **2.11** suitable for X-Ray diffraction study.
Yield = 0.814 g (1.107 mmol), 39 % w.r.t. **2.2**.

^{1}H NMR (benzene-d_6, 399.5 MHz, 303 K): δ_H 6.88 (s, 2H, COT-H), 5.98 (m, 2H, COT-H), 5.66 (m, 2H, COT-H), 1.98 (s, 6H, Cp-CH_3), 1.70 (s, 6H, Cp-CH_3), 1.58 (septet, $|^3J_{HH}|$ = 7.41 Hz, 6H, ^{i}Pr-CH), 1.32 (d, $|^3J_{HH}|$ = 7.51 Hz, 18H, ^{i}Pr-CH_3), 1.24 (d, $|^3J_{HH}|$ = 7.51 Hz, 18H, ^{i}Pr-CH_3), 0.34 (s, 9H, Si-CH_3).
^{13}C{^{1}H} NMR (benzene-d_6, 100.5 MHz, 303 K): δ_C 125.86 (Cp*C*CH_3), 124.03(Cp*C*CH_3), 119.24 (Cp*C*Si), 113.43 (COT-*C*H), 100.43 (COT-*C*H), 100.27 (COT-*C*Si), 93.50 (COT-*C*H), 19.59 (^{i}Pr-*C*H_3), 19.52 (^{i}Pr-*C*H_3), 15.65 (Cp*C*H_3), 12.78 (^{i}Pr-*C*H), 12.69 (Cp*C*H_3), 2.50 (CpSi*C*H_3).
^{29}Si{^{1}H} NMR (benzene-d_6, 79.4 MHz, 303 K): δ_{Si} 10.48 (s, Si^{i}Pr$_3$), -7.26 (s, $SiCH_3$).
MS (EI)$^+$: m/z = 545 (100 %), 735 (M^+ 3 %), 690 (M^+ -^{i}Pr 4 %), 545 (M^+ -Cp$^{Me4(TMS)}$).
Elemental analysis calcd (%) for $C_{38}H_{69}ClSi_3Zr$: C 61.80, H 9.28; found: C 61.94, H 9.44.

Crystal data for **2.11**: Yellow air-sensitive prism 0.22 × 0.20 × 0.09 mm^3, $C_{38}H_{69}ClSi_3Zr$, a = 39.4051(6), b = 8.6243(1), c = 24.9173(4) Å, α = 90°, β = 108.989(1)°, γ = 90°, U = 7975.0(2) $Å^3$, monoclinic, C 2/c, Z = 8, total reflections 57242, independent reflections 8771, R_{int} = 0.063, θ_{max} = 27.10, R_1 [I >2σ(I)] = 0.036, wR^2 = 0.077 and 417 parameters.

2.11.10 Synthesis of [Hf(η^8-C_8H_6{Si^{i}Pr$_3$-1,4}$_2$)(Cp$^{Me4(TMS)}$)Cl (2.12)

A white suspension of $KCp^{Me4(TMS)}$ (0.721 g, 3.108 mmol) in toluene (20 cm^3) was added *via* cannula to a yellow solution of **2.4** (2.057 g, 1.549 mmol) in toluene (30 cm^3) at ambient temperature with stirring, turning brighter yellow on addition. This mixture was allowed to heat at reflux (120 °C) overnight resulting in an orange solution with pale precipitate. Solvent was removed at reduced pressure and the product taken up in pentane. This was freeze-thawed three times in liquid nitrogen before filtration *via* filter cannula. Storage of a concentrated solution at -50 °C afforded yellow needle-like crystals. Subsequent recrystallisation from DME afforded crystals of **2.12** that were suitable for X-ray diffraction study.

Yield = 1.599 g (1.945 mmol), 63 % w.r.t. **2.4**.

^{1}H NMR (toluene-d_8, 399.5 MHz, 303K): δ_H 6.80 (s, 2H, COT-H), 5.84 (m, 2H, COT-H), 5.61 (m, 2H, COT-H), 2.05 (s, 6H, Cp-CH_3), 1.76 (s, 6H, Cp-CH_3), 1.56 (septet, $|^3J_{HH}|$ = 7.50 Hz, 6H, ^{i}Pr-CH), 1.32 (d, $|^3J_{HH}|$ = 7.41 Hz, 18H, ^{i}Pr-CH_3), 1.22 (d, $|^3J_{HH}|$ = 7.61 Hz, 18H, ^{i}Pr-CH_3), 0.30 (s, 9H, Si-CH_3).

^{13}C{^{1}H} NMR (toluene-d_8, 100.5 MHz, 303K): δ_C 124.02 (Cp-*C*CH_3), 122.78 (Cp-*C*CH_3), 117.39 (Cp-*C*Si), 113.40 (COT-*C*H), 99.29 (COT-*C*H), 98.76 (COT-*C*Si), 89.84 (COT-*C*H), 20.11 (^{i}Pr-*C*H_3), 20.01 (^{i}Pr-*C*H_3), 15.96 (Cp-*C*H_3), 13.44 (^{i}Pr-*C*H), 12.96 (Cp-*C*H_3), 2.94 (CpSi*C*H_3).

^{29}Si{^{1}H} NMR (toluene-d_8, 79.4 MHz, 303 K): δ_{Si} 10.30 (s, Si^{i}Pr$_3$), -7.21 (s, $SiMe_3$).

MS $(EI)^+$: m/z = 631 (100 %), 824 (M^+, 27 %), 781 (M^+ -^{i}Pr, 38 %), 631 (M^+, -Cp$^{Me4(TMS)}$, 100 %).

Elemental analysis calcd (%) for $C_{38}H_{69}ClHfSi_3$: C 55.37, H 8.44; found: C 55.57, H 8.56.

Crystal data for **2.12**: Yellow air-sensitive needles 0.20 × 0.04 × 0.04 mm^3, $C_{38}H_{69}ClSi_3Hf$,

a = 38.9412(15), b = 8.6080(4), c = 24.9700(10) Å, α = 90°, β = 108.2910(10)°, γ = 90°, U = 7947.2(6) Å^3, monolinic, C2/c, Z = 8, total reflections 53417, independent reflections 8085, R_{int} = 0.0720, θ_{max} = 26.37, R_1 [I >2σ(I)] = 0.0431, wR^2 = 0.1006 and 388 parameters.

2.11.11 Synthesis of [Zr(η^8-C_8H_6{Si^{i}Pr$_3$-1,4}$_2$)(Ind^{Me7})Cl] (2.13)

A pale orange suspension of KInd^{Me7} (0.325 g, 1.290 mmol) in toluene (20 cm^3) was added dropwise with stirring, *via* cannula to a stirring orange solution of **2.2** (0.746 g, 6.453 mmol) in toluene (20 cm^3), turning green on addition. The reaction mixture was allowed to heat under reflux (120 °C) for 48 hours during which time the mixture become orange/green in colour with the appearance of a fine precipitate. This was filtered on a frit through dry Celite and washed with 3 x 20 cm^3 toluene to yield a green solution. Crystallisation from pentane at -50 °C yielded **2.13** as large orange crystals suitable for X-ray diffraction studies.
Yield = 0.439 g (0.581 mmol), 45 % w.r.t. **2.2**.

^{1}H NMR (benzene-d_6, 399.5 MHz, 303 K): δ_H 6.81 (s, 2H, COT-H), 5.86 (m, 2H, COT-H), 5.48 (m, 2H, COT-H), 2.47 (s, 2H, Ind-CH), 2.32 (s, 2H, Ind-CH), 2.11 (s, 2H, Ind-CH), 1.81 (s, 1H, Ind-CH), 1.51 (septet, $|^3J_{HH}|$ = 7.47 Hz, 6H, ^{i}Pr-CH), 1.34 (d, $|^3J_{HH}|$ = 7.25 Hz, 18H, ^{i}Pr-CH$_3$), 1.21 (d, $|^3J_{HH}|$ = 7.32 Hz, 18H, ^{i}Pr-CH$_3$).
^{13}C{^{1}H} NMR (benzene-d_6, 100.5 MHz, 303K): δ_C 131.58 (Ind-*C*), 128.18 (Ind-*C*CH$_3$), 127.94 (Ind-*C*CH$_3$), 124.80 (Ind-*C*CH$_3$), 113.14 (COT-*C*H), 110.42 (Ind-C*C*H$_3$), 102.44 (COT-*C*H), 99.72 (COT-*C*Si), 95.28 (COT-*C*H), 19.73 (^{i}Pr-*C*H$_3$), 19.51 (^{i}Pr-*C*H$_3$), 17.88 (Ind-*C*H$_3$), 16.67 (Ind-*C*H$_3$), 16.09 (Ind-*C*H$_3$), 13.05 (^{i}Pr-*C*H), 12.78 (Ind-*C*H$_3$).
^{29}Si{^{1}H} NMR (benzene-d_6, 79.4 MHz, 303 K): δ_{Si} 10.62 (s, Si^{i}Pr$_3$).
MS (EI)$^+$: m/z = 199 (100 %), 755 (M$^+$ 1 %), 711 (M$^+$ -^{i}Pr 6 %).
Crystal data for **2.13**: Yellow air-sensitive prism 0.23 × 0.19 × 0.16 mm^3, $C_{42}H_{69}ClSi_2Zr$, a = 8.8796(2), b = 19.3965(3), c = 12.5711(3) Å, α = 90°, β = 109.913(1)°, γ = 90°, U = 2035.71(7) Å^3, monoclinic, P 2$_1$, Z = 2, total reflections 33308, independent reflections

9154, R_{int} = 0.054, θ_{max} = 27.48, R_1 [I >2σ(I)] = 0.028, wR^2 = 0.061 and 422 parameters.

2.11.12 Synthesis of [Hf(η^8-C_8H_6{Si^{i}Pr$_3$-1,4}$_2$)(Ind^{Me7})Cl] (2.14)

A pale orange suspension of KInd^{Me7} (0.193 g, 0.753 mmol) in toluene (20 cm^3) was added dropwise *via* cannula to a stirring orange solution of **2.4** (0.497 g, 0.376 mmol) in toluene (20 cm^3), turning green in colour and becoming cloudy on further addition. The reaction mixture was allowed to heat to reflux (120 °C) for 24 hours, during which time the mixture become bright orange-red in colour with the appearance of a fine precipitate. This was filtered on a frit through dry Celite and washed with 3 x 20 ml toluene, which was subsequently removed to yield an orange sticky solid. Crystallisation from pentane at -20 °C yielded small yellow crystals of **2.14** unsuitable for single crystal diffraction studies.
Yield = 0.144 g (0.171 mmol), 23 % w.r.t.**2.4**.

^{1}H NMR (benzene-d_6, 399.5 MHz, 303 K): δ_H 6.81 (s, 2H, COT-H), 5.78 (m, 2H, COT-H), 5.38 (m, 2H, COT-H), 2.46 (s, 2H, Ind-CH_3), 2.39 (s, 2H, Ind-CH_3), 2.13 (s, 2H, Ind-CH_3), 1.91 (s, 1H, Ind-CH_3), 1.52 (septet, $|^3J_{HH}|$ = 7.40 Hz, 6H, ^{i}Pr-CH), 1.36 (d, $|^3J_{HH}|$ = 7.40 Hz, 18H, ^{i}Pr-CH_3), 1.21 (d, $|^3J_{HH}|$ = 7.16 Hz, 18H, ^{i}Pr-CH_3).
^{13}C{^{1}H} NMR (benzene-d_6, 100.5 MHz, 303K): δ_C 131.37 (Ind-*C*), 128.20 (Ind-*C*CH_3), 127.50 (Ind-*C*CH_3), 123.60 (Ind-*C*CH_3), 112.18 (COT-*C*H), 107.44 (Ind-C*C*CH_3), 100.59 (COT-*C*H), 96.92 (COT-*C*Si), 91.10 (COT-*C*H), 19.68 (^{i}Pr-*C*H_3), 19.54 (^{i}Pr-*C*H_3), 17.91 (Ind-*C*H_3), 16.55 (Ind-*C*H_3), 15.81 (Ind-*C*H_3), 13.14 (^{i}Pr-*C*H), 12.92 (Ind-*C*H_3).
^{29}Si{^{1}H} NMR (benzene-d_6, 79.4 MHz, 303 K): δ_{Si} 10.04 (s, Si^{i}Pr$_3$).
MS (EI)$^+$: m/z = 59 (100 %), 826 (M^+ -Me, 1 %), 808 (M^+ -Cl, 2 %), 794 (M^+ -Me, 7 %), 765 (M^+ -Me, 7 %).

2.11.13 Electrochemical analysis of compounds 2.7 – 2.12

Electrochemical studies were performed in dry THF containing 0.1 M [N^{n}Bu$_4$][PF$_6$] as the supporting electrolyte using a BASi Epsilon-EC potentiostat under computer control, performed by A. Kilpatrick of the University of Sussex. Cyclic voltammetry experiments were performed using a three-electrode configuration with a glassy carbon disc having an area of 7.0 mm^2 as the working electrode, a platinum wire as the counter electrode and a silver wire as the pseudoreference electrode. The Ag wire pseudoreference electrode was calibrated to the ferrocene/ferrocenium couple in THF, relative to which all of the standard potentials are reported. Ferrocene (*ca*. 3 mg) was added to a 0.1 M solution of electrolyte in THF (5 cm^3) containing the dissolved metal compounds (3 – 6 mM).

2.12 References for Chapter Two

1. J. Blenkers, P. Bruin and J. H. Teuben, *J. Organomet. Chem.*, 1985, **297**, 61-67.
2. R. D. Rogers and J. H. Teuben, *J. Organomet. Chem.*, 1989, **359**, 41-47.
3. W. J. Highcock, R. M. Mills, J. L. Spencer and P. Woodward, *J. Chem. Soc. Dalton Trans.*, 1986, 821-827.
4. P. Berno, C. Floriani, A. Chiesi-Villab and C. Rizzoli, *J. Chem. Soc. Dalton Trans.*, 1991, 3093-3095.
5. N. A. Morley-Smith, *D.Phil Thesis, University of Sussex*, 2001.
6. S. C. P. Joseph, *D.Phil. Thesis, University of Sussex*, 1994.
7. D. J. Brauer and C. Krüger, *Inorg. Chem.*, 1975, **14**, 3053-3056.
8. D. A. Fletcher, R. F. McMeeking and D. Parkin, *J. Chem. Inf. Comput. Sci.*, 1996, **46**, 746-749.
9. F. H. Allen, *Acta Crystallogr., Sect. B: Struct. Sci*, 2002, **58**, 380-388.
10. I. J. Bruno, J. C. Cole, P. R. Edgington, M. Kessler, C. F. Macrae, P. McCabe, J. Pearson and R. Taylor, *Acta Crystallogr., Sect. B: Struct. Sci*, 2002, **58**, 389-397.
11. F. G. N. Cloke, P. B. Hitchcock and S. C. P. Joseph, *J. Chem. Soc., Chem. Commun.*, 1994, 1207-1208.
12. P. Berno, C. Floriani, A. Chiesi-Villa and C. Guastini, *J. Chem. Soc., Chem. Commun.*, 1991, 109-110.
13. P. Berno, S. Stella, C. Floriani, A. Chiesi-Villa and C. Guastini, *J. Chem. Soc., Dalton Trans.*, 1990, 2669-2677.
14. P.-J. Sinnema, A. Meetama and J. H. Teuben, *Organometallics*, 1993, **12**, 184-189.
15. P. Binger, S. Leininger, K. Günther and U. Bergsträßer, *Chem. Ber.*, 1997, **130**, 1491-1494.
16. P. Berno, C. Floriani, A. Chiesi-Villab and C. Rizzoli, *J. Chem. Soc., Dalton Trans.*, 1991, 3085-3091.
17. A. F. Hill and M. K. Smith, *Organometallics*, 2007, **26**, 3900-3903.
18. Y. Mu, W. E. Piers, L. R. MacGillivray and M. J. Zaworotko, *Polyhedron*, 1995, **14**, 1-10.

19. M. Horácek, P. Stepnicka, J. Kubis, K. Fejfarová, R. Gyepes and K. Mach, *Organometallics*, 2003, **22**, 861-869.
20. D. J. Cardin, M. F. Lappert and C. L. Raston, *Chemistry of Organo-Zirconium and - Hafnium Compounds*, 1st edn., Ellis Horwood Limited, Chichester, 1986.
21. D. O'Hare, V. Murphy, G. M. Diamond, P. Arnold and P. Mountford, *Organometallics*, 1994, **13**, 4689-4694.
22. J. C. Gallucci, B. Gautheron, M. Gugelchuk, P. Meunier and L. A. Paquetter, *Organometallics*, 1987, **6**, 15-19.
23. M. D. Rausch, K. J. Moriarty, J. L. Atwood, W. E. Hunter and E. Samuel, *J. Organomet. Chem.*, 1987, **327**, 39-54.
24. L. A. Paquette, K. J. Moriarty, P. Meunier, B. Gautheron, C. Sornay, R. D. Rogers and A. L. Rheingold, *Organometallics*, 1989, **8**, 2159-2167.
25. L. A. Paquette, K. J. Moriarty and R. D. Rogers, *Organometallics*, 1989, **8**, 1506-1511.
26. T. Repo, M. Klinga, L. Mutikainen, Y. Su, M. Leskela and M. Polamo, *Acta Chem. Scand.*, 1996, **50**, 1116.
27. M. A. Schmid, H. G. Alt and W. Milius, *J. Organomet. Chem.*, 1996, **514**, 45-49.
28. R. Kempe, A. Spannenberg, N. Peulecke and U. Rosenthal, *Z. Kristallogr. - New Cryst. Struct.*, 1998, **213**, 629.
29. N. Peuleckea, W. Baumanna, R. Kempea, V. V. Burlakovb and U. Rosenthal, *Eur. J. Inorg. Chem.*, 1998, **1998**, 419-424.
30. M. Rahim, N. J. Taylor, S. Xin and S. Collins, *Organometallics*, 1998, **17**, 1315-1323.
31. N. W. Alcock, H. J. Clase, D. J. Duncalf, S. L. Hart, A. McCamley, P. J. McCormack and P. C. Taylor, *J. Organomet. Chem.*, 2000, **605**, 45-54.
32. R. Fischer, D. Walther, P. Gebhardt and H. Görls, *Organometallics*, 2000, **19**, 2532-2540.
33. J. R. Ascenso, C. G. d. Azevedo, M. J. Correia, A. R. Dias, M. T. Duarte, J. L. F. d. Silva, P. T. Gomes, F. Lourenço, A. M. Martins and S. S. Rodrigues, *J. Organomet. Chem.*, 2001, **632**, 58-66.

34. P. Binger, P. Müller, S. Podubrin, S. Albus and C. Krüger, *J. Organomet. Chem.*, 2002, **656**, 288-298.

35. H. Sun, A. Spannenberg, V. V. Burlakov, W. Baumann, P. Arndt and U. Rosenthal, *Z. Kristallogr. - New Cryst. Struct.*, 2002, **217**, 237.

36. A. M. Martins, J. R. Ascenso, C. G. d. Azevedo, A. R. Dias, M. T. Duarte, J. F. d. Silva, L. F. Veiros and S. S. Rodrigues, *Organometallics*, 2003, **22**, 4218-4228.

37. A. Spannenberg, P. Arndt, W. Baumann, V. V. Burlakov, U. Rosenthal, S. Becke and T. Weiss, *Organometallics*, 2004, **23**, 3819-3825.

38. E. Verguet, R.-V. Fortune, P. O. Oguadinma and F. Schaper, *Acta Crystallogr. Sect. E: Struct. Rep. Online*, 2007, **63**, m2539.

39. S. Ren, E. Igarashi, K. Nakajima, K.-i. Kanno and T. Takahashi, *J. Am. Chem. Soc.*, 2009, **131**, 7492-7493.

40. T. M. Trnka, J. B. Bonanno, B. M. Bridgewater and G. Parkin, *Organometallics*, 2001, **20**, 3255-3264.

3 CHAPTER THREE: REDUCTION OF ZIRCONIUM AND HAFNIUM MIXED-RING CHLORIDES

3.1 Introduction

Whilst the synthesis of a U(III) mixed-sandwich complex proceeds *via* a series of U(III) intermediates (as described in chapter 1), this direct approach cannot be applied to the zirconium and hafnium congeners. The starting material, uranium triiodide, can be isolated cleanly and in good yield[1, 2] and is unusually stable considering the low oxidation state of the metal. However, the synthesis of clean zirconium and hafnium trihalides is more challenging and time-consuming, requiring harsh conditions. A report by Corbett *et al* suggests that disproportion of a mixture of ZrX_4 and ZrX (X = Cl, Br, I) at 350 – 600 ºC for 10 days results in a highly pure and crystalline product in a quantitative yield. A later investigation into the use of low-temperature aluminium halide melts by Larsen *et al*[3] involved the dissolution of ZrX_4 in liquid AlX_3 at the eutectic composition before reduction by either zirconium or aluminium metal at 220 – 300 ºC to again produce a highly crystalline and pure product, although the absence of aluminium in the final compound cannot be guaranteed. Although these preparative steps do not require the extremely high pressures as seen with earlier investigations[4], there still remains a non-stoichiometry when X = I, resulting in $ZrI_{3.4}$, and no method has been found suitable for the clean production of hafnium trihalide.

Due to the ease with which both zirconium and hafnium tetrahalides can be obtained and purified by sublimation, the production of the mixed-ring metal chlorides and their subsequent reduction to the active +3 compound was pursued in this work. The first example of a mixed ring Zr(III) compound, where the aromatic moieties are COT and Cp^{Me5}, was described by Teuben and coworkers in 1985,[5] with details from single crystal X-ray diffraction studies published shortly afterwards.[6, 7] This compound was the first thermally stable paramagnetic organozirconium(III) compound isolated in the solid state to be published. Difficulties were experienced, however, in isolation of the

hafnium analogue, with sublimation and subsequent identification revealing a diamagnetic hydridic Hf(IV) compound. Examples of fully characterised mononuclear Zr(III) and Hf(III) organometallic complexes remain rare due to their instability and relative inaccessibility.[8-12]

Based on the similar physical properties of zirconium and hafnium complexes with respect to bond lengths, ionic radii and redox potentials, it was assumed that both metals would respond similarly under the same reaction conditions to produce the mixed-ring chlorides (described in Chapter 2) and this was indeed the case. With such sterically bulky ligands used in these M(IV) complexes, successful reduction should occur similarly for both zirconium and hafnium compounds resulting in the desired M(III) centre. The attempts of synthesis, isolation and characterisation of [M(η^8-$C_8H_6\{Si^iPr_3\text{-}1,4\}_2$)($Cp^{Me4R}$)] will be described in this chapter.

3.2 Reduction of zirconium mixed-ring complexes

Many different reduction conditions were attempted on the zirconium systems discussed in this work, the results of which are summarised in **Table 3.1**. Whilst elemental magnesium and magnesium anthracene appeared to be successful reductants, difficulties in isolating the product without contamination from magnesium dichloride or anthracene prevented further pursuit of these methods. Use of the potassium graphite (**Scheme 3.1**) intercalation compound KC_8 resulted in less soluble by-products that were easier to remove from the desired product, whilst it became clear that the use of THF led to an increased range of unidentifiable impurities as observed by ^{1}H NMR spectroscopy. This possibly results from the ring-opening or polymerisation susceptibility of the solvent. Tractable, cleaner products were accessed when toluene was instead employed.

Table 3.1: Summary of attempted reductions of [Zr(η^8-C_8H_6{Si^{i}Pr$_3$-1,4}$_2$)(Cp^{Me5})Cl]. In each case, the product was extracted with pentane before attempted recrystallisation from a saturated solution at low temperatures.

Reducing Agent and Conditions	Result
LiDBB[a] THF, -78 ºC → RT, 16 h	Incomplete reduction DBB contamination
MgAn[b](THF)$_3$ THF, 0 ºC → RT, 16 h	Intractable dark red product with anthracene contamination
Finely divided magnesium THF, -78 ºC → RT, 16 h	Intractable dark red product. Difficult to remove $MgCl_2$
KC_8 THF, -78 ºC → RT, 1 week	Intractable dark red product
KC_8 Toluene, -78 ºC → RT, 1 week	Dark red crystals isolated from pentane

[a] : Di-*tert*-butylbiphenyl, [b] : anthracene

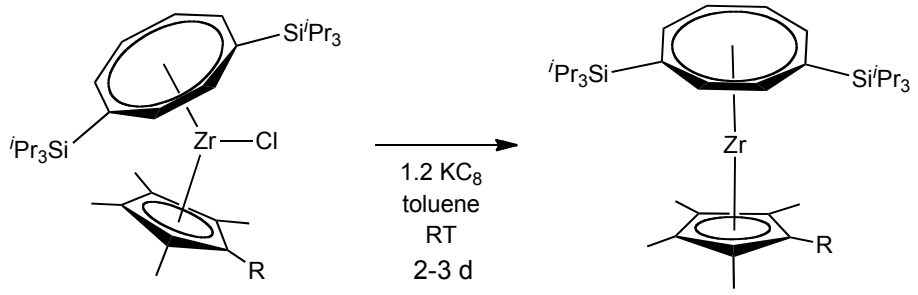

Scheme 3.1: Synthesis of reduced zirconium species for R = H (**3.1**), R = Me (**3.2**) and R = TMS (**3.3**).

It was noted that the Zr(III) compounds were highly soluble in all common hydrocarbon solvents to the point of precluding crystallisation and X-ray diffraction studies. Occasionally crystallisation was possible from pentane, although this proved to be an unreliable method that was not always reproducible. However, cooling saturated solutions of [Zr(η^8-C_8H_8)(Cp^{Me4R})] in $(Me_3Si)_2O$ to -35 °C yielded clean, crystalline material where R = H, Me, TMS.

3.3 Synthesis and characterisation of [Zr(η^8-C_8H_6{Si^{i}Pr$_3$-1,4}$_2$)(Cp^{Me4R})]

Toluene was added to an ampoule charged with [Zr(η^8-C_8H_8)(Cp^{Me4R})Cl] and a slight excess of KC_8 at ambient temperature, to give a yellow solution with bronze-coloured solids. This suspension was allowed to stir for 2-3 days resulting in a dark red solution with insoluble black precipitate. Extraction with $(Me_3Si)_2O$ and subsequent storage at -35 °C resulted in X-ray quality dark red crystals of [Zr(η^8-C_8H_6{Si^{i}Pr$_3$-1,4}$_2$)(Cp^{Me4R})] (**3.1**, R = H; **3.2**, R = Me; **3.3**, R = TMS) in poor yields. The purity of the compounds was confirmed by elemental analysis and mass spectrometry, with parent ions at m/z 627, 641 and 699 for compounds **3.1**, **3.2** and **3.3** respectively. The identity of the compounds was unable to be confirmed directly by ^{1}H NMR spectroscopy due to significant paramagnetic broadening of all resonances that could not be modelled, whilst the paramagnetic nature of the compounds precluded acquisition of useful ^{13}C{^{1}H} NMR spectra. However, ^{29}Si{^{1}H} NMR spectroscopy was possible in each case, with assignment through HMBC analysis. A significant upfield shift was seen for the isopropyl silyl group in **3.3** to δ_{Si} -50.53 compared to the chloride precursor, whilst

the trimethyl silyl resonance was less shifted and observed slightly downfield at δ_{Si} 6.98. Compound **3.1** displayed a resonance at δ_{Si} -20.50 whilst the ^{29}Si signal for **3.2** was shifted to a less significantly lower frequency at 7.17 ppm.

The paramagnetic nature of a chemical compound can be determined by a variety of methods, including SQUID (superconducting quantum interface device), use of the Gouy balance and Evans ^{1}H NMR spectroscopic method. Due to the small amount of **3.1**, **3.2** and **3.3** available for analysis and their highly air-sensitive nature, the Evans method was employed.[13, 14] Here, the paramagnetic shift of the solvent signal was compared to an internal standard and applied to the formula below. The third correction factor was ignored as due to the dilute nature of the solution required for successful ^{1}H NMR spectroscopy, the density of the solution (d_s) effectively equals the density of the solvent (d_o), thus leading the third term to equal zero. The second term is neglected in order to reduce error.[15] Conversion of χ_g resulted in an effective magnetic susceptibility (μ_{eff}) value, which can be approximately related to the number of unpaired electrons in each case. The results of these calculations are shown in **Table 3.2**. Whilst these calculations work well for the first row of the transition elements, for those in the second and third row, values of μ_{eff} are usually to be lower than expected. This is due to the greater crystal field splitting and greater spin-orbit coupling in complexes of the heavier transition metals.[16] Taken into account with other observations including the highly broadened ^{1}H NMR spectra and the molecular structures obtained by single crystal X-ray diffraction studies, *vide infra*, these zirconium complexes can be unambiguously assigned as d^1 complexes.

$$\chi_g = (-3\Delta f)/(4\pi fm) + \chi_o + [\chi_o(d_o - d_s)]/m$$

χ_g = mass susceptibility of the solute / $cm^3.g^{-1}$
Δf = observed frequency shift of the reference resonance / Hz
f = spectrometer frequency / Hz
χ_o = mass susceptibility of the solvent / $cm^3.g^{-1}$
m = mass of substance per cm^3 of solution / g
d_o = density of solvent / $g.cm^{-3}$
d_s = density of solution / $g.cm^{-3}$

Table 3.2: Number of unpaired electrons calculated for compounds **3.1** (R = H), **3.2** (R = Me) and **3.3** (R = TMS)

Compound Number	μ_{eff}
3.1	1.06
3.2	1.00
3.3	1.13

Single crystal X-ray diffraction analysis was completed on each compound, with the major features summarised in **Table 3.3**. In each case, the average Cp C-C and COT C-C distances observed in the ligands are consistent with those seen in the mixed-ring halide examples described in the previous chapter, measuring 1.414(9), 1.418(4) and 1.43(3) Å for the Cp moiety.

For compounds **3.1** – **3.3** (**Figure 3.1**,**Figure** 3.2 and **Figure** 3.3 respectively), the loss of the chlorine atom has resulted in a distinctly more linear $COT_{cent.}$-M-$Cp_{cent.}$ angle: these values have increased significantly from approximately 146° to 169.88(10)° (**3.1**), 170.64(16)° (**3.2**) and 168.2(6)° (**3.3**), coincident with a decrease in steric congestion.

This decrease in steric crowding has caused a significant shortening of the zirconium-centroid distances, with the Zr-$COT_{cent.}$ and Zr-$Cp_{cent.}$ distances now significantly shorter than those observed in the chloride starting materials **2.7**, **2.8** and **2.9**. The metal-centroid distances in the only other similar Zr(III) system[7] [Zr(η^8-C_8H_8)(Cp^{Me5})] are significantly shorter than in **3.1** – **3.3**, a feature attributed to the unsubstituted nature of the COT ligand in that particular example. The reduced metal-centroid distances in complexes **3.1** – **3.3** are comparable with the average literature values discussed in Chapter Two.

The linearity and metal-ring distances are comparable to those seen in the cycloheptatrienyl Zr(IV) compounds [Zr(η^7-C_7H_7)(Cp^R)] (R = Me_5,[17] H,[18] H_4(TMS), H_4Me[19] and $H_4CH_2CHCH_2$[19]), despite the significantly less bulky ligands employed.

For compounds **3.1** – **3.3**, the eight-membered ring is distinctly less puckered than seen with the chloride precursors.

Table 3.3: Selected bond angles (deg) and distances (Å) for [Zr(η^8-C_8H_6{Si^{i}Pr$_3$-1,4}$_2$)(Cp^{Me4R})]: **3.1** (R = H), **3.2** (R = Me), **3.3** (R = TMS). $COT_{cent.}$ and $Cp_{cent.}$ indicates the centroid of the COT and Cp rings.

Compound	**3.1**	**3.2**	**3.3**
Zr-$COT_{cent.}$	1.6704(3)	1.688(3)	1.668(12)
Zr-$Cp_{cent.}$	2.201(2)	2.206(3)	2.210(12)
$COT_{cent.}$-Zr-$Cp_{cent.}$	169.88(10)	170.64(16)	168.2(6)
COT C-C range	1.394(8) – 1.432(8)	1.406(3) – 1.4196(19)	1.39(2) – 1.43(3)
Av. Cp C-C	1.414(9)	1.418(4)	1.43(3)

Each Zr(III) compound crystallised with different symmetry, with **3.1** crystallising in the orthorhombic space group $Pna2_1$ with the Cp ring oriented so that the C-H group is in-line with a tri*iso*propyl silyl group, presumably to lessen the steric congestion between the two ring moieties. Complex **3.2** crystallised in the monoclinic space group $P2_1/m$, with a plane of symmetry bisecting the COT and Cp moieties, whilst **3.3** crystallised in the monoclinic space group $P2_1/c$. In the latter case, the trimethylsilyl group is aligned in a staggered configuration between the two tri*iso*propyl silyl groups.

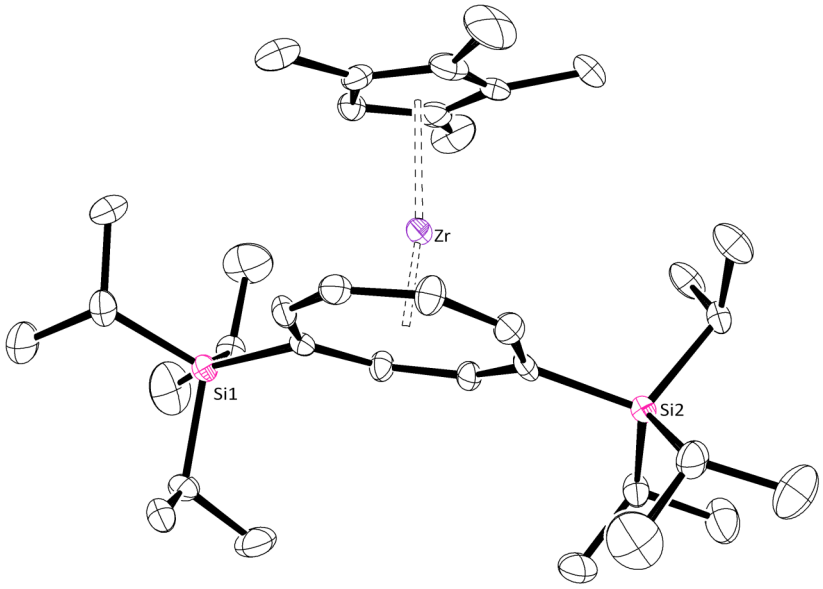

Figure 3.1: Molecular structure of [Zr(η^8-C_8H_6{Si^{i}Pr$_3$-1,4}$_2$)(Cp^{Me4H})] (**3.1**). Hydrogen atoms are omitted for clarity. Thermal ellipsoids at 50 % probability level.

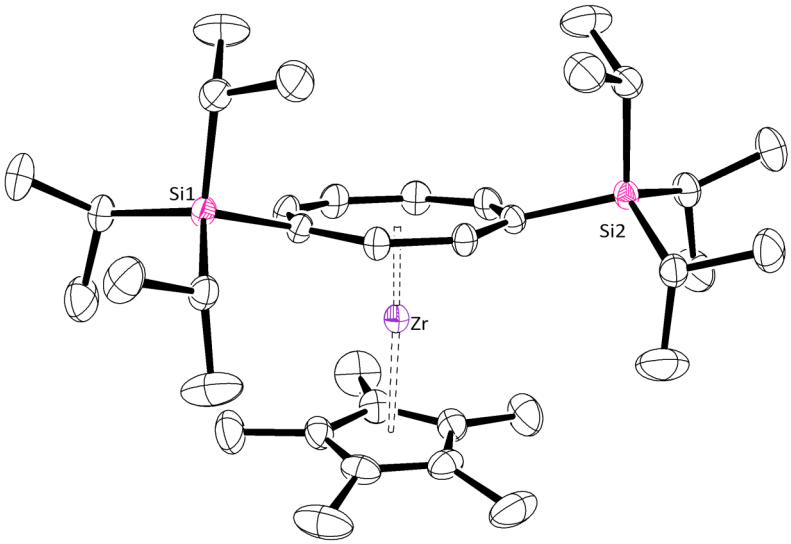

Figure 3.2: Molecular structure of [Zr(η^8-C_8H_6{Si^{i}Pr$_3$-1,4}$_2$)(Cp^{Me5})] (**3.2**). Hydrogen atoms are omitted for clarity. Thermal ellipsoids at 50 % probability level.

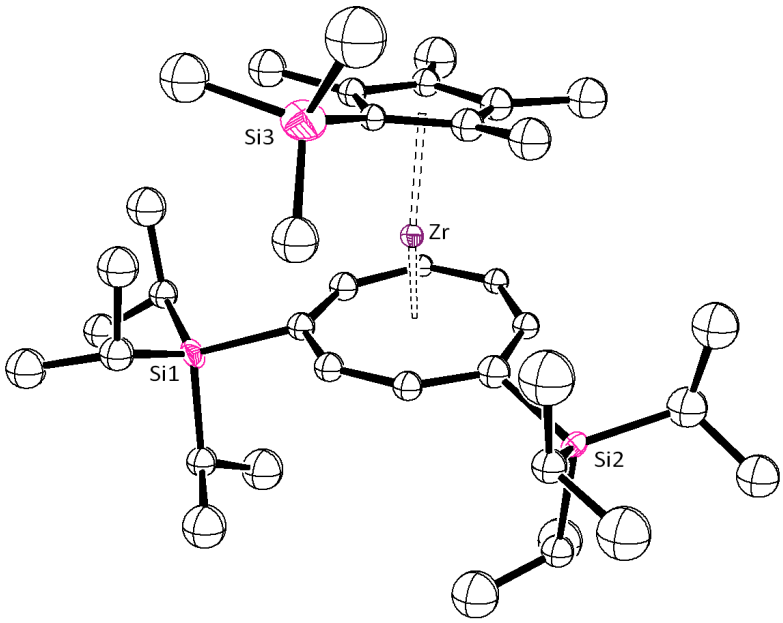

Figure 3.3: Molecular structure of [Zr(η^8-C_8H_6{Si^{i}Pr$_3$-1,4}$_2$)(Cp$^{Me4(TMS)}$)] (**3.3**). Hydrogen atoms are omitted for clarity. Thermal ellipsoids at 50 % probability level.

3.4 Synthesis and characterisation of [Hf(η^8-C_8H_6{Si^{i}Pr$_3$-1,4}$_2$)(Cp^{Me4R})]

Once a successful reduction method was established for the synthesis and subsequent isolation of the low valent zirconium compounds, experiments were initiated to reduce the mixed-ring hafnium analogues. However, despite similar reaction conditions and comparable observations, Hf(III) complexes could not be reliably isolated. The crude materials from these reactions all showed broadened resonances by ^{1}H NMR spectroscopy, consistent with a paramagnetic metal centre, and were found to be highly soluble in all common hydrocarbon solvents. With behaviour similar to that observed with the zirconium congeners, crystallisation from $(Me_3Si)_2O$ was attempted. However, on dissolution of the Hf(III) complexes in this solvent, immediate discolouration of the solvent and a pale precipitate was observed.

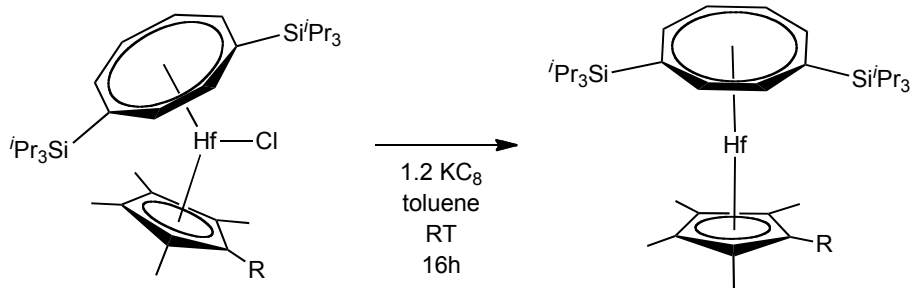

Scheme 3.2: Synthesis of reduced hafnium species for R = H (**3.4**) and R = Me (**3.5**).

However and in contrast to the synthesis of the Zr congeners, when toluene was added to an ampoule charged with [Hf(η^8-C_8H_6{Si^{i}Pr$_3$-1,4}$_2$)(Cp^{Me4R})Cl] (R = H, Me) and a slight excess of KC_8 at ambient temperature, reaction ensued, affording a yellow solution with bronze-coloured precipitate (**Scheme 3.2**). This suspension was allowed to stir overnight, resulting in a deep red solution with a black precipitate. Filtration and subsequent storage at -80 °C in a toluene/pentane solution overnight resulted in small black X-ray quality crystals of **3.4** and **3.5** in poor yields (**Figure 3.4** and **Figure** 3.5). The purity of **3.4** was confirmed by elemental analysis and mass spectrometry, with the parent ion observed at m/z 717, consistent with the reduced complex, with Evan's method calculating μ_{eff} = 1.02. The purity of **3.5** could not be confirmed by mass spectrometry, ^{1}H NMR spectroscopy or elemental analysis and as such Evans analysis was not pursued. These fortuitous isolations of Hf(III) compounds could not, however, be reliably reproduced. Upon prolonged storage of a solution, further intermolecular reactions, typically leading to an unusual dimeric compound in which a C-C bond is formed between the COT moieties on two neighbouring molecules, were observed. This dimerisation reaction is described more fully in the next section.

Attempts were made to produce solvent adducts of the Hf(III) complexes that might prove less soluble in common hydrocarbon solvents and assist isolation of a clean product. However, in our hands, KC_8 appeared to show reactivity towards both DME and diethyl ether. Reaction in THF proceeded smoothly and preliminary spectroscopic evidence tentatively suggested that the product contained butoxy group or similar moiety derived from ring-opened THF. However, this new Hf(IV) complex could not be definitively identified by ^{1}H NMR spectroscopy or mass spectrometry.

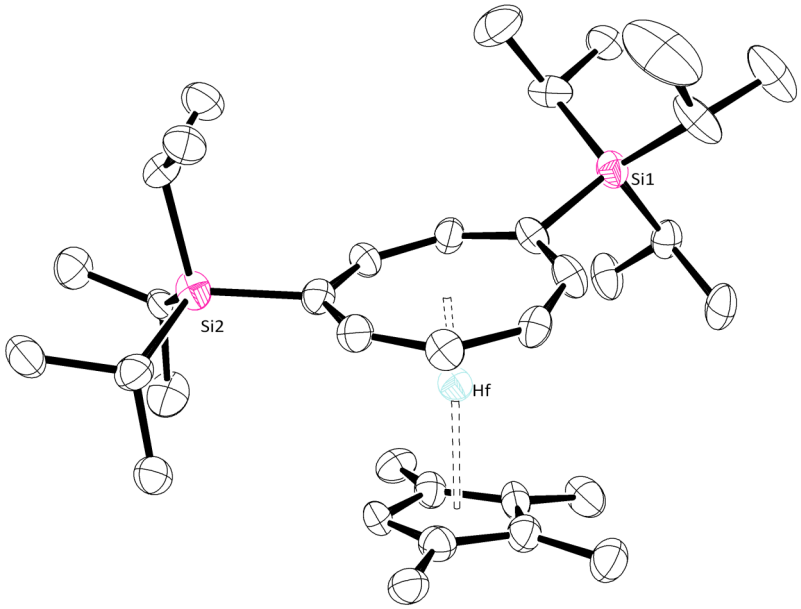

Figure 3.4: Molecular structure of [Hf(η^8-C_8H_6{Si^{i}Pr$_3$-1,4}$_2$)(Cp^{Me4H})] (**3.4**). Hydrogen atoms are omitted for clarity. Thermal ellipsoids at 50 % probability level.

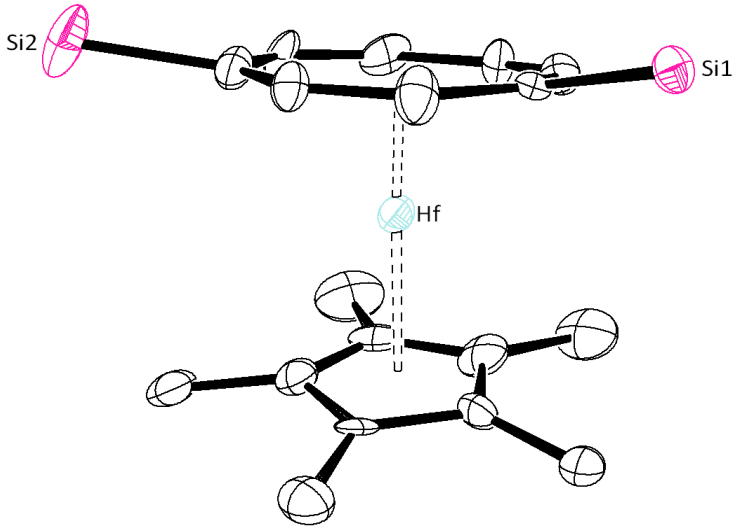

Figure 3.5: Molecular structure of [Hf(η^8-C_8H_6{Si^{i}Pr$_3$-1,4}$_2$)(Cp^{Me5})] (**3.5**). Hydrogen atoms and disordered ^{i}Pr groups are omitted for clarity. Thermal ellipsoids at 50 % probability level.

The reduced hafnium compounds exist in different space groups to each other and with respect to their zirconium analogues: **3.4** crystallises in the monoclinic space group $P2_1/c$ and **3.5** in the orthorhombic space group Pcan. In **3.4**, the C-H group on the Cp ring is aligned with an *iso*propyl silyl group, presumably to relieve steric congestion. The physical data obtained from single crystal X-ray diffraction studies (**Table 3.4**) are consistent with those discussed for the zirconium analogues, although with slightly smaller metal-centroid distances for both the COT and Cp moieties. The C-C distances are consistent with the previous complexes discussed. There is a slight decrease in linearity in the $COT_{cent.}$-Hf-$Cp_{cent.}$ angles when compared to the zirconium analogues, but these compounds are distinctly less bent than the chloride precursors. Although not examples of a reduced hafnium centre, the [Hf(η^7-C_7H_7)(Cp^R)] examples described by Rogers and Teuben (R = Me_5)[17] and Tamm and coworkers (R = H_5)[20] display a similar linearity. It is also noteworthy that the COT moiety has greater planarity when compared to the Hf(IV) starting material.

The metal centroid distances here are significantly shorter than those observed in the related mixed ring hafnium chloride compound, although direct literature comparisons cannot be made here due to the lack of examples of Hf-COT compounds. These M-$COT_{cent.}$ distances of 1.642(15) and 1.6481(6) Å are similar to the average Zr-COT distance reported in the literature (1.66(6) Å) and discussed more fully in the previous chapter. The Hf-$Cp_{cent.}$ length of 2.16(3) Å for the tetramethyl derivative is comparable with the average literature figure of 2.24(3) Å. In the case of the pentamethyl Cp ligand, the Hf-$Cp_{cent.}$ distance of 2.152(6) Å is also directly comparable with the literature average of 2.21(3) Å.

Table 3.4: Selected bond angles (deg) and distances (Å) for [Hf(η^8-C_8H_6{Si^{i}Pr$_3$-1,4}$_2$)(Cp^{Me4R})] **3.4** (R = H), **3.5** (R = Me). $COT_{cent.}$ and $Cp_{cent.}$ indicate the centroid of the COT and Cp rings.

Compound	**3.4**	**3.5**
Hf-$COT_{cent.}$	1.642(15)	1.6481(6)
Hf-$Cp_{cent.}$	2.16(3)	2.1562(6)
$COT_{cent.}$-Hf-$Cp_{cent.}$	168.7(8)	167.89(3)
COT C-C range	1.39(2) – 1.440(18)	1.381(18) – 1.442(17)
Av. Cp C-C	1.42(2)	1.419(19)

3.4.1 Synthesis of [Hf(η-Cp^{Me4R})]$_2$(μ-η^7:η^7-(C_8H_6{Si^{i}Pr$_3$-1,4}$_2$$C_8H_6${Si^{i}Pr$_3$-1,4}$_2$)]

In a similar manner to that described for the synthesis of **3.4** and **3.5,** and represented in **Scheme 3.3**, toluene was added at ambient temperature to an ampoule charged with [Hf(η^8-C_8H_6{Si^{i}Pr$_3$-1,4}$_2$)(Cp^{Me4R})Cl] and excess KC_8 affording a bronze suspension. This was allowed to stir for 7 days before filtration and subsequent storage at -35 °C. Small red X-ray quality crystals of **3.6** (R = H), **3.7** (R = Me) and **3.8** (R = TMS) were isolated in poor yields for **3.6** and good yields for **3.7** and **3.8**. These compounds were found to be insoluble in all common hydrocarbon solvents and react with chlorinated solvents to give unidentified products, making acquisition of informative NMR spectroscopy impossible. The identity and dimeric nature of the products was confirmed by mass spectrometry, with the distinctive dinuclear hafnium isotope pattern observed at m/z 1430 and 1458 for compounds **3.6** and **3.7** respectively. The expected parent ion was not observed for **3.8**, with the highest mass peak at m/z 1179 corresponding to the loss of HfCp$^{Me4(TMS)}$ from the parent molecule. The purity of the product was confirmed by elemental analysis in the cases of **3.7** and **3.8**.

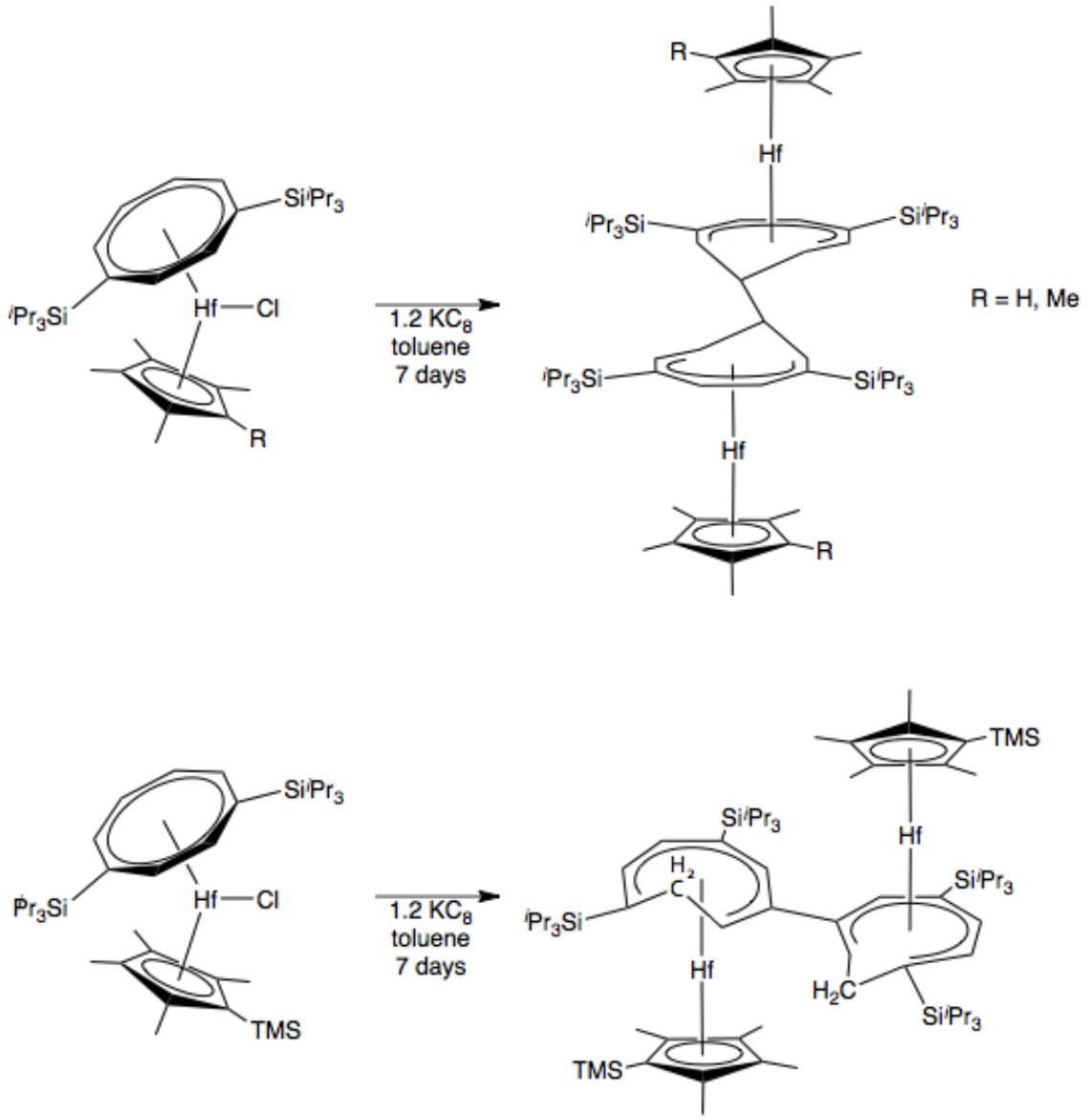

Scheme 3.3: Reduction and subsequent dimerisation of Hf(III) complexes to result in Hf(IV) dimers.

On following the attempted reduction of complexes **2.8**, **2.10** and **2.12** *via* ^{1}H NMR spectroscopy, it is suggested that a paramagnetic compound is produced during the course of the reaction, apparent from broadening of the resonances. This isolation of only **3.6**, **3.7** and **3.8** (**Figure 3.6, Figure** 3.7 and **Figure** 3.8), must thus be attributed to the highly reactive nature of the d^1 metal centre leading to dimerisation through COT-COT bonding. It is possible that this dinuclear compounds represents a favourable thermodynamic product that is easily accessible *via* the labile Hf(III) intermediate.

These dimeric complexes can be considered to be electronically similar to [Hf(CHT)(Cp^R)], where the cycloheptatrienyl ligand formally possesses a 3- charge.[21] This would indicate that following initial reduction by KC_8, the hafnium centres have undergone subsequent oxidation resulting in the more stable dimeric Hf(IV) complexes.

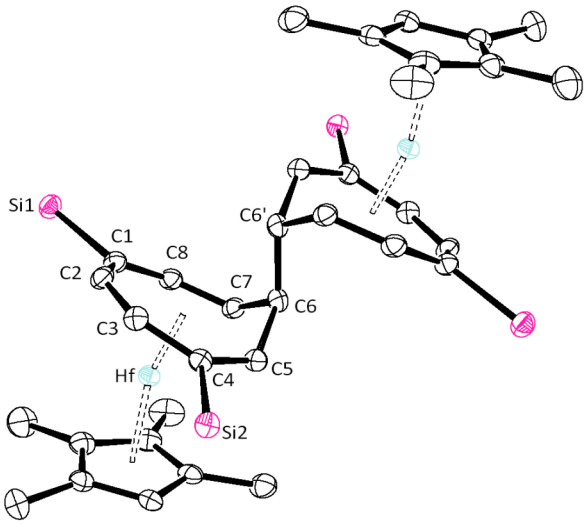

Figure 3.6: Molecular structure of [Hf(η-Cp^{Me4R})]$_2$[(μ-η^7.η^7-(C_8H_6{Si^{i}Pr$_3$-1,4}$_2$$C_8H_6${Si^{i}Pr$_3$-1,4}$_2$)] (**3.6**). Hydrogen atoms and ^{i}Pr groups are omitted for clarity. Thermal ellipsoids at 50 % probability level.

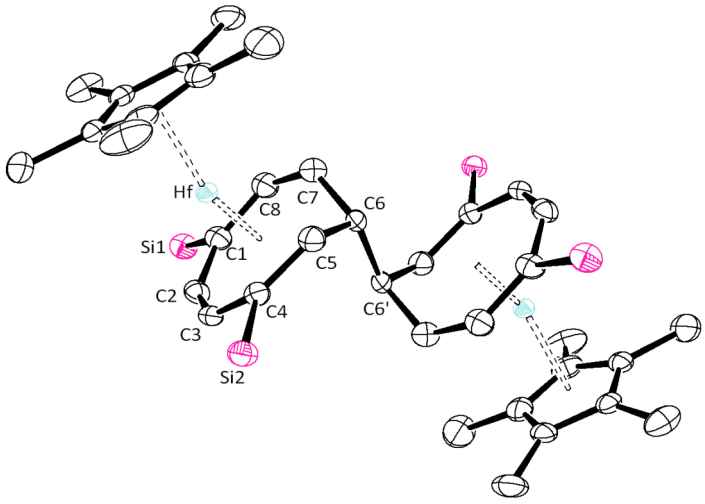

Figure 3.7: Molecular structure of [Hf(η-Cp^{Me5})]$_2$[(μ-η^7.η^7-(C_8H_6{Si^{i}Pr$_3$-1,4}$_2$$C_8H_6${Si^{i}Pr$_3$-1,4}$_2$)] (**3.7**). Hydrogen atoms and ^{i}Pr groups are omitted for clarity. Thermal ellipsoids at 50 % probability level.

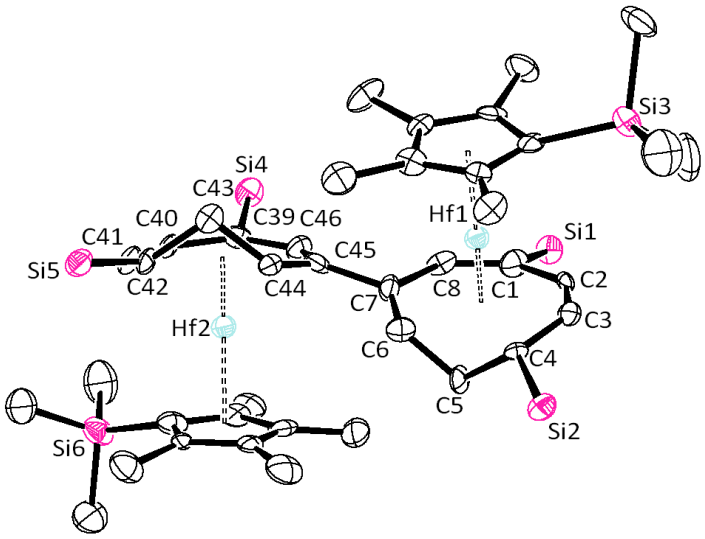

Figure 3.8: Molecular structure of $[Hf(\eta\text{-}Cp^{Me4(TMS)})]_2[(\mu\text{-}\eta^7.\eta^7\text{-}(C_8H_6\{Si^iPr_3\text{-}1,4\}_2C_8H_6\{Si^iPr_3\text{-}1,4\}_2)]$ (**3.8**). Hydrogen atoms and ^{i}Pr groups are omitted for clarity. Thermal ellipsoids at 50 % probability level.

This dimerisation of two aromatic COT units is rare and sparsely documented in the literature. Dimerisation of the antiaromatic ligand is well known, occurring *via* Diels Alder processes[22-24] or more traditional olefinic chemistry.[25-27] The most relevant examples of aromatic COT coupling are described by Bachmann *et al*[28] and Lavallo and Grubbs.[29] Bachmann's work discusses the attempted synthesis of [V(COT)(Cp)] (**Scheme 3.4**) *via* $CpVCl_2(PEt_3)_2$ and the subsequent isolation of a dimeric compound akin to that observed for **3.6** and **3.7**. Also described in this paper is the attempted synthesis of the anionic monomer $[V(COT)(Cp)]^-$ *via* $[CpVCl(PEt_3)]_2$, also resulting in a COT-bridged compound that has undergone a 1,2-hydrogen shift similar to that observed in **3.8** (**Scheme 3.5**). Here, the change in the vanadium starting material employed results in selectivity between the formation of unshifted and the 1,2-shifted products. With the hafnium-based dimers, this selectivity appears to be controlled *via* the differently substituted cyclopentadienyl ligands.

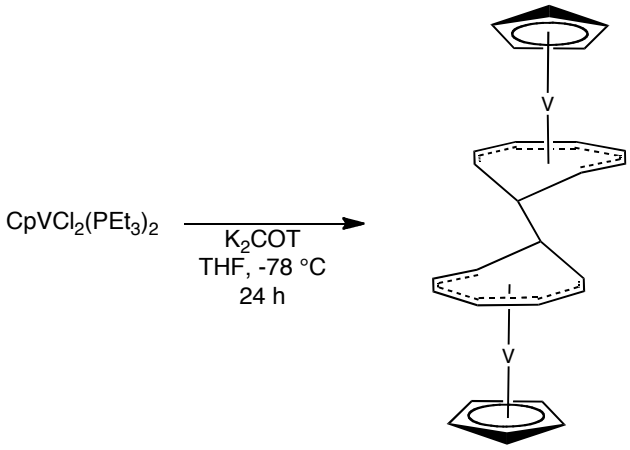

Scheme 3.4: Synthesis of vanadium dimer similar to **3.6** and **3.7** as described by Bachmann *et al*.

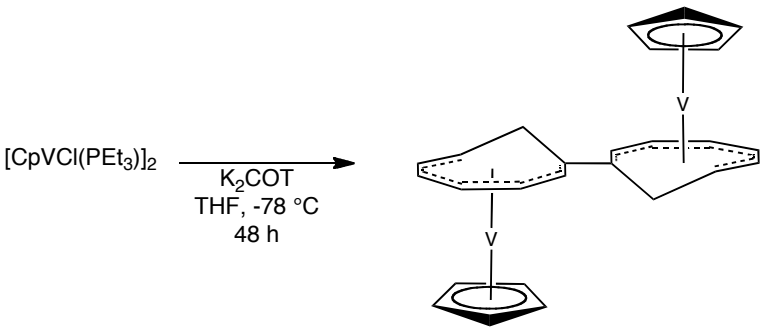

Scheme 3.5: Synthesis of vanadium dimer similar to **3.8**. 1,2-hydrogen shift is observed with this preparation by Bachmann *et al*.

Lavallo and Grubbs described the synthesis of a tetranuclear iron complex (**Scheme 3.6**) bridged by two adjoined COT ligands, again having dimerised and rearranged *via* a 1-2 hydrogen shift. Nowhere has a 1,3 shift similar to that seen in **3.8** been identified; whether the preference for a 1,3-shift in the latter can be attributed to the presence of $SiMe_3$ is unclear at this stage.

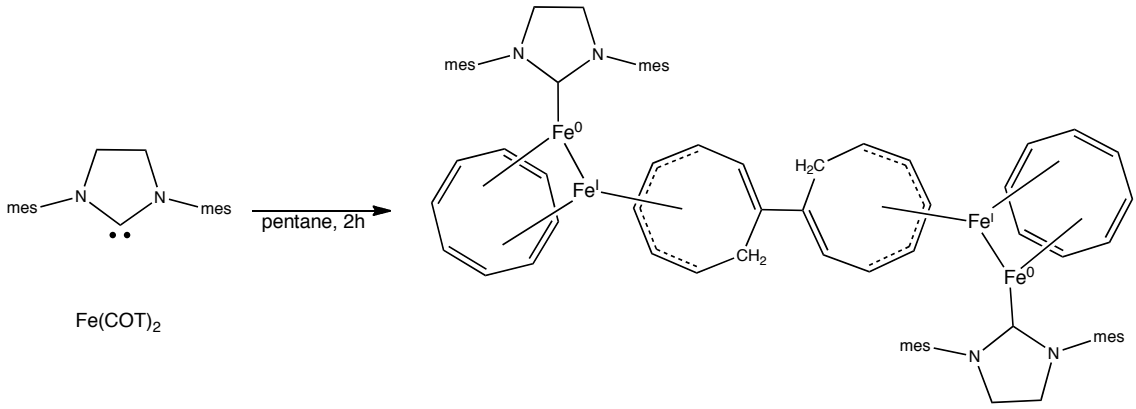

Scheme 3.6: Generation of COT-COT bond, followed by 1,2-hydrogen shift reported by Lavallo and Grubbs.

With compound **3.8**, formation of the new C-C bond occurs with a rearrangement: the hydrogen atom shifts from the sp^3-hybridised bridging carbon to the neighbouring carbon two bonds away (C5, C43). This leads to the bridging carbons (C7, C45) regaining their sp^2 hybridisation and returning to a more planar conformation with respect to each COT ring. Atoms C43 and C47 now bear the extra hydrogens, becoming sp^3-hybridised, no longer aromatic and thus out of the plane of the ring.

The cyclopentadienyl ligands appear to be unaffected by the unusual dimerisation of these monomers. The Hf-$Cp_{cent.}$ distances (**Table 3.5**) for **3.6** and **3.7** are comparable with those seen in **3.4** and **3.5**, measuring 2.1616(3) and 2.181(5) Å respectively. For all three dimers, these distances are only marginally shorter than the lengths observed in the M(IV) precursors **2.8**, **2.10** and **2.12**. The $COT_{cent.}$-Hf-$Cp_{cent.}$ angle of **3.6** is relatively linear (169.06(2)°) and deviates little from those observed in the unstable Hf(III) monomer, however, there is a slight loss in linearity in the case of R = Me (162.8(3)°). Compound **3.8** shows the greatest linearity (174.8(9), 176.6(9)°) of the mixed ring complexes described here so far; this is possibly due to C7 and C45 regaining unsaturation, thus preventing the ring-slip associated with the COT-COT bonding in the other two examples. Values for a $CHT_{cent.}$-Hf-Cp angle in the literature suggest an expected figure of 169.4 to 176.6°,[20, 30] consistent with **3.6** and **3.8**, but not **3.7**.

Table 3.5: Selected bond angles (deg) and distances (Å) for [Hf(η-Cp^{Me4R})]$_2$(μ-η^7.η^7-(C_8H_6{Si^{i}Pr$_3$-1,4}$_2C_8H_6${Si^{i}Pr$_3$-1,4}$_2$)] **3.6** (R = H), **3.7** (R = Me), **3.8** (R = TMS). $COT_{cent.}$ and $Cp_{cent.}$ indicate the centroid of the COT and Cp rings.

Compound	**3.6**	**3.7**	**3.8**
Hf-$COT_{cent.}$	1.4846(3)	1.602(5)	1.494(14) 1.490(14)
Hf-$Cp_{cent.}$	2.1612(3)	2.183(5)	2.176(14) 2.177(14)
$COT_{cent.}$-Hf-$Cp_{cent.}$	169.06(2)	162.8(3)	176.6(9) 174.8(9)
COT C-C range	1.408(4) – 1.537(4)	1.394(5) – 1.569(5)	1.424(14) – 1.534(13) 1.397(14) – 1.548(13)
Bridging C-C	1.548(5)	1.525(6)	1.549(14)
Av. Cp C-C	1.417(4)	1.416(6)	1.424(14) 1.430(16)

The Hf-$COT_{cent.}$ distances in **3.6** and **3.8** are significantly shorter than anything observed so far in this work. The same parameter for **3.7** is unexpectedly long compared to the other two dimeric compounds, although it still remains significantly shorter than seen in **3.5** and the chloride precursor. Hf-$CHT_{cent.}$ distances from mixed-ring examples published by Tamm and coworkers[20, 30] and Rogers and Teuben[17] range from 1.614 to 1.618 Å, significantly longer than observed herein.

The bridging C-C distances are consistent with C-C single bond lengths, at 1.548(5), 1.525(6) and 1.549(14) Å for **3.6** – **3.8** respectively, with the C-C distances within the COT ligand ranging from 1.394(5) to 1.569(5), showing the presence of aromatic and single bonds within the eight-membered structure. For **3.6**, the longest C-C bonds are between C5-C6 and C6-C7 (1.537(4) and 1.508(4) Å) and are consistent with C-C

single bonds, with the rest of the COT ring C-C distances within a narrow range between 1.408(4) – 1.459(4) Å. In the case of **3.7**, the longest COT C-C distances are again seen either side of C6, with C5-C6 measuring 1.569(5) Å and C6-C7 significantly shorter at 1.490(5) Å, although this is still reasonable for a Csp^3-Csp^2 distance. The remaining C-C bonds in the COT ligand in this case range from 1.394(5) – 1.462(5) Å, a much wider range than with **3.6**.

Complex **3.8** shows longer C-C distances within the aromatic portion of the COT moiety than previously observed, ranging from 1.397(14) – 1.488(14) Å, with the longest distances furthest from the C-C bridge. The single bonds within the ring leading to the out-of-plane CH_2 units range from 1.505(13) – 1.548(13) Å in length, consistent with Csp^3-Csp^3 bonds.

It is unclear why the unusual hydrogen shift only occurs when R = TMS, as the COT rings are all similarly substituted. However, crystallographic evidence suggests that the results discussed above are consistently reproducible.

3.5 Conclusions

The reduction of the mixed-ring zirconium chloride complexes described in Chapter 2 has proven problematic due to the suspected reactivity of Zr(III) towards polar solvents, and the high solubility in common hydrocarbon solvents. However, it has proven possible to isolate these reduced compounds in moderate yields and they appear to be relatively stable in solid form and in solution under an inert atmosphere. The hafnium(III) analogues show inherent instability in solution over a period of time, dimerising to afford insoluble Hf(IV) complexes in variable yields. These resulting dimers are highly insoluble, with analysis relying on mass spectrometry and single crystal X-ray diffraction.

3.6 Experimental details for Chapter Three

3.6.1 Synthesis of [Zr(η^8-C_8H_6{Si^{i}Pr$_3$-1,4}$_2$)(Cp^{Me4H})] (3.1)

An ampoule was charged with **2.7** (0.526 g, 0.793 mmol) and KC_8 (0.134 g, 0.993 mmol) before addition of toluene (25 cm^3) at ambient temperature *via* cannula leading to a bronze-coloured suspension which was allowed to stir for 3 days resulting in a dark red solution with black precipitate. This was extracted into $(Me_3Si)_2O$, before subsequent storage at -35 ºC yielding **3.1** as small red crystals suitable for X-ray diffraction studies.
Yield = 0.156 g (0.25 mmol), 31 % w.r.t. **2.7**.

Due to the paramagnetic nature of the product, ^{1}H NMR and ^{13}C{^{1}H} NMR spectroscopic data could not be obtained.
^{29}Si NMR (benzene-d_6, 79.4 MHz, 303 K): δ_{Si} -20.50.
MS (EI)$^+$: m/z = 67 (100 %), 627 (M$^+$, 22 %), 541 (M$^+$ - ^{i}Pr -^{i}Pr -Me, 50 %).
Elemental analysis calcd (%) for $C_{35}H_{61}Si_2Zr$: C 66.8, H 9.77; found: C 66.70, H 9.92.
Crystal data for **3.1**: Red air-sensitive needle 0.20 × 0.20 × 0.10 mm^3, $C_{35}H_{61}Si_2Zr$, a = 15.8450(6), b = 23.1166(10), c = 9.6436(2) Å, α = 90º, β = 90º, γ = 90º, U = 3532.3(2) Å^3, orthorhombic, Pna2$_1$, Z = 4, total reflections 15654, independent reflections 6133, R_{int} = 0.0790, θ_{max} = 26.73, R_1 [I >2σ(I)] = 0.0583, wR^2 = 0.1102 and 343 parameters.

3.6.2 Synthesis of [Zr(η^8-C_8H_6{Si^{i}Pr$_3$-1,4}$_2$)(Cp^{Me5})] (3.2)

Prepared in a similar way to **3.1**, an ampoule was charged with **2.9** (0.545 g, 0.805 mmol) and KC_8 (0.226 g, 1.67 mmol) before addition of toluene (25 cm^3) at ambient temperature *via* cannula with stirring. Stirring for 3 days resulted in black precipitate in a dark red solution. Extraction into $(Me_3Si)_2O$ and storage -35 ºC yielded the reduced species **3.2** as red plate-like crystals suitable for single crystal X-ray diffraction study.
Yield = 0.086 g (0.149 mmol), 17 % w.r.t. **3.1**.

Due to the paramagnetic nature of the product, ^{1}H NMR and ^{13}C{^{1}H} NMR spectroscopic data could not be obtained.

^{29}Si NMR (benzene-d_6, 79.4 MHz, 303 K): δ_{Si} 7.17.

MS (EI)$^{+}$: m/z = 525 (100 %), 641 (M^{+}, 50 %), 541 (M^{+} - ^{i}Pr -^{i}Pr -Me, 50 %), 525 (M^{+} - ^{i}Pr -^{i}Pr -Me -Me, 100 %).

Elemental analysis calcd (%) for $C_{36}H_{63}Si_2Zr$: C 67.3, H 9.81; found: C 67.16, H 9.84.

Crystal data for **3.2**: Red air-sensitive plate 0.30 × 0.20 × 0.12 mm^3, $C_{36}H_{63}Si_2Zr$, a = 8.7791(1), b = 22.2176(4), c = 9.5499(2) Å, α = 90º, β = 100.616(1)º, γ = 90º, U = 1830.83(5) Å^3, monoclinic, $P2_1/m$, Z = 2, total reflections 31486, independent reflections 4285, R_{int} = 0.052, θ_{max} = 27.48, R_1 [I >2σ(I)] = 0.028, wR^2 = 0.068 and 184 parameters.

3.6.3 Synthesis of [Zr(η^8-C_8H_6{Si^{i}Pr$_3$-1,4}$_2$)(Cp$^{Me4(TMS)}$)] (3.3)

Similarly to the synthesis of **3.1** and **3.2**, an ampoule was charged with **2.11** (0.424 g, 0.577 mmol) and KC_8 (0.094 g, 0.696 mmol) before the addition of toluene (25 cm^3) at ambient temperature *via* cannula with stirring. After 2 days, the reduced zirconium species was extracted into $(Me_3Si)_2O$, with subsequent storage at -35 °C yielding small red crystals suitable for X-ray diffraction studies.

Yield = 0.095 g (0.136 mmol), 24 % w.r.t. **2.11**.

Due to the paramagnetic nature of the product, ^{1}H NMR and ^{13}C{^{1}H} NMR spectroscopic data could not be obtained.

^{29}Si NMR (benzene-d_6, 79.4 MHz, 303 K): δ_{Si} 6.98 (s, $SiMe_3$), -50.53 (s, Si^{i}Pr$_3$).

MS (EI)$^{+}$: m/z = 699 (M^{+} 100 %), 541 (M^{+} - ^{i}Pr -^{i}Pr -Me -$SiMe_3$, 50 %), 525 (M^{+} - ^{i}Pr -^{i}Pr -Me -Me -$SiMe_3$, 100 %).

Elemental analysis calcd (%) for $C_{38}H_{69}Si_3Zr$: C 65.07, H 9.91; found: C 64.92, H 9.82.

Crystal data for **3.3**: Red air-sensitive needle 0.08 × 0.04 × 0.02 mm^3, $C_{76}H_{138}Si_6Zr2$, a = 14.7791(3), b = 24.2182(5), c = 22.5627(4) Å, α = 90º, β = 92.2210(10)º, γ = 90º, U = 8069.6(3)() Å^3, monoclinic, $P2_1/c$, Z = 4, total reflections 83330, independent reflections 11555, R_{int} = 0.2908, θ_{max} = 23.28, R_1 [I >2σ(I)] = 0.1787, wR^2 = 0.3873 and 377 parameters.

3.6.4 Synthesis of [Hf(η^8-C_8H_6{Si^{i}Pr$_3$-1,4}$_2$)(Cp^{Me4H})] (3.4)

An ampoule was charged with **2.8** (0.429 g, 0.570 mmol) and KC_8 (0.152 g, 1.126 mmol) before addition of toluene (25 cm^3) at ambient temperature *via* cannula leading to a bronze-coloured suspension. This was allowed to stir overnight resulting in a dark red solution with black precipitate. Filtration *via* cannula and pentane addition to a concentrated solution and storage at -80 °C yielded small, black crystals of **3.4** suitable for single crystal X-ray diffraction study.
Yield = 0.062 g (0.0865 mmol), 15 % w.r.t. **2.8**.

Due to the paramagnetic nature of the product, ^{1}H NMR ^{13}C{^{1}H} NMR spectroscopic data could not be obtained.
MS (EI)$^+$: m/z = 561 (100 %), 717 (M$^+$, 72 %), 631 (M$^+$ - ^{i}Pr -^{i}Pr -Me, 20 %).
Elemental analysis calcd (%) for $C_{35}H_{61}Si_2Hf$: C 58.7, H 8.59; found: C 58.53, H 8.50.
Crystal data for **3.4**: Red air-sensitive needle 0.24 × 0.18 × 0.1 mm^3, $C_{35}H_{61}Si_2Hf$, a = 15.9171(14), b = 9.4819(9), c = 25.170(2) Å, α = 90º, β = 112.126(6)º, γ = 90º, U = 3519.0(6) Å^3, monoclinic, $P2_1/c$, Z = 4, total reflections 27170, independent reflections 6017, R_{int} = 0.183, θ_{max} = 25.02, R_1 [I >2σ(I)] = 0.104, wR^2 = 0.162 and 347 parameters.

3.6.5 Synthesis of [Hf(η^8-C_8H_6{Si^{i}Pr$_3$-1,4}$_2$)(Cp^{Me5})] (3.5)

An ampoule was charged with **2.10** (0.808 g, 1.058 mmol) and KC_8 (0.285 g, 2.111 mmol) before addition of toluene (25 cm^3) at ambient temperature *via* cannula with stirring. After 3 days, filtration and storage of a concentrated pentane solution at -80 °C yield large red X-ray quality crystals of **3.5** in poor yield.
Yield = 0.146 g (0.200 mmol), 19 % w.r.t. **2.10**.

Due to the paramagnetic nature of the product, ^{1}H NMR ^{13}C{^{1}H} NMR spectroscopic data could not be obtained.
Crystal data for **3.5**: Red air-sensitive block 0.18 × 0.14 × 0.10 mm^3, $C_{36}H_{63}Si_2Hf$, a = 11.7530(2), b = 16.8027(3), c = 19.6881(3) Å, α = 99.778(1)º, β = 107.251(1)º, γ =

90.039(1)º, U = 3652.82(11) $Å^3$, triclinic, $P\bar{1}$, Z = 4, total reflections 56162, independent reflections 14702, R_{int} = 0.061, θ_{max} = 26.73, R_1 [I >2σ(I)] = 0.034, wR^2 = 0.069 and 741 parameters.

3.6.6 Synthesis of [Hf(*η*-Cp^{Me4H})]$_2$(*μ*-*η*^{7}.*η*^{7}-(C_8H_6{Si^{i}Pr$_3$-1,4}$_2$$C_8H_6${Si^{i}Pr$_3$-1,4}$_2$)] (3.6)

An ampoule was charged with **2.8** (0.128 g, 0.170 mmol) and KC_8 (0.028 g, 0.0207 mmol) before the addition of toluene (15 cm^3) at ambient temperature *via* cannula with stirring. The mixture was allowed to stir for 7 days before filtration and subsequent storage at -35 °C resulting in **3.6** as dark red needles in very poor yield and suitable for single crystal X-ray diffraction studies.

Due to the insoluble nature of this product, solution NMR analysis has not proved possible.

MS $(EI)^+$: m/z = 718 (100 %, M^+ -Hf(η^8-COT{Si^{i}Pr$_3$-1,4}$_2$)(Cp^{Me4H})), 1430 (1% M^+).

Crystal data for **3.6**: Red air-sensitive needle 0.30 × 0.10 × 0.10 mm^3, $C_{70}H_{122}Si_4Hf_2$, a = 11.1056(2), b = 24.8924(4), c = 12.6004(2) Å, α = 90º, β = 99.2180º, γ = 90º, U = 3438.33(10) $Å^3$, monoclinic, $P2_1/c$, Z = 2, total reflections 44120, independent reflections 7835, R_{int} = 0.0486, θ_{max} = 27.46, R_1 [I >2σ(I)] = 0.0273, wR^2 = 0.0529 and 343 parameters.

3.6.7 Synthesis of [Hf(η-Cp^{Me5})]$_2$[(μ-η^7.η^7-(C_8H_6{Si^{i}Pr$_3$-1,4}$_2$$C_8H_6${Si^{i}Pr$_3$-1,4}$_2$)] (3.7)

In a similar manner to that employed for the synthesis of **3.6**, an ampoule was charged with **2.10** (0.148 g, 0.194 mmol) and KC_8 (0.033 g, 0.244 mmol) before the addition of toluene (20 cm^3) at ambient temperature with stirring. The resulting mixture was allowed to stir for 7 days before filtration and storage at -35 °C giving **3.7** in good yields as large red crystals, suitable for X-ray diffraction studies.

Yield = 0.096 g (0.0658 mmol), 68 % w.r.t. **2.10**.

Due to the highly insoluble nature of the product, solution NMR analysis was not possible.

MS $(EI)^+$: m/z = 616 (100 %), 1458 (1% M^+), 731 (63% M^+ -Hf(η^8-COT{Si^{i}Pr$_3$-1,4}$_2$)(Cp^{Me5})).

Elemental analysis calcd (%) for $C_{72}H_{126}Hf_2Si_4$: C 59.18, H 8.69; found: C 59.30, H 8.77.

Crystal data for **3.7**: Red air-sensitive plate 0.24 × 0.20 × 0.13 mm^3, $C_{72}H_{126}Si_4Hf_2$, a = 14.0891(2), b = 18.3487(4), c = 15.8885(3) Å, α = 90º, β = 120.090(1)º, γ = 90º, U = 3553.92(11) Å^3, monoclinic, $P2_1/c$, Z = 2, total reflections 52709, independent reflections 8327, R_{int} = 0.062, θ_{max} = 27.89, R_1 [I >2σ(I)] = 0.032, wR^2 = 0.071 and 357 parameters.

3.6.8 Synthesis of [Hf(η-$Cp^{Me4(TMS)}$)]$_2$[(μ-η^7.η^7-(C_8H_6{Si^{i}Pr$_3$-1,4}$_2$$C_8H_6${Si^{i}Pr$_3$-1,4}$_2$)] (3.8)

To an ampoule charged with **2.12** (0.155 g, 0.188 mmol) and KC_8 (0.035 g, 0.259 mmol) toluene (20 cm^3) was added at ambient temperature with stirring. After 7 days, filtration of the resulting dark solution and storage at -35 °C led to large dark red crystals of **3.8** in moderate yield and suitable for X-ray diffraction study.

Yield = 0.053 g (0.0337 mmol), 36 % w.r.t. **2.12**.

Due to the highly insoluble nature of the product, solution NMR analysis was not possible.

MS $(EI)^+$: m/z = 73 (100 %), 1179 (22 % M^+ - $HfCp^{Me4(TMS)}$).

Elemental analysis calcd (%) for $C_{76}H_{138}Hf_2Si_6$: C 57.94, H 8.77; found: C 57.65, H 8.63.

Crystal data for **3.8**: Red air-sensitive plate 0.20 × 0.03 × 0.03 mm^3, $C_{76}H_{138}Si_6Hf_2$, a = 10.7685(5), b = 31.235(2), c = 25.6103(16) Å, α = 90º, β = 112.139(3)º, γ = 90º, U = 7979.0(8) Å^3, monoclinic, $P2_1/c$, Z = 4, total reflections 62170, independent reflections 13773, R_{int} = 0.175, θ_{max} = 25.03, R_1 [I >2σ(I)] = 0.075, wR^2 = 0.124 and 765 parameters.

References for Chapter Three

1. J. D. Corbett, *Inorganic Synthesis*, 1983, **22**, 31.
2. F. G. N. Cloke and P. B. Hitchcock, *J. Am. Chem. Soc.*, 2002, **124**, 9352-9353.
3. E. M. Larsen, J. S. Wrazel and L. G. Hoard, *Inorg. Chem.*, 1982, **21**, 2619-2624.
4. E. M. Larsen and J. J. Leddy, *J. Am. Chem. Soc.*, 1956, **78**, 5983-5987.
5. J. Blenkers, P. Bruin and J. H. Teuben, *J. Organomet. Chem.*, 1985, **297**, 61-67.
6. D. Gourier, E. Samuel and J. H. Teuben, *Inorg. Chem.*, 1989, **28**, 4663-4667.
7. R. D. Rogers and J. H. Teuben, *J. Organomet. Chem.*, 1989, **359**, 41-47.
8. I. F. Urazowski, V. I. Ponomaryev, I. E. Nifant'ev and D. A. Lemenovskii, *J. Organomet. Chem.*, 1989, **368**, 287-294.
9. P. B. Hitchcock, M. F. Lappert, G. A. Lawless, H. Olivier and E. J. Ryan, *J. Chem. Soc., Chem. Commun.*, 1992, 474-476.
10. M. D. Fryzuk, M. Mylvaganam, M. J. Zawarotko and L. R. MacGillivray, *Polyhedron*, 1996, **15**, 689-703.
11. B. Ray, T. G. Neyroud, M. Kapon, Y. Eichen and M. S. Eisen, *Organometallics*, 2001, **20**, 3044-3055.
12. D. Pun, S. M. Leopold, C. A. Bradley, E. Lobkovsky and P. J. Chirik, *Organometallics*, 2009, **28**, 2471-2484.
13. D. F. Evans, *J. Chem. Soc. (Resumed)*, 1959, 2003-2005.
14. E. M. Schubert, *J. Chem. Educ.*, 1992, **69**, 62.
15. C. Piguet, *J. Chem. Educ.*, 1997, **74**, 815-816.
16. J. Lewis and R. G. Wilkins, *Modern Coordination Chemistry*, Interscience Publishers, New York, 1964.
17. R. D. Rogers and J. H. Teuben, *J. Organomet. Chem.*, 1988, **354**, 169-176.
18. M. Tamm, A. Kunst, T. Bannenberg, E. Herdtweck and R. Schmid, *Organometallics*, 2005, **24**, 3163-3171.
19. A. Glöckner, M. Tamm, A. M. Arif and R. D. Ernst, *Organometallics*, 2009, **28**, 7041-7046.
20. S. Büschel, T. Bannenberg, C. G. Hrib, A. Glöckner, P. G. Jones and M. Tamm, *J. Organomet. Chem.*, 2009, **694**, 1244-1250.

21. C. E. Davies, I. M. Gardiner, J. C. Green, M. L. H. Green, N. J. Hazel, P. D. Grebenik, V. S. B. Mtetwa and K. Prout, *J. Chem. Soc., Dalton Trans.*, 1985, 669-683.

22. A. P. Humphries and S. A. R. Knox, *J. Chem. Soc., Dalton Trans.*, 1978, **1978**, 1514-1523.

23. R. Goddard and P. Woodward, *J. Chem. Soc., Dalton Trans.*, 1979, 661-667.

24. A. H. Connop, F. G. Kennedy, S. A. R. Knox, R. M. Mills, G. H. Riding and P. Woodward, *J. Chem. Soc., Chem. Commun.*, 1980, 518-520.

25. R. Goddard, S. A. R. Knox, R. F. D. Stansfield, F. G. A. Stone, M. J. Winter and P. Woodward, *J. Chem. Soc. Dalton Trans.*, 1982, 147-158.

26. B. Fischer, J. Boersma, B. Kojić-Prodić and A. L. Spek, *J. Chem. Soc., Chem. Commun.*, 1985, 1237-1239.

27. R. P. Aggarwal, N. G. Connelly, B. J. Dunne, M. Gilbert and A. G. Orpen, *J. Chem. Soc. Dalton Trans.*, 1991, 1-9.

28. B. Bachmann, J. Heck, G. Meyer, J. Pebler and T. Schleid, *Inorg. Chem.*, 1992, **31**, 607-614.

29. V. Lavallo and R. H. Grubbs, *Science*, 2009, **326**, 559-562.

30. S. Büschel, A.-K. Jungton, T. Bannenberg, S. Randoll, C. G. Hrib, P. G. Jones and M. Tamm, *Chem. Eur. J.*, 2009, **15**, 2176-2184.

4 CHAPTER FOUR: THE ACTIVATION OF CARBON MONOXIDE AND CARBON DIOXIDE BY LOW VALENT ZIRCONIUM(III) COMPOUNDS

4.1 Introduction

Despite the large volume of research that has been conducted with regards to small molecule activation by zirconium complexes and fully discussed in Chapter 1, none have so far utilised a discrete Zr(III) starting material, with preference instead for *in situ* reduction of Zr(IV) complexes under a blanket of CO or CO_2. In addition to Zr(III) chemistry being generally ill-defined with few examples in existence, fewer reports exist for CO_2 activation by zirconium complexes than for CO. In this chapter, the activity of the three well defined Zr(III) complexes (**3.1**, **3.2** and **3.3**, illustrated in **Figure 4.1**), characterised in Chapter Three, towards the carbon oxides will be discussed.

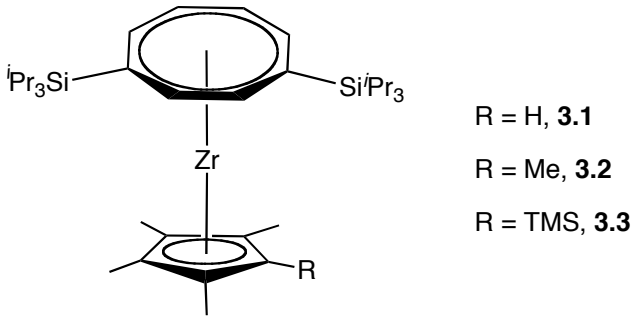

Figure 4.1: Zr(III) complexes for reaction with small molecules.

4.2 Reactivity of [Zr(η^8-C_8H_6{Si^{i}Pr$_3$-1,4}$_2$)(Cp^{Me4R})] with ^{13}CO

Addition of isotopically labelled ^{13}CO, *via* Toepler line to a cooled (-78 °C) dark red solution of **3.1** or **3.2** in toluene resulted in new resonances observed by $^{13}C\{^1H\}$ NMR spectroscopy after approximately fifteen minutes.

After being allowed to reach ambient temperature while stirring overnight, the samples were isolated and stored at -35 °C leading to isolation of X-ray quality small red crystals for R = Me (**4.1)** and small black crystals for R = H (**4.2**), albeit in poor yields (*vide infra*). No difference in reactivity was observed with one equivalent or excess gas, and in the case of **3.3**, no reactivity was observed even upon heating to 80 °C. Addition of a mixture of ^{13}CO and H_2 did not afford any other products than those observed from carbon monoxide alone, with **3.3** still showing no reactivity, presumably due to subtle electronic and steric effects caused by the TMS group present on the Cp ligand.

4.2.1 Identification and characterisation of 4.1

X-ray diffraction analysis showed **4.1** to be a dimeric compound (**Scheme 4.1**, **Figure 4.2**) constructed from 14 electron monomers linked by a zig-zag OC-CO unit bonded to both zirconium atoms. The new carbon atoms each form bridgeheads between C2 and C5 of the COT ring, resulting in C2 and C5 becoming sp^3 hybridised and C3 and C4 bending away from the metal atom. A large single peak corresponding to the zig-zag core is observed at δ_C 104 by $^{13}C\{^1H\}$ NMR spectroscopy, representing the major product. Arrayed $^{13}C\{^1H\}$ NMR spectra of the reaction mixture at approximately nine minute intervals over eleven hours shows little variation in resonances, with the major peak at δ_C 104 and a number of much smaller peaks corresponding to isotopically labelled ^{13}C in as yet unidentified minor products. Further analysis by ^{13}C NMR spectroscopy was inconclusive regarding further product elucidation.

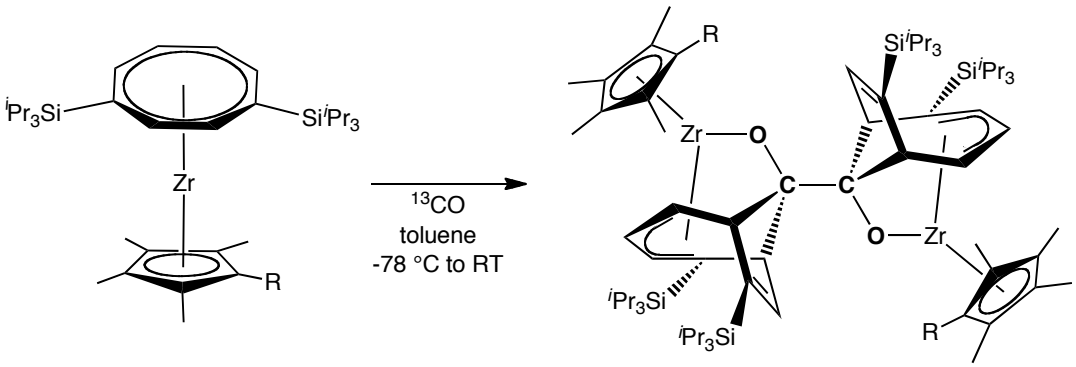

Scheme 4.1: Synthetic route for generation of **4.1** (R = H).

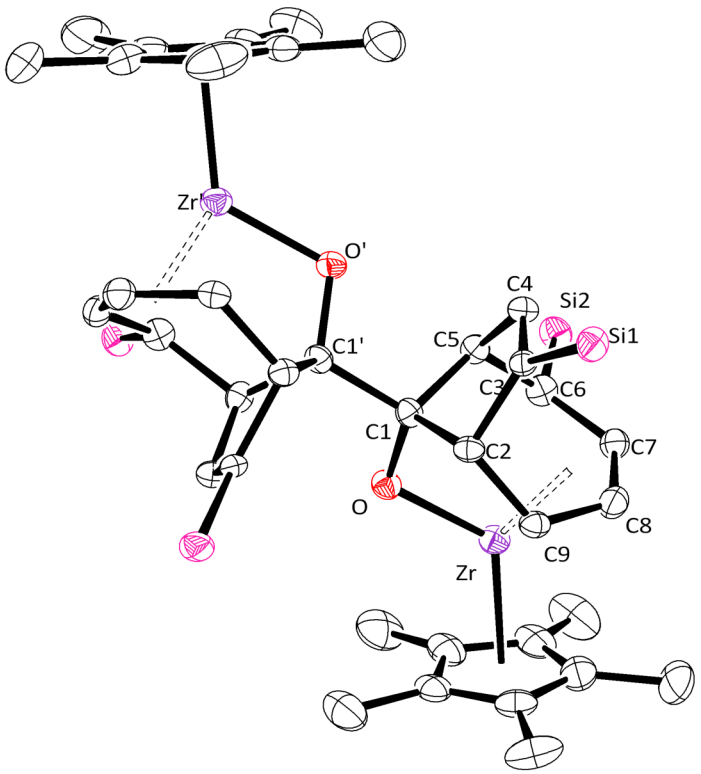

Figure 4.2: Molecular structure of $[Zr(\eta^4\text{-}C_8H_6\{Si^iPr_3\text{-}1,4\}_2)(Cp^{Me5})^{13}CO]_2$ (**4.1**). Hydrogen atoms and ^{i}Pr groups are omitted for clarity. Thermal ellipsoids at 50 % probability levels.

The zirconium atoms in **4.1** are still bound to the COT moiety, although now in an η^4 manner, and can be considered as Zr(IV) centres by ^{1}H NMR spectroscopic evidence and electron counting considerations. Green's guide to electron counting regards cyclopentadienyl as an L_2X, alkoxide as X and the deformed COT ring as an LX_2 ligand, thus leading to the conclusion that this dimer consists of two 14 electron monomers each containing a +4 zirconium centre.

The identity of **4.1** was confirmed by mass spectrometry, with the parent ion appearing at m/z 1340. Analysis of the pure product by ^{1}H NMR spectroscopy identified six separate COT-H resonances between 6.30 and 3.00 ppm, in agreement with the significant change in COT environment from the starting material. A singlet corresponding to the Cp group was observed at δ_H 1.85, with resonances due to the *iso*propyl silyl groups merged into a broad multiplet between 1.42 and 1.21 ppm. Two resonances are seen by ^{29}Si{^{1}H} NMR spectroscopy at δ_{Si} 6.03 and 4.02 and again confirm the loss of symmetry in the COT ligand in **4.1**. Assignment of ^{1}H and ^{13}C{^{1}H} NMR spectra was by recourse to 2D techniques including COSY, HSQC and HMBC. Data from X-ray diffraction studies including bond lengths and angles are summarised alongside those data from **4.2** in **Table 4.1**.

4.2.2 Identification and characterisation of 4.2

In the case of **4.2**, two doublets observed by ^{13}C{^{1}H} NMR spectroscopy at 145 and 128 ppm were indicative of the resultant compound, which was shown by X-ray diffraction studies to again be a dimeric complex (**Scheme 4.2**, **Figure 4.3**). Despite again consisting of two 14 electron monomers and containing the same atoms, **4.2** is very different from **4.1**. Here, both zirconium atoms are bonded to the same COT ligand that is bent along the C001/C005 plane, with an OC=CO linkage between the metal atoms which is itself bonded to the remaining COT ring. Arrayed ^{13}C{^{1}H} NMR spectra of the reaction mixture at approximately nine minute intervals over fourteen hours detected a resonance at δ_C 106 and is attributable to a metastable intermediate which decomposes to give rise to the pair of doublets indicative of **4.2**. With this initial resonance occurring at a frequency similar to that observed for **4.1**, it is presumed to correspond to the tetramethylated cyclopentadienyl

analogue of **4.1**, which then undergoes an intramolecular rearrangement to afford the major product **4.2** (**Scheme 4.3**).

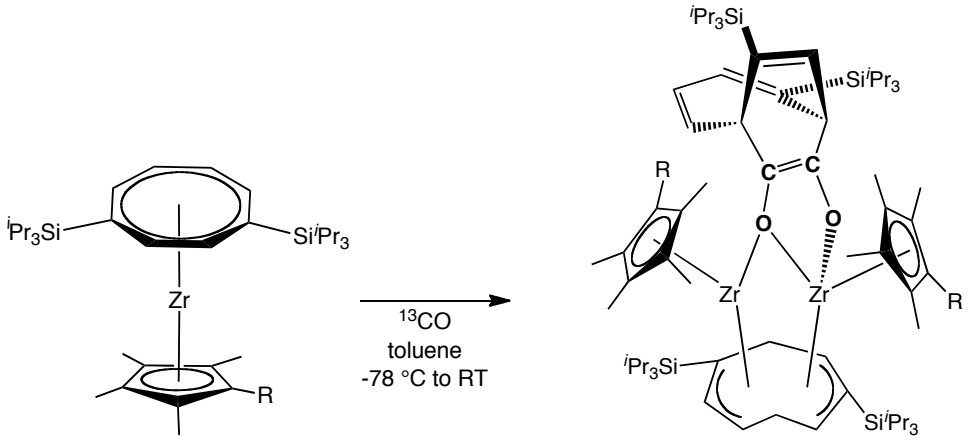

Scheme 4.2: Synthetic route for generation of **4.2** (R = Me).

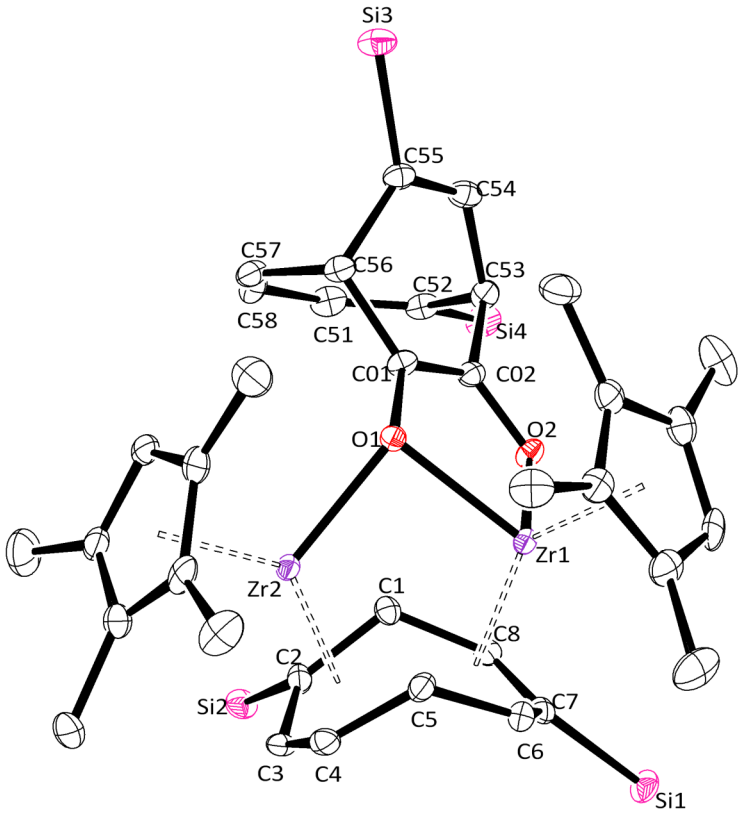

Figure 4.3: Molecular structure of $[Zr(C_8H_6\{Si^{i}Pr_3\text{-}1,4\}_2)(Cp^{Me4H})^{13}CO]_2$ (**4.2**). Hydrogen atoms and ^{i}Pr groups are omitted for clarity. Thermal ellipsoids at 50 % probability level.

The identity of **4.2** was indicated by mass spectrometry, although the anticipated parent ion was not observed at m/z 1340: the greatest value peak occurred at m/z 1298 and corresponded to the loss of an *iso*propyl group from the molecule. Purity was confirmed by elemental analysis. The resonances observed in the ^{1}H NMR spectrum are consistent with that of a diamagnetic compound, with no paramagnetic broadening observed. However, similar electron counting considerations to those discussed for **4.1** suggest that both zirconium centres could exist in the +3 oxidation state and spin-pair due to their proximity to each other to give rise to a singlet state, or they could exist in oxidation states different to each other as a Zr(II)/Zr(IV) pair: both situations giving rise to the diamagnetic ^{1}H NMR spectra observed.

Analysis of pure **4.2** by ^{1}H NMR spectroscopy identified twelve separate COT-H resonances between 6.54 and 2.72 ppm, in agreement with two eight-membered ligands in different environments. The Cp resonances were observed as two singlets (δ_H 6.14, 5.32) corresponding to the Cp-H groups, with five further singlets at lower frequencies (δ_H 2.39, 2.22, 2.05, 1.91, 1.84), corresponding to the methyl environments. The *iso*propyl silyl groups merged into a broad multiplet between 1.50 and 1.05 ppm, with it impossible to conclusively identify the resonances caused by the CH and CH_3 units. Three resonances are seen by ^{29}Si{^{1}H} NMR spectroscopy at δ_{Si} 4.17, 3.23, 0.65, detectable *via* the 2D technique HMBC, whilst assignment of ^{1}H NMR spectra was by recourse to COSY. Selected data from X-ray diffraction analysis are summarised in **Table 4.1**.

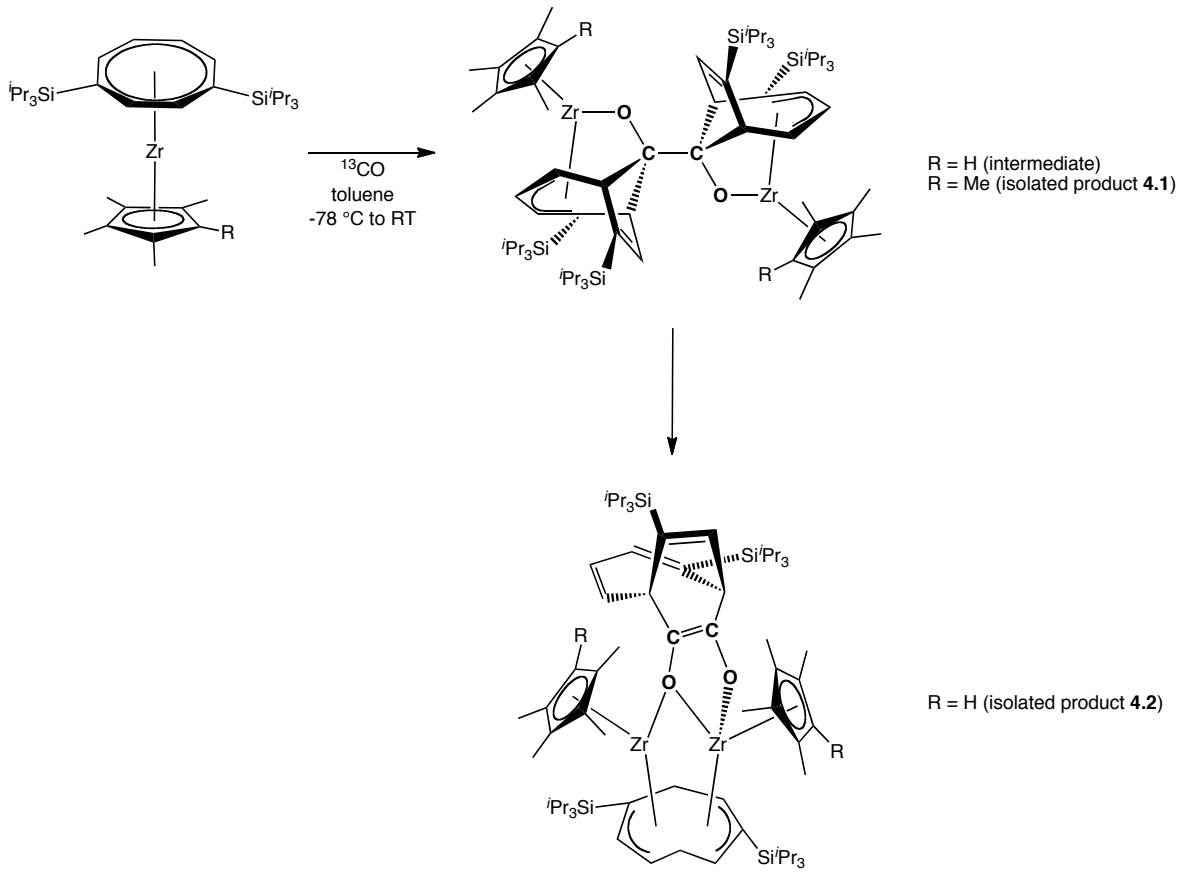

Scheme 4.3: Synthetic route to **4.1** and **4.2**, where **4.1** is analogous to an intermediate in the generation of **4.2.**

Table 4.1: Selected bond angles (deg) and distances (Å) for [Zr(η^8-C_8H_6{Si^{i}Pr$_3$-1,4}$_2$)(Cp^{Me4R})(CO)]$_2$ (**4.1**, R = Me; **4.2**, R = H). $COT_{cent.}$ and $Cp_{cent.}$ indicate the centroid of the COT and Cp rings

Compound	**4.1**	**4.2**
C-C	1.618(8)	1.325(5)
C-O	1.440(5)	1.411(4), 1.345(4)
Zr-O	1.9637(3)	2.177(2), 2.197(2), 2.133(2)
Zr-$Cp_{cent.}$	2.200(4)	2.2380(22), 2.2414(16)
Zr-$COT_{cent.}$	1.952(4)	1.9855(17), 1.8145(19)
Cp C-C range	1.401(8) – 1.435(8)	1.403(5) – 1.431(5)
COT C-C range	1.344(6) – 1.577(6)	1.391(5) – 1.520(5)

NB: COT C-C range refers to the eight-membered ligand bound to the zirconium atom(s)

Since no similar dinuclear OCCO-bridged compounds exist, direct comparisons are impossible for **4.1** and **4.2**. For compound **4.1**, the C-C and C-O distances in the zig-zag moiety are consistent with those expected for singly bonded units (1.618(8) and 1.440(5) Å respectively), with the C-C distance corresponding to a lengthened bond with respect to a traditional C-C single bond. In the case of **4.2**, the C-C distance is significantly shorter and comparable to that expected for a doubly bonded unit at 1.325(5) Å. The C1-O1 distance in **4.2** measures 1.411(4) Å and represents a singly bonded fragment, while the distance calculated for the C2-O2 bond is significantly shorter (1.345(4) Å) and is comparable to the delocalised C-O arrangement in carboxylic acids.

When literature data for Zr-O distances are examined, (where the oxygen atom is bound to two atoms), a bimodal histogram results, with a high frequency of bond lengths measuring between 1.945 and 1.970 Å and between 2.195 and 2.220 Å (**Figure 4.4**). On consideration

of the literature examples, is unclear why there are two modal frequencies in this case. The Zr-O bond distance in **4.1** measures 1.9637(3) Å and corresponds to this first modal length, whilst the Zr-O distances in **4.2** are longer at 2.177(2), 2.197(2) and 2.133(2) Å and correspond to the second modal length.

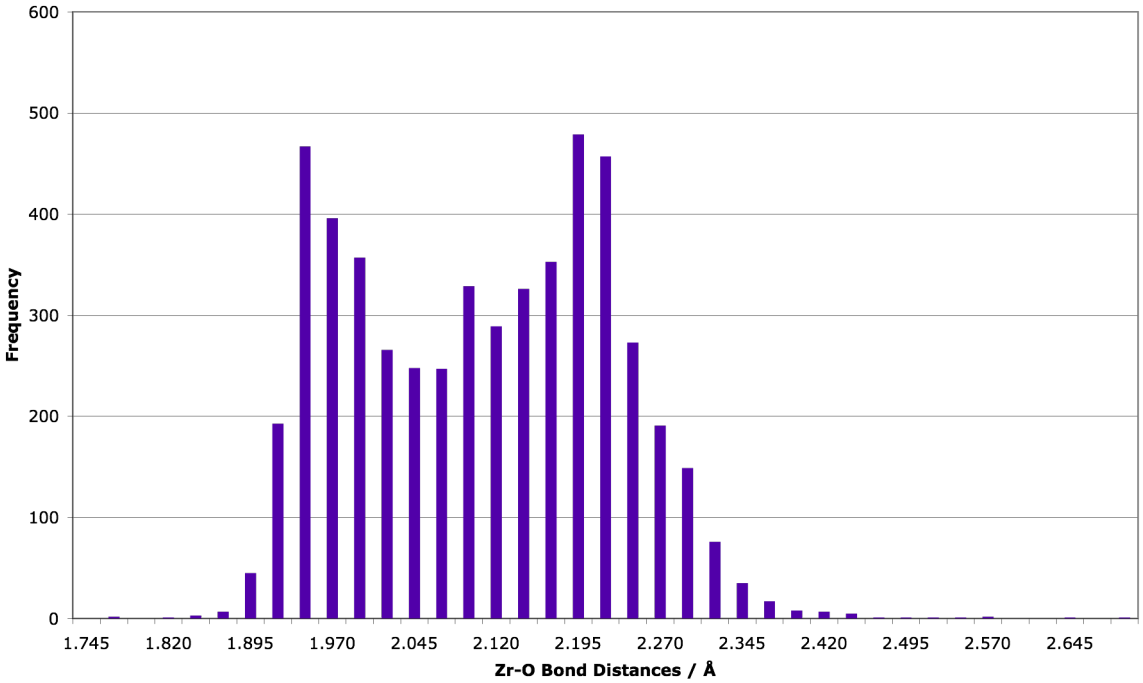

Figure 4.4: Zr-O distances where the oxygen atom is only bound to two atoms.[1-3]

The Zr-$Cp_{cent.}$ and cyclopentadienyl C-C distances in complexes **4.1** and **4.2** are consistent with those previously documented for the Zr-Cp moiety. Due to the deformation of the COT ligand in both cases, the C-C distances now range from aromatic to singly-bound C-C units (**Figure 4.5**). In each case, the sections of the eight-membered ligand that possess that shorter C-C bonds are coordinated to the zirconium atoms. For **4.1**, deformation of the eight-membered ring is concurrent with the formation of the new bridgehead across C2 and C5, and subsequent sp^3 hybridisation of those carbon atoms. The shortest C-C distances are between C7 and C8, and C3 and C4, with the former bond the furthest point from the new bridgehead. In the case of **4.2**, the ligand is bent along the C1/C5 axis so that the ring is no longer planar, with longer distances from C1 and C5 to C2, C8, C4 and C6 than seen

in the remainder of the ligand. The migrated eight-membered ring in **4.2** (C51 – C58) bound to the OC=CO core possess double bonds between C51/C52, C54/C55 and C57/C58, while the other C-C bonds in the fragment are calculated as being significantly longer.

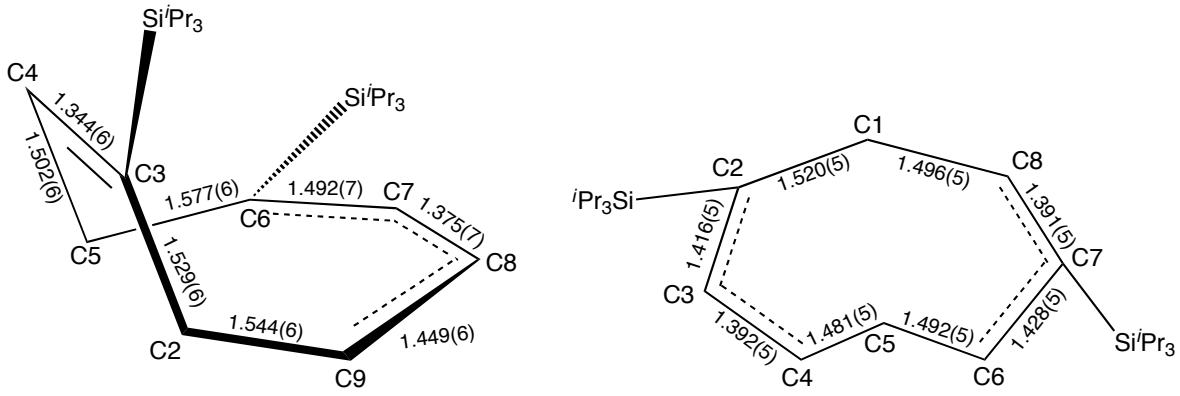

Figure 4.5: Deformed zirconium-bound COT ligands (with bond lengths in Å) for **4.1** (left) and **4.2** (right).

4.2.3 Theoretical calculations on the formation of 4.1

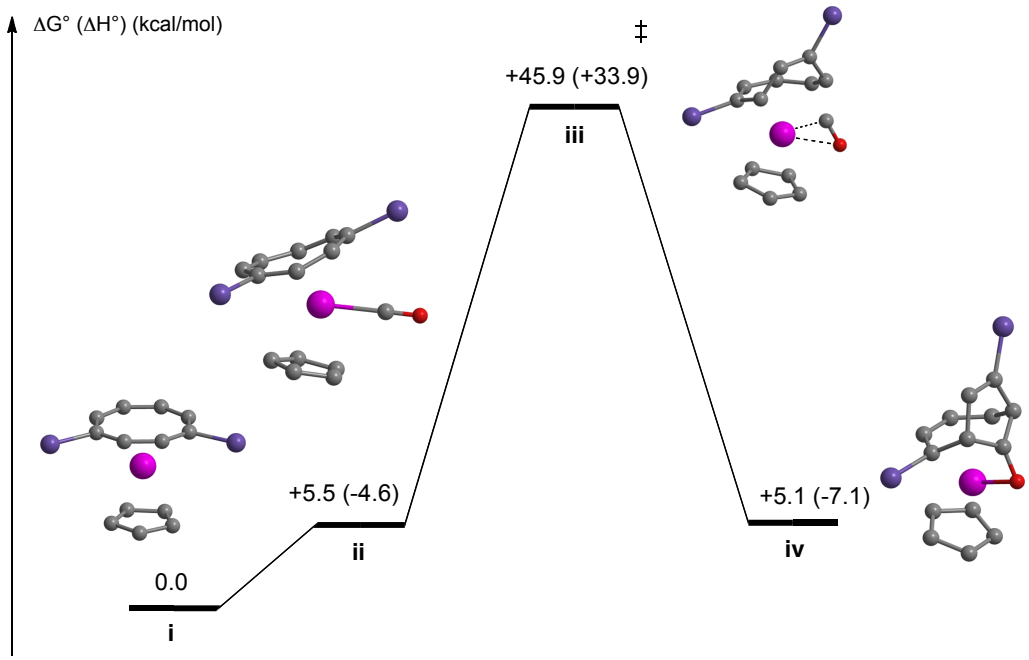

Figure 4.6: Formation of **4.1** from **3.2**. A zirconium-carbon bond is the first to form, before rearrangement resulting in a zirconium-oxygen bond. The values calculated are entropy, whilst those in parenthesis are enthalpy values.

Theoretical studies have been completed by Prof. L. Maron regarding the formation of **4.1** from **3.2** (**Figure 4.6**). Due to the difficulty in calculating entropy in the gas phase, a larger than expected ΔG° value results, implying the need for thermal activity (+ 45.9 kcal.mol^{-1}) between **ii** and **iii**. However, the reaction actually proceeds at ambient or sub-ambient temperatures and is more appropriately described using the enthalpy term (+ 33.9 kcal.mol^{-1}).

The CO carbon atom initially forms a bond with the zirconium atom in **ii**, with only a small increase in energy from the Zr(III) starting material. Compound **ii** undergoes a

rearrangement with rotation of the CO unit and initial deformation of the eight-membered ring to form **iii**, before formation of the zirconium-oxygen bond and C-COT bonds to afford **iv**. The final product (**iv**) is more stable than the Zr(III) starting material by 7.1 kcal.mol^{-1}, if enthalpy only is considered, and marginally more favourable than the first intermediate (**ii**) which possesses the Zr-C bond. Calculations have yet to be completed for the formation of **4.2**.

4.3 Reactivity of [Zr(η^8-C_8H_6{Si^{i}Pr$_3$-1,4}$_2$)(Cp^{Me4R})] with $^{13}CO_2$

Under similar conditions to those employed for the synthesis of **4.1** and **4.2**, $^{13}CO_2$ was added to a toluene solution of **3.1**, **3.2** or **3.3**, in each case yielding a bright orange solution upon warming to ambient temperature. These mixtures were allowed to stir overnight before decantation and storage at -35 °C. In the case of R = H (**4.3**) and R = Me (**4.4**), low yields of bright orange X-ray quality crystals were obtained, while those afforded for R = TMS (**4.5**) were red in colour and also low-yielding. In each case, addition of one equivalent or excess $^{13}CO_2$ made no noticeable difference to products isolated or their yield. Compounds **4.3**, **4.4** and **4.5** each display one significant resonance attributable to the isotopically labelled ^{13}C at *ca*. 167 ppm corresponding to a carbonate core (*vide infra*).

4.3.1 Identification and characterisation of 4.3, 4.4 and 4.5

For compounds **4.3**, **4.4** and **4.5**, X-ray diffraction analysis showed the crystalline products to be tetranuclear compounds as illustrated in **Figure 4.7**. In these compounds, it appears that four Zr(III) molecules have been bound together by two bridging carbonate and oxo groups with concomitant loss of two COT ligands to yield [$OZr_2(CO_3)_2Zr_2O$]^{Me4R} (R = H, **4.3**; R = Me, **4.4**; R = TMS, **4.5**). Following the loss of the COT units, the remaining eight-membered ligands each bridge two zirconium atoms. In terms of electron counting, the structure illustrated in **Figure 4.6** can be rationalised as described in **Table 4.2**, leading to the conclusion that the tetramer possess 64 electrons, equating to four 16 electron monomers, each of which contain a zirconium(IV) centre.

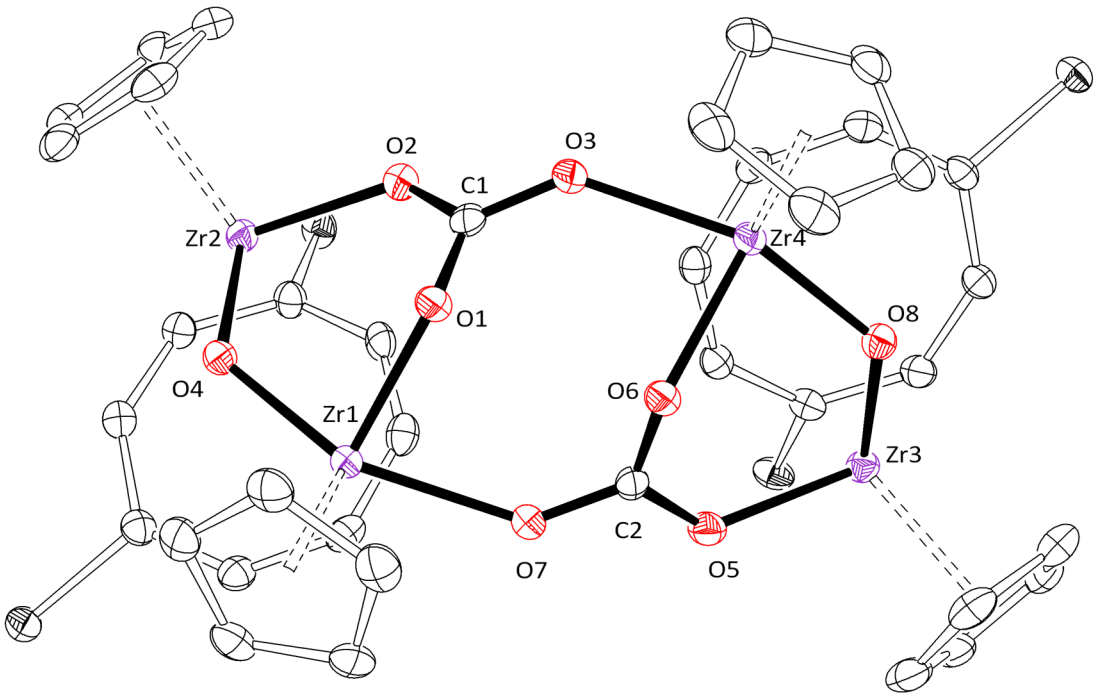

Figure 4.7: Molecular structure of $[OZr_2(CO_3)_2Zr_2O]^{Me4R}$ (**4.3**, R = H; **4.4**, R = Me; **4.5**, R = TMS). Example **4.3** is shown here and is isostructural to **4.4** and **4.5**. Hydrogen atoms, Me, TMS and ^{i}Pr groups are omitted for clarity. Thermal ellipsoids at 50 % probability levels.

Table 4.2: Green's electron counting considerations for **4.3**, **4.4** and **4.5**.

Fragment	L_nX_y per fragment	Electrons in fragment	Total electrons
Zr	-	4	16
Cp	L_2X	5	20
COT	L_3X_2	8	16
CO_3	LX_2	4	8
O	X_2	2	4

$$CO_2 + 2e^- \longrightarrow CO + O^{2-} \qquad \text{(Equation 1)}$$

$$2CO_2 \longrightarrow CO_3^{2-} + CO \qquad \text{(Equation 2)}$$

The carbonate and oxo groups in these compounds have presumably been generated *via* the reduction and disproportionation (**Equations 1** and **2**) of $^{13}CO_2$, with free ^{13}CO detectable by *in situ* $^{13}C\{^1H\}$ NMR spectroscopy of the reaction mixture supporting this assumption. If the reactions are analysed by $^{13}C\{^1H\}$ NMR spectroscopy overnight *via* an array of short data collections, the main product peak at *ca*. 167 ppm appears immediately, and does not grow in intensity over time. Peaks corresponding to the ^{13}CO products **4.1** and **4.2** appear along with the expected resonance for free carbon monoxide, presumably as residual Zr(III) reacts with the CO molecules generated upon formation of **4.3** and **4.4**. In the synthesis of **4.5**, only three resonances attributable to labelled-^{13}C are detected (δ_C 172.97, 164.83 and 76.17). The second resonance is due to the isolated compound **4.5**, with the first resonance also observed during the synthesis of **4.3** and **4.4**, although like the third peak, it is yet to be conclusively identified.

In the case of **4.3**, mass spectrometry indicated the identity of the product, although it was not possible to observed the anticipated parent ion, with the greatest value mass peak observed at m/z 1298, corresponding to the loss of one COT and one Cp ligand from the parent molecule. No meaningful data from mass spectrometric analysis was obtained for **4.4** and **4.5**, although elemental analysis confirmed the purity of **4.3** and **4.5**. Analysis of ^1H NMR spectra for **4.3** and **4.4** identified eight resonances corresponding to twelve COT protons between δ_H 7.56 and 5.56, with the *iso*propyl resonances occurring upfield between δ_H 1.70 and 0.90 as overlapping resonances, indicating that the COT ligands in the final product are inequivalent. The Cp^{Me5} ligand is recorded as four resonances integrating 24: 24: 4: 4: 4 between 2.19 and 1.88 ppm, again indicative of inequivalent ligand environment. For **4.3**, the Cp-H groups are observed amongst the COT-H resonances as two singlets (δ_H 6.85 and 6.27), with the methyl groups apparent as eight singlets, each integrating to six protons between 2.59 and 1.83 ppm. The silicon environments were detectable by $^{29}Si\{^1H\}$ NMR spectroscopy, with resonances at δ_{Si} 7.01 and 5.50 for **4.3** and

four resonances at δ_{Si} 1.35, 1.29, 1.08 and 0.85 for **4.4**. Finally, the bridging carbonate groups were apparent at δ_C 166.97, 167.39 and 164.83 for compounds **4.3**, **4.4** and **4.5** respectively. Due to the very small amount of **4.5** isolated, ^{1}H, $^{13}C\{^{1}H\}$ and $^{29}Si\{^{1}H\}$ NMR spectroscopic data have not been obtained. Selected bond lengths and angles are summarised in **Table 4.3**.

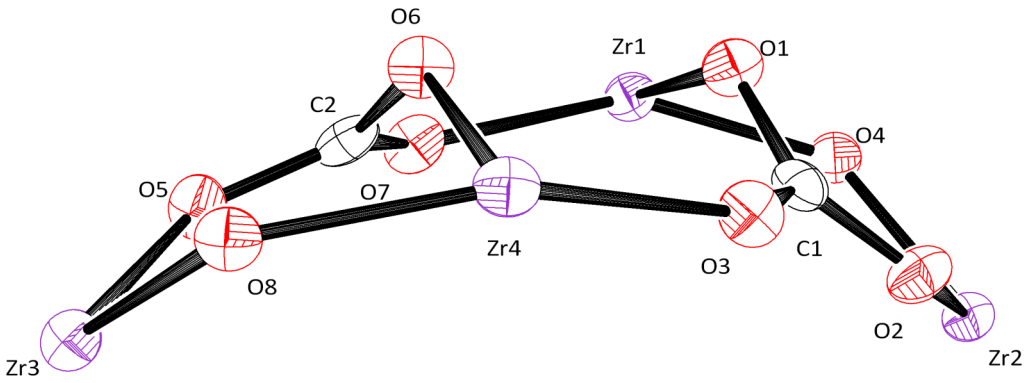

Figure 4.8: "Side-on" view of molecular structure of carbonate/oxo core of $[OZr_2(CO_3)_2Zr_2O]^{Me4R}$ (**4.3**, R = H; **4.4**, R = Me; **4.5**, R = TMS). Hydrogen atoms, COT and Cp ligands are omitted for clarity. Thermal ellipsoids at 50 % probability levels. The zirconium atoms are linked through the core of the molecule *via* oxo and carbonate units, with this central moiety taking on a 'curved' appearance in which the COT ligands would be aligned along the shorter, inner curve, while the Cp ligands project outward from the O1/O6 face.

Table 4.3: Selected bond angles (deg) and distances (Å) for $[OZr_2(CO_3)_2Zr_2O]^{Me4R}$ (**4.3**, R = H; **4.4**, R = Me; **4.5**, R = TMS). O_{oxo} and O_{CO3} indicate to whether the oxo or carbonate moieties are referred.

Compound	**4.3**	**4.4**	**4.5**
Zr-O_{oxo} range	1.952(19) – 1.9942(19)	1.921(3) – 2.006(3)	1.9323(2) – 2.0005(2)
Zr-O_{CO3} range	2.1054(19) – 2.200(2)	2.096(3) – 2.190(3)	2.1000(3) – 2.2068(2)
C-O_{CO3} range	1.269(3) – 1.293(3)	1.274(5) – 1.303(5)	1.263(10) – 1.305(9)
Zr-O-Zr	124.94(9), 126.33(10)	125.34(17), 127.35(14)	127.0(3), 127.0(3)
Cp C-C range	1.407(4) – 1.425(4)	1.403(6) – 1438(6)	1.392(16) – 1.443(13)
COT C-C range	1.400(4) – 1.450(4)	1.391(6) – 1.443(6)	1.382(14) – 1.455(12)

There are no significant differences in the measured bond lengths and angles between compounds **4.3**, **4.4** and **4.5**. The Cp and COT C-C ranges are typical for the ligands concerned, with a relatively narrow range of C-C distances measured. The Zr-O_{oxo} and Zr-O_{CO3} distances (1.921(3) to 2.2068(2) Å) are also comparable with literature values as illustrated in **Figure 4.4** (*vide supra*). The C-O bonds in the carbonate units are as expected, corresponding to elongated double bonds or single bonds with partial double bond character.

4.4 Conclusions

Although the Zr(III) complexes **3.1**, **3.2** and **3.3** exhibit distinctly different reactivity to that displayed by the U(III) analogues, C-C bond formation and the synthesis of novel products has been possible. Variation of the sterics of the cyclopentadienyl ligand results in different products, with the most sterically encumbered system, **3.3**, failing to react at all with carbon monoxide. The slightly less hindered **3.2** results in a product (**4.1**) that is believed to be similar to an intermediate detected by $^{13}C\{^{1}H\}$ NMR spectroscopy in the synthesis of the **4.2**. In the reaction of **3.1** with CO, it is believed that the metastable intermediate, similar to **4.1**, undergoes a rearrangement process affording **4.2**.

Despite the differences in reactivity towards carbon monoxide demonstrated by the Zr(III) compounds, the three reduced zirconium compounds all react with carbon dioxide to yield very similar products, $[OZr_2(CO_3)_2Zr_2O]^{Me4R}$ (**4.3**, R = H; **4.4**, R = Me; **4.5**, R = TMS) with concomitant release of CO *via* reduction and reductive disproportionation of CO_2. Analysis of $^{13}C\{^{1}H\}$ NMR spectra obtained during the synthesis of **4.3**, **4.4** and **4.5** suggest that a number of other products are formed in these reactions, although their identities are yet to be unambiguously confirmed.

4.5 Experimental details for Chapter Four

4.5.1 Synthesis of [Zr(η^4-C_8H_6{Si^{i}Pr$_3$-1,4}$_2$)(Cp^{Me5})^{13}CO]$_2$ (4.1)

To an ampoule charged with a dark red solution of **3.2** (0.115 g, 0.18 mmol) in d_8-toluene (0.5 cm^3) was added one equivalent of ^{13}CO gas *via* Toepler line at -78 ºC before warming to ambient temperature. Shortly after addition the solution appeared more orange-red in colour. Storage at -35 °C of a toluene solution afforded small red crystals which were suitable for X-Ray diffraction studies in poor yield.
Yield = 0.0058 g (0.0043 mmol), 5 % w.r.t. **3.2**.

^{1}H NMR (toluene-d_8, 399.5 MHz, 303K): δ_H 6.30 (s, 1H, COT-H), 4.89 (d, $|^3J_{HH}|$ = 8.90 Hz, 1H, COT-H), 4.41 (t, $|^3J_{HH}|$ = 9.60 Hz, 1H, COT-H), 3.98 (s, 1H, COT-H), 3.43 (s, 1H, COT-H), 3.00 (d, $|^3J_{HH}|$ = 8.90 Hz, 1H, COT-H), 1.85 (s, 15H, Cp-CH_3), 1.21-1.42 (m, 42H, ^{i}Pr-CH and ^{i}Pr-CH_3).
^{13}C{^{1}H} NMR (toluene-d_8, 100.5 MHz, 303K): δ_C 152.04 (COT-*C*H), 132.66 (COT-*C*H), 120.53 (COT-*C*H), 118.70 (Cp-*C*CH$_3$), 106.99 (COT-*C*Si), 104.27 (O-C), 103.82 (COT-*C*Si), 91.96 (COT-*C*H), 80.09 (COT-*C*H), 63.87 (COT-*C*H), 20.72 (^{i}Pr-C), 20.29 (^{i}Pr-C), 19.88 (^{i}Pr-C), 19.80 (^{i}Pr-C), 13.45 (Cp-*C*H$_3$), 13.23 (Cp-*C*H$_3$), 1313 (Cp-*C*H$_3$), 12.74 (Cp-*C*H$_3$), 11.66 (Cp-*C*H$_3$).
^{29}Si{^{1}H} NMR (toluene-d_8, 79.4 MHz, 303 K): δ_{Si} 6.03 (Si^{i}Pr$_3$), 4.02 (Si^{i}Pr$_3$).
MS (EI)$^+$: m/z = 59 (100 %), 1340 (M$^+$, 83 %).
Crystal data for **4.1**: Red plates 0.36 × 0.22 × 0.06 mm^3, $C_{74}H_{126}Si_4Zr_2$, a = 21.6997(4), b = 22.2120(8), c = 15.2503(5) Å, α = 90 °, β = 93.914(2) °, γ = 90 °, U = 7333.4(4) Å^3, monolinic, C 2/c, Z = 4, total reflections 44731, independent reflections 7461, R_{int} = 0.102, θ_{max} = 26.37, R_1 [I >2σ(I)] = 0.068, wR^2 = 0.153 and 370 parameters.
An unidentified residual peak of 3.0 e is located 0.85 Å from C6, which does not make any chemical sense. (Note: this was present in several crystals from the original batch, and also on a subsequent batch of independently synthesised crystals). In this solution, attempted anisotropic refinement of C6 gave unrealistic ellipsoids, and it was therefore left isotropic.

4.5.2 Synthesis of [Zr(COT{Si^{i}Pr$_3$-1,4}$_2$)(Cp^{Me4H})^{13}CO]$_2$ (4.2)

To an ampoule charged with a dark red solution of **3.1** (0.069 g, 0.0110 mmol) in d_6-benzene (0.5 cm^3) was added one equivalent of ^{13}CO gas *via* Toepler line at -78 ºC before warming to ambient temperature. Immediately after addition the solution appeared more orange-red in colour. Storage of a toluene solution at -35 °C afforded small black X-ray quality crystals in poor yield.
Yield = 0.002 g (0.00152 mmol), 3 % w.r.t. **3.2**.

^{1}H NMR (benzene-d_6, 399.5 MHz, 303K): δ_H 6.54 (m, 2H, COT-H), 6.14 (s, 1H, Cp-H), 6.04 (s, m, COT-H), 5.76 (d, $|^3J_{HH}|$ = 7.53 Hz, 1H, COT-H), 5.65 (m, 1H, COT-H), 5.37 (d, $|^3J_{HH}|$ = 9.15 Hz, 1H, COT-H), 5.32 (s, 1H, Cp-H), 4.00 (m, 2H, COT-H), 3.86 (m, 2H, COT-H), 2.72 (t, $|^3J_{HH}|$ = 10.07 Hz, 1H, COT-H), 2.39 (s, 2H, CH_3), 2.22 (s, 2H, CH_3), 2.05 (s, 4H, CH_3), 1.91 (s, 2H, CH_3), 1.84 (s, 2H, CH_3), 1.50-1.05 (m, Si^{i}Pr$_3$).
Meaningful ^{13}C{^{1}H} NMR spectroscopic data is yet to be obtained for **4.2**. The only resonances that can be reliably assigned are those due to the doubly-bonded isotopically labelled ^{13}C atoms.
^{13}C{^{1}H} NMR (benzene-d_6, 100.5 MHz, 303K): δ_C 144.76 (d, $|^1J_{CC}|$ = 85.77 Hz, ^{13}C-^{13}C), 127.76 (d, $|^1J_{CC}|$ = 85.96 Hz, ^{13}C-^{13}C).
^{29}Si{^{1}H} NMR (benzene-d_6, 79.4 MHz, 303 K): δ_{Si} 4.17 (Si^{i}Pr$_3$), 3.23 (Si^{i}Pr$_3$), 0.65(Si^{i}Pr$_3$)
MS (EI)$^+$: m/z = 157 (100 %), 1298 (M$^+$ - ^{i}Pr, 1 %).
Elemental analysis calcd (%) for $C_{72}H_{122}O_2Si_4Zr_2$: C 65.7, H 9.30; found: C 66.0, H 9.42
Crystal data for **4.2**: Red plates 0.40 × 0.06 × 0.04 mm^3, $C_{72}H_{122}O_2Si_4Zr_2$, a = 13.1662(3), b = 15.1978(4), c = 20.2688(5) Å, α = 71.3300(10) °, β = 83.6170(10) °, γ = 80.6610(10) °, U = 3783.77(16) Å^3, triclinic, $P\bar{1}$, Z = 2, total reflections 60578, independent reflections 16032, R_{int} = 0.0887, θ_{max} = 26.76, R_1 [I >2σ(I)] = 0.0563, wR^2 = 0.1123 and 784 parameters.

4.5.3 Synthesis of $[OZr_2(CO_3)_2Zr_2O]^{Me4H}$ (4.3)

To an ampoule charged with a dark red solution of **3.1** (0.064 g, 0.102 mmol) in d_6-benzene (0.5 cm^3) was added one equivalent of $^{13}CO_2$ gas *via* Toepler line at -78 ºC and warmed to ambient temperature, at which point the solution turned bright orange. Subsequent storage of a toluene solution at -35 °C afforded orange X-ray quality crystals in poor yield.
Yield = 0.006 g (0.00327 mmol), 13 % w.r.t. **3.1**.

^{1}H NMR (benzene-d_6, 399.5 MHz, 303K): δ_H 7.56 (d, $|^3J_{HH}|$ = 9.06 Hz, 2H, COT-H), 7.04 (d, $|^3J_{HH}|$ = 11.62 Hz, 2H, COT-H), 6.96 (d, $|^3J_{HH}|$ = 7.41 Hz, 1H, COT-H), 6.95 (d, $|^3J_{HH}|$ = 7.63 Hz, 1H, COT-H), 6.85 (s, 2H, Cp-H), 6.71 (d, $|^3J_{HH}|$ = 11.53 Hz, 2H, COT-H), 6.27 (s, 2H, Cp-H), 6.24 (d, $|^3J_{HH}|$ = 11.72 Hz, 2H, COT-H), 5.83 (d, $|^3J_{HH}|$ = 7.62 Hz, 1H, COT-H), 5.81 (d, $|^3J_{HH}|$ = 7.62 Hz, 1H, COT-H), 2.59 (s, 6H, Cp-CH_3), 2.47 (s, 6H, Cp-CH_3), 2.21 (s, 6H, Cp-CH_3), 2.06 (s, 6H, Cp-CH_3), 2.03 (s, 6H, Cp-CH_3), 1.83 (s, 6H, Cp-CH_3), 1.83 (s, 6H, Cp-CH_3), 1.83 (s, 6H, Cp-CH_3), 1.68 (septet, $|^3J_{HH}|$ = 7.42 Hz, 6H, ^{i}Pr-CH), 1.42 (d, $|^3J_{HH}|$ = 7.44 Hz, 18H, ^{i}Pr-CH_3), 1.39 (m, 6H, ^{i}Pr-CH), 1.33 (d, $|^3J_{HH}|$ = 7.46 Hz, 18 Hz, ^{i}Pr-CH_3), 1.28 (d, $|^3J_{HH}|$ = 7.44 Hz, 18 Hz, ^{i}Pr-CH_3), 0.99 (d, $|^3J_{HH}|$ = 6.85 Hz, 18 Hz, ^{i}Pr-CH_3).
$^{13}C\{^1H\}$ NMR (benzene-d_6, 100.5 MHz, 303K): δ_C 166.97 ($^{13}CO_3$), 126.19 (Cp*C*CH_3), 125.28 (COT-*C*H), 124.01 (COT-*C*H), 123.76 (Cp*C*CH_3), 123.32 (Cp*C*CH_3), 123.29 (Cp*C*CH_3), 121.93 (Cp*C*CH_3), 121.51 (Cp*C*CH_3), 121.19 (Cp*C*CH_3), 116.18 (COT-*C*H), 111.17 (COT-*C*Si), 109.61 (Cp*C*H), 108.92 (Cp*C*H), 102.94 (COT-*C*H), 99.62 (COT-*C*Si), 99.32 (COT-*C*H), 95.29 (COT-*C*H), 20.51 (Si-*C*CH_3), 20.10 (Si-*C*CH_3), 19.97 (Si-*C*CH_3), 14.98 (Cp-*C*H_3), 14.65 (Cp-*C*H_3), 14.16 (Si-*C*H), 13.66 (Cp-*C*H_3), 13.45 (Cp-*C*H_3), 12.85 (Si-*C*H), 12.24 (Cp-*C*H_3), 11.35 (Cp-*C*H_3), 10.72 (Cp-*C*H_3), 10.42 (Cp-*C*H_3).
$^{29}Si\{^1H\}$ NMR (benzene-d_6, 79.4 MHz, 303 K): δ_{Si} 7.01 (Si^{i}Pr$_3$), 5.50 (Si^{i}Pr$_3$).
MS $(EI)^+$: m/z = 873 (100 %), 1298 (M^+ - COT{Si^{i}Pr$_3$-1,4}$_2$, - Cp^{Me4H}, 1 %).
Elemental analysis calcd (%) for $C_{88}{}^{13}C_2H_{148}O_8Si_4Zr_4$: C 59.0, H 8.07; found: C 59.4, H 7.47.
Crystal data for **4.3**: Orange plates 0.25 × 0.24 × 0.20 mm^3, $C_{90}H_{148}O_8Si_4Zr_4(C_6H_6)$, a = 13.1463(2), b = 18.2248(2), c = 21.8206(3) Å, α = 100.283(1) °, β = 93.637(1) °, γ = 94.901(1) °, U = 5108.65(12) $Å^3$, triclinic, $P\bar{1}$, Z = 2, total reflections 118597, independent

reflections 23232, R_{int} = 0.056, θ_{max} = 27.48, R_1 [I >2σ(I)] = 0.042, wR^2 = 0.122 and 1079 parameters.

4.5.4 Synthesis of $[OZr_2(CO_3)_2Zr_2O]^{Me5}$ (4.4)

To an ampoule charged with a dark red solution of **3.2** (0.056 g, 0.0872 mmol) in d_6-benzene (0.5 cm^3) was added one equivalent of $^{13}CO_2$ gas *via* Toepler line at -78 ºC before warming to ambient temperature, at which point the solution turned bright orange. Subsequent storage of a toluene solution of the sample at -35 °C afforded orange X-ray quality crystals in poor yield.
Yield = 0.003 g (0.00159 mmol), 7 % w.r.t. **3.2**.

^{1}H NMR (benzene-d_6, 499.1 MHz, 303K): δ_H 7.37 (d, $|^3J_{HH}|$ = 8.68 Hz, 2H, COT-H), 7.08 (s, 1H, COT-H), 7.05 (s, 1H, COT-H), 7.02 (s, 1H, COT-H), 7.00 (m, 1H, COT-H), 6.72 (d, 2H, $|^3J_{HH}|$ = 11.96 Hz, COT-H), 6.03 (d, 2H, $|^3J_{HH}|$ = 10.65, COT-H), 5.56 (m, 2H, COT-H), 2.19 (s, 24H, Cp-CH_3), 2.15 (s, 24H, Cp-CH_3), 2.11 (s, 4H, Cp-CH_3), 2.02 (s, 4H, Cp-CH_3), 1.88 (s, 4H, Cp-CH_3), 1.70 (septet, $|^3J_{HH}|$ = 7.4 Hz, 6H, ^{i}Pr-CH), 1.36 (m, 45H, ^{i}Pr-CH_3), 1.16 (m, 25H, ^{i}Pr-CH and ^{i}Pr-CH_3), 0.90 (m, 14H, ^{i}Pr-CH_3).
$^{13}C\{^1H\}$ NMR (benzene-d_6, 100.5 MHz, 303K): δ_C 167.39 ($^{13}CO_3$), 130.55 (COT-*C*H), 129.33 (COT-*C*H), 123.95 (COT-*C*H), 123.08 (Cp*C*CH_3), 121.30 (Cp*C*CH_3), 117.88 (COT-*C*H), 112.02 (COT-*C*Si), 105.01 (COT-*C*H), 100.20 (COT-*C*H), 99.18 (COT-*C*Si), 92.30 (COT-*C*H), 20.64 (^{i}Pr-*C*H_3), 20.29 (^{i}Pr-*C*H_3), 20.15 (^{i}Pr-*C*H_3), 19.99 (^{i}Pr-*C*H_3), 19.12 (^{i}Pr-*C*H), 18.96 (^{i}Pr-*C*H_3), 14.74 (^{i}Pr-*C*H_3), 13.18 (^{i}Pr-*C*H), 12.72 (Cp*C*H_3), 12.33 (Cp*C*H_3)
$^{29}Si\{^1H\}$ NMR (benzene-d_6, 79.4 MHz, 303 K): δ_{Si} 1.35 (Si^{i}Pr$_3$), 1.29 (Si^{i}Pr$_3$), 1.08 (Si^{i}Pr$_3$), 0.85 (Si^{i}Pr$_3$).
Meaningful MS analysis was not possible for this sample.
Crystal data for **4.4**: Orange plates 0.18 × 0.12 × 0.08 mm^3, $C_{94}H_{156}O_8Si_4Zr_4$, a = 13.5626(3), b = 16.6449(3), c = 23.4625(3) Å, α = 97.821(1) °, β = 102.409(1) °, γ = 99.798(1) °, U = 5014.73(16) $Å^3$, triclinic, $P\bar{1}$, Z = 2, total reflections 104977, independent reflections 23055, R_{int} = 0.114, θ_{max} = 27.57, R_1 [I >2σ(I)] = 0.059, wR^2 = 0.127 and 1074

parameters.

4.5.5 Synthesis of $[OZr_2(CO_3)_2Zr_2O]^{Me4(TMS)}$ (4.5)

To an ampoule charged with a dark red solution of **3.3** (0.021 g, 0.0300 mmol) in d_6-benzene (0.5 cm^3) was added one equivalent of $^{13}CO_2$ gas *via* Toepler line at -78 ºC before warming to ambient temperature, at which point the solution turned bright orange. Subsequent storage of a toluene solution of the sample at -35 °C afforded bright red X-ray quality crystals in poor yield.

Yield = 0.003 g (0.0014 mmol), 19 % w.r.t. **3.3**.

Conclusive ^1H, $^{13}C\{^1H\}$ and $^{29}Si\{^1H\}$ NMR spectroscopic data is yet to be obtained for this compound.

Meaningful MS analysis was not possible for this sample.

Elemental analysis calcd (%) for $C_{100}{}^{13}C_2H_{180}O_8Si_4Zr_4 \bullet C_7H_8$: C 58.6, H 8.45; found: C 58.3, H 8.81.

Crystal data for **4.5**: Red needles 0.30 × 0.20 × 0.10 mm^3, $C_{68.67}H_{84}O_{5.3}Si_{5.3}Zr_{2.7}$, a = 13.4480(10), b = 20.2840(10), c = 22.4400(10) Å, α = 86.685(10) °, β = 82.739(10) °, γ = 74.608(10) °, U = 5852.4(6) $Å^3$, triclinic, $P\bar{1}$, Z = 3, total reflections 80900, independent reflections 25486, R_{int} = 0.0712, θ_{max} = 27.10, R_1 [I >2σ(I)] = 0.01198, wR^2 = 0.3049 and 1009 parameters.

4.6 References for Chapter Four

1. D. A. Fletcher, R. F. McMeeking and D. Parkin, *J. Chem. Inf. Comput. Sci.*, 1996, **46**, 746-749.
2. F. H. Allen, *Acta Crystallogr., Sect. B: Struct. Sci*, 2002, **58**, 380-388.
3. I. J. Bruno, J. C. Cole, P. R. Edgington, M. Kessler, C. F. Macrae, P. McCabe, J. Pearson and R. Taylor, *Acta Crystallogr., Sect. B: Struct. Sci*, 2002, **58**, 389-397.

5 CHAPTER FIVE: SYNTHESIS AND REACTIVITY OF MIXED SANDWICH THORIUM(IV) HALIDES

5.1 Introduction

The chemistry of thorium(III) is poorly defined, with only a handful of unambiguously characterised examples known. In 1982, Marks and coworkers[1] identified a number of presumed Th(III) compounds *via* the photochemical reduction of $[Th(Cp)_3(^nBu)]$, $[Th(Cp^{MeH4})_3(^iPr)]$ and $[Th(Ind)_3(C_4H_9)]$ to yield the corresponding *tris*cyclopentadienyl species (**Figure 5.1**). The trivalent nature of the metal centre in each case was confirmed through addition of chloroform or iodine to yield the corresponding Th(IV) mono-chlorides and -iodides. However, single crystal X-ray diffraction studies were not possible on the isolated Th(III) examples, and despite the distinctively broadened and shifted resonances expected by ^1H NMR spectroscopy that would support the assignment of a reduced thorium core, these data was not provided by the authors.

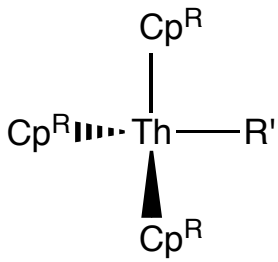

Figure 5.1: Th(IV) compounds that are thought to have been reduced photochemically.

It was four years later that Lappert and coworkers unambiguously identified the first Th(III) compound through X-ray diffraction studies.[2] This compound was obtained through the reduction of $[Th(Cp^{(TMS)2})_2Cl_2]$ with NaK. This reduction was claimed to proceed through the divalent *bis*-Cp complex which underwent disproportionation and ligand rearrangement to afford $[Th(Cp^{(TMS)2})_3]$, similar to those previously documented. Isolation of similar trivalent compounds $[Th(Cp^{(SiMe2R)2})_3]$ (R = Me, ^{t}Bu) was reported more recently, accessed *via* an identical synthetic route.[3] Later attempts by this group to reduce $[Th(LL)_2Cl_2]$ (LL = $\{N(TMS)C(Ph)\}_2CH$) $[Th(LL)_2Cl_2]$ (LL =

{N(TMS)C(Ph)}$_2$CH) *via* NaK resulted in material that showed broadened resonances by ^{1}H NMR spectroscopy as anticipated for a paramagnetic Th(III) centre.[4] Although more definitive characterisation through X-ray diffraction studies was not possible, this particular example represents the first successful use of ligands in generation of a Th(III) complex that are not based on the cyclopentadienyl skeleton.

More recent investigations into trivalent thorium have also embraced different ligands, with Cloke and coworkers' thoracene anion[5] [Th(η^8-C$_8$H$_6${1,4-Si^{t}BuMe$_2$})$_2$]$^-$ [K(DME)$_2$]$^+$ and Gambarotta *et al's* sterically congested complex[6] {2,5-[(C$_4$H$_3$N)CPh$_2$]$_2$[C$_4$H$_2$N]}$_2$Th[K(DME)]$_2$. The latter group subsequently performed DFT calculations on another Th(III) complex, [{η^5-1,3-[(η^5-2-C$_4$H$_3$N)(CH$_3$)$_2$C]$_2$C$_6$H$_4$}ThK-(μ-Cl)$_3$][Li(DME)$_3$], the synthesis of which is described in the same publication. Although broadened signals observed by ^{1}H NMR spectroscopy coupled with low magnetic moment measurements suggest a Th(III) centre, theoretical studies indicate that the lone electron is located on the organic ligands that surround a formal Th(IV) centre.

The chemistry of low valent thorium remains ill-defined, with many Th(III) compounds only existing as unisolable, transient complexes. Only four Th(III) complexes have been unambiguously reported to date and few data are available regarding the Th(IV)/Th(III) reduction potential, suggesting that the trivalent thorium centre would be highly reducing and could be expected to show reactivity towards small molecules. In this chapter, attempts to prepare low valent thorium centres with the application of sterically encumbered ligands are discussed, alongside attempts to reduce CO and CO_2 *via* these Th(III) compounds. Electrochemistry of the mixed-ring thorium(IV) halides and the resultant reduction potentials will also be discussed.

5.2 Synthesis of mixed-ring thorium(IV) halides

In an attempt to mirror the reactivity towards small molecules exhibited by [U(η^8-C$_8$H$_6${Si^{i}Pr$_3$-1,4}$_2$)(Cp^{Me5})], it was deemed desirable to synthesise a thorium analogue. However, although the uranium mixed-ring complexes are synthesised directly from a U(III) source, maintaining this oxidation state throughout the synthetic procedure, this

is not possible in the case of thorium. As with the zirconium and hafnium compounds described in Chapters Two and Three, attempts were made to generate mixed-ring thorium(IV) halide compounds with the aim of reducing these to low valent mixed-sandwich complexes prior to small molecule activation.

5.3 Attempted synthesis of $[Th(\eta^8\text{-}C_8H_6\{Si^iPr_3\text{-}1,4\}_2)Cl_2]_2$

An NMR tube was charged with equimolar amounts of $ThCl_4$ and $[Th(\eta^8\text{-}COT\{Si^iPr_3\text{-}1,4\}_2)_2]$ (**5.1**) in d_8-THF before being degassed by freeze-thaw the and sealing the tube under vacuum. No new resonances nor shifts in the existing peaks were observed by ^1H NMR spectroscopy after heating to 80 °C for 96 hours, so the sample was heated to 100 °C for two weeks. However, as repeated ^1H NMR spectroscopy continued to show no change from the starting materials, this attempted method of synthesis was abandoned.

Following this unsuccessful attempt to replicate the synthetic route applied with the zirconium and hafnium analogues described in chapter 2, an alternative synthesis was developed. In this case, the synthetic route routinely used to access the uranium analogue was modified according to the work by Mintz *et al*[7] and applied to the thorium system.

5.4 Synthesis and characterisation of $[Th(\eta^8\text{-}C_8H_6\{Si^iPr_3\text{-}1,4\}_2)(Cp^{Me5})X]$

5.4.1 Synthesis of $[Th(\eta^8\text{-}C_8H_6\{Si^iPr_3\text{-}1,4\}_2)(Cp^{Me5})Cl]$

To an ampoule charged with equimolar amounts of $ThCl_4$ and $MgCp^{Me5}Cl(THF)$ was added 1,4-dioxane and THF at ambient temperature. Upon stirring fro two days, the initially white suspension became off-white in colour. Extraction with 1,4-dioxane and dichloromethane, and subsequent storage as a THF/pentane solution at -50 °C resulted in colourless needle-like crystals of $ThCp^{Me5}Cl_3(thf)_{0.6}$ (**5.3**) in good yields that were unsuitable for X-ray diffraction studies. The identity of **5.3** was confirmed by ^1H NMR spectroscopy, with THF resonances observed as broad singlets at 3.79 and 1.27 ppm;

the Cp ligand was observed as a sharp singlet at δ_H 2.35. Relative integration of these peaks indicated the presence of 0.6 moles of THF per Cp^{Me5} ligand. Compound **5.3** was taken up in THF and cooled to -78 °C and to this was added a pale green solution of one equivalent of $[K_2(\eta^8\text{-}C_8H_6)\{Si^iPr_3\text{-}1,4\}_2]$ in THF, immediately affording a fine white precipitate. This was allowed to stir, reaching ambient temperatures overnight, before extraction into pentane and subsequent storage at 0 °C, resulting in large off-white X-ray quality crystals of $[Th(\eta^8\text{-}C_8H_6\{Si^iPr_3\text{-}1,4\}_2)(Cp^{Me5})Cl]$ (**5.4**) in moderate to good yields (**Scheme 5.1**). Bond lengths and angles are summarised in **Table 5.1**.

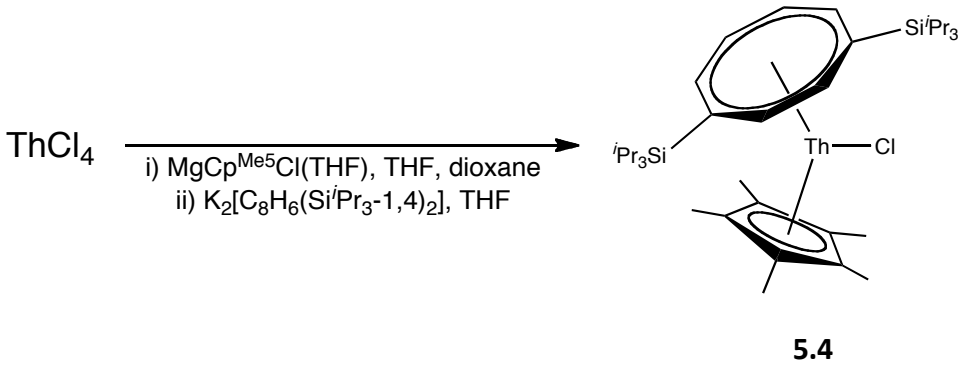

5.4

Scheme 5.1: Synthesis of **5.4** from thorium tetrachloride.

5.4.2 Synthesis of $[Th(\eta^8\text{-}C_8H_6\{Si^iPr_3\text{-}1,4\}_2)(Cp^{Me5})I]$

Thorium turnings previously cleaned by sonication in hydrofluoric acid with a catalytic amount of hydrochloric acid were weighed into a Schlenk before addition of THF and subsequent cooling to 0 °C to give a dark grey suspension. To this was added 1.6 equivalents of elemental I_2 in four portions, with continuous stirring. On each addition, the suspension turned red-brown in colour before fading back to dark grey. Following the final addition, the mixture was allowed to reach ambient temperature overnight to yield a pale brown solution and fine grey powder. This was filtered before extraction into 40-60 petroleum ether. The resultant pale grey powder was isolated in moderate to good yield and identified as $ThI_4(THF)_4$ (**5.5**). Following the preparative steps outlined in the synthesis of **5.4** (*vide supra*), attempts were made to obtain the iodide analogue $[Th(\eta^8\text{-}C_8H_6\{Si^iPr_3\text{-}1,4\}_2)(Cp^{Me5})I]$ (**5.7**) from **5.5**. However, what was presumed to be $ThCp^{Me5}I_3(THF)_x$ (**5.6**) was found to be highly unstable, often decomposing to unidentified bright purple solids on work-up, precluding the isolation and

characterisation of the triiodide compound. Attempted syntheses of **5.7** from crude samples of **5.6** yielded material that that could not be unambiguously identified by ^{1}H NMR spectroscopy or mass spectrometry.

As the above synthetic route did not result in clean **5.7**, halide exchange *via* addition of TMSI to **5.4** was instead attempted (**Scheme 5.2**). An excess of TMSI was added to a pale yellow solution of **5.4** in toluene, before being allowed to stir for three days at ambient temperature. Removal of volatiles and addition of more toluene afforded, upon storage at -35 °C, pale yellow X-ray quality block crystals of **5.7** in good yield.

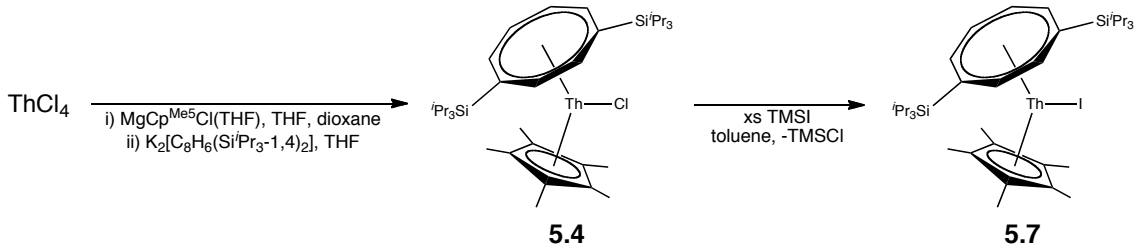

Scheme 5.2: Synthesis of mixed-ring thorium chloride and iodide compounds.

5.4.3 Characterisation of [Th(η^8-C_8H_6{Si^{i}Pr$_3$-1,4}$_2$)(Cp^{Me5})Cl] (5.4) and [Th(η^8-C_8H_6{Si^{i}Pr$_3$-1,4}$_2$)(Cp^{Me5})I] (5.7)

The identities of **5.4** (**Figure 5.2**) and **5.7** (**Figure 5.3**) were confirmed by mass spectrometry, with the parent ions observed at m/z 818 and 910 respectively, while purity was confirmed by elemental analysis. As observed for the zirconium and hafnium analogues, the COT ligand was apparent from the characteristic AA'BB'X_2 pattern in the ^{1}H NMR spectrum, with resonances at approximately 7.1, 6.7 and 6.4 ppm. The *iso*propyl silyl groups were observed upfield as a septet and two doublets at δ_H 1.6, 1.3 and 1.2, with the Cp^{Me5} ligand seen as a singlet at 2.0 ppm. The silyl groups were observed by ^{29}Si{^{1}H} spectroscopy at δ_{Si} 11.0, while full assignment of ^{1}H ^{13}C{^{1}H} and ^{29}Si{^{1}H} shifts were by recourse to 2D techniques, including COSY, HSQC and HMBC experiments.

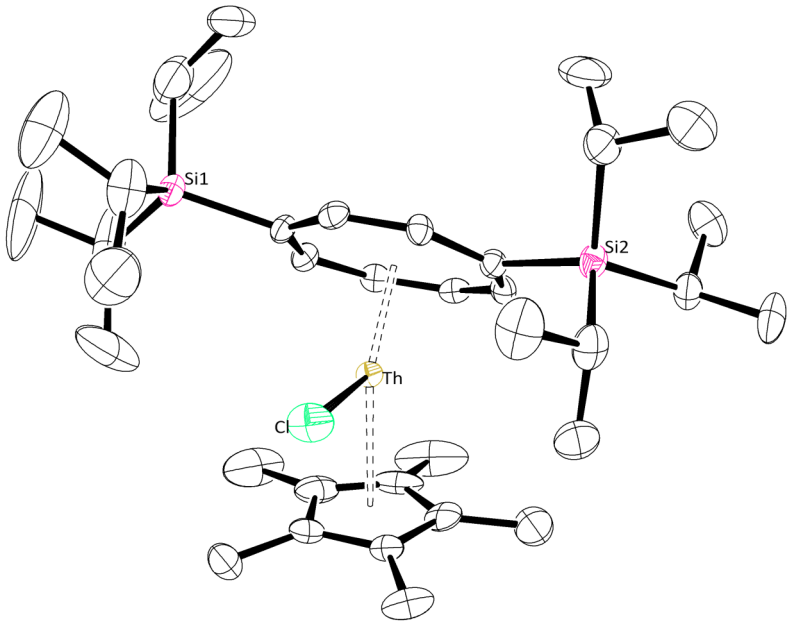

Figure 5.2: Molecular structure of [Th(η^8-C_8H_6{Si^{i}Pr$_3$-1,4}$_2$)(Cp^{Me5})Cl] (**5.4**). Hydrogen atoms are omitted for clarity. Thermal ellipsoids at 50 % probability level.

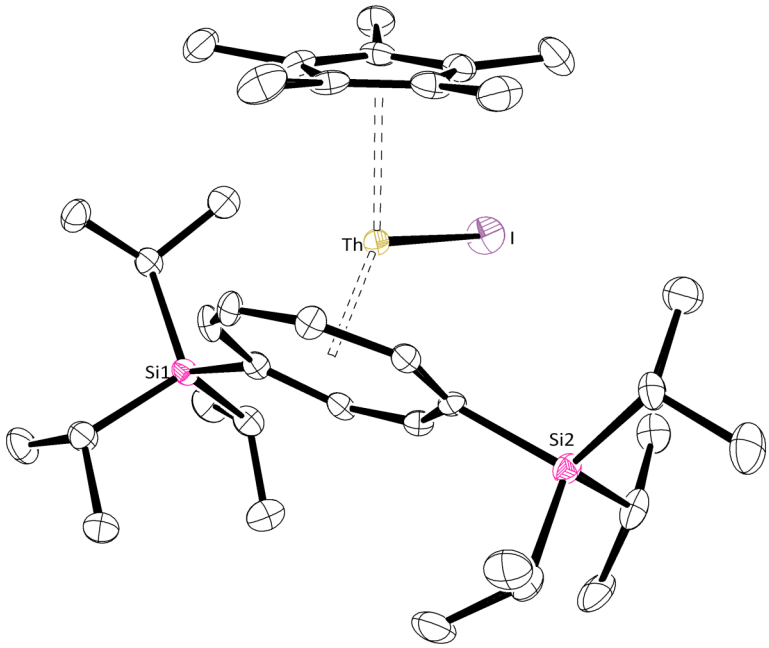

Figure 5.3: Molecular structure of [Th(η^8-C_8H_6{Si^{i}Pr$_3$-1,4}$_2$)(Cp^{Me5})I] (**5.7**). Hydrogen atoms are omitted for clarity. Thermal ellipsoids at 50 % probability level.

Both the chloride and iodide complexes crystallise in the triclinic space group $P\bar{1}$, with two molecules in the unit cell; selected bond angles and distances are summarised in **Table 5.1**. Both compounds have similarly acute $COT_{cent.}$-Th-$Cp_{cent.}$ angles that are only slightly less linear than seen with the zirconium and hafnium analogues described earlier (140.531(15) and 140.2(4) ° for **5.4** and **5.7** respectively, *cf*. 145.5(6) and 145.9(19) °). There is only one comparable mixed-ring thorium compound reported in the literature,[8] $[(Cp^{Me5})(COT)Th]_2(COT)$, which possess a $COT_{cent.}$-Th-$Cp_{cent.}$ angle of 132.1 °, somewhat less linear than observed in **5.4** and **5.7**.

Table 5.1: Selected bond angles (deg) and distances (Å) for [Th(η^8-C_8H_6{Si^{i}Pr$_3$-1,4}$_2$)(Cp^{Me5})X] (**5.4**, X = Cl; **5.7**, X = I). $COT_{cent.}$ and $Cp_{cent.}$ indicate the centroid of the COT and Cp rings.

Compound	**5.4**	**5.7**
Th-X	2.6865(16)	3.1104(5)
Th-$COT_{cent.}$	1.9846(3)	1.980(18)
Th-$Cp_{cent.}$	2.5292(3)	2.530(7)
$COT_{cent.}$-Th-$Cp_{cent.}$	140.531(15)	140.2 (4)
COT C-C range	1.406(9) – 1.428(8)	1.407(8) – 1.431(8)
Cp C-C range	1.401(9) – 1.429(11)	1.416(9) – 1.431(9)

The mean Th-X distances (2.6865(16) Å for **5.4**, 3.1104(5) Å for **5.7**) are consistent with those reported and summarised in **Figure 5.4** for literature examples of terminal halides (Th-X) at 2.70(6) and 3.09(9) Å, although few data are available regarding Th-I bond lengths,[9-11 12, 13] due to a paucity of examples. The shortest Th-Cl bond length reported was by Lappert and coworkers,[4] in [{Th(LL')(μ_3-Cl)(μ-Cl)$_2$K(OEt$_2$)}$_\infty$] (LL' = [N(TMS)C(^{t}But)CH(TMS)]). This highly unusual compound contains three Th-Cl bonds of lengths 2.413(6), 3.093(8) and 3.204(6) Å, with the shortest measurement corresponding to a Th-Cl fragment where the chlorine atom also interacts with two potassium atoms.

The internal COT and Cp C-C distances in **5.4** and **5.7** are as anticipated for these ligands and the range of bond lengths is narrow.

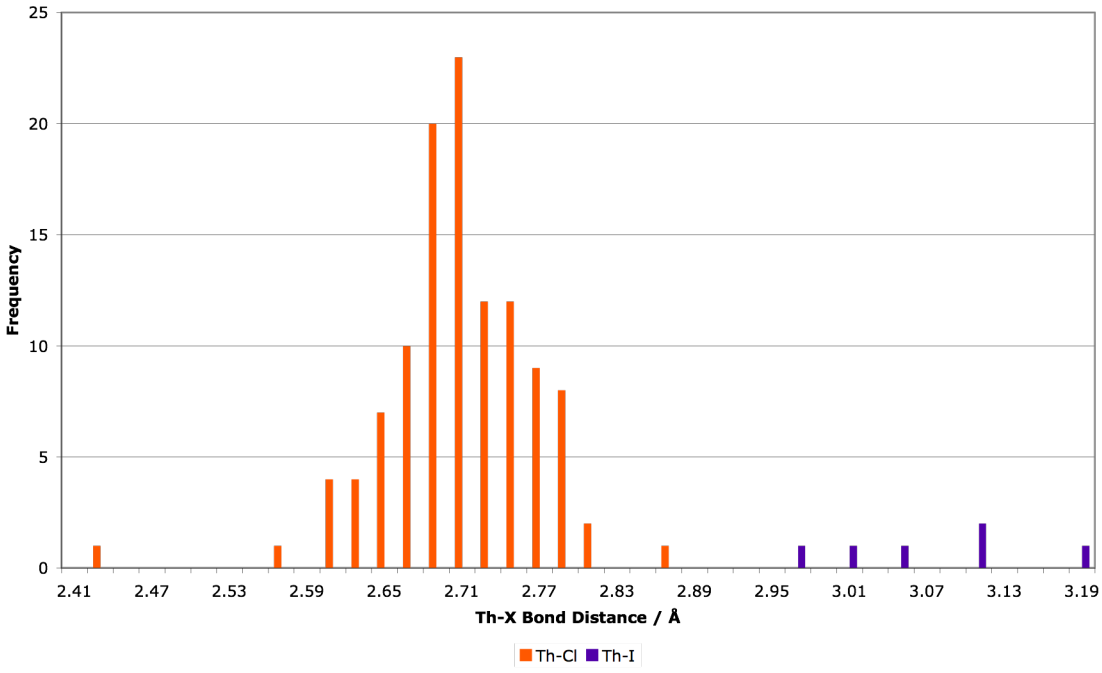

Figure 5.4: Th-X distances where the halide is the terminal moiety.[14, 15]

No other examples of the *iso*propylsilyl-substituted cyclooctatetraene bonded to a thorium atom exist, however, examples do exist of thorium bound to differently substituted COT, so these will be compared to **5.4** and **5.7**. There is no difference in Th-$COT_{cent.}$ distances in **5.4** and **5.7** (1.9846(3) and 1.980(18) Å), which are slightly shorter than those recorded in the literature, with the average measuring 2.03(3) Å. The Th-$COT_{cent.}$ lengths here are similar to those seen with other bulky substituted COT ligands such as COT{1,4-Si^{t}BuMe$_2$} (1.998 Å)[5] and COT{1,4-SiMe$_3$} (1.986 Å).[16]

More data are available for Th-$Cp^{Me5}_{cent.}$ distances, the average literature length being 2.55(7) Å, which is in accord with **5.4** and **5.7** (2.5292(3) and 2.530(7) Å). The largest Th-$Cp_{cent.}$ distance published is 2.68 Å,[17] in bis(N-(diphenylmethylene)-N'-benzylhydrazonato-N,N')-bis(Cp^{Me5})-thorium(IV), with the extended distance attributable to steric encumbrance exerted by surrounding phenyl groups. The Th-

$Cp_{cent.}$ distances in **5.4** and **5.7** are slightly shorter when compared to the only similar mixed-ring Th(IV) in the literature (2.575 Å).[8]

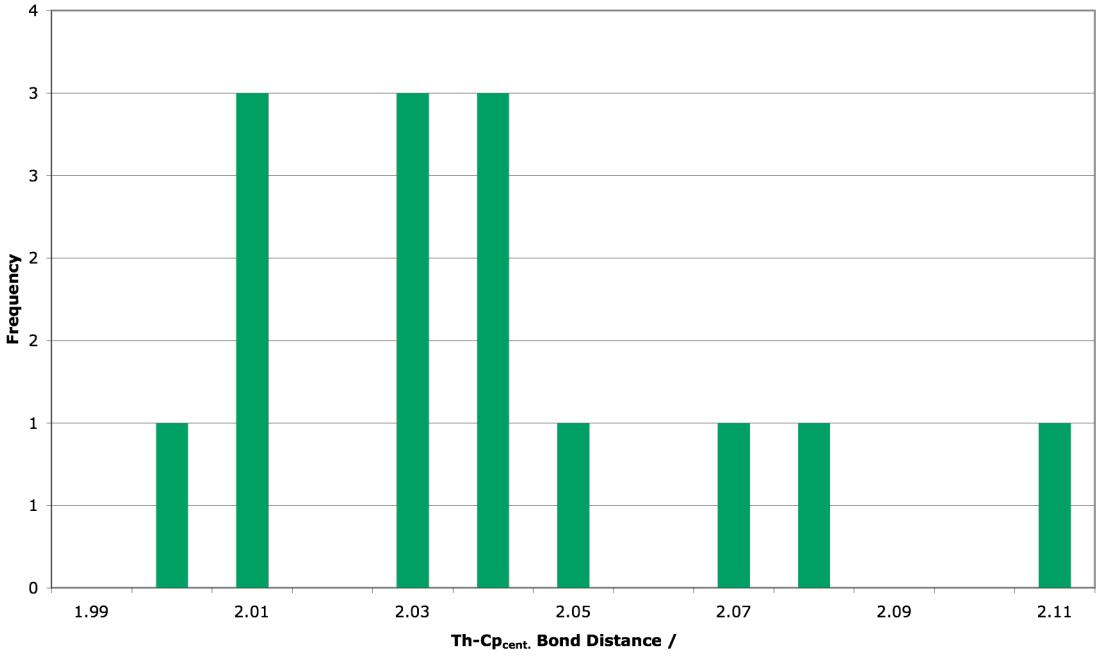

Figure 5.5: Th-$COT_{cent.}$ distances for variously substituted planar COT ligands.[14, 15]

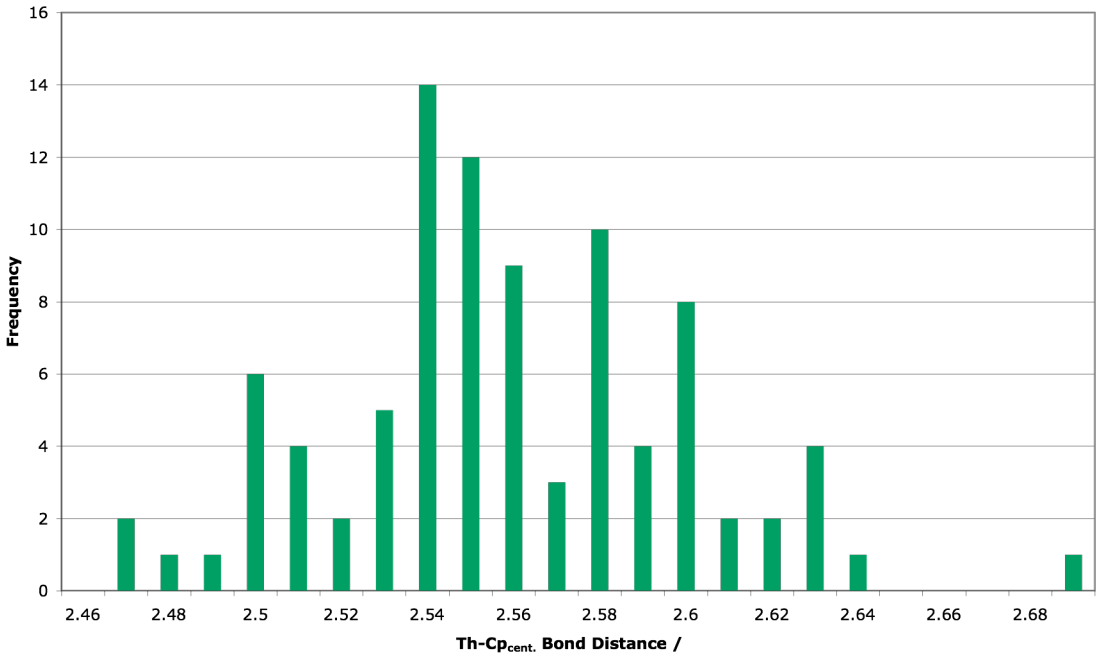

Figure 5.6: Th-$Cp_{cent.}$ distances for pentamethylated cyclopentadienyl.[14, 15]

5.5 Cyclic voltammetry of [Th(η^8-C_8H_6{Si^{i}Pr$_3$-1,4}$_2$)(Cp^{Me5})X]

As little is known about Th(III), apart from its relative instability, compounds **5.4** and **5.7** were analysed by cyclic voltammetry in THF. These results should allow a comparison with existing data and the reduction potentials of the Group IV analogues described earlier in this work.

For compounds **5.4** and **5.7** a reduction wave was observed at approximately -3.3 V (**Table 5.2**) with respect to the ferrocene/ferrocenium couple and corresponding to a one electron reduction of the metal centre (**Figure 5.**) from Th(IV) to Th(III). Shortly after this event was detected, immediate breakdown of the thorium complexes ensued, apparent from discolouration of the solution and deposition of material on the working electrode. Due to the instability of the Th(III) complex, repeated scans on the solution were not possible. There is no significant difference between the reduction potentials of the chloride or iodide complex.

The calculated E_p^{red} values for **5.4** and **5.7,** of -3.33 and -3.32 V respectively, are much more negative than those observed for the zirconium and hafnium congeners **2.9** and **2.10** (-2.96 and -3.12 V), indicating the decreased stability of Th(III) compared to Zr(III) and Hf(III). The values obtained for the thorium compound are in accordance with the literature, where values have been measured between -2.9 and -3.7 V.[18, 19]

Table 5.2: Electrode potentials *versus* $FeCp_2^{0/+}$ in 0.1 M [N^{n}Bu$_4$][PF$_6$] in THF at a silver electrode at 27 °C.

Compound	E_p^{red} / V
5.4	-3.33
5.7	-3.32

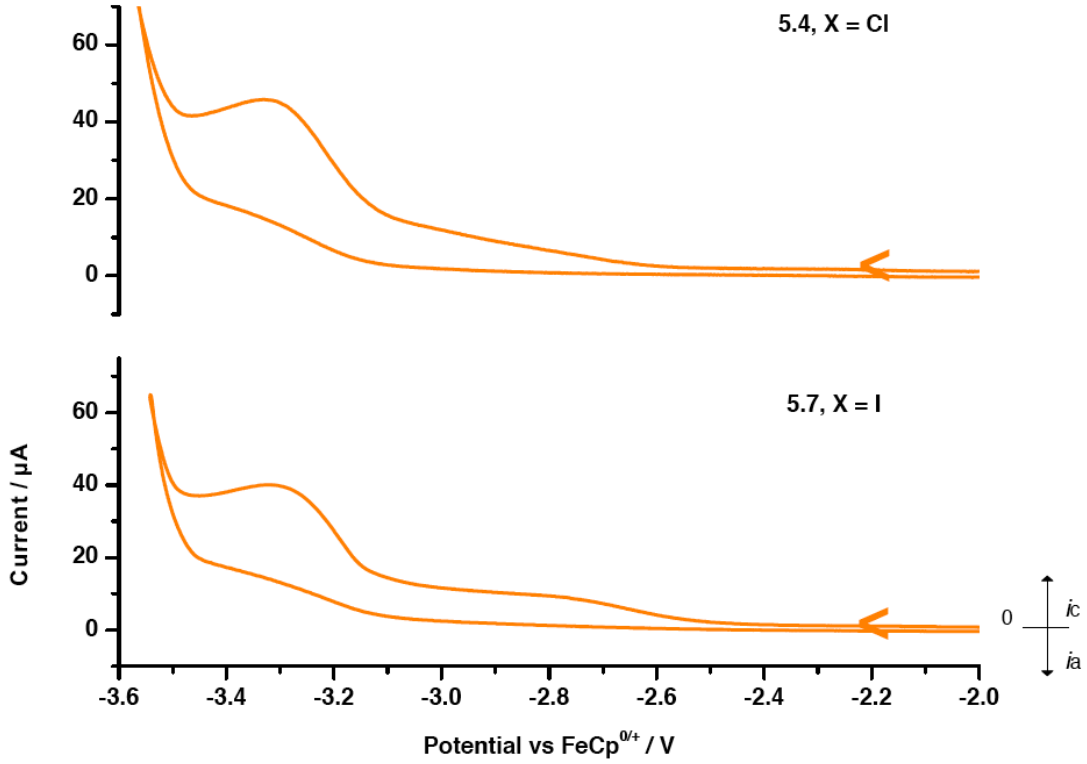

Figure 5.7: Cyclic voltammograms of **5.4** (7.70 mM) and **5.7** (5.27 mM) in THF containing 0.1 M [N^{n}Bu$_4$][PF$_6$]. The scan rate was 100 mV.s^{-1}.

5.6 Attempted reduction of [Th(η^8-C$_8$H$_6${Si^{i}Pr$_3$-1,4}$_2$)(Cp^{Me5})X]

A number of different attempts were made to reduce compounds **5.4** and **5.7**, with limited success. Stirring of a toluene solution of **5.4** with excess KC_8 for three days resulted in no change from the Th(IV) starting material, with subsequent sonication of the mixture having no effect. Addition of excess NaK and stirring at ambient temperature for a further nine days also failed to effect any reduction. Subsequent sonication of the NaK mixture for 30 minutes resulted in the appearance of an insoluble blue-grey solid, presumed to be elemental thorium, and a bright yellow solution that was identified by ^{1}H NMR spectroscopy to be the thoracene **5.1**. This bis-COT compound is identified by a distinctive ^{1}H NMR spectrum, with a lack of Cp^{Me5} resonance and a shift to a lower frequency in the unresolved COT multiplet usually observed at higher frequencies. Due to the paramagnetism of Th(III), it would be

expected that the presence of such a species would result in a significantly broadened resonances in the ^{1}H NMR spectrum, which was not observed in this case.

Further attempts were made reduce to the mixed-ring iodide, as it was presumed that the weaker Th-I bond would be easier to break. Sonication of a toluene suspension of **5.7** with excess KC_8 led to no observable changes by ^{1}H NMR spectroscopy; heating to 80 °C for six days also failed to produced the desired Th(III) product. A solution of **5.7** in toluene stirred over excess NaK at ambient temperature became brighter yellow in colour, with the appearance of a brown precipitate. Subsequent ^{1}H NMR spectroscopy again indicated conversion of **5.7** to **5.1** and intractable by-products.

It appears that if any Th(III) species were produced in these reactions they were clearly transient and highly reactive, undergoing immediate disproportionation in solution resulting in elemental thorium and **5.1.** Due to this behaviour, efforts to isolate Th(III) were discontinued and attention concentrated on the *in situ* reduction of [Th(η^8-C_8H_6{Si^{i}Pr$_3$-1,4}$_2$)(Cp^{Me5})X] under an atmosphere of CO or CO_2.

5.7 Reactivity of [Th(η^8-C_8H_6{Si^{i}Pr$_3$-1,4}$_2$)(Cp^{Me5})X] with NaK and CO, CO_2

Due to the presence of elemental alkali metals in the sample, these reactions could not be tracked over a period of time *via* ^{1}H or ^{13}C{^{1}H} NMR spectroscopy. The corrosive nature of NaK also precluded *in situ* observation of the reaction by IR spectroscopy, as the IR probe is encased in a metal housing.

In the case of both **5.4** and **5.7**, no reactivity was observed with ^{13}CO when a toluene solution was treated with excess NaK and allowed to stir for two weeks. Whilst compound **5.4** also failed to show any reactivity toward excess $^{13}CO_2$ when a toluene solution was treated with excess NaK and allowed to stir over a period of ten days. No changes in the resonances observed by ^{1}H NMR spectroscopy were noted, with no signals attributable to isotopically labelled ^{13}C atoms seen by ^{13}C{^{1}H} NMR spectroscopic analysis. In the case of **5.7**, no reactivity was observed after four days,

however allowing the reaction to proceed for two weeks in total resulted in conversion to the thoracene **5.1**, observed by ^{1}H NMR spectroscopy, as seen during the attempted reduction of **5.7** described earlier.

Stirring of a toluene solution of **5.7** with an excess of NaK and $^{13}CO_2$ for five days at ambient temperatures led to the observation of new resonances in the crude material (172 and 167 ppm) by $^{13}C\{^{1}H\}$ NMR spectroscopy (**Scheme 5.3**). When stored at -35 °C, off-white X-ray quality crystals were isolated in poor yield and identified as the dinuclear thorium(IV) oxalate molecule **5.8** (**Figure 5.**), corresponding to the resonance observed at 172 ppm. When allowed to stir under similar conditions for twelve days, the same ^{13}C resonances were observed in the crude material, with subsequent storage at -35 °C affording off white X-ray quality crystals of the dinuclear thorium(IV) carbonate compound **5.9** (**Figure 5.**) in poor yield, with the resonance at δ_C 167 attributable to the carbonate moiety. The bond lengths and angles of **5.8** and **5.9** are summarised in **Table 5.3**. Compound **5.4**, proved to be unreactive under similar conditions, with only starting material observed by ^{1}H and $^{13}C\{^{1}H\}$ NMR spectroscopy and no resonances attributable to the isotopically labelled ^{13}C observed.

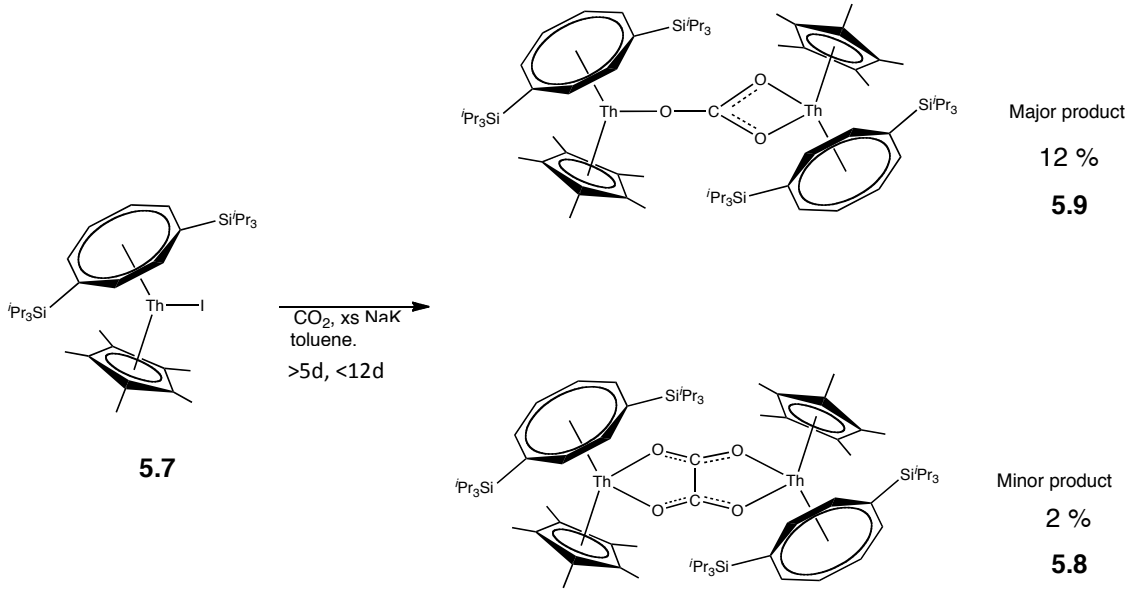

Scheme 5.3: Reaction of **5.7** with CO_2 in the presence of excess NaK, produces a mixture of products including the dinuclear bridging oxalate and carbonate compounds.

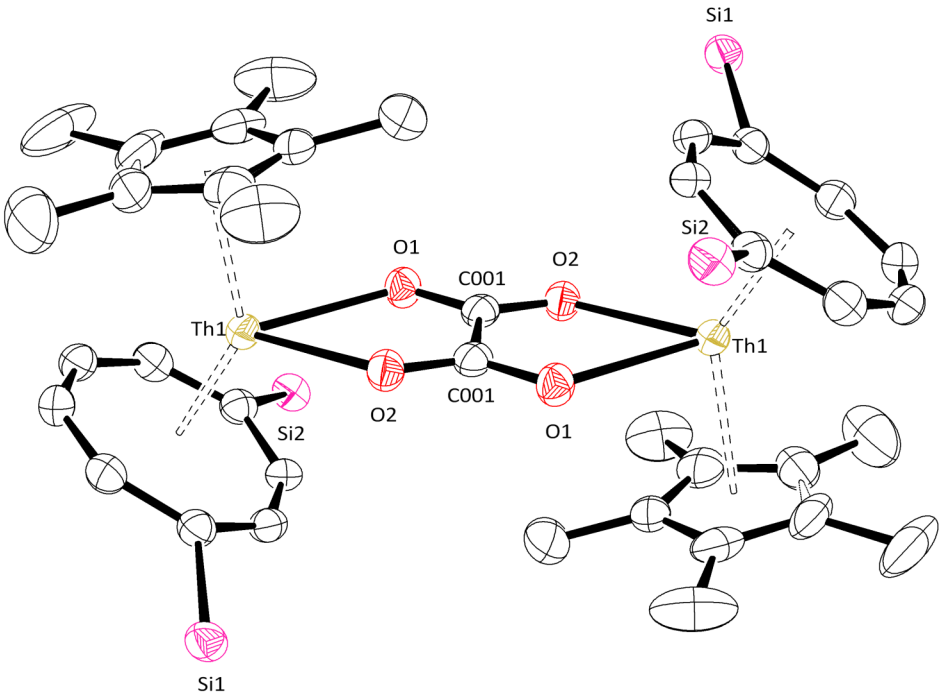

Figure 5.8: Molecular structure of [Th(η^8-C_8H_6{Si^{i}Pr$_3$-1,4}$_2$)(Cp^{Me5})]$_2C_2O_4$ (**5.8**). Hydrogen atoms and ^{i}Pr groups are omitted for clarity. Thermal ellipsoids at 50 % probability level.

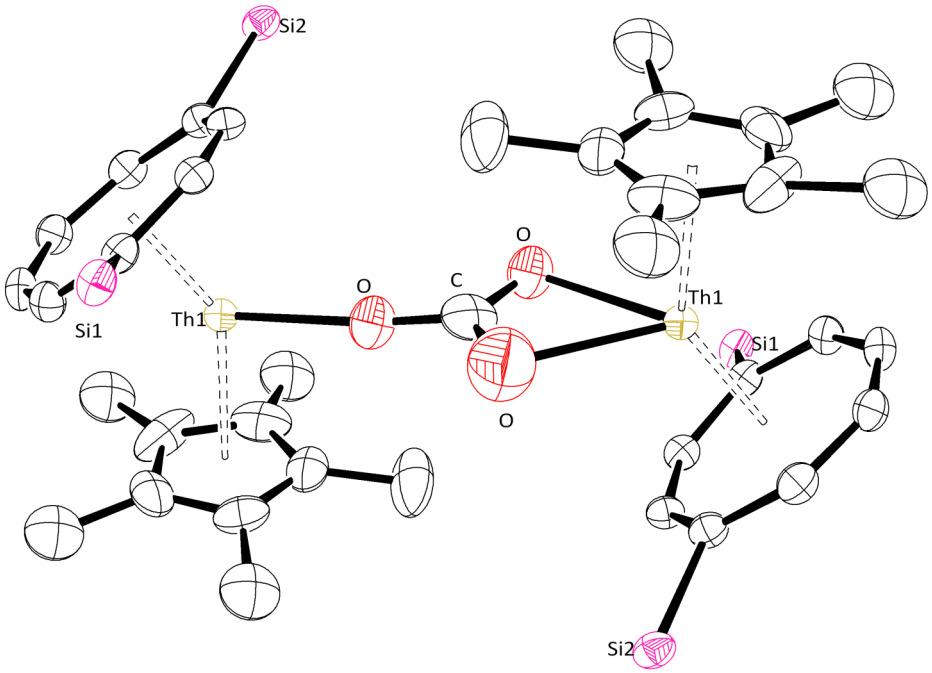

Figure 5.9: Molecular structure of [Th(η^8-C_8H_6{Si^{i}Pr$_3$-1,4}$_2$)(Cp^{Me5})]$_2CO_3$ (5.9). Hydrogen atoms and ^{i}Pr groups are omitted for clarity. Thermal ellipsoids at 50 % probability level.

5.7.1 Characterisation of 5.8 and 5.9

The identity and purity of **5.8** and **5.9** was confirmed by ^{1}H NMR spectroscopy, with the anticipated resonances identified for the cyclopentadienyl ligand and *iso*propyl silyl groups. The AA'BB'X_2 splitting pattern due to the COT protons merged such that only two signals were observed. The identity of each product was further confirmed by mass spectrometry, with the parent ion detected at m/z 1657 for **5.8**. The anticipated parent ion was not observed for **5.9**, with the highest mass peak seen at m/z 1494, corresponding to the loss of one Cp^{Me5} ligand. Combustion analysis confirmed the purity of the carbonate compound, but was precluded for the oxalate compound due to the very small amount of product obtained.

Table 5.3: Selected bond angles (deg) and distances (Å) for [Th(η^8-C_8H_6{Si^iPr_3-1,4}$_2$)(Cp^{Me5})]$_2C_nO_y$ (**5.8**, n = 2, y = 4; **5.9**, n = 1, y = 3).

Compound	**5.8**	**5.9**
Th-O	2.473(2), 2.475(3)	No reliable figure due to inversion centre in structure
C-O	1.264(4), 1.260(4)	As above
Th-C	-	As above
C-C	1.518(7)	-
Th-$COT_{cent.}$	2.02932(17)	2.0226(9)
Th-$Cp_{cent.}$	2.54142(17)	2.5388(11)
$COT_{cent.}$-Th-$Cp_{cent.}$	139.402(7)	138.88(3)
COT C-C range	1.402(5) – 1.428(5)	1.405(5) – 1.435(5)
Cp C-C range	1.395(7) – 1.432(7)	1.380(7) – 1.433(8)

Both **5.8** and **5.9** crystallised in the triclinic space group $P\bar{1}$, with one dinuclear thorium molecule in the unit cell. In both cases, significantly longer Th-$COT_{cent.}$ distances were observed compared to **5.7**, though they are themselves comparable (2.02932(17) Å for

5.8, 2.0226(9) Å for **5.9**). The $COT_{cent.}$-Th-Cp_{cent} angles are again similar in the oxalate and carbonate compounds, and slightly less linear than observed for the starting material The Th-$Cp_{cent.}$ distances are not significantly longer than in **5.7**, and while the COT C-C bond lengths are still within narrow range of values, this is not the case for the Cp C-C distances, which are typically longer than in the starting material.

No examples of organometallic thorium complexes containing carbonate or oxalate have been described previously; additionally, there are only two structurally characterised thorium oxalates,[20] so direct comparisons to similar compounds are not possible for **5.8** and **5.9**. In the case of the oxalate unit, the two carbon atoms are bound by a single bond measuring 1.518(7) Å, with the bond distance between the C-O atoms corresponding to a double bond (1.264(4) and 1.260(4) Å). The Th-O distances in **5.8** are consistent with those reported in the literature (average of 2.4(1)Å), where the oxygen atom is not terminal (**Figure 5.10**). An unusually long Th-O bond distance of 2.947 Å was reported by Alcock *et al*[21] for their hexanitrothorate(IV) complex, although all other Th-O bonds in the same molecule are more consistent with the average figure calculated from the literature values.

Unfortunately, due to the disorder associated with the CO_3 core of **5.9**, Th-O and C-O lengths cannot be reliably calculated and so preclude further comparisons with **5.8**.

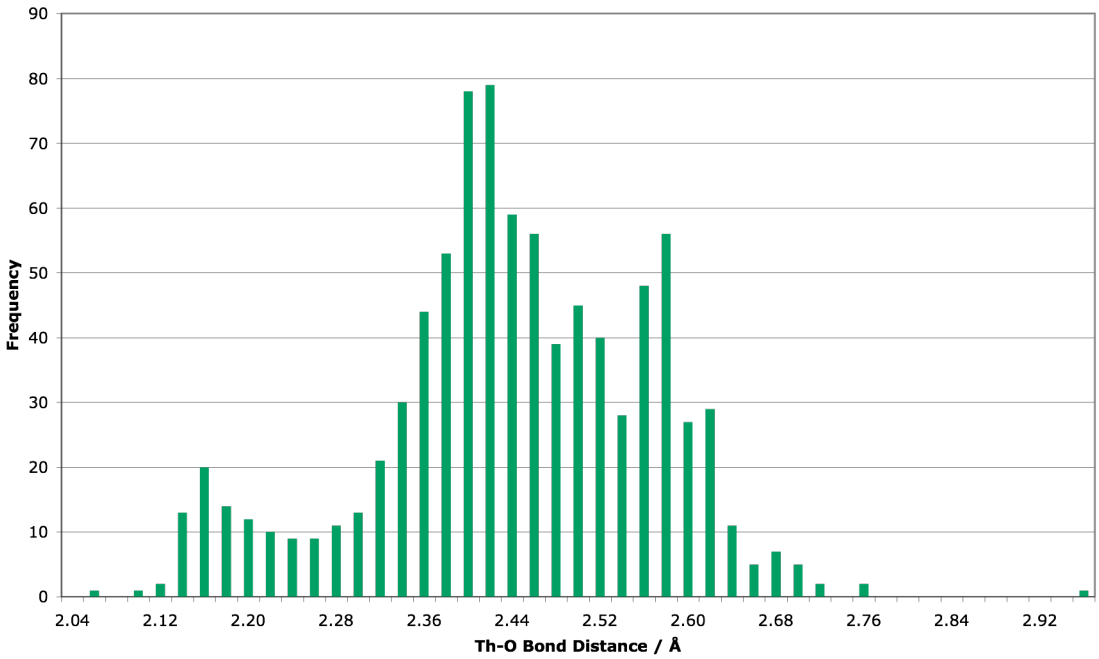

Figure 5.10: Th-O distances, where oxygen is not a terminal moiety.[14, 15]

5.8 The mechanism of formation of 5.8 and 5.9

5.8.1 Thorium(III)-mediated formation of 5.8 and 5.9

Given the issues precluding in-depth ^{1}H and $^{13}C\{^{1}H\}$ NMR and IR spectroscopic analysis during the reaction, experimental data pertaining to intermediates are not available. However, calculations performed by Prof. L. Maron (**Figures 5.11** and **5.12**) suggest two possible mechanistic pathways concerning the reactions illustrated in **Scheme 5.3**.

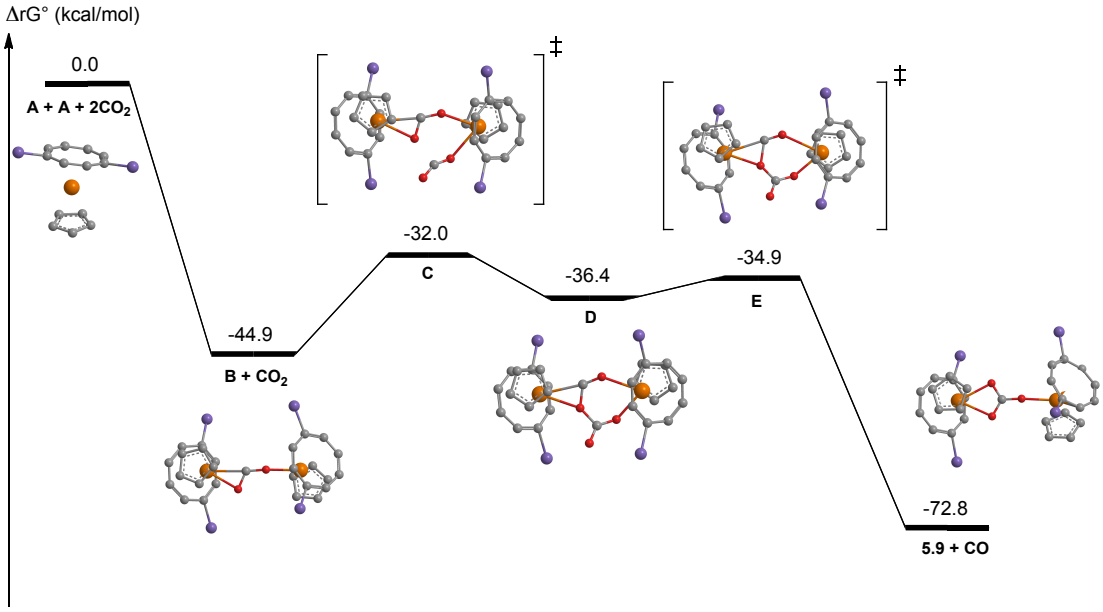

Figure 5.6: Suggested reaction pathway for the synthesis of the thorium(IV) bridging carbonate compound 5.9 from a discrete thorium(III) compound, provided by Prof. L. Maron.

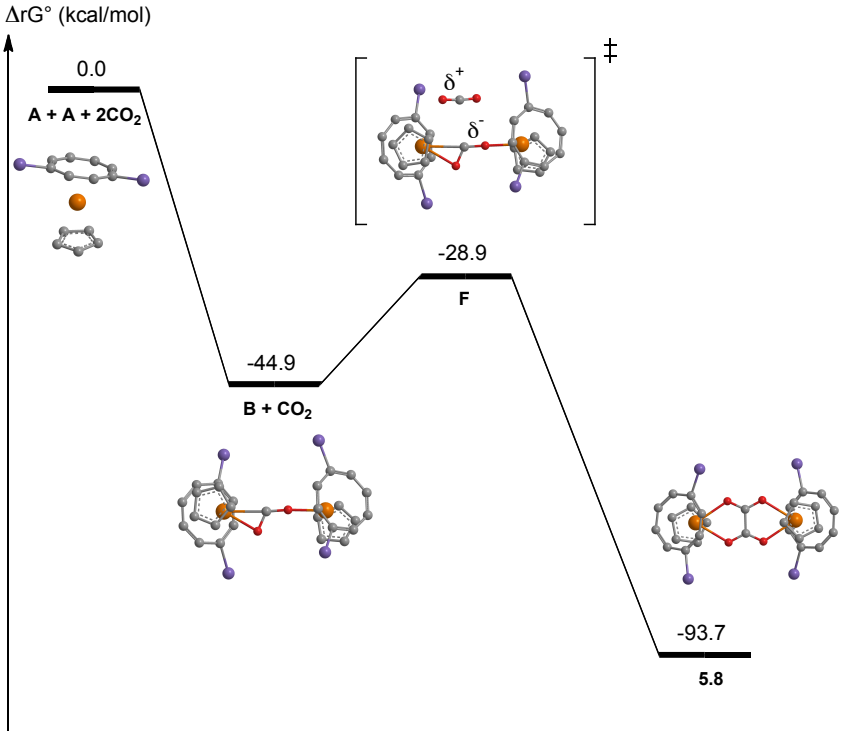

Figure 5.7: Suggested reaction pathway for the synthesis of the thorium(IV) bridging oxalate compound **5.8** from a discrete thorium(III) compound, provided by Prof. L. Maron.

For both **5.8** and **5.9**, the same meta-stable intermediate (**B**) is observed 44.9 kcal.mol^{-1} lower in energy than the transient Th(III) starting material (**A**). Intermediate **B** consists of an η^2,η^1-CO_2 unit between the two thorium nuclei. The two COT ligands are positioned so that they are as far away from each other as possible, presumably to decrease steric encumbrance caused by clashing *iso*propyl groups.

Formation of **5.9** requires a second CO_2 molecule to approach **B** and form a further Th-O bond leading to the higher energy (+12.9 kcal.mol^{-1}) transition state **C**. This undergoes a rearrangement to result in the metallocycles **D**, with formation of a C-O bond between the two CO_2 units, ultimately resulting in the transfer of an oxygen atom between the two. Subsequent loss of carbon monoxide results in complex **5.9**. Due to the nature of work up in this case, it was not possible to detect CO in the reaction solution.

The cyclic intermediate **D** and following transition state **E** described in **Figure 5.6** are generally similar to the isolated mononuclear iridium complex as crystallographically defined by Herskovitz[22] (**Figure 5.8**). Here, two carbon dioxide units are bound to the iridium centre, with examination of the bond lengths indicating that one C-O bond has become significantly lengthened with respect to others present. This example shows CO_2 disproportionation through binding of two carbon dioxide units similar to a calculated stage in the pathway of **5.9** formation.

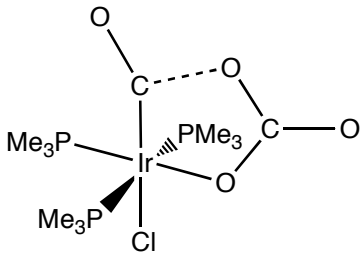

Figure 5.8: Binding of two carbon dioxide molecules to an iridium complex showing possible route to carbonate and carbon monoxide formation.

With respect to formation of oxalate **5.8**, the second CO_2 approaches **B** from the opposite side of the η^2,η^1-CO_2 core with respect to **5.9**, inducing carbon polarisation, leading to transition state **F** that is 3.1 kJ.mol^{-1} greater in energy than **C**, representing a

slightly larger barrier of activation to ultimate formation of **5.8**. Subsequent formation of the C-C bond and two Th-O bonds and breakage of the Th-C bond occur in a final concerted step.

The energy barrier difference between carbonate and oxalate formation is small, *ca.* 3 kcal.mol^{-1}, and is in favour of carbonate formation, despite **5.8** being -20 kcal.mol^{-1} more stable than **5.9**. Experimental data support these calculations: the carbonate compound is isolated in greater quantities than the oxalate complex.

5.8.2 Alternative formation of 5.8 and 5.9

As alkali metals are well known to react with CO_2, it is possible that compounds **5.8** and **5.9** are generated by transmetallation between **5.7** and M_2CO_3 or $M_2C_2O_4$ (M = Na, K), following reaction between NaK and carbon dioxide. However, attempts at recreating this proposed transmetallation *via* addition of excess $Na_2C_2O_4$ or a mixture of excess Na_2CO_3 and K_2CO_3 to **5.7** failed to result in any change from the starting material after eleven days. Neither **5.8**, **5.9,** nor other products were observed by ^{1}H and $^{13}C\{^{1}H\}$ NMR spectroscopy of the crude material after this time.

5.9 Conclusions

Compound **5.4** can be easily generated *via* a modification of an established route to uranium analogues. The same procedure is not applicable to the iodide congener, with addition of TMSI to **5.4** leading to a facile halogen exchange to access the more labile iodide complex. Despite a number of attempts to prepare and isolate a Th(III) complex *via* the reduction of the chloride or iodide compounds, isolation was not possible due to the inherent instability of the +3 oxidation state. Neither the chloride nor iodide compound shows reactivity towards carbon monoxide as deduced by ^{1}H and $^{13}C\{^{1}H\}$ NMR spectroscopic analysis; the chloride complex also fails to show reactivity towards carbon dioxide. Compound **5.7** shows activity towards carbon dioxide under reducing conditions producing bridging carbonate and oxalate dithorium compounds

competitively as supported by theoretical studies. Compound **5.7** does not appear to react with $Na_2C_2O_4$, Na_2CO_3 or K_2CO_3 *via* transmetallation to form **5.8** or **5.9**.

5.10 Experimental details for Chapter Five

5.10.1 Synthesis of $ThCp^*Cl_3(THF)_{0.6}$ (5.3)

To an ampoule charged with $ThCl_4$ (0.234 g, 0.629 mmol) and $MgCp^{Me5}Cl(THF)$ (0.171 g, 0.633 mmol) was added 1,4-dioxane (10 cm^3) and THF (10 cm^3) at ambient temperature. The resulting white suspension was allowed to stir for 2 days before being extracted into 1,4-dioxane (5 cm^3) and dichloromethane (5 cm^3). Cooling to 0 °C and extraction with THF (2 cm^3) and pentane (2 cm^3) before subsequent storage at -50 °C yielded white needle-like crystals of **5.3** that were unsuitable for X-ray diffraction studies.

Yield = 0.213 g (0.414 mmol), 66 % w.r.t. $ThCl_4$.

^1H NMR (benzene-d_6, 399.5 MHz, 303 K): δ_H 3.79 (br s, 4H, THF-CH_3), 2.35 (s, 15H, Cp-CH_3), 1.27 (s, 4H, THF-CH_3).

^{13}C {^1H} NMR (benzene-d_6, 100.5 MHz, 303 K): δ_C 25.44 (Cp-CCH_3), 12.47 (Cp-CH_3).

EI MS analysis on this product has not proved possible.

5.10.2 Synthesis of $[Th(\eta^8\text{-}COT\{Si^iPr_3\text{-}1,4\}_2)(Cp^{Me5})Cl]$ (5.4)

A green solution of $K_2(\eta^8\text{-}C_8H_6)\{Si^iPr_3\text{-}1,4\}_2$ (0.674 g, 1.364 mmol) in THF (5 cm^3) was added dropwise over 5 minutes to a white suspension of **5.3** (0.740 g, 1.436 mmol) in THF at -78 ºC, with stirring, with observation of a fine white precipitate. This mixture was allowed to warm to ambient temperature overnight extraction with pentane. Subsequent storage of this pentane solution at 0 °C resulted in large off-white block crystals of **5.4** in good yield, suitable for X-ray diffraction studies.

Yield = 0.565 g (0.691 mmol), 48 % w.r.t. **5.3**.

^1H NMR (benzene-d_6, 399.5 MHz, 303K): δ_H 7.12 (s, 2H, COT-H), 6.70 (m, 2H, COT-H), 6.41 (m, 2H, COT-H), 1.95 (s, 15H, Cp-CH_3), 1.59 (septet, $|^3J_{HH}|$ = 7.45 Hz, 6H, ^{i}Pr-CH), 1.32 (d, $|^3J_{HH}|$ = 7.55 Hz, 18H, ^{i}Pr-CH_3), 1.22 (d, $|^3J_{HH}|$ = 7.47 Hz, 18H, ^{i}Pr-CH_3).

$^{13}C\{^1H\}$ NMR (benzene-d_6, 100.5 MHz, 303K): δ_C 127.59 (Cp-*C*CH_3), 113.48 (COT-*C*H), 107.55 (COT-*C*H), 107.14 (COT-*C*Si), 105.02 (COT-*C*H), 20.05 (^{i}Pr-*C*H_3), 19.68 (^{i}Pr-*C*H_3), 11.77 (Cp-*C*H_3).

$^{29}Si\{^1H\}$ NMR (benzene-d_6, 79.4 MHz, 303 K): δ_{Si} 11.04 (s, Si-^{i}Pr).

MS $(EI)^+$: m/z = 683 (100 %), 818 (M^+, 95 %), 775 (M^+ -^{i}Pr,33 %) 683 (M^+ -Cp^{Me5}, 100%).

Elemental analysis calcd (%) for $C_{36}H_{63}ClSi_2Th$: C 52.8, H 6.97; found: C 52.62, H 7.16.

Crystal data for **5.4**: Yellow air-sensitive plates 0.02 × 0.02 × 0.02 mm^3, $C_{47}H_{69}ClSi_2Th$, a = 8.67790(10), b = 12.8594(2), c = 20.8423(4) Å, α = 92.8860(10)°, β = 99.1770(10)°, γ = 109.519(2)°, U = 2150.66(6) $Å^3$, triclinic, $P\bar{1}$, Z = 2, total reflections 26587, independent reflections 9259, R_{int} = 0.0673, θ_{max} = 27.06, R_1 [I >2σ(I)] = 0.0444, wR^2 = 0.1091 and 361 parameters.

5.10.3 Synthesis of $ThI_4(THF)_4$ (5.5)

To a Schlenk charged with dark grey thorium turnings (5.024 g, 21.655 mmol) was added THF (40 cm^3) before cooling to 0 ºC. Elemental I_2 (9.050 g, 35.629 mmol) was added in 4 portions with stirring, causing the suspension to turn red-brown in colour before fading to dark grey. After the final addition the mixture was allowed to reach ambient temperature overnight resulting in a pale brown solution with fine grey powder. The supernatant was isolated *via* filter cannula and the residues washed with THF (2 x 20 cm^3) before removal of solvent under reduced pressure to give a sticky grey/brown solid. To this was added 40-60 petroleum-ether (50 cm^3), followed by stirring, sonication and trituration, resulting in the appearance of $ThI_4(THF)_4$ as fine pale grey powder that was further extracted with 40-60 petroleum-ether.

Yield = 17.038 g (16.6 mmol), 77 % w.r.t. Th.

EI MS and ^1H and $^{13}C\{^1H\}$ NMR spectroscopy was not possible on this compound.

5.10.4 Synthesis of [Th(η^8-COT{Si^{i}Pr$_3$-1,4}$_2$)(Cp^{Me5})I] (5.7)

To a pale yellow solution of **5.4** (0.420 g, 0.513 mmol) in toluene (20 cm^3) was added trimethylsilyliodide (0.552 g, 2.760 mmol) at ambient temperature. The mixture was allowed to stir for 3 days with no observable colour changes before removal of volatiles under reduced pressure to give pale solids. These were taken up in toluene and on subsequent storage at -35 °C, resulted in pale yellow block crystals of **5.7** in good yields which were suitable for X-ray diffraction studies.
Yield = 0.277 g (0.304 mmol), 59 % w.r.t. **5.4**.

^{1}H NMR (benzene-d_6, 399.5 MHz 303K): δ_H 7.18 (s, 2H, COT-H), 6.70 (m, 2H, COT-H), 6.38 (m, 2H, COT-H), 2.00 (s, 15H, Cp-CH$_3$), 1.62 (septet, $|^3J_{HH}|$ = 7.57 Hz, 6H, ^{i}Pr-CH), 1.33 (d, $|^3J_{HH}|$ = 7.49 Hz, 18H, ^{i}Pr-CH$_3$), 1.24 (d, $|^3J_{HH}|$ = 7.49 Hz, 18H, ^{i}Pr-CH$_3$).
^{13}C{^{1}H} NMR (benzene-d_6, 100.5 MHz, 303K): δ_C 128.78 (Cp-*C*CH$_3$), 114.38 (COT-*C*H), 109.02 (COT-*C*Si), 107.64 (COT-*C*H), 104.73 (COT-*C*H), 20.27 (^{i}Pr-*C*H$_3$), 20.19 (^{i}Pr-*C*H$_3$), 12.98 (^{i}Pr-*C*H), 12.71 (Cp-*C*H$_3$).
^{29}Si{^{1}H} NMR (benzene-d_6, 79.4 MHz, 303 K): δ_{Si} 10.96 (s, Si^{i}Pr$_3$).
MS (EI)$^+$: m/z = 157 (100 %), 910 (M$^+$, 13 %), 867 (M$^+$ - ^{i}Pr, 10 %), 775 (M$^+$ - Cp^{Me5}, 32 %).
Elemental analysis calcd (%) for $C_{36}H_{63}ISi_2Th$: C 47.5, H 6.97; found: C 47.64, H 6.87
Crystal data for **3.7**: Yellow blocks 0.36 × 0.22 × 0.06 mm^3, $C_{36}H_{63}ISi_2Th$, a = 8.7050(4), b = 12.5835(6), c = 18.1400(8) Å, α = 89.126(2)°, β = 83.109(2)°, γ = 71.906(3)°, U = 1874.63(15) Å^3, triclinic, $P\bar{1}$ (No.2), Z = 2, total reflections 35631, independent reflections 8609, R_{int} = 0.057, θ_{max} = 27.53, R_1 [I >2σ(I)] = 0.041, wR^2 = 0.098 and 366 parameters.

5.10.5 Synthesis of [Th(η^8-COT{Si^{i}Pr$_3$-1,4}$_2$)(Cp^{Me5})]$_2$(C_2O_4) (5.8)

To a pale yellow solution of **5.7** (0.100 g, 0.110 mmol) in toluene (1 cm^3) was added an excess of NaK before cooling to -78 °C and subsequent addition of $^{13}CO_2$ (5 eq). This mixture was allowed to stir for 5 days before filtration. Storage at -35 °C yielded pale yellow rectangular crystals of **5.8** in poor yield that were suitable for X-ray diffraction analysis.
Yield = 0.002 g (0.00122 mmol), 2 % w.r.t. **5.7**.

^{1}H NMR (benzene-d_6, 399.5 MHz 303K): δ_H 6.82 (m, 2H, COT-H), 6.70 (m, 4H, COT-H), 1.99 (s, 15H, Cp-CH_3), 1.63 (septet, $|^3J_{HH}|$ = 7.59 Hz, 6H, ^{i}Pr-CH), 1.31 (d, $|^3J_{HH}|$ = 7.51 Hz, 18H, ^{i}Pr-CH_3), 1.28 (d, $|^3J_{HH}|$ = 7.51 Hz, 18H, ^{i}Pr-CH_3).
^{13}C{^{1}H} NMR (benzene-d_6, 125.72 MHz, 303K): δ_C 172.09 (C_2O_4), 128.35 (Cp*C*CH_3), 109.90 (COT-*C*H), 105.33 (COT-*C*H), 105.21 (COT-*C*H), 20.14 (^{i}Pr-*C*H_3), 19.79 (^{i}Pr-*C*H_3), 12.94 (^{i}Pr-*C*H), 11.74 (Cp-*C*H_3).
^{29}Si{^{1}H} NMR (benzene-d_6, 79.4 MHz, 303 K): δ_{Si} 9.04 (s, Si^{i}Pr$_3$).
MS (EI)$^+$: m/z = 59 (100 %), 1657 (M^+, 1 %), 1552 (M^+ - Cp^{Me5}, 1 %), 783 (M^+ - [Th(η^8-COT{Si^{i}Pr$_3$-1,4}$_2$)(Cp^{Me5})](C_2O_4), 1%).
Crystal data for **5.8**: Yellow plates 0.04 × 0.02 × 0.02 mm^3, $C_{88}H_{142}O_4Si_4Th_2$, a = 12.3722(5), b = 13.3983(4), c = 15.7276(7) Å, α = 65.525(2)°, β = 67.618(2)°, γ = 72.722(2)°, U = 2163.84(15) Å^3, triclinic, $P\bar{1}$ (No.2), Z = 1, total reflections 28262, independent reflections 9819, R_{int} = 0.0534, θ_{max} = 27.54, R_1 [I >2σ(I)] = 0.0346, wR^2 = 0.0667 and 454 parameters.

5.10.6 Synthesis of [Th(η^8-COT{Si^{i}Pr$_3$-1,4}$_2$)(Cp^{Me5})]$_2$(CO_3) (5.9)

To a pale yellow solution of **5.7** (0.090 g, 0.0989 mmol) in toluene (1 cm^3) was added an excess of NaK before cooling to -78 °C and subsequent addition of $^{13}CO_2$ (3 eq). This mixture was allowed to stir for 16 days before filtration. Storage at -35 °C yielded pale yellow rectangular crystals of **5.9** in poor yield that were suitable for X-ray diffraction analysis.
Yield = 0.010 g (0.00615 mmol), 12 % w.r.t. **5.7**.

^{1}H NMR (toluene-d_8, 399.5 MHz 303K): δ_H 6.73 (m, 4H, COT-H), 6.53 (m, 2H, COT-H), 2.01 (s, 15H, Cp-CH_3), 1.62 (septet, $|^3J_{HH}|$ = 7.45 Hz, 6H, ^{i}Pr-CH), 1.32 (d, $|^3J_{HH}|$ = 7.38 Hz, 18H, ^{i}Pr-CH_3), 1.24 (d, $|^3J_{HH}|$ = 7.75 Hz, 18H, ^{i}Pr-CH_3).

^{13}C{^{1}H} NMR (toluene-d_8, 100.5 MHz, 303K): δ_C 177.53 (Cp-*C*CH_3), 167.84 (CO_3), 111.05 (COT-*C*H), 108.24 (COT-*C*H), 106.50 (COT-*C*H), 105.50 (COT-*C*H), 20.67 (^{i}Pr-*C*H_3), 20.51 (^{i}Pr-*C*H_3), 13.46 (^{i}Pr-*C*H), 11.88 (Cp-*C*H_3).

^{29}Si{^{1}H} NMR (toluene-d_8, 79.4 MHz, 303 K): δ_{Si} 9.79 (s, Si^{i}Pr$_3$).

MS (EI)$^+$: m/z = 784 (100 %), 1494 (M^+ - Cp^{Me5}, 1 %), 1449 (M^+ - Cp^{Me5}, - ^{i}Pr, 2 %).

Elemental analysis calcd (%) for $C_{73}H_{126}O_3Si_4Th_2$: C 46.9, H 6.74; found: C 47.05, H 6.56.

Crystal data for **5.9**: Yellow blocks 0.16 × 0.08 × 0.06 mm^3, $C_{37}H_{63}O_2Si_2Th$, a = 12.283(3), b = 13.356(3), c = 15.689(3) Å, α = 65.03(3)°, β = 67.92(3)°, γ = 72.30(3)°, U = 2142.8(8) Å^3, triclinic, $P\bar{1}$ (No.2), Z = 2, total reflections 31500, independent reflections 9766, R_{int} = 0.0581, θ_{max} = 27.88, R_1 [I >2σ(I)] = 0.0295, wR^2 = 0.0675 and 444 parameters.

5.10.7 Electrochemical analysis of compounds 5.4 and 5.7

Electrochemical studies were performed in dry THF containing 0.1 M [N^{n}Bu$_4$][PF_6] as the supporting electrolyte using a BASi Epsilon-EC potentiostat under computer control, performed by A. Kilpatrick of the University of Sussex. Cyclic voltammetry experiments were performed using a three-electrode configuration with a glassy carbon disc having an area of 7.0 mm^2 as the working electrode, a platinum wire as the counter electrode and a silver wire as the pseudoreference electrode. The Ag wire pseudoreference electrode was calibrated to the ferrocene/ferrocenium couple in THF, relative to which all of the standard potentials are reported. Ferrocene (*ca*. 3 mg) was added to a 0.1 M solution of electrolyte in THF (5 cm^3) containing the dissolved metal complexes (5 – 8 mM).

5.11 References for Chapter Five

1. J. W. Bruno, D. G. Kalina, E. A. Mintz and T. J. Marks, *J. Am. Chem. Soc.*, 1982, **104**, 1860-1869.
2. P. C. Blake, M. F. Lappert, J. L. Atwood and H. Zhang, *J. Chem. Soc. Chem. Comm.*, 1986, 1148-1149.
3. P. C. Blake, N. M. Edelstein, P. B. Hitchcock, W. K. Kot, M. F. Lappert, G. V. Shalimoff and S. Tian, *J. Organomet. Chem.*, 2001, **636**, 124-129.
4. P. B. Hitchcock, J. Hu, M. F. Lappert and S. Tian, *J. Organomet. Chem.*, 1997, **536-537**, 473-480.
5. J. S. Parry, F. G. N. Cloke, S. J. Coles and M. B. Hursthouse, *J. Am. Chem. Soc.*, 1999, **121**, 6867-6871.
6. A. Arunachalampillai, P. Crewdson, I. Korobkov and S. Gambarotta, *Organometallics*, 2006, **25**, 3856-3866.
7. E. A. Mintz, K. G. Moloy, T. J. Marks and V. W. Day, *J. Am. Chem. Soc.*, 1982, **104**, 4692-4695.
8. W. J. Evans, K. A. Miller, S. A. Kozimor, J. W. Ziller, A. G. DiPasquale and A. L. Rheingold, *Organometallics*, 2007, **26**, 3568-3576.
9. R. S. Sternal, C. P. Brock and T. J. Marks, *J. Am. Chem. Soc.*, 1985, **107**, 8270-8272.
10. D. Rabinovich, S. G. Bott, J. B. Nielsen and K. D. Abney, *Inorg. Chim. Acta*, 1998, **274**, 232-235.
11. D. M. Barnhart, T. M. Frankcom, P. L. Gordon, N. N. Sauer, J. A. Thompson and J. G. Watkin, *Inorg. Chem.*, 1995, **34**, 4862-4867.
12. D. M. Barnhart, D. L. Clark, J. C. Gordon, J. C. Huffman, J. G. Watkin and B. D. Zwick, *Inorg. Chem.*, 1995, **32**, 5416-5423.
13. W. J. Evans, J. R. Walensky and J. W. Ziller, *Organometallics*, 2010, **29**, 101-107.
14. D. A. Fletcher, R. F. McMeeking and D. Parkin, *J. Chem. Inf. Comput. Sci.*, 1996, **46**, 746-749.
15. I. J. Bruno, J. C. Cole, P. R. Edgington, M. Kessler, C. F. Macrae, P. McCabe, J. Pearson and R. Taylor, *Acta Crystallogr., Sect. B: Struct. Sci*, 2002, **58**, 389-397.

16. W. Clegg and A. McCamley, *Private Communication*, 2005.
17. T. Cantat, C. R. Graves, K. C. Jantunen, C. J. Burns, B. L. Scott, E. J. Schelter, D. E. Morris, P. J. Hay and J. L. Kiplinger, *J. Am. Chem. Soc.*, 2008, **130**, 17537-17551.
18. R. Srinivasan and S. N. Flengas, *Can. J. Chem.*, 1963, **42**, 1315-1322.
19. S. Cotton, *Lanthanide and Actinide Chemistry*, John Wiley and Sons, Ltd., 2006.
20. N. Clavier, N. Hingant, M. Rivenet, S. Obbade, N. Dacheux, N. Barr e and F. Abraham, *Inorg. Chem.*, 2010, **49**, 1921-1931.
21. N. W. Alcock, S. Esperås, K. W. Bagnall and W. Hsian-Yun, *J. Chem. Soc., Dalton Trans.*, 1978, 638-646.
22. T. Herskovitz, *J. Am. Chem. Soc.*, 1977, **99**, 2391-2392.

A APPENDIX ONE: EXPERIMENTAL DETAILS

A1.1 General Procedures

High vacuum Schlenk-line techniques[1] were used for the manipulation of air-sensitive compounds and their spectroscopic measurements, under an atmosphere of dry nitrogen or catalytically dried and deoxygenated argon, or under catalytically dried and deoxygenated nitrogen in an MBraun glove box < 1 ppm H_2O and < 3 ppm O_2, or catalytically dried and deoxygenated argon in an MBraun glove box < 0.1 ppm H_2O and < 0.1 ppm O_2. Nitrogen and argon gases were supplied by BOC Gases UK. All glassware was dried by storage in an oven at 120 °C with subsequent cooling at 10^{-3} mbar vacuum followed by repeated alternate evacuation and purging with argon. Celite 545 filter aid was store in an oven at 200 °C and flame dried *in vacuo* before use. Filter cannulae equipped with Whatman® 25 mm glass microfibre filters were dried in an oven at 120 ° prior to use.

A1.2 Purification of Solvents

Where necessary, solvents were dried for a minimum of 72 hours over sodium wire before refluxing over the appropriate dying agents: sodium-potassium alloy (pentane, diethyl ether, petroleum ether), potassium (thf), sodium (toluene, DME, $(Me_3Si)_2O$) or calcium hydride (dichloromethane). Dried solvents were collected, degassed and stored in potassium mirrored ampoules except in the case of thf , DME and DCM, which were stored over activated 4 Å molecular sieves. All were degassed prior to use.

Deuterated NMR solvents were obtained from GOSS Scientific Ltd. and dried over potassium (d_6-benzene, d_8-thf) or sodium (d_8-toluene). These were vacuum transferred into ampoules followed by freeze-thaw degassing and stored under dinitrogen prior to use.

A1.3 Instrumentation

NMR analysis was undertaken by the author using Varian Direct Drive 400 MHz, 500 MHz or 600 MHz spectrometers. Chemcal shifts are reported in parts per million (δ) and are given relative to the residual protio chemical shift of the deuterated solvent in the case of ^{1}H NMR and $^{13}C\{^{1}H\}$ NMR. $^{11}B\{^{1}H\}$ NMR and $^{29}Si\{^{1}H\}$ NMR were referenced externally to $BF_3.OEt_2$ and TMS. In accordance with IUPAC convention, downfield refers to a positive shift.

Single crystal X-ray diffraction analysis was performed by Dr P. B. Hitchcock, Dr M. P. Coles or Dr S. M. Roe at 173 K using a Enraf-Nonius CAD4 diffractometer or by the National Crystallography Service at Southampton using a Bruker-Nonius Roper CCD diffractomer, each using graphite-monochromated Mo K α radiation (λ = 0.71073 Å). Data collection was handled using KappaCCD software, final cell parameter calculations performed using program package WinGX. The data were corrected for absorption using the MULTISCAN program. Refinement was performed using SHELXL-97, and the thermal ellipsoid plots drawn using Shelxtl-XP. SADI restraints, isotropic C atoms, H atoms are omitted, except where specified. Full details of the structures are given in Appendix Two.

Elemental analysis were carried out by S. Boyer at the Elemental Analysis Service, London Metropolitan University or by Mikroanalytisches Labor Pascher in Remagen, Germany.

Mass spectra were recorded by Dr. A. Abdul-Sada using a VG Autospec Fisons instrument (electron ionisation at 70 eV) or a Kratos MS25 mass spectrometer.

Electrochemical studies (cyclic voltammetry) were carried in dry THF containing 0.1 M $[N^{n}Bu_4][PF_6]$ as the supporting electrolyte using a BASi Epsilon-EC potentiostat under computer control, performed by A. Kilpatrick of the University of Sussex. Cyclic voltammetry experiments were performed using a three-electrode configuration with a glassy carbon disc having an area of 7.0 mm^2 as the working electrode, a platinum wire as the counter electrode and a silver wire as the pseudoreference electrode. The Ag

wire pseudoreference electrode was calibrated to the ferrocene/ferrocenium couple in THF, relative to which all of the standard potentials are reported. Ferrocene (*ca*. 3 mg) was added to a 0.1 M solution of electrolyte in THF (5 cm^3) containing the dissolved metal complexes (5 – 8 mM).

Quantum chemical calculations were performed by Prof. L. Maron of the Université Paul Sabatier. Thorium atoms were treated with two different effective core potentials. The 5f-in-core effective core potential adapted to the thorium +4 oxidation state was used in combination with its adapted basis set and additional f and g polarisation functions[2] in order to account for reactions involving dinuclear thorium(IV) complexes. The small Stuttgart-Dresden RECP (realistic effective core potential) was also used in combination with its adapted basis set[3-5] to study the oxidation step from +3 to +4. Carbon, oxygen and hydrogen atoms have been described with the double-zeta 6-31G)d,p) basis set.[6] Silicon atoms were treated with the Stuttgart-Dresden ECP in combination with its adapted basis set and additional d polarisation functions.[7,8] Calculations were carried out at the DFT level of theory using the B3PW91 functional.[9,10] Geometry optimisations were performed without any symmetry restrictions and the nature of the extreme (minima and transition states) was verified with analytical frequency calculations. Gibbs free energies were obtained at T = 298, 15 K within the harmonic approximation. IRC (Intrinsic Reaction Coordinate) calculations were performed to confirm th te connections of the optimised transition states. DFT calculations were carried out with the Gaussian 09 suite of programs.[11]

A1.4 Commercially Supplied Reagents

The following material were supplied by Sigma-Aldrich®: cyclooctadiene, tri*iso*propyl silane and triflic acid, these reagents were used as received. ^{n}BuLi (*ca*. 2.5 % in hexanes) was purchased from Sigma-Aldrich and titrated to determine exact molarity. $ZrCl_4$ and $HfCl_4$ were also supplied by Sigma-Aldrich and were sublimed and Fluka-supplied $KN(TMS)_2$ was recrystallised from toluene prior to use.[12] Isotopically enriched gases ^{13}CO (99 %) and $^{13}CO_2$ (99 %) were supplied by Cambridge Isotopes, and added *via* Toepler line. Thorium turnings were supplied by BNFL.

A1.5 Synthesis of Starting Materials

KC_8, NaK_3, K/Hg, MgCp*Cl(thf), 2,3,4,5-tetramethylcyclopent-2-enone, $ThCl_4$ and [Th(η^8-COT{Si^{i}Pr$_3$-1,4}$_2$)$_2$] were donated by Prof. F. G. N. Cloke and Ind^{Me7} by Dr J. H. Farnaby of the University of Sussex. ThI_4,[13] K_2(COT{Si^{i}Pr$_3$-1,4}$_2$),[14] and $AgBPh_4$[15] were synthesised according to published procedures. HCp^{Me4H},[16] HCp^{Me5},[17] HCp$^{Me4(TMS)}$,[16] HCp$^{Me4(nBu)}$ [18] were synthesised as described in the literature before potassiation by K(NTMS)$_2$ to give the potassium salts.

A1.6 References for Appendix One

1. D. F. Shriver and M. A. Drezdzon, *The Manipulation of Air-Sensitive Compounds*, 2nd edn., Wiley-Blackwell, 1986.
2. A. Moritz, X. Cao and M. Dolg, *Theor. Chem. Acc.*, 2007, 118, 845.
3. W. Kuechle, M. Dolg, H. Stoll and H. Preuss, *J. Chem. Phys.*, 1994, 100, 7535.
4. X. Cao, M. Dolg and H. Stoll, *J. Chem. Phys.*, 2003, 118, 487.
5. X. Cao and M. Dolg, *THEOCHEM*, 2004, 673, 203.
6. W. J. Hehre, R. Ditchfield and J. A. Pople, *J. Chem. Phys.*, 1972, 56, 2257.
7. A. Bergner, M. Dolg, W. Kuechle, H. Stoll and H. Preuss, *Mol. Phys.*, 1993,80, 1431.
8. A. W. Ehlers, M. Böhme, S. Dapprich, A. Gobbi, A. Höllwarth, V. Jonas, K. F. Köhler, R. Stegmann, A. Veldkamp and G. Frenking, *Chem. Phys. Lett.*, 1993, 208, 111.
9. A. D. Becke, *J. Chem. Phys.*, 1993, 98, 5648.
10. K. Burke, J. P. Perdew and W. Yang, *Electronic Density Functional Theory: Recent Progress and New Directions*, 1998.
11. M. J. Frisch, G. W. Trucks, H. B. Schlegel, G. E. Scuseria, M. A. Robb, J. R. Cheeseman, G. Scalmani, V. Barone, B. Mennucci, G. A. Petersson, H. Nakatsuji, M. Caricato, X. Li, H. P. Hratchian, A. F. Izmaylov, J. Bloino, G. Zheng, J. L. Sonnenberg, M. Hada, M. Ehara, K. Toyota, R. Fukuda, J. Hasegawa, M. Ishida, T. Nakajima, Y. Honda, O. Kitao, H. Nakai, T. Vreven, J. J. A. Montgomery, J. E. Peralta, F. Ogliaro, M. Bearpark, J. J. Heyd, E. Brothers, K. N. Kudin, V. N. Staroverov, R. Kobayashi, J. Normand, K. Raghavachari, A. Rendell, J. C. Burant, S. S. Iyengar, J. Tomasi, M. Cossi, N. Rega, J. M. Millam, M. Klene, J. E. Knox, J. B. Cross, V. Bakken, C. Adamo, J. Jaramillo, R. Gomperts, R. E. Stratmann, O. Yazyev, A. J. Austin, R. Cammi, C. Pomelli, J. W. Ochterski, R. L. Martin, K. Morokuma, V. G. Zakrzewski, G. A. Voth, P. Salvador, J. J. Dannenberg, S. Dapprich, A. D. Daniels, Ö. Farkas, J. B. Foresman, J. V. Ortiz, J. Cioslowski, D. J. and Fox, Gaussian, Inc., Wallingford CT, A2 edn., 2009.
12. W. L. F. Armarego and D. D. Perrin, *Purification of Laboratory Chemicals*, 4th Ed., Butterworth-Heinemann, 1997.

13. D. L. Clark, Tracey M. Frankcom, M. M. Miller and J. G. Watkin, *Inorg. Chem.*, 1992, 31, 1628-1633.
14. N. C. Burton, F. G. N. Cloke, P. B. Hitchcock, H. C. d. Lemos and A. A. Sameh, *J. Chem. Soc. Chem. Comm.*, 1989, 1462-1464.
15. G. Balazs, F. G. N. Cloke, J. C. Green, R. M. Harker, A. Harrison, P. B. Hitchcock, C. N. Jardine and R. Walton, *Organometallics*, 2007, 26, 3111-3119.
16. P. Courtout, R. Pichone and T. Y. Salaun, *Can. J. Chem.*, 1991, 69, 661-672.
17. F. X. Kohl and P. Jutzi, *J. Organomet. Chem.*, 1983, 243, 119-121.
18. S. Kaita, Y. Takeguchi, Z. Hou, M. Nishiura, Y. Doi and Y. Wakatsuki, *Macromolec.*, 2003, 36, 7923-7926.